

Geckofluidics: A strong and reliable reversible bonding technique for microfluidics

by

Abdul Wasay

A thesis submitted in partial fulfillment of the requirements for the degree of

Master of Science

Department of Mechanical Engineering
University of Alberta

© Abdul Wasay, 2016

Abstract

Towards minimizing the cost of Micro Total Analysis Systems (μ TAS) or Lab on a chip (LoC) systems, it is important to minimize manufacturing and assembly cost and time, and lower material costs. While the choice of material does govern material costs and the manufacturing process required and thereby, the time, it has been observed that the assembly (bonding) and interfacing time is one of the major rate limiting steps for the entire process. This work is an attempt to introduce a new bonding technique for microfluidics by using synthetic gecko inspired adhesives. This technique is being referred to as Geckofluidics. It doesn't require the use of any solvents or glues or surface activation or application of high pressure and/or temperature and is achievable in a process which doesn't require any additional equipment or add to the cost. It provides for a strong and reliable, reversible bonding technique, with bond strengths being on par with traditional irreversible bond strengths in elastomers.

This work characterizes the manufacturing feasibility of geckofluidic devices with various thermoplastic elastomers. A finite element simulation was also implemented in order to study the effect of some of the remedial measures taken to improve the adhesion strength, and also to study the minimum number of adhesive features required to effectively support the integration with microfluidics. A rapid mass manufacturing technique is also demonstrated using thermocompressive molding in thermoplastic elastomers. The resulting devices have been demonstrated for use for both pressurized and non-pressurized microfluidic systems against various substrates.

Preface

This thesis is an original work by Abdul Wasay under the supervision of Dr. Dan Sameoto. All of the work presented henceforth was conducted in the Polymer Microfabrication lab and nanoFab located at the University of Alberta. Sections of chapter 3, 4,5 and 6 have been published as journal article: ‘Wasay, A; Sameoto, D. Gecko Gaskets For Self-Sealing And High-Strength Reversible Bonding Of Microfluidics. Lab On A Chip. 15, 13, 2749-2753, 2015. Issn: 14730197’; and conference articles, ‘A.Wasay And D. Sameoto ,“Geckofluidics”: A New Concept In Reversible Bonding Of Microfluidic Channels, Solid-State Sensors, Actuators And Microsystems Workshop, Hilton Head 2014, Hilton Head, Sc, USA’; ‘D. Sameoto ; A. Wasay; Materials Selection And Manufacturing Of Thermoplastic Elastomer Microfluidics, Proc. Spie 9320, Microfluidics, Biomems, And Medical Microsystems Xiii, 932001 (March 5, 2015); Doi:10.1117/12.2081291’; ‘A.Wasay And D. Sameoto, Geckoadhesives For Microfluidics: A Strong And Reversible Bonding Technique, Proc. Int. Conf. Miniaturized Syst. Chem. Life Sci., 18th, 2014, 2530–2531’; ‘D. Sameoto And A. Wasay; Multi-Layer Strong Reversible Bonding Via Gecko-Inspired Gasket Architecture , Napa Institute 2015, Enabling Future Health Care- The Role Of Micro And Nano Technologies, Napa, CA, USA’

I was responsible for data collection and analysis as well as the manuscript composition. Dr.Dan Sameoto assisted with the data collection , concept ideation and development and contributed to manuscript edits.

Acknowledgements

I would like to sincerely thank my supervisor, Dr.Dan Sameoto, for his immense support and guidance, which imbibed in me a great deal of scientific and technical expertise and also for his encouragement to work on a topic I was passionate about. His ideas and experimentation at the lab helped me cultivate a research ethic and develop hands on creative skills and also laid a substantial groundwork for most of this thesis. I would also like to thank Dr.Stephan Warnat , who collaborated on the MEMS integration of the concept.

I would like to acknowledge the support and contribution of my fellow lab mates, Ben Bsbaden, Walid bin Khaled, Babak Soltannia, Mersedeh Zandavakili and Hasan Khodoker. I would specifically like to thank Walid bin Khaled, for his valuable discussions, nanoFab orientations and his help with my academics. I would also like to thank Matthew Reynolds for his help in getting me acquainted with the microfabrication process in the nanoFAB , David Sloan for his help in setting up the PXI set-up and the LabVIEW code and Saul Caverhill for collaborating on the electromagnetic field based separation of magnetic beads.

Also thanks to the great group of friends, Pankaj, Talat, Agni, Heena, Pallavi x2, Loki, Raheem, Khaleel, Hande, Nitya, PJ and Priya, who helped me adapt in a new country and created the home away from home. Finally thanks to my parents who have always loved me and trusted me to do what I love to do. Thanks to my sisters and brother, for being the source of limitless support, fun, love and strength throughout the course of this thesis and life.

Table of Contents

List of Tables	ix
List of Figures	x
List of Abbreviations	xv
CHAPTER 1: INTRODUCTION	1
1.1 What is Microfluidics?	2
1.2 Why Lab on Chip?	5
1.3 Motivation	8
1.4 Gecko Adhesion:	9
1.5 Research objective:	10
CHAPTER 2. LITERATURE REVIEW	12
2.1 Material Selection for microfluidics	12
2.1.1 Silicon	13
2.1.2 Glass	13
2.1.3 Polymers for microfluidics	8
2.1.3.1 Properties of Polymers	9
2.1.3.2 Classification of Polymers	11
2.1.3.3 PDMS Microfluidics	13
2.3.3.4 Thermoplastic Elastomers for microfluidics	14
2.2 Fabrication of Microfluidic chips	15
2.2.1 Photolithography	16
2.2.2 Deposition	17
2.2.4 Etching	17
2.2.5 Soft Lithography	18
2.2.6 Polymer machining	19
2.2.6.1 Micro-milling and Laser Machining	19

2.2.6.2 3D Printing.....	23
2.2.7 Polymer thermo-forming	24
2.2.7.1 Injection molding.....	20
2.2.7.2 Hot embossing	22
2.2.7.3 Mold insert fabrication.....	24
2.3 Bonding of Microfluidics.....	26
2.3.1 Irreversible bonding methods	27
2.3.1.1 Surface activated bonding.....	27
2.3.1.2 Thermal bonding.....	29
2.3.1.3 Localized Welding.....	30
2.3.1.4 Solvent bonding	32
2.3.1.5 Adhesive bonding	32
2.3.2 Reversible bonding	33
2.3.2.1 Bonding by self-adhesive property	34
2.3.2.2 Sealing by active sources	34
2.3.2.3 Reversible bonding with adhesives.....	35
2.4 World to chip interfaces.....	36
2.5 Gecko Inspired Adhesives	41
CHAPTER 3: STUDY OF MANUFACTURING FEASIBILITY WITH SEBS.....	49
3.1 Introduction.....	49
3.2 Replication studies	56
3.3 Results and discussion	62
3.4 Conclusion	69
CHAPTER 4: FIBER DESIGN GUIDELINES	70
4.1 Introduction.....	70
4.1 Integration with microfluidics.....	74
4.3 Results.....	77
4.3.1 Mesh:.....	77
4.3.2 Boundary Conditions	78

4.3.3 Governing Equations	78
4.3.4: Stress Distribution Without backing Layer	80
4.3.5 : Stress Distribution With Rigid Backing	85
4.4 Results and Discussion	86
4.5 Conclusion	94
CHAPTER 5: FABRICATION	95
5.1 Introduction.....	95
5.2. Mask Designs.....	97
5.3 Master mold fabrication.....	99
5.3.1 The development process.....	102
5.3.1.1 75% SU-8 Developer-25% IPA	104
5.3.1.2 50% SU-8 Developer-50% IPA	105
5.3.1.3 25%SU-8 Developer-75%IPA	106
5.3.1.4 100% IPA.....	107
5.4 Daughter Mold Fabrication.....	109
5.5 Device preparation	110
5.5.1 Thermocompressive molding.....	110
5.5.2 Roller Thermocompressive molding.....	113
5.6 World to chip interface manufacturing	116
5.7 Conclusion	118
CHAPTER 6: TESTS AND APPLICATIONS.....	119
6.1 Introduction.....	119
6.2 Non pressure driven systems:	119
6.2.1 Pinch Injection in a Capillary electrophoresis device:.....	119
6.2.3 Flexile microfluidics	124
6.2.4 Integration with MEMS	125

6.3 Pressure driven microfluidics:	126
6.3.1 Blister burst test	126
6.3.2 Micromixing:	131
6.3.3 Droplet Generator	133
6.3.4 Valves	136
6.3.5 Electromagnetic Field based Microbead Capture	137
6.4 World to chip interface	139
CHAPTER 7: CONCLUSION	142
7.1. Summary	142
7.2. Future Work	144
LIST OF PUBLICATIONS	146
REFERENCES.....	147
APPENDICES.....	171
Appendix A.....	171
Appendix B.....	180
Appendix C.....	184
Appendix D.....	185
Appendix E.....	188

List of Tables

Table 1. Overview of materials for microfluidic device fabrication.	7
Table 2: Comparison of properties of PDMS, TPE and hard thermoplastics (TP) materials properties for microfluidic technology	14
Table 3: Comparison of SEBS to PDMS and PS.....	55
Table 4: Overview of the thermoplastic elastomers	57
Table 5 :Average roughness values for dfferent replicated polymers	65
Table 6: Summary of results	67

List of Figures

<p>Fig. 1. A typical Lab on a chip device. The microfluidic chip is shown in purple, which is a cartridge that can be interfaced to the reader unit via electrical interconnects. The microfluidics chip cartridge should ideally cost < 1\$. [1] [Reprinted by permission of John Wiley & Sons, Inc.].....</p> <p>Fig. 2. a) Hierarchical imaging of Gecko feet [Reproduced with permission from [39], Copyright © 2006, Springer-Verlag], b) SEMs of nanoscaled gecko-spatulae terminal elements [40].....</p> <p>Fig. 3 Photolithography with a) positive resist b) Negative resist.....</p> <p>Fig. 4. Etching Process.....</p> <p>Fig. 5. Molding process for fabrication of stamp (similar for replica molding).....</p> <p>Fig. 6. Micro end mill tool images: (a) optical image showing all sections of a tool, (b) SEM image of the cutting end of an end mill, and (c) SEM image of a corner of the tool. [Reprinted from [112], with permission from Elsevier].....</p> <p>Fig. 7. (a) Micromilling machine (Image courtesy: Minitech Machinery Corporation) (b) SEM of an end mill in comparison to a leg of an ant. (Photo courtesy of Texas A&M University- via Permormance microtools).....</p> <p>Fig. 8. (a) Conceptual layout of a 3D printing setup (A) DLW concept (B)DMD concept [Reprinted with permission from [116]] (b) an integrated valving unit integrated with microfluidic system manufactured via 3D printing [Reproduced from [114], with permission of The Royal Society of Chemistry].....</p> <p>Fig. 9.(a) Schematic of Injection Molding Process flow (i) Polymer loading in the nozzle (ii) Clamping (iii) Polymer injection followed by cooling (iv) demolding) [Adapted from [119]] b) Pressure-Temperature Diagram for Injection Molding (Partially adapted from ISO 294-1:1996(E)).....</p> <p>Fig. 10.(a) Schematic of Hot Embossing Process flow[Adapted from [121]] b) Pressure-Temperature Diagram for Hot Embossing. [Adapted from [119]].....</p> <p>Fig. 11 Mold inserts fabricated by different processes: (a) milling with a CNC machine, (b) laser-manufactured tool with different surface roughness, (c) x-ray lithography and electroplating,(LIGA) (d) silicon etching (courtesy of Jenoptik Mikrotechnik GmbH), (e) photolithography with SU8, and (f) electric discharge machining (courtesy of Institut für Mikrotechnik Mainz) [125] [© IOP Publishing. Reproduced with permission. All rights reserved].....</p> <p>Fig. 12. (a) Chemistry of Plasma bonding (b) Plasma Cleaner Unit (Source: Harrick plasma).....</p> <p>Fig. 13.(a) Ultrasonic bonding Schematic of the bonding principle. The energy director material is contained within the groove resulting in no added height. [Adapted from [144], with permission from The Royal Society of Chemistry] (b) Cross-section of a 500 μm square microchannel in PMMA sealed by ultrasonic bonding, with deformed energy concentration structures evident on either side of the channel opening[Reprinted from [145], Springer 2006] (c) Ultrasonic Bonder Unit (Branson 2000X).....</p>	<p>2</p> <p>10</p> <p>16</p> <p>18</p> <p>19</p> <p>22</p> <p>22</p> <p>24</p> <p>21</p> <p>23</p> <p>25</p> <p>27</p> <p>30</p>
--	--

Fig. 14. (a) Schematic of the punching process and the interconnect fabrication method (Adapted from [174]) (b) Metal interconnects embedded in PMMA holder chip and sealed by a two part epoxy.....	37
Fig. 15. (a,b) “sleeve”-type coupler that fits the inner and outer diameter of the capillary tubing and prevents adhesive seeping into the microchannel.[Reprinted from [176], with permission from Elsevier] (c) Interconnect modules in silicon , for interfacing on a silicon microfluidic chip [Reprinted with permission [177], Copyright © 2002, Kluwer Academic Publishers]	38
Fig. 16. Double side adhesive tape bonded world to chip inter connects for paper based microfluidics.(a) Schematic arrangement for the WTC interconnects (b) sample unit T-channel for and (c) serial dilution device. [Reproduced from [175] with permission from The Royal Society of Chemistry]	39
Fig. 17. (a) Microfluidic Fit to Flow adapter[Reprinted from [178] with permission from The Royal Society of Chemistry] (b)press and screw fit connectors (c) Force fit interconnects in PTFE (the force is applied with a holder by means of tightening screws) [Reprinted from [179] with permission from The Royal Society of Chemistry]	39
Fig. 18. (a) Magnet based world to chip interconnects (b) Interface gasketing provided by (i) Polyimide tape (ii) Polyester tape (iii) PDMS and (iv) rubber O-ring [Reprinted from [180] with permission from The Royal Society of Chemistry]	40
Fig. 19. Synthetic gecko inspired adhesives: (a)Wedge shaped adhesive fibers in PDMS manufactured by dual layer SU-8 lithography in on quartz wafer[209] b)vertical fibres in polypropylene manufactured over polycarbonate filter by pressure filling in vacuum at 200 °C ,scale bar equals 10 microns [Reprinted with permission from [210], Copyright 2006 by the American Physical Society] c) polyurethane mushroom shaped fibers [Reprinted with permission from [211] Copyright 2009 American Chemical Society] d) hierarchical mushroom shaped adhesives in polyurethane with each layer hierarchical layer formed in separate steps and assembling by joining interfaces with liquid polyurethane and curing. [Reprinted with permission from [212] Copyright 2009 American Chemical Society].	47
Fig. 20. (a) Physical structure of SEBS (adapted from [217]) (b) Chemical formula of SEBS	50
Fig. 21.Economics of scale based on manufacturing process. [Reprinted from [221] with permission from The Royal Society of Chemistry]	53
Fig. 22. The Rhodamine dye test analysis performed by Borysiak <i>et al.</i> With Rhodamine B dye filled channel: (a), SEBS (b), PDMS and (c); the intensity variation along the width of the channel . after flushing the dye, (d), SEBS (e) PDMS and (f) intensity variation. [Reprinted with permission from The Royal Society of Chemistry].....	54
Fig. 23. a. Kraton G 1657 (pellet form) b. Kraton G1651 (Fluffy crumbs) c. Dryflex C series (SEBS-carbon black composite pellets) d. Proform EVA (Sheet) e. Dryflex SEBS T series f. thermoplastic polyurethane (cylindrical pellets).....	58
Fig. 24: Replication study results for various polymers*	60

Fig. 25.(a) Charging plumes (in the background) at gun voltages of ~5kV in a PS sample without gold coating (b) Low resolution images with low gun voltages (G1657) Extent of poor replication with (c) Proform EVA and (d) C3 6068.....	61
Fig. 26. Surface profile for Kraton G1657, without curve fitting.....	63
Fig. 27. Surface profile for Kraton G1657,after curve fitting,.....	64
Fig. 28. T909 (Maximum Roughness).....	65
Fig. 29. Kraton G1657M (Minimum Roughness)	66
Fig. 30: Setae geometry on feet of <i>Episyrphus balteatus</i> , a fly. PL- End Plate;Lu- Lumen and DL- electron dense layer Image from [224].....	70
Fig. 31. Fiber geometries tested for maximum adhesion strength.....	71
Fig. 32. Idealized failure modes [Adapted from [226], with permission from The Royal Society of Chemistry]	73
Fig. 33. Stress distribution for (a) flat punch and Mushroom Caps : (b)thin, (c) optimum and (d) thick [Adapted from [226], with permission from The Royal Society of Chemistry].....	73
Fig. 34: Geometry and geometric definitions for mushroom shaped micro fibers	74
Fig. 35. A schematic layout of a geckofluidics device	75
Fig. 36: SEM of the modelled adhesive fiber	77
Fig. 37. Illustration of modelled geometry and meshing scheme	77
Fig. 38. Description of boundary conditions used for simulation.....	78
Fig. 39. Geckofluidics: (a) Normal stress distribution (deflected). (b) Normal stress distribution in Gasket (c) 3D stress distribution in the gasket.	81
Fig. 40. Vertical punch geometry: (a) Normal stress distribution (deflected). (b) Normal stress distribution in Gasket (c) 3D stress distribution in the gasket.	83
Fig. 41. The inflation of the blisters as observed in practical application	83
Fig. 42. Geckofluidics with rigid backing: (a) Normal stress distribution (deflected). (b) Normal stress distribution in Gasket (c) 3D stress distribution in the gasket.....	86
Fig. 43. Geckofluidics without Rigid Backing: (Green: von mises; Blue: Normal Stress)	87
Fig. 44. Geckofluidics with Rigid Backing:	87
Fig. 45. Vertical Punch geometry: without Rigid backing	88
Fig. 46. Vertical Punch geometry: With Rigid backing.....	88
Fig. 47.A relative comparison of the peak Normal Stresses.....	89
Fig. 48. Geckofluidics: Without backing: one fixed fiber beyond the gasket	91
Fig. 49.Geckofluidics with rigid backing	91
Fig. 50.The variation of peak stress in the geckofluidic gasket with respect to variation in backing layer thickness	92
Fig. 51: The variation of peak stress in the geckofluidic gasket with respect to number of fibers in loading beyond the gasket, without backing layer.....	92
Fig. 52.The variation of peak stress in the geckofluidic gasket with respect to number of fibers in loading beyond the gasket, with backing layer.....	93
Fig. 53. Process layout for fabrication of Geckofluidic devices.....	98
Fig. 54. Prepared post development solvent compositions.....	103

Fig. 55. Post development in 75% SU-8 Developer-25% IPA, (a) 5X (b)20X (c) Naked eye view	104
Fig. 56. Post development in 50% SU-8 Developer-50% IPA, (a) 5X (b)20X (c) Naked eye view	105
Fig. 57. Post development in 25% SU-8 Developer-75% IPA, (a) 5X (b) 20X (c) Naked eye view	106
Fig. 58. Post development in 100% IPA: (a) 5X (b) 20X (c) Naked eye view (d) Inside the developer bath	107
Fig. 59. Variation of channel height with respect to exposure dose (in hrs) [See Appendix C for height details].....	109
Fig. 60. Visual depiction of the fabrication process. a) SU-8 patterned PMMA Wafer. b) UV exposed, post etched PMMA wafer, c) silicone daughter mold d) thermo-compressive molding process	112
Fig. 61. Roller- Thermo compressive molding.....	114
Fig. 62 (a) SEM Image of a Geckofluidic device replica in PS (b) cross section of a geckofluidics channel.....	115
Fig. 63. Dual master thermocompressive molding.....	117
Fig. 64. (a) A casting with some of the molded features (b) Dual master thermocompression molded interconnect with a patterned gasket	118
Fig. 65. A Geckofluidic channel with square tipped fibers	121
Fig. 66. Conceptual illustration of pinch injection	122
Fig. 67. (a) An assembled Capillary Electrophoresis Chip (b) Demonstration of pinch injection.....	123
Fig. 68. (a)A micromixer on the neck of an erlenmeyer flask (b) Flexible electrodes patterned on thin PS, integrated with a CE device (c) Ga-In (liquid metal) filled channels for stretchable antennas.....	124
Fig. 69. (a) Assembly of the MEMS chip with the geckofluidic channel. (b) The assembled device an enlarged view of the MEMS gripper section [Partially adapted from [250]](c) the gripper in action (image courtesy: Dr.Stephan Warnat, Dalhousie University)	125
Fig. 70. (a) Inflation in Geckofluidic blisters (b) Set up of the burst pressure test (inset: Schematic of the blister arrangement (R)igid backing- (B)lister- (S)ubstrate) [Partially adapted from [250]]	127
Fig. 71. (a) The blister arrangement on the substrate (b) SEM of the Blister.....	128
Fig. 72.: Burst pressure test results against different substrates.[Partially adapted from [250]].....	129
Fig. 73. Micromixer with focus regions.....	131
Fig. 74. Mixing in a Y-channel with a serpentine section – (a)High flow rates, (b) Low flow rate (at specified focus regions).....	132
Fig. 75.(a) The droplet generation equipment set-up (b) the droplet generator chip[Partially adapted from [250]].....	134
Fig. 76. Droplet Generation and coalescence results[Partially adapted from [250]].....	135

Fig. 77. (a) Fluid introduction (b) fluid deflecting the memberane (c) the breach (d) reseal 137

Fig. 78. Conceptual illustration of the electromagnetic field based bead capture. 138

Fig. 79 (a) A Geckofluidic channel on a PCB (b) Aggregation of magnetic beads in the magnetic field lines with an input current of 1 A and immediately after turning off the field 139

List of Abbreviations

LoC: Lab On a Chip

μ TAS: micro Total Analysis Systems

UV: Ultraviolet

PMMA: Poly (methyl methacrylate)

PDMS: Polydimethylsiloxane

COC: Cyclic Olefin Copolymer

TPU: Thermoplastic Polyurethane

PS: Polystyrene

SBS: styrene butadiene styrene

SEBS: styrene ethylene butylene styrene

SEPS: styrene ethylene propylene styrene

PC: Polycarbonate

TPE: Thermo Plastic Elastomer

NOA: Norland Optical Adhesive

REM: replica molding

μ CP: microcontact printing

MIMIC: micromolding in capillaries

SAMIM: Solvent assisted micromolding

nTP: nanotransfer printing

CHAPTER 1: INTRODUCTION

Micro Total Analysis Systems (μ TAS) are miniature diagnostic tools often used for chemical and biological analysis. The key application areas include, life sciences research, drug discovery and environment and Point of Care (PoC) health diagnostics. Also referred to as Lab on a Chip(LoC), these systems can either be standalone systems with complete functionality to offer detailed quantitative results, or instant point of care qualitative results. Ideally, the complete systems may be hand held, but in certain circumstances, owing to technological limitations for detection systems, these systems, may be bulky, yet portable. Immaterial of the size, these systems utilize small sample and reagent volumes and provide rapid analysis of the input sample. A LoC device is a complex integration of miniaturized fluidics, sensors and electronics. A typical LoC device consists of a microfluidics chip, sample processing unit, sample flow control unit, a detection mechanism and a data analysis and output unit. All laboratory tasks like sample preparation, reagent mixing, flow control, sensing, and analysis are carried out on the chip, often without manual intervention. The underlying concept weaving together these individual systems is microfluidics.

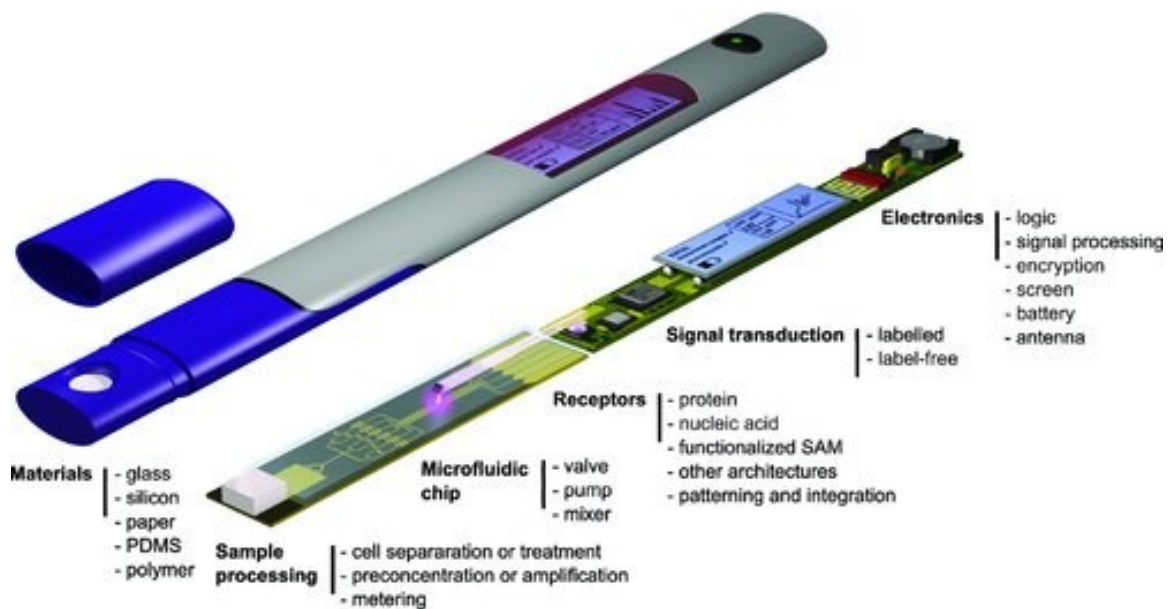


Fig. 1. A typical Lab on a chip device. The microfluidic chip is shown in purple, which is a cartridge that can be interfaced to the reader unit via electrical interconnects. The microfluidics chip cartridge should ideally cost < 1\$. [1] [Reprinted by permission of John Wiley & Sons, Inc.]

1.1 What is Microfluidics?

“Microfluidics is the science and engineering of systems in which flow behavior differs from conventional flow theory primarily due to the length scale of the system” [2]. Microfluidics has also been referred to as a tool box for research and development in the fields of chemistry, physics, biology and material sciences [3]. It is a science of manipulating very small amounts of fluids in miniaturized channels (10-100s of microns) thereby offering “control of concentrations of molecules in space and time” [4]. Since the typical sample format in μ TAS systems are liquids like plasma or other processed biological samples, this thesis limits the context of microfluidics to Newtonian liquids.

Microfluidic flow often exhibits low Reynolds number, typically $Re < 10$ (most applications working at $Re < 1$ and $Re \rightarrow 0$) [5].

$$Re = \frac{\text{inertial forces}}{\text{viscous forces}} = \frac{\rho u D_H}{\eta} = \frac{u D_H}{\nu} \quad \dots\dots\dots \text{Eq. 1}$$

Where, ρ is density of the fluid, u is the velocity of flow, η is dynamic viscosity, ν is kinetic viscosity and D_H is called the Hydraulic diameter, which is given by

$$D_H = \frac{4A}{P} \quad \dots\dots\dots \text{Eq. 2}$$

Where, A = Area of cross section, and P is the wetted perimeter.

The type of flow is often classified based on the value of Reynolds number. The flow is considered,

- *laminar* for $Re < 2300$
- *transient* for $2300 < Re < 4000$
- And *turbulent* $Re > 4000$

Hence, microfluidic flow is laminar and mixing is achieved purely by diffusion. At this scale properties like capillary forces and surface energies are the dominating forces.

The basic continuity equation for fluids stands as,

$$\frac{\partial \rho}{\partial t} + \nabla \cdot (\rho u) = 0 \quad \dots\dots\dots \text{Eq. 3}$$

Where t is time and $\nabla = (\frac{\partial}{\partial x}, \frac{\partial}{\partial y}, \frac{\partial}{\partial z})$

Since the fluids typically being used are incompressible, the variation in density is insignificant, the density can be assumed to be constant, implying, $\frac{\partial \rho}{\partial t} = 0$. Thus,

$$\nabla \cdot u = 0 \quad \dots\dots\dots \text{Eq. 4}$$

is the continuity equation for microfluidics flow regime.

The Navier stokes equation relates the velocity vector and pressure as,

$$\rho \left(\frac{\partial u}{\partial t} + u \cdot \nabla u \right) = -\nabla p + \mu \nabla^2 u + f_b \quad \dots\dots \text{Eq. 5}$$

Inertia= pressure gradient+ viscosity effect+ body forces

The inertial term includes unsteady acceleration effects, $\frac{\partial u}{\partial t}$ and $u \cdot \nabla u$ is the advection term, which describes the bulk flow behavior of the fluid.

For typical microfluidics regime, certain simplifications can be introduced. The body forces are primarily the self weight (gravity) effects of the fluid, which can be neglected. Since the flow regime is a low Reynolds number flow, at a distance beyond the entrance or the exit, the variations in bulk flow are negligible. Thus,

$$\rho \left(\frac{\partial u}{\partial t} \right) = -\nabla p + \mu \nabla^2 u \quad \dots\dots \text{Eq. 6}$$

While further simplifications may be introduced depending on specific conditions of flow, Eq.6 can be considered as the basic Navier Stokes equation for microfluidics.

The engineering aspect with microfluidics revolves around leveraging these inherent properties into developing optimized solutions and integration with other engineering domains.

1.2 Why Lab on Chip?

LoC systems open up a whole new paradigm of personalized and point of care diagnostics. With improving technologies pushing the boundaries of microfabrication each day, LoC systems could soon be regular feature for most biological fluids based diagnostics [4]. The key features pushing this acceptance are,

1. Miniature size

LoC device cartridges can, on the smallest size, be a few square millimeters to the largest being about of the size of a credit card. The entire LOC unit are often handheld or at least portable.

2. Low reagent and sample requirements

The sample volumes are often a few micro liters compared to milliliters required for the parent assay. Droplet microfluidics use volumes of the order of nanoliters to perform various high throughput computations.

3. Low bio-wastes

Since the input volumes are small, the output waste is less and requires minimal efforts for disposal.

4. Quick results

Most tests often take a fraction of time of the parent assay due to faster reaction kinetics.

5. Low power consumption

With miniaturized and more efficient electronics being developed, the power consumption on a LOC device is very small.

6. High throughput

With faster processing times, parallel processing of multiple samples can be carried out

on the same analyzer Droplet microfluidics[6], microfluidic arrays/ matrices [7] etc. are some of the examples of high throughput systems.

7. Multiplexing

Customized LOC systems with either serial or parallel processing can help perform multiple analyte detection tests on single sample [8, 9].

8. Improved sensitivity and results

Depending on the type of sensing in the microchannel, 2D or 3D, reliable and repeatable results can be obtained due to larger surface area to volume ratio (due to larger flow across the analysis surface). With minimal manual intervention and digital readout, the scope for errors is minimized. Also , various manipulation and detection techniques like fluorescence microscopy, raman spectroscopy, surface plasmon resonance etc, can be easily integrated with microfluidic systems and demonstrate high sensitivities for small analyte detection [10, 11].

9. Low cost

The advancements in microfabrication technologies can potentially allow fabrication costs to be minimized for the LOC devices. Novel materials like paper for microfluidics help drive the material cost to negligible and are becoming a popular choice for LoC devices [12].

10. Integration and Global health

With improved technologies, Lab on chip systems can communicate and update patient history, at the same time the recent impetus for integration with cellular phone cameras can help healthcare professionals and policy makers identify any epidemic outbreaks [13] with logging of localized patient count.

With all the stated advantages, LOC diagnostic devices have the potential to be used for personalized diagnostics, point of care testing in emergency rooms or doctor's office or hospital and most importantly in low resource setting and for global health, but the translation of academic research to commercialization has been challenging. Chin *et al.* [14] have discussed, in detail, both the technical and business challenges associated with commercialization of point of care diagnostic devices. A few companies with very small panel of tests have begun commercializing LoC products with low to moderate commercial success. A report by Research and Markets identifies the current in vitro microfluidics market to be worth 949.6 million in 2013 and predicts [15] it to reach 3.3 Billion USD by 2019.

While Cepheid and Caliper Life Sciences (now, Perkin Elmer) were the first companies for LoC systems, some of the major player in the industry are, Abbott (Abbott point of care division acquired iSTAT in 2003), Alere (Earlier, Inverness Medical acquired Biosite in 2007 and Epocal in 2009), Johnson & Johnson (acquired Amic in 2008), and Hewlett Packard (Agilent- a HP company- microfluidics instrumentation). iSTAT was amongst the first commercially successful company.

On the technical front, there are significant challenges associated at every detail in a lab on chip device. Many reviews on detection methods [16-18], reagent storage [19], sample preparation, separations, mixing and pumping [20-25] have addressed the existing techniques and challenges of each aspect. In this work, I have tried to address the challenges associated with bonding and interfacing using a low cost material and a rapid manufacturing process that together can provide a cost and time effective solution.

1.3 Motivation

Microfluidic chips are often fabricated in elastomeric materials as they provide a wide range of material properties and access to well characterized and established manufacturing techniques. Amongst the elastomers, PDMS has been the most commonly used material, but its potential as an industrial polymer for microfluidics is quite weak [26-28]. But elastomers are the only class of polymers that can support valves [29, 30] and hence recent developments have revolved around identifying other elastomers that can provide the preferred properties of PDMS, and at the same time be convenient for manufacturing. These materials are typically classified as thermoplastic elastomers.

A microchannel patterned in a polymer needs to be interfaced with a MEMS, microelectronics, chemical sensors coated or blank chip in order to make a functional device. This bonding step is often complex and a low yield process. Typical irreversible bonding techniques like plasma bonding, thermo-compressive bonding, solvent bonding, though provide a good seal, often require external apparatus and chemicals which may sometimes be incompatible in the presence of pre-patterned biological reagents [31, 32]. Reversible bonding techniques rely on simple contacting of two clean interfaces and the self sealing property of either of the polymers in contact, which has to preferentially be an elastomer. This bonding technique is often too weak for a reliable operation of the microfluidic chip. Use of suction aspiration, magnets [33] and adhesive tapes [34] has been proposed to improve this bonding technique.

From a cost analysis of a typical LoC device, the bulk of the cost may often be of the sensor, MEMS and Microelectronics components. While most of these components, except the polymeric chip, can be reused or regenerated [35, 36], the use of irreversible bonding techniques would prevent the reuse.

Hence to address all these challenges a strong yet reliable reversible bonding technique is desired. This work proposes a technique that relies on the integration of Gecko inspired adhesives with microfluidics. A brief insight into Gecko Adhesion will help us understand the solutions at hand.

1.4 Gecko Adhesion:

Geckos can stick to arbitrary surfaces purely by van der Waals intermolecular forces. Counter narratives attributing the adhesion to capillary forces have been disproved by experimentation [37]. This strong adhesion strength can be attributed to the hierarchical structures present on the Gecko's feet. The feet pads branch out into microscopic hair like structures called Setae, each of which in turn splits into sub-micron spatula shaped features. A single setae on a tokay gecko can generate upto $200\mu\text{N}$ force , with a cumulative maximum adhesion force per gecko foot being 100N ($\sim 10\text{atm}$) [38]. Synthetic versions emulating gecko adhesion have been fabricated using microfabrication technologies.

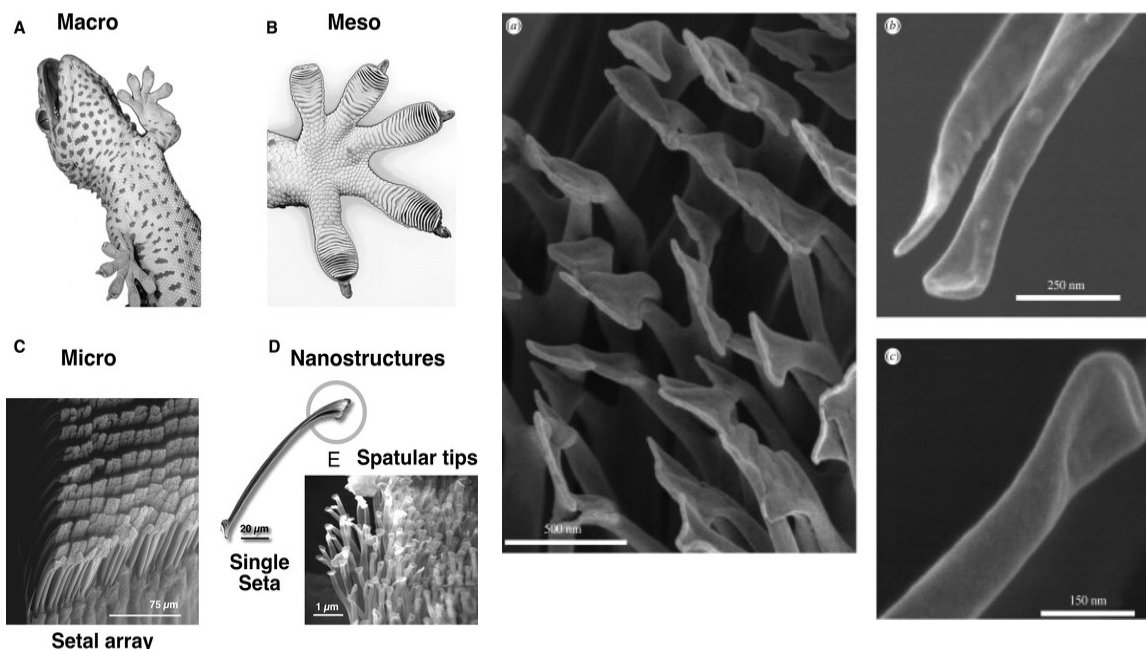


Fig. 2. a) Hierarchical imaging of Gecko feet [Reproduced with permission from [39], Copyright © 2006, Springer-Verlag], b) SEMs of nanoscaled gecko-spatulae terminal elements [Reproduced with permission from [40], The Royal Society]

1.5 Research objective:

The underlying theme across this thesis is to develop low cost and mass manufacturable microfluidic chips. μTAS or LOC systems hold huge promise and social value with their objective of providing quicker, personalized and improved diagnostics. The primary factor that would influence the acceptance of these systems over existing technologies is cost. In order to achieve these objectives, minimizing the cost is critical, which can only be achieved, when mass produced with cheaper material alternatives and minimal instrumentation. One objective of this thesis is to explore thermoplastic elastomers for microfluidics from a manufacturing standpoint. Another objective is to provide a microfluidic chip bonding and world to chip interfacing solution. Despite being

independent problems in their own way, this thesis addresses these problems with an integrated solution. After solving these issues, the solution is validated by multiple conceptual application studies.

A detailed material study follows a fabrication feasibility and replication fidelity study for thermoplastic elastomers in Chapter 3. Chapter 4 focusses on identifying the design parameters for the adhesive components of the geckofluidics concept. An FEA study has been included to study the design changes included for manufacturing feasibility. Chapter 5 includes the fabrication protocols and improved development techniques. It also introduces the thermo-compressive molding technique and outlines a potential serial mass manufacturing technique using roller thermo-compressive molding process. Chapter 6 describes some of the proof of concept applications classified under a superficial classification as pressure driven and non pressure driven applications. It also includes the burst pressure test used to characterize the peak adhesion against a few commonly used substrates.

The bonding and world to chip integration is addressed by integrating Gecko inspired adhesives with microfluidics, which provides for an instant strong and reversible bonding solution. Both the fabrication and adhesive integration is integrated into a single fabrication step, which is the highlight of this thesis.

This thesis tries to answer one of Dr.George Whitesides doubts as addressed in this discussion,

“ “As far as I know, every other polymer requires an adhesive,” says Whitesides. “Using an adhesive in a system with 50- μm channels on its surface can be very challenging and may not lend itself well to manufacturing”.[26]”

CHAPTER 2. LITERATURE REVIEW

2.1 Material Selection for microfluidics

While the origins of microfluidics trace back to the advent of microanalytical systems- Gas Chromatography, High Performance Liquid Chromatography (HPLC) and Capillary Electrophoresis (CE), the combination of microfluidics with the concept of a Lab on a Chip, as evident in modern context can be traced to the pioneering article by Manz in 1990 [41]. The early microfluidic chips, were manufactured using photolithography and associated technologies, borrowed from traditional silicon microelectronics and MEMS fabrication techniques [4]. Hence, early devices were mostly manufactured in silicon or glass. Subsequently polymer based microfluidic devices have been developed to address the shortcomings of silicon and glass based microfluidic devices, such as their opaque nature (in the case of silicon), high cost of manufacturing and challenges in bonding. Polymers in contrast can be manufactured in many different ways other than with traditional lithography and potentially at costs low enough to permit disposable systems to be produced profitably. There are many factors which need to be considered in the process of material selection for microfluidics. An overview of these factors, based on general classification of materials for microfluidics, is discussed in Table 1 [42]. Apart from the inherent physical and chemical properties, properties such as ease of fabrication, scalability and cost also play a critical role. Hybrid devices, like silicon-polymer, glass-polymer and dissimilar polymer hybrids are fast gaining recognition towards integrating better separation, sensing and detection functions with an added ease of fabrication. Where most initial microfluidic devices were manufactured from a set of materials good from a microfabrication point of view (due to appropriation of existing infrastructure and processes), there is a greater trend now to use

the most appropriate materials for the desired application and develop the manufacturing techniques and integration tools to produce the appropriate microstructures.

2.1.1 SILICON

Being the fundamental material at the origin of the very field of microfluidics, Silicon remains an important material for LOC applications. While the early LOC systems employed silicon for microfluidics [4, 43], modern LOC systems usually limit the use of silicon for MEMS-based sensing technologies. The quality of fabrication of microfluidic channels in silicon can yield the highest surface quality, due the crystal plane specific wet etching properties of crystalline silicon. The resolution, surface stability and solvent compatibility are the benchmark standards. Unfortunately, silicon is opaque to visible light, making it incompatible with fluorescence detection methods, and its electrically conductive nature prevents its use with separation techniques like CE, which require high voltages across channels. While modifications can be made (for example, a transparent lid bonded to silicon, or thermal oxide grown to provide an insulating layer), they increase the complexity of the full fabrication process. Due to the impeccable manufacturing quality, silicon is used to aid in the rapid prototyping of molds for polymer based microfluidics using methods like injection molding and hot embossing, by providing high quality mold inserts [44-46]. Unfortunately, its relative fragility and brittle nature limits its applicability for long term use in these molds.

2.1.2 GLASS

Glass has been used in conjugation with silicon and other polymer as a sealing substrate and also independently used for LOC devices. With the added advantage of the best optical properties, glass can also be micro-machined using the silicon fabrication

techniques [47], and hence was preferred over silicon in optical detection based microfluidic devices. Though at a nascent stage, modern fabrication techniques using femtosecond lasers have enabled 3D micromachining in glass [48]. Capillary Electrophoresis (CE) has been a major application of glass based devices, because of its stable electroosmotic mobility on the surface [49].

Despite the wide acceptance of polymeric devices, glass and silicon still have a few advantages, like superior electrical customization feasibility, well defined and consistent manufacturing properties, which render them superior over other polymers and continue to be used for LOC application [50].

Table 1. Overview of materials for microfluidic device fabrication.
(Reproduced with permission from [42]. Copyright 2013 American Chemical Society)

Property	Silicon/glass ^a	Elastomers	Thermoset	Thermoplastics	Hydrogel	Paper
Young's (tensile) modulus (GPa)	130–180/50–90	~0.0005	2.0–2.7	1.4–4.1	Low	0.0003–0.0025
Common technique for microfabrication^b	Photolithography	Casting	Casting, photopolymerization	Thermomolding	Casting, photopolymerization	Photolithography, printing
Smallest channel dimension	<100 nm	<1 μm	<100 nm	~100 nm	~10 μm	~200 μm
Channel profile	Limited 3D	3D	Arbitrary 3D	3D	3D	2D
Multilayer channels	Hard	Easy	Easy	Easy	Medium	Easy
Thermostability	Very high	Medium	High	Medium to high	Low	Medium
Resistance to oxidizer	Excellent	Moderate	Good	Moderate to good ^c	Low	Low
Solvent compatibility	Very high	Low	High	Medium to high	Low	Medium
Hydrophobicity	Hydrophilic	Hydrophobic	Hydrophobic	Hydrophobic	Hydrophilic	Amphiphilic
Surface charge	Very stable	Not stable	Stable	Stable	N/a	N/a
Permeability to oxygen (Barrer^d)	<0.01	~500	0.03–1	0.05–5	>1	>1
Optical transparency	No/high	High	High	Medium to high	Low to medium	Low

a) Photosensitive glass can be considered as thermoset.

b) Most of the materials can be fabricated by laser ablation, but compared with those obtained with lithographic or molding methods the ablated features usually have a rougher surface and are often misshaped.

c) Excellent for Teflon. ^d 1 Barrer = 10⁻¹⁰ [cm³ O₂(STD)] cm

2.1.3 POLYMERS FOR MICROFLUIDICS

Polymers are macromolecular materials with multiple similar or dissimilar monomeric units which can be crosslinked by a chemical or mechanical stimulus like a chemical initiator, light, pressure or temperature. Polymers with only one type of monomeric units are called homopolymers, while those with multiple monomeric units are referred to as copolymers.

Polymers have been used for microfluidics most prominently due to the lower cost for the materials and ease of manufacturability (depending on the specific polymer). The material and fabrication costs of microfluidic chip in polymers doesn't necessarily vary with complications in design. Polymers also offer a huge range of properties and processing parameters to choose from. They can have excellent replication fidelity (down to 10s of nm) [51] and offer scope for rapid prototyping using larger features and technologies like 3D printing(smallest ~100nm) [52]. While the optical properties, high surface quality and chemically stable properties make silicon and glass highly desirable, very few microfluidic applications require that high a quality. Polymers also provide the flexibility of combining multiple properties of materials either via surface coatings, blends, or composite materials to achieve desirable properties, which may otherwise not be available in the individual polymers themselves.

To identify the most appropriate polymers for a specific microfluidic application, it is important to understand the properties of polymers.

2.1.3.1 Properties of Polymers

From a manufacturing perspective, the important properties are as follows [53],

- Glass transition temperature
- Melting temperature
- Coefficient of Thermal Expansion
- Melt flow index
- Hardness
- Elasticity

while from an applications perspective, the properties to be considered are,

- Electrical insulation (Dielectric Strength and Electrical Resistance)
- Microchannel surface charge
- Thermal conductivity
- Moisture absorption
- Chemical resistance
- Optical properties
- Permeability
- Analyte absorption (Surface energy)
- Biocompatibility (material and/or additives)

The temperature at which, during the cooling phase, rubbery state converts to a solid [54]/ glassy state is called the glass transition temperature. It is also the inflection point on the specific volume [54] or specific heat capacity [55] vs temperature curve for amorphous and semi-crystalline polymers. At this temperature a polymer loses its mechanical strength but can still retain its preexisting shape. The properties of the polymer radically change due to internal movement of the polymer chains. At and slightly above this temperature, the

polymers can be worked to form a new shape via embossing. Beyond the glass transition temperature, exists a temperature at which the polymer deforms and eventually melts. This temperature is referred to as the melting temperature. Processes like injection molding are carried out at this temperature. The polymer retains its chemical integrity until the melting temperature. At the degradation temperature, the polymer loses both its mechanical and chemical integrity and can no longer be worked.

The coefficient of thermal expansion is an important parameter to determine the shrinking of the polymer after cooling down to the room temperature after manufacturing. Appropriate tolerances are decided to accommodate this coefficient. It is also an important parameter to be considered for thermal bonding. The melt flow index helps to understand the quality of filling and thereby determine approximate work pressures and hold times for high temperature manufacturing modes. Hardness is a critical parameter in room temperature fabrication of microfluidics via stamping processes.

Electro-osmotic flow is the most common flow driving mechanism in Lab on a chip systems. In order to be conducive for this flow mechanism, it is necessary that the surface exhibit dielectric properties to create a surface charge rather than being electrically conductive. The surface charge varies with the material, and mode of fabrication of the channel in that material [53]. The surface energy, which governs the hydrophobicity or hydrophilicity of the material, dictates the flow regime in the microfluidic devices. It is also important to note that hydrophobic surfaces tend to adsorb proteins and other analytes [56] from the solution in the channel. Depending on the porosity and permeability of the materials, the solutions in the channel may be absorbed by the channels, or providing gas permeation/ breathability to the device [57, 58]. While other visible colorimetric methods are also used, one of the most prevalent forms of detection systems for Lab on a chip

systems is often fluorescence detection. This requires that the microfluidic devices have good optical properties, especially low auto fluorescence.

2.1.3.2 Classification of Polymers

Polymers can be classified based on their source of origin, structure, type of polymerisation, and degree of cross linking. A superficial classification can also be made based on Physical properties, especially thermal properties, as these properties dictate the manufacturing. Based on physical properties, polymers are classified as,

1. Thermosets and
2. Thermoplastic materials
3. Elastomer

Thermoset polymers have covalently bonded polymer chains which produce a crosslinked matrix. These covalent bonds prevent melting of the thermosets, and generally increases solvent and temperature tolerance over thermoplastic materials. These polymers can soften and reflow, initially, but in the due process of crosslinking, form an infusible solid [59]. Eg: Thermoset Polyesters Polyurethane Methacrylate (PUMA), Norland Optical Adhesive 81(NOA), Polyimides, etc

Thermoplastics are polymers which have polymer chains held together by intermolecular forces. These polymers soften at glass transition temperature and melt at melting temperature, and can be repeatedly shaped into products without significant degradation. They can be processed for large scale manufacturing on tools like injection molding and hot embossing. Eg: PMMA, COC, PC

Elastomeric materials have weakly cross-linked polymer chains, which can regain the original state after removal of an external stress. These are also referred to as rubbers, and

demonstrate extreme elastic extensibility, some even as high as 1000% of original lengths, even under low mechanical stresses [59]. They have a low Young's modulus and a high yield strain. Elastomeric polymers include both thermosets and thermoplastics, which can be either naturally occurring or synthetic polymers.

There is a class of thermoplastic polymers called Thermoplastic elastomers (TPE), which is often overlooked for microfluidic applications. Thermoplastic elastomers exhibit the temperature dependent properties of thermoplastics, at the same time have the rubbery mechanical properties of elastomers. Thermoplastic elastomers have multiple temperature based transition points. A perfect definition of glass transition temperature for TPE's is debatable [60], due to glass transition temperatures of the individual polymers in the TPE [61], which dictate the net behavior. Thermoplastic elastomers are of three types,

1. Block copolymers
2. Rubber/plastic blends
3. Dynamically vulcanized rubber/plastic alloys, called thermoplastic vulcaisates [62]

Styrenic Block Copolymers are discussed in detail in chapter 3 of this thesis.

Thermoset Elastomers have been the most popular choice of materials for prototyping and research in the field of microfluidics. They are flexible and offer the temperature stability of thermosets. They are thermally stable over the range of operations of most LOC applications. Natural rubbers [63], Silicones and polyurethanes[64] are the family of polymers which have traditionally been used for elastomeric microfluidics. Other polymers like, perfluoropolyether (PFPE) [65-67], also referred as liquid Teflon, Fluorinated-Norbornene [66, 67], perfluorinated Silicone (PFPE SIFEL) [68, 69], Fluorocarbon Rubber (FKM), commonly known as viton[70] and a few other fluorinated polymers have also been demonstrated for use for microfluidics.

2.1.3.3 PDMS Microfluidics

Amongst the Silicones too, PDMS, specifically Sylgard 184, is the most predominant choice for microfluidics. It is a synthetic polymer, which was invented by M.K.Chaudhury at Dow Chemicals [26] and first adapted for microfluidics by the George Whitesides group. It offers very good optical and gas permeation properties and has a well-informed bio compatibility [71], and can be rapid prototyped with a sub 0.1 μ m fidelity [72]. It also exhibits a low surface energy which helps in the easy demolding from the master molds. The rapid prototyping argument is valid when compared to the then existing microfluidics fabrication technologies in silicon and glass. The relatively low cost and the simplicity of fabrication, especially without the requirement of high cost apparatus makes it quite attractive. The ease of multi layer device fabrication also helps reduce the foot print of the typical devices. PDMS also allows for multimaterial composites in order to add electrical [73] or magnetic [74] functionality to the polymers

Protein adsorption, oligomer leaching and water vapor permeability have been some of the drawbacks of PDMS, and have been addressed by surface modifications and coatings [75-77]. Problems concerning pressure induced deformations have been repeatedly come to the fore, but considering that most common driving modes appear to be non-pressurised systems, it could be deprioritized. IBM developed a high modulus variant of PDMS, referred to as h-PDMS (hard-PDMS) [78], which could help limit these deformation. Also, *Inglis* proposed to sandwich a thin layer of PDMS between two rigid materials like glass [79] in order to drastically reduce these deformation. Being an elastomer, it also supports the integration of microvalves, [29, 30, 80-82] and offers simple plug and play world to chip interconnection feasibility. The valves in PDMS also tend to be highly durable and show no signs of wear or fatigue even after more than 4 million

actuators [29]. While PDMS has been largely successful in academia, partially owing to the lack of competing materials, its drawbacks as a large scale manufacturing material are well established [26, 28].

Table 2: Comparison of properties of PDMS, TPE and hard thermoplastics (TP) materials properties for microfluidic technology [Adapted from [83], with permission of The Royal Society of Chemistry]

Property	PDMS	TPE	TP
Optical transparency	++	+	+
Young modulus	0.1–5 MPa	1–100 MPa	1–10 GPa
Thermoforming cycle	very slow	fast	fast
Gas permeability	high	moderate	low
Cost (\$/Lbs)	10–50	0.1–5	0.1–5
Reversible bonding	+	+	impossible
Irreversible bonding	+	++	—
Resolution	50 nm	10 nm - 100 nm	10 nm
Ease of de-molding	++	++	—

2.3.3.4 Thermoplastic Elastomers for microfluidics

Thermoplastic Elastomers have only recently found application for microfluidics, with the earliest publication in 2005 [84], while they were demonstrated for use for microcontact printing a little earlier in 2003 [85]. The recent and more elaborate push for the use of TPEs has been by the Posner Group at University of Washington and The Veres group from Industrial Materials Institute, National Research Council, Canada.

TPEs provide an alternative to PDMS and also facilitate true rapid prototyping via melt processing, like the thermoplastics. They also address the issues of lowers Young's

modulus, low tear strengths and protein adsorption of PDMS. Being bulk polymers, unlike the porous matrix of PDMS, the reagent evaporation is highly regulated in TPEs (and thermoplastics). Apart from their lucrative hybrid properties, they are cheaper than most elastomers and thermoplastics. They also do not require the expensive tooling of thermoplastics or the long curing hours of PDMS.

Sudarsan *et al.* have demonstrated the biocompatibility studies with SEBS [84], while Borysiak *et al.* performed cell culture, surface stability, absorption and optical studies with SEBS [86]. Geissler *et al.* demonstrated patterning of DNA arrays on Versaflex CL30 [87], which is another styrenic block copolymer, and performed analysis by fluorescence intensity read outs. Sudarsan *et al.* demonstrated dean flow induced hydrodynamic mixing in SEBS microchannels [88]. Borysiak *et al.* performed detailed zeta potential measurements [89] with and without plasma treatments on SEBS and demonstrated it to be compatible for electrokinetic applications like isotachopheresis and loop mediated isothermal amplification (LAMP) for nucleic acid detection [90]. While there are a few other polymers available with similar properties, SEBS remains the most well characterized and most preferred thermoplastic elastomer for microfluidics.

2.2 Fabrication of Microfluidic chips

Depending on the material of choice and application, different manufacturing strategies are adopted for microfabrication. The choice of fabrication also varies with the scale of fabrication. Since silicon and glass were the pioneering materials used in the early development of microfluidics, few of the techniques have been extended without or with minimal modification for fabrication in some polymers. A brief discussion of the processes is discussed in order to get an insight into polymer micromachining for microfluidics.

2.2.1 PHOTOLITHOGRAPHY

Lithography is the technique of writing unilateral 3D structures or patterns on substrates using radiations. Depending on the type of radiation, lithography can be subdivided into photolithography (visible Light or UV), X-Ray lithography, electron beam (e-beam) lithography, and ion beam lithography [2]. There are two aspects to lithography, firstly, the resolution of the images on the substrate, and secondly, registration (alignment) of the pattern [91]. The process involves coating the required surface with a radiation sensitive coating, called a resist, which upon exposure to the radiation, will undergo chemical changes, and thereby in a development process yield the structure or pattern. The lithography process involves either the use of a mask to incident patterns on the substrate or a computer controlled source guide (in a direct writing process). Mask based photolithography also proceeds as two options, contact exposure and projection exposure. Projection exposure (non-contact exposure) uses optics to allow for reduction in feature sizes, thereby improving resolution over traditional contact lithography.

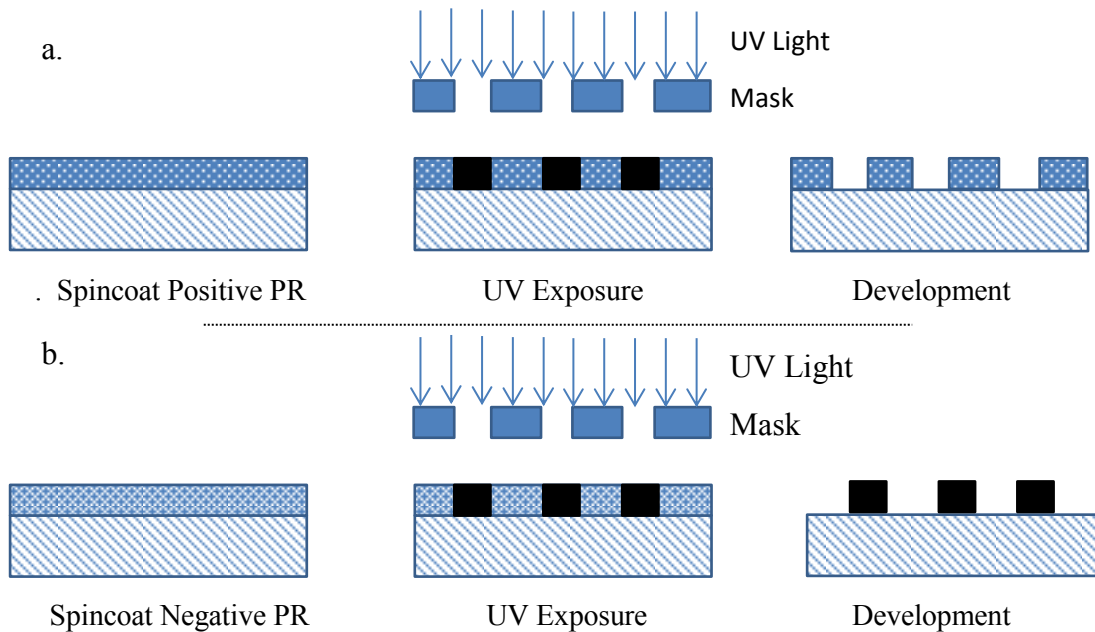


Fig. 3 Photolithography with a) positive resist b) Negative resist

2.2.2 DEPOSITION

In order to create metal or metallic alloy films, deposition techniques are used. These additive processes and can be classified into two main types, Chemical Vapor Deposition (CVD) and Physical Vapor Deposition (PVD). CVD involves creating a surface reaction of gaseous reactants on the substrate in order to form a solid film. PVD involves removing a target material from the source and depositing it on the substrate. This is done either by evaporating the metal, and depositing the vapor on the surface of the substrate, or creating a plasma of inert gas, which bombards the target material source and removes material from it, which later condenses on the substrate (a process known as sputtering). The cross-linked photoresists used for patterning the metal is removed by a stripping process involving resist specific organic solvents.

2.2.4 ETCHING

Etching is a subtractive process, involving removal of either the substrate or a target material. While physical dry etching involving ions, photons and electrons exists, Etching in practice is generally a chemical process. It involves identifying appropriate chemistries to react with the material across a passive resist. Wet etching involves immersing the substrates in etchant solutions for appropriate times depending on the etch rate and concentration of the etchant and the etch depth required. Dry chemical etching involves etching by gasses. Plasma cleaning is an example of chemical dry etching. Physical-Chemical etching processes like Reactive Ion Etching are the some of the commonly employed etching methods. They involve creating ions of reactive gasses, which under low pressure and high electric fields bombard the substrate to remove the material.

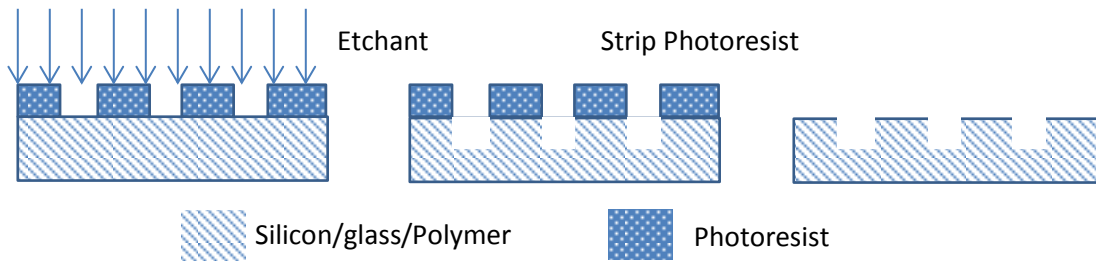


Fig. 4. Etching Process

2.2.5 SOFT LITHOGRAPHY

Soft Lithography is an umbrella term used to refer to a large number of processes like, replica molding (REM)[92], microcontact printing (μ CP)[93], microtransfer molding[94], micromolding in capillaries (MIMIC)[95], Solvent assisted micromolding (SAMIM)[96], Phase shifting edge lithography[97], nanotransfer printing (nTP) [98] and nano skiving [99]. It is preferred over other methods as it requires minimal skills, and no major equipment. The underlying principle for all these process involves the use of an elastomeric stamp, and hence the name, Soft Lithography. This stamp is fabricated via a molding process over a master mold which may be fabricated via other micromachining techniques either in Silicon or Glass or other polymers. While any compatible polymer may be used, the typical fabrication is carried out with liquid prepolymers like 2 or 3 part elastomeric pre polymers, epoxies or dissolved thermoplastics. Depending on the polymer and the type of prepolymer mix , the replication fidelity may vary. PDMS has been the choice of material for most microfluidics applications, due to its great optical properties, inertness, low surface energy and non-toxicity. Feature sizes as small as 50-100nm may be fabricated with PDMS [100].

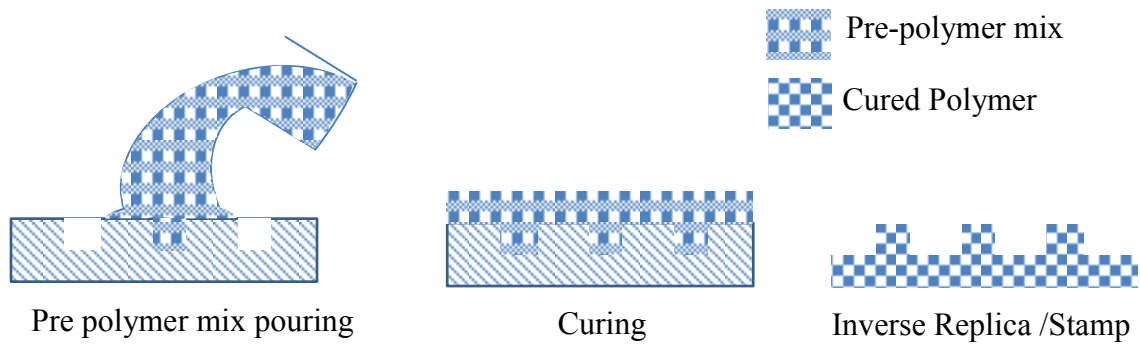


Fig. 5. Molding process for fabrication of stamp (similar for replica molding)

This molding process along with replica molding forms a part of the basis of the fabrication process in this thesis. Hence only replica molding is explained.

Replica molding proceeds via the same technique as the fabrication of stamp from the master mold, except that the master mold for replica molding is an elastomeric polymer. A dissimilar polymer to the stamp should be the ideal choice of polymer, but similar polymers have also been used especially with PDMS. Molding of PDMS against PDMS requires a silane surface treatment, in order to avoid fusion.

The molding and replica molding are simple processes, but require considerable time as the curing rates for different polymers vary and are often a few hours at elevated temperatures to a few days at room temperature.

2.2.6 POLYMER MACHINING

2.2.6.1 Micro-milling and Laser Machining

Subtractive machining processes like micro-milling and laser micromachining are some of the most common machining methods used with polymers. These are most effective with rigid polymers. Micromilling involves use of precisely machined milling

tools ,available for feature size up to 5 Microns(<http://www.pmtnow.com/end-mill/micron>) to remove materials from a stock piece. With this small the dimension of the end mills, handling and machining is a very delicate operation. Micro-milling machines employ computer numeric controls (CNC) which automate the process, thereby improving repeatability and precision. The designs are fed to the machine as G-codes. Alternately, the designs can be created on a designing software like AutoCAD, and fed to the machine via software like MasterCAM , which convert the designs into G-codes. Most operational issues arise out of tool failures, but adequate chip building measures can ensure reliability [101].

Laser machining is another important tool for microfluidics chip fabrication. Different forms of lasers sources offer different wavelengths and thereby a range of minimum resolutions. Shorter wavelength lasers can produce smaller features. Short wavelength lasers include UV (266-355nm) and excimer lasers, while Nd:YAG (1064nm) and CO₂ Lasers (10.6 μ m) offer higher wavelengths. The fabrication involves focusing a laser beam controlled on an X-Y stage. The energy associated with the laser point breaks down the polymer chains in the focused region which when continued along X and Y can produce suitable structures. The nature of breaking these bonds varies with respect to the laser source. The contactless manufacturing offers rapid and repeatable manufacturing without the concern of tools wear. Lasers have also been used for surface modification via surface micro-structuring or chemical grafting. *Malek* published a two part extensive review on the use of lasers for bio-microfluidics [102, 103], which also covers at length the principles of laser machining and the challenges associated incontext with bio-microfluidics. CO₂ laser based machining is the most common machining tool used by the microfluidics community primarily for prototyping, as it is also the cheapest of the lasers. It offers relatively quick machining times and can be used for machining thermoplastics [104-

106] or PDMS [107] or even thin metal [108, 109]. The results are particularly good with PMMA due to its high absorbance in the IR with low heat capacity. Laser machining in glass is challenging due to poor thermal conducting properties of glass compounded with brittleness, which risks inducing microcracks, and thereby also high surface roughness. Thus high energy low exposure times are required, which are feasible with UV, Nd-YAG or Ti:Sapphire with nano[110] to femto-second exposures [111].

The features produced by both micro-milling and laser machining generally have significant roughness and are avoided for optics based microfluidic sensing devices. The micro-milled features are generally orthogonal, and do vary slightly depending on the wear of the end mill, whereas the profiles for a laser cut microchannel could vary between shallow curves to deep converging trenches, depending on the aspect ratio of the channels. They are preferred for the ease of fabricating multi height devices in a single run. Nano-femtosecond laser based manufacturing reduces the extent of roughness significantly. These processes can be combined with electroforming techniques to manufacture molds for other fabrications processes like hot embossing or injection molding.

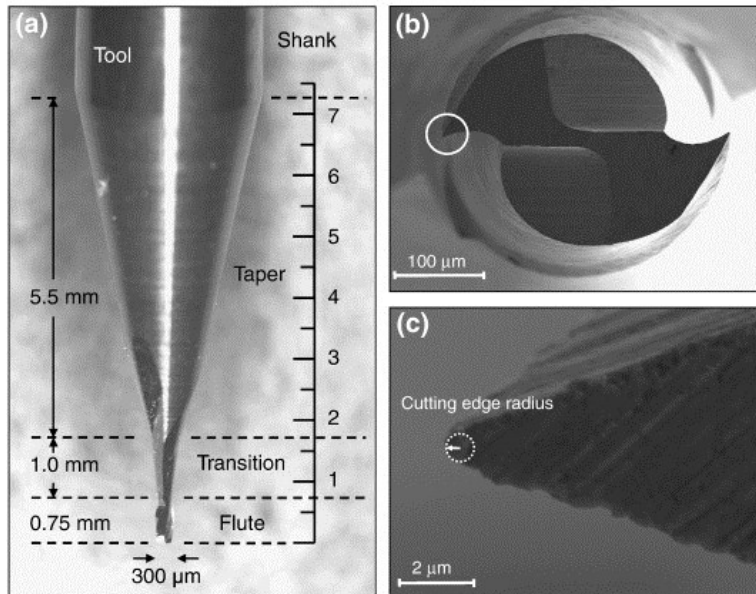


Fig. 6. Micro end mill tool images: (a) optical image showing all sections of a tool, (b) SEM image of the cutting end of an end mill, and (c) SEM image of a corner of the tool. [Reprinted from [112], with permission from Elsevier]

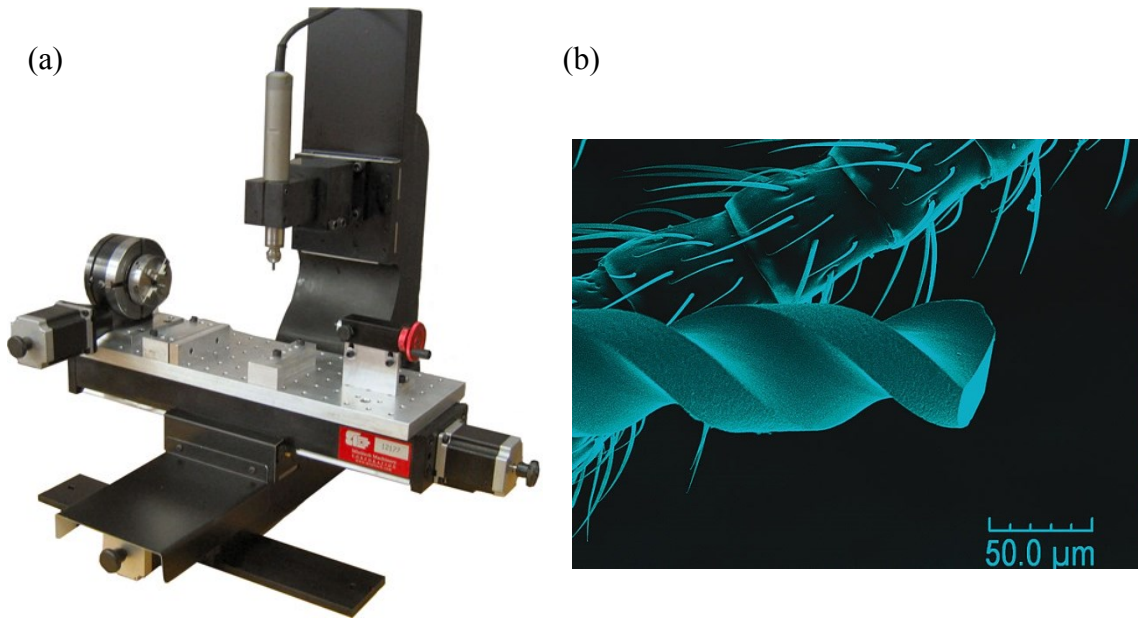


Fig. 7. (a) Micromilling machine (Image courtesy: Minitech Machinery Corporation) (b) SEM of an end mill in comparison to a leg of an ant. (Photo courtesy of Texas A&M University- via Performance microtools)

2.2.6.2 3D Printing

3D printing of microfluidics is the most recent addition to the list of manufacturing techniques for microfluidics. Stereolithography is a form of 3D printing, wherein a focused beam of light (mostly UV) produces arbitrary 3-d shapes based on a CAD file input, in a polymer from a photoresin precursor, held on a controlled receding pedestal. While the traditional systems involved a scanner tracing the structures based on CAD input, also referred to as Direct Laser Writing (DLW), modern systems rely on digital image projection techniques, in packages called Digital Mirror Display (DMD) Technologies. To create channels, the channel walls are polymerized by light and the uncured resin is drained [113], forming the channel. Integrated valves with microfluidics have been created via stereolithography [114].

3D printing is a very laborious process and involves significant sophistication. The surface quality and geometric integrity is debatable depending on the level of sophistication of the equipment and the polymer. Most of the low to medium cost printers suffer from poor resolutions, while the high end systems could cost as high as \$100,000-125,000. O’Niel *et al.* [115] have briefly discussed the advancements in stereolithography for microfluidics and cite that the expiration of patents is and will drive the cost down in the near future, but also express that more research is required in terms of new resins and in removal of supporting structures at the scale for use in microfluidics. The technology is still at a nascent stage to be adopted for mass manufacturing and can be promising with advancements in polymer sciences. For now, 3D printed molds can be used as templates for complex microfluidic geometries.

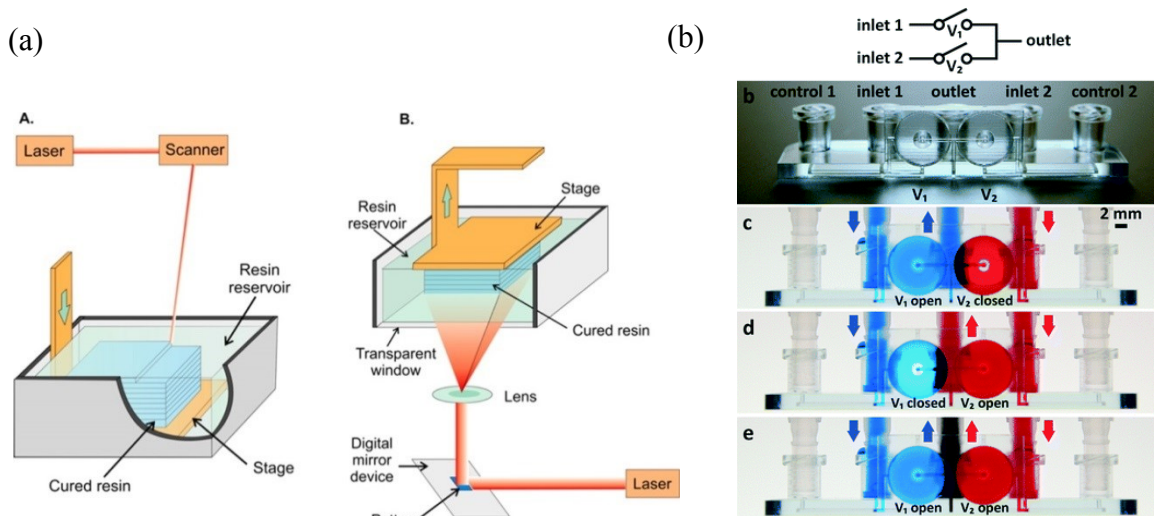


Fig. 8. (a) Conceptual layout of a 3D printing setup (A) DLW concept (B)DMD concept [Reprinted with permission from [116]] (b) an integrated valving unit integrated with microfluidic system manufactured via 3D printing [Reproduced from [114], with permission of The Royal Society of Chemistry]

While none of these processes, under polymer machining are ideal for large scale manufacturing, they are great tools for early developmental stage, which requires significant design iterations.

2.2.7 POLYMER THERMO-FORMING

Thermoplastic polymers have the potential to be thermo-formed into required geometries and structures, via processes like injection molding, hot embossing, injection compression molding and thermoforming. Thermo-forming of polymers has been in existence for long and are a fairly well characterized processes for macro sized products. This know-how can be extended to micromolding processes with small modifications. While polymer related properties do define the processes, the molding parameters for the processes vary with different machines, and complexity of the molds.

2.2.7.1 Injection molding

Injection molding is a variotherm process [117] involving cycling the mold temperatures between above and below glass transition temperature of the polymer. The mold cavity houses a microfabricated mold insert. For the process, the cavity is closed and evacuated, and the mold is heated before a measured quantity of melted polymer is injected at high pressures into the cavity. After a complete filling, the temperature of the mold is reduced and the solidified structured polymer is ejected. Metering size and hold times have been shown to have the most significant effect on the molding quality, based on DOE experimentation by Zhao *et al.* [118]. Some of the other important parameters are, mold temperature, injection speed, injection pressure and melt temperature. Fig. 9(b) shows the variation of pressure and the temperature (as described by International Standards Organization (ISO) 294-1:1996 protocols) and the process layout (Fig. 9 (a)) [119].

Microinjection molding is the mostly commonly used method for large scale fabrication of microfluidic devices and the fabricated chips could cost only a few pennies. Submicron and high aspect ratio feature sizes are achievable. Despite the low manufacturing cost, the capital costs often run into 6-7 figure amounts. While the process could be outsourced, most commercial injection molding contractors operate away from clean rooms, while fabrication of these devices requires operating in a dedicated clean room facility, which again adds to the cost [120].

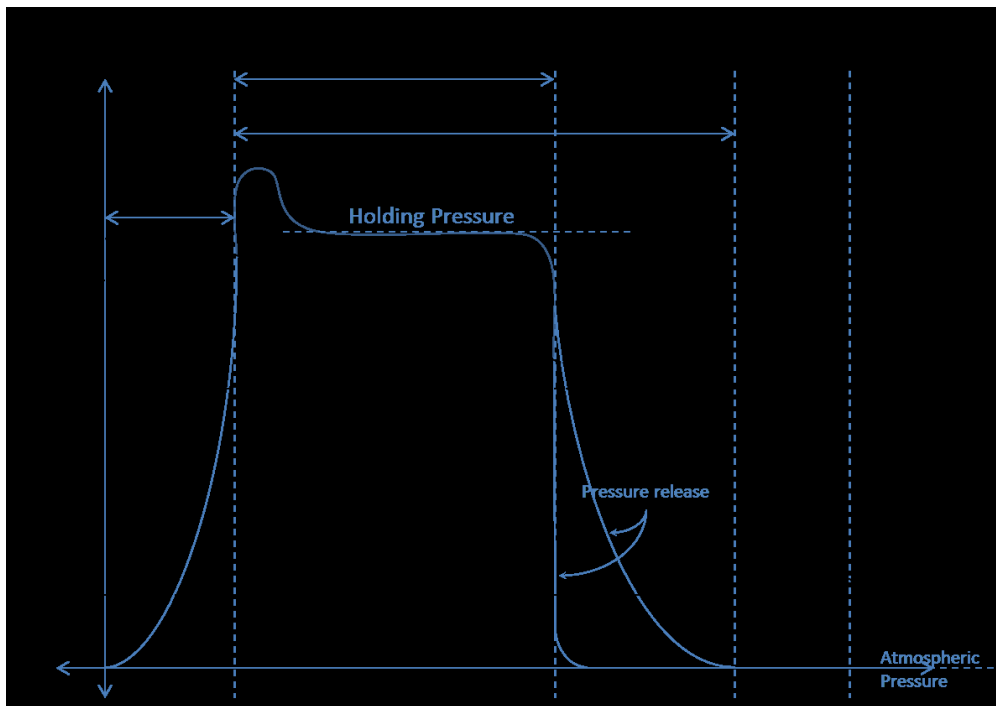
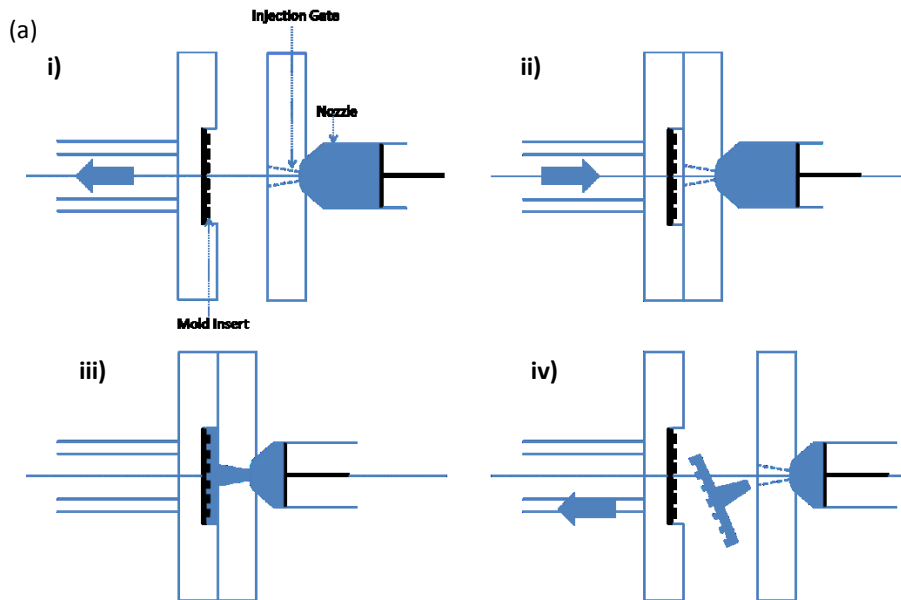


Fig. 9.(a) Schematic of Injection Molding Process flow (i) Polymer loading in the nozzle (ii) Clamping (iii) Polymer injection followed by cooling (iv) demolding) [Adapted from [119]]
 b) Pressure-Temperature Diagram for Injection Molding (Partially adapted from ISO 294-1:1996(E))

2.2.7.2 Hot embossing

The variation between injection molding and hot embossing arises out of the state of polymers being introduced into the molds for structuring. Hot embossing uses a solid thermoplastic polymer sheet, which is pressed into with a micro-structured mold insert at the glass transition temperature. After cooling the mold opens and the molded part is ejected. A pressure and temperature relationship over the hot embossing process cycle [121] and schematic process layout is as in Fig. 10 [119].

Modifications to the embossing process, through the development of roll to plate and roll to roll hot embossing have made possible series mass manufacturing of microfluidic/ microfabricated systems. In these processes unlike regular hot embossing, the temperature of the imprinting roll is set to be higher than T_g while the holding roll/plate is held at below T_g . The stamps are fabricated on thin sheet of electroformed metals (generally Nickel) or in polymers and wrapped around rollers embedded with heaters. The roller scan speeds are very low (of the order of 0.1-2mm/sec) [122].

Low temperature embossing processes like ultrasonics assisted embossing provide high fidelity structures without the warping issues generally associated with hot embossing.

Sahli *et al.* [123] concluded from their detailed scanning mechanical microscopy analysis that the quality of structures produces via either injection molding or hot embossing is completely identical.

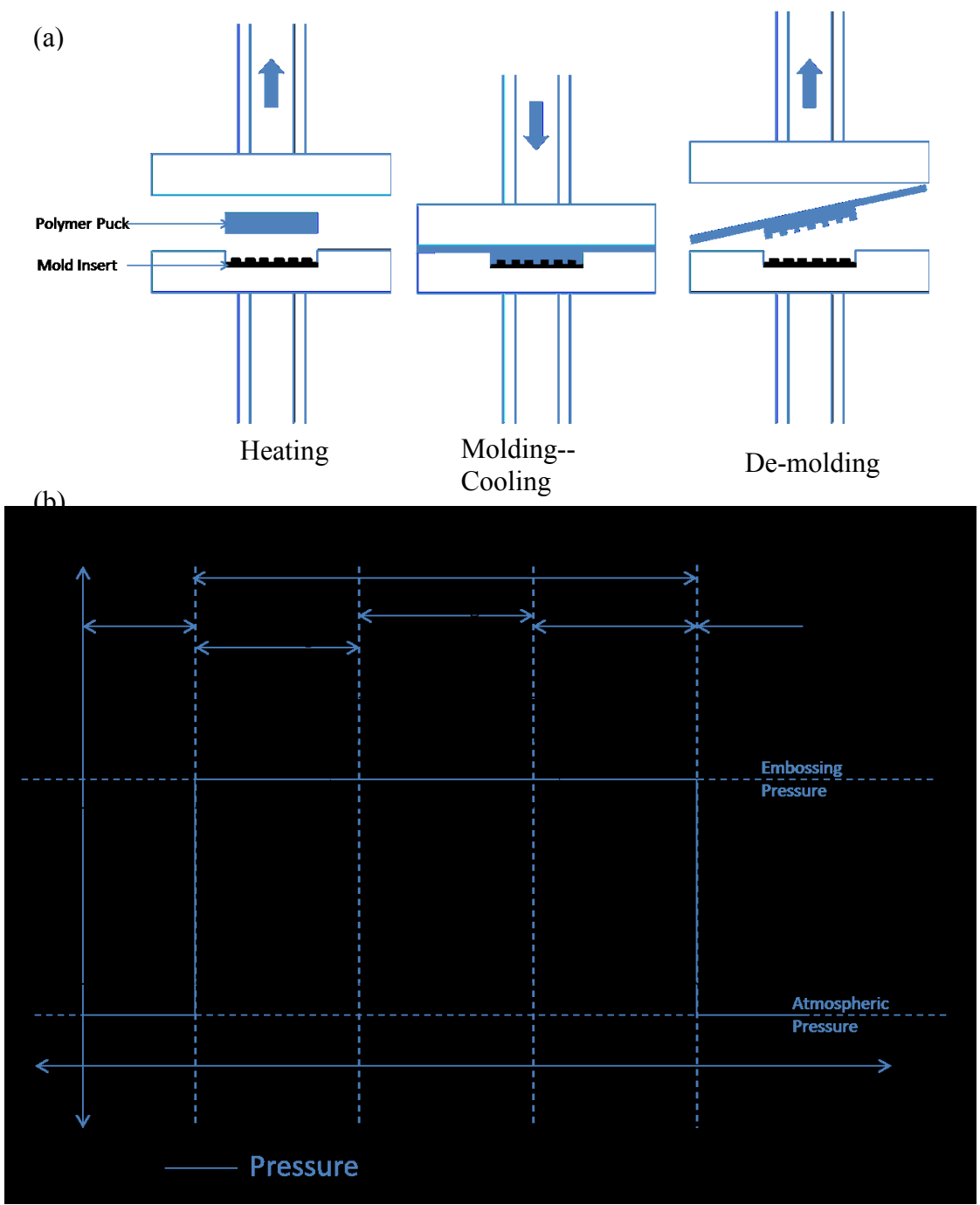


Fig. 10.(a) Schematic of Hot Embossing Process flow[Adapted from [121]] b) Pressure-Temperature Diagram for Hot Embossing. [Adapted from [119]]

2.2.7.3 Mold insert fabrication

Molds for injection molding and hot embossing can be fabricated via,

1. LIGA or DEEMO
2. Micro-Electro Discharge Machining (μ EDM)
3. Micromilling or laser ablation
4. Silicon etching or Photoresist based

Fabrication via Silicon etching, photoresists, micromilling and laser ablation have been discussed earlier. Mold inserts fabricated by micromilling or laser ablation can be fabricated at low cost but are of inferior quality. Molds fabricated via photoresists are generally for small batch fabrication.

The LIGA and DEEMO process of mold fabrication is used for very high quality molds. LIGA is a German acronym for Lithography, Electroplating and Molding, while DEEMO stands for Dry etching, Electroplating and Molding [124][45]. For the LIGA process, a thick film resist is photolithographically patterned using X-ray synchrotron radiation. The resist is developed and then electroformed generally with Nickel or Nickel alloys. This electroplated template can be used for molding [124]. In the DEEMO process, instead of using a thick film resist and the hassles of specialized X-ray lithography, a thin film resist is patterned on silicon, followed by DRIE to achieve the high aspect ratio features. The etched wafer is then subjected to electroforming with Nickel or its alloys to yield the required template for molding [45].

The proposed fabrication process, in the following chapters, gets rid of the need for these expensive mold inserts and the huge and expensive tools. Adding to this cost saving, the fabrication process requires little to no time in a very rapid manufacturing technique.

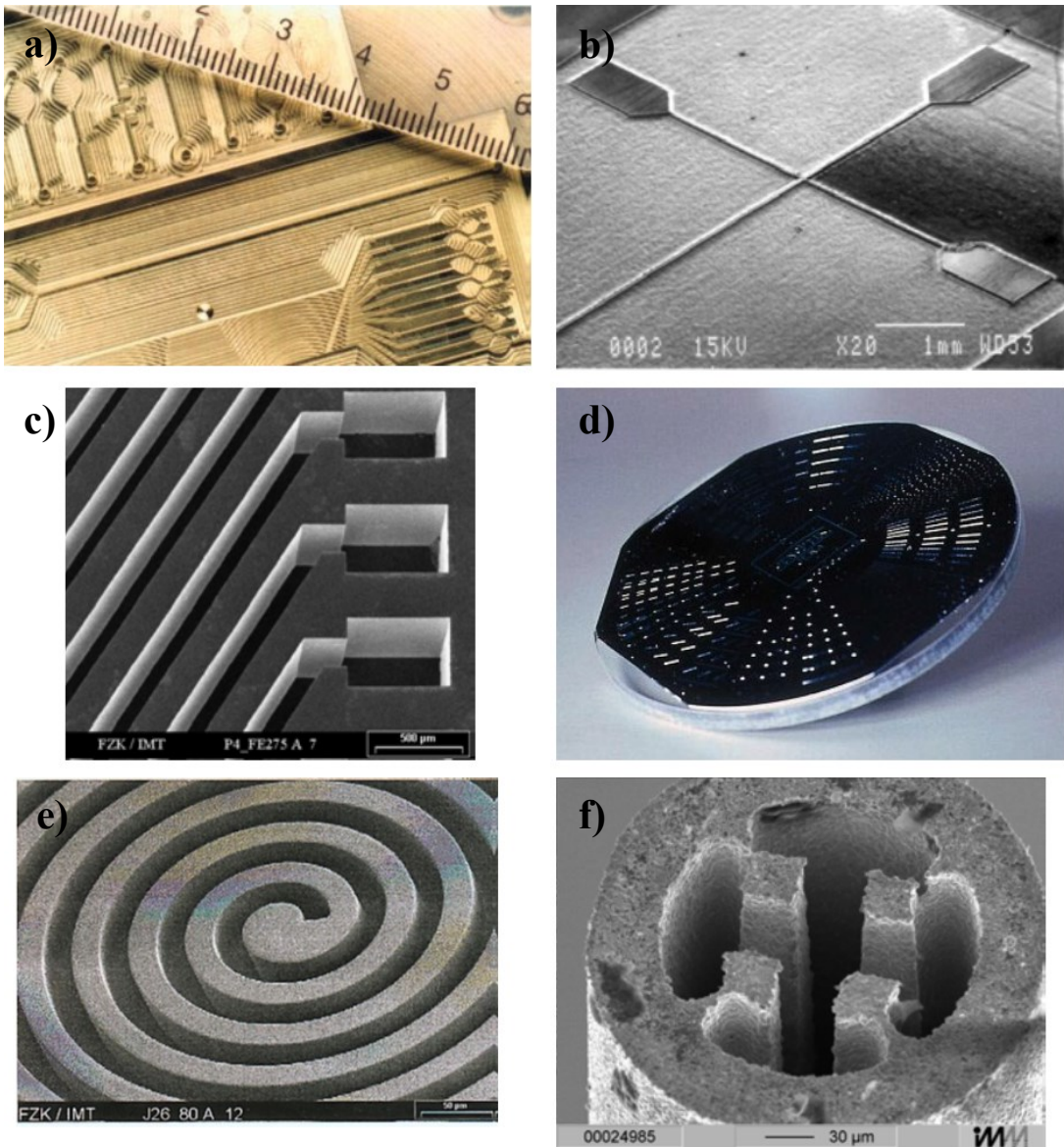


Fig. 11 Mold inserts fabricated by different processes: (a) milling with a CNC machine, (b) laser-manufactured tool with different surface roughness, (c) x-ray lithography and electroplating,(LIGA) (d) silicon etching (courtesy of Jenoptik Mikrotechnik GmbH), (e) photolithography with SU8, and (f) electric discharge machining (courtesy of Institut für Mikrotechnik Mainz) [125] [© IOP Publishing. Reproduced with permission. All rights reserved].

2.3 Bonding of Microfluidics

In order to yield a functional device, a microfabricated microfluidic chip has to be sealed either to a blank substrate or another microfluidic chip (in case of multilayered devices). This operation in a chip manufacturing process is often the most delicate, complicated and low yield process [126, 127]. The bonding operation may also include providing an interface for chip to world interconnection. It is important to first identify the scope of bonding. A bonding operation should seal a channel so that the fluid sample is in the control region for any of the fluidic driver modes, prevent external reagents from cross contaminating, support integration of sensing mechanisms and minimize dead volumes for interconnections.

Bonding of silicon and glass substrates can be equally as challenging as the fabrication process itself. Anodic bonding is the most common method used to produce hermetic seal between silicon and glass. This process involves heating both the surfaces to temperatures of 300-600°C and a high voltage is applied between the two surfaces, between 200-2kV. The surfaces must be very smooth ($R_a \sim 5\text{nm}$) for this process to work and the bonding occurs due to high electrostatic fields. In chemical terms, a thin oxide layer (Si-O-Si) formed at the interface holds the both the surfaces together. The high temperatures and extreme requirements of surface roughness make this process difficult to integrate with metal electrodes and temperature sensitive materials.

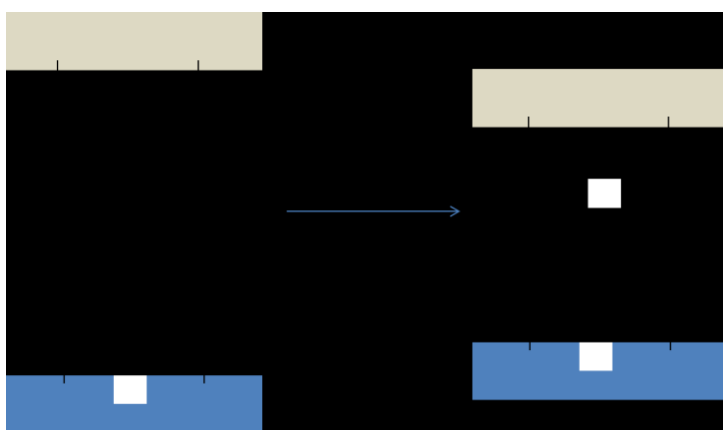
Bonding of polymers can be achieved by many ways, by exploiting either physical or chemical properties. External fixtures and adhesives may also be used can also be used depending on the desired bond strength. Bonding can primarily be classified as reversible and irreversible bonding. This classification is based on the type of failure mechanism. An adhesive failure identifies a reversible bond whereas a cohesive failure at the interface is

considered an irreversible bond. Irreversible bonding exhibits high adhesion strength and as the name implies is a process used for substrates to be permanently bonded, whereas reversible bonding are low strength bonds and is preferred for low pressure systems.

2.3.1 IRREVERSIBLE BONDING METHODS

2.3.1.1 Surface activated bonding

(a)



(b)



Fig. 12. (a) Chemistry of Plasma bonding (b) Plasma Cleaner Unit (Source: Harrick plasma)

Bonding between low surface energy surfaces can be challenging [128], thus increasing the surface energy helps to improve bonding due to higher electrostatic interactions and creation of hydrogen or covalent bonds [127]. Increasing surface energy of polymers can be performed in two ways, one approach could be to break down the bonds at the interface of the polymer to produce highly reactive sites, while the other method would involve modifying the polymers at the interface or grafting new polymers / free radicals at the interface. Both these approaches can be achieved with different methods and sources.

The widely accepted standard procedure for irreversible bonding of microfluidics made from PDMS is plasma activated bonding. This process involves creating functional groups at the surface using plasma. Various gases like Ar, Ne, He, NH₃, CO, CO₂, H₂O, N₂, NO₂ and F₂ can be used [129], but O₂ is the most prominent source for bonding of PDMS against PDMS, Glass or silicon. Activation via O₂ entails creation of a silanol group at the interface. PDMS has repeated $-\text{O-Si}(\text{CH}_3)-$ units, the surface molecules of which shed a methyl group and a silanol group (-OH). When the two activated surfaces are brought in contact, being polar compounds, the silanol groups of both the surfaces react to form an interfacial Si-O-Si, after dropping a water molecule (Fig.9(a)). Bhattacharya *et al.*, performed detailed parametric studies of PDMS-PDMS and PDMS-Glass bonding and reported a maximum bond pressures of PDMS-Glass bonding to be 74 ± 2 psi, which was tested via a burst pressure test similar to the one reported later in this thesis [130]. Bonding against other surfaces may proceed via different activations, some of which may use a mixture of gases [131-133]. Apart from specific gases, vacuum and atmospheric air have also been used as sources for plasma generation.[134-136]. Similar plasma based techniques in context with thermoplastics, have also been discussed by Tsao *et al.*[127]. Bhattacharya *et al.* [130] also tested a few sources of plasma generators, namely, Inductively Coupled Plasma Reactive Ion Etching (ICP-RIE) and Plasma Enhanced Chemical Vapor Deposition (PECVD) and concluded to also have effect on the bond quality. Based on recent articles, Harrick Plasma cleaner is one of the most common cleanroom plasma generator (Fig 9 (b)).

UV exposure dose also aids the bonding process by activating the surface, but cannot be a standalone bonding mechanism. The surface activation helps reduce the glass transition temperature of thermoplastic polymers, which as a result can be bonded at temperatures far below their actual glass transition temperatures [137]. This works by virtue

of creating oxygen free radicals in the process of converting atmospheric or source derived oxygen to ozone, which react with the low molecular weight polymers on the surface, thereby creating a high surface energy interface [138]. Ethanol in conjunction with UV exposure have been demonstrated to partially dissolve and break down the interfacing surface of PMMA, which can be brought together to form a strong bond.

Creating a new chemically active interface also helps the bonding process. This can be achieved by either grafting new polymers or subjecting the surface to form new compound via chemical reactions. Roy *et al.* demonstrated photo grafting of 2-hydroxyethyl methacrylate via UV in COC [139]. Beh *et al.* demonstrated that a treatment of PDMS interfaces in Methacryloxypropyl-trimethylsilane (MAP-TMS)+ NAIO_4 +Methanol followed by UV exposure initiates a polymerization reaction on the surface and thereby bond together[140]. Bonding PDMS to surfaces which cannot be activated via plasma or UV treatments requires activation via chemical grafting. This requires treatment of the substrate to be bonded to PDMS, with ‘mercaptosilane’ via immersion for 1-5 min, followed by subjecting both the substrate and PDMS to a corona or oxygen plasma for 2min. After this both substrates are brought incontact and held for 10 minutes to achieve an irreversible bond [141].

2.3.1.2 Thermal bonding

Bonding of thermoplastics usually takes the route of thermal bonding. Unlike for elastomers, bonding of thermoplastic arises out of molecular entanglement. Since these materials can be processed at T_g at the same time maintain the maintain the channel integrity, thermal bonding involves fusing the substrate and the device using a high pressure at this temperature. This technique is best adapted when both the device and the substrate have been heated to similar temperature and are preferably of the same material. The

bonding temperatures can be reduced to below T_g by surface activation via UV or corona discharge treatment [137, 142]. Thin film lamination is a modern thermal bonding technique and offers quick bonding times compared to traditional techniques [143].

2.3.1.3 Localized Welding

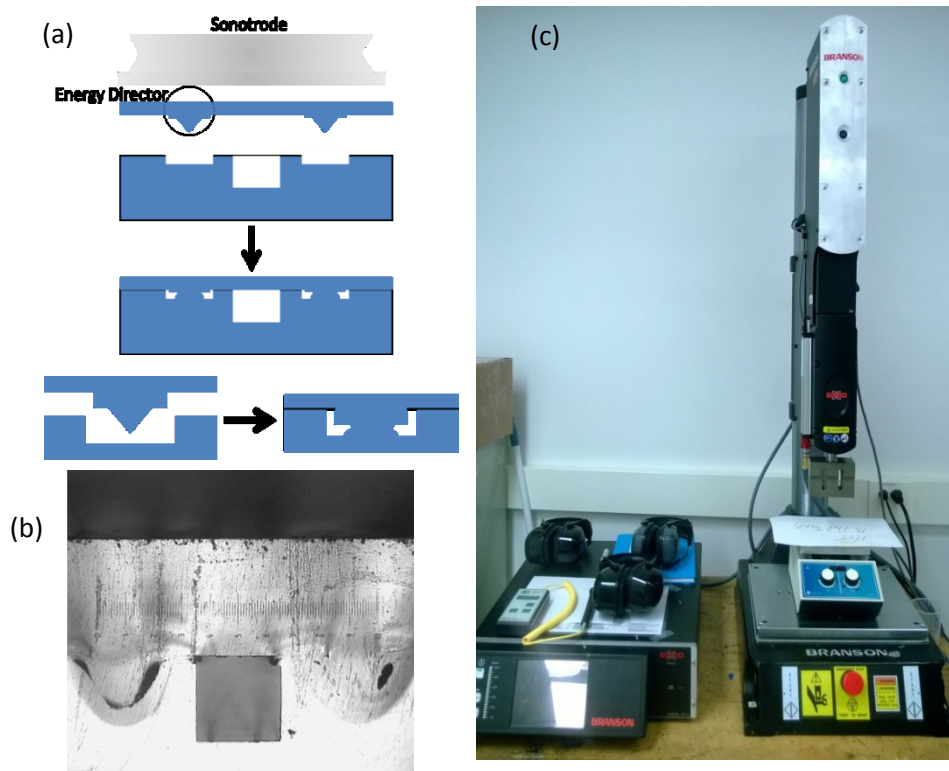


Fig. 13.(a) Ultrasonic bonding Schematic of the bonding principle. The energy director material is contained within the groove resulting in no added height. [Adapted from [144], with permission from The Royal Society of Chemistry] (b) Cross-section of a 500 μm square microchannel in PMMA sealed by ultrasonic bonding, with deformed energy concentration structures evident on either side of the channel opening [Reprinted from [145], Springer 2006] (c) Ultrasonic Bonder Unit (Branson 2000X)

Localized welding involves creating a small high temperature zone where the polymers can be bonded, without having to heat up the bulk material. The most common method under localized welding is Ultrasonic bonding. Ultrasonic bonding involves localized heating of the interfacial surface, using ultrasonic vibrations. This process requires using energy directors [144] to focus the energy of ultrasonic vibrations into a specific bonding zone. The temperatures rise up in these zones, creating a melt flow and under pressure, form a localized seal. There are various factors that govern the bonding process, the amplitude and frequency of ultrasonic vibrations, the applied pressure, preheat temperature and the time of application of the ultrasonic energy [146]. Truckenmuller *et al.* first introduced the concept of ultrasonic welding to microfluidics[147]. This required designing the energy directors to run parallel on either sides of the microchannel. The ultrasonic welders are a reasonably expensive piece of equipment (~\$10,000) but the welding times are very short (a few tens of seconds). The investment for such a tool may be a justified for a large scale manufacturing line. Thermal and solvent assisted ultrasonic bonding techniques have also been proposed, which donot require the energy directors [148, 149].

Another form of localized welding is microwave bonding. This technique involves heating the interface surface via the use of conductive heating by embedded thin metal films. The polymer itself is generally transparent to the microwave frequencies, but the embedded metal heats up to melt the interfacial surface and thereby form a localized weld. Full interface deposition of metal [150] or selective masked deposition [151] may be pursued. This process can be performed in commercial microwave unit [151], rendering it significantly cost effective over many other bonding techniques like the thermal, ultrasonic or plasma bonding, in terms of capital costs.

2.3.1.4 Solvent bonding

All thermoplastic polymers are soluble to some degree in organic solvents. The solubility of a polymer is given by Hildebrandt parameter (δ). For amorphous non-polar polymers, if the δ value of a polymer and solvent are similar or close, the molecules of both materials readily coexist, and therefore the polymer can easily dissolve [152]. For amorphous polar polymers, Hansen's theory is used, which accounts for other forces in the bond, the permanent dipole-permanent dipole forces and the hydrogen forces, apart from the London dispersion forces as with the standard Hildebrandt parameter [153]. Though these approaches are effective, there is still no understanding of explicit interactions between the two molecules [154]. Solvent bonding of thermoplastics involves selecting an appropriate solvent to dissolve a very small volume of the interfacial surface so that the polymer chains get intertwined, once the solvent evaporates. This process creates exceptionally strong bonds but requires significant care to prevent any damage to the channels. Umbrecht *et al.* demonstrated a peak bond strength of 7.8 ± 1.0 MPa with a $9.2 \pm 2.3\%$ deformation, measured via an tensile pull-off test on Instron, in PMMA substrates bonded by Ethylene glycol dimethacrylate solvent [155]. Kelly *et al.* realized the maximum bond strength to be 15.2 MPa by applying internal pressure, in PMMA substrates bonded via acetonitrile [156]. The interfacial surface also tends to show significant crazing around stressed microfluidic channels, due to sudden release of these manufacturing induced stresses. Annealing of substrates for a long period and solvent vapor based bonding techniques for bonding of PMMA and COC [157] have shown to minimize crazing.

2.3.1.5 Adhesive bonding

Adhesive bonding introduces a new material between two structural materials specifically for adhesion enhancing properties. Adhesives like pressure sensitive adhesives and UV curing adhesives have been frequently used for both sealing of microfluidic chips and also to provide world to chip interconnections. Norland Optical Adhesives (NOA), a

brand of UV curing adhesives, are a popular choice due to their optical properties like low fluorescence and high transmission in UV and/or visible light range, and wide range of mechanical properties after curing [158]. Using liquid based adhesives risks the channels or other systems getting clogged during application, and this possible loss of micro-sized features is the biggest challenge when working with curable adhesives. Modified forms of applying adhesives, similar to the inking of stamps [159], have been used to minimize the feature loss, but are successful under specific applications with moderately wider channels. Arayanarakool *et al.* demonstrated the application of UV curable adhesive using rollers to demonstrate bonding of microchannels as wide as 20 μ m without any contamination [160]. Adhesive bonding in context with microfluidics doesn't necessarily limit to using an adhesive solution. Using semi-cured polymer substrates of the similar polymer as that of the patterned substrate eliminates a lot challenges associated with liquid adhesives, except that it is limited to curable polymers and is not compatible with heterogeneous material bonding. Tuomikoski *et al.* demonstrated this concept with SU-8[161], while functional PDMS based devices bonded via the partial cure method have been demonstrated by Eddings *et al.* [162] and Sang Go *et al.* [163]. Sang Go *et al.* also characterized an optimum 'cure ratio' for the maximum bond strength. Thermoset Polyester, Polyurethane methacrylate and NOA have been stated to adopt a similar semi-cured polymer based bonding process [164]. Complementary polymer grafting / coating aided bonding has sometimes also been referred to as adhesive bonding [165].

2.3.2 REVERSIBLE BONDING

Reversible bonding allows for easy assembly and disassembly of microfluidic devices, thereby allowing high throughput and reusability. Being low bond strength systems, small dislodging forces could potentially affect the performance of the chip.

Though not desirable for a commercial system, it is the most preferred choice of bonding in research environment as it allows for repeatable bonding trails for proper alignment and temporary sealing. Apart from being used for bonding of prototypes it is also used for patterning of micro electrodes, cells and other bio-molecules.

2.3.2.1 Bonding by self-adhesive property

Elastomeric materials like PDMS can be bonded to various other substrates like silicon, glass or itself by creating a simple conformal contact with the required substrate. This bonding is facilitated by van der Waals forces and can support up to 5psi of fluid pressure [130]. Electrostatic charge based bonding has been demonstrated for bonding of Rigiflex PEG-DA mold with gold or silicon substrates to create nano capillaries. The electrostatic charge was generated by mechanical friction due to peeling of the PEG-DA film from a silicon master.[166].

Adhesive property based bonding can be leaky even with flow rates as low as 1 $\mu\text{l}/\text{min}$ [167] .To support any pressures and to ensure leak proofing, external gripping sources like patch clamp have been suggested[167].

2.3.2.2 Sealing by active sources

Bonding by aspiration method involves using a negative pressure source to induce an effect similar to a suction cup. The device is fabricated in a way so as to ensure the microchannel is unaffected by the vacuum, while the net suction cup effect and the material stiffness help hold the microchannel against the bonded surface [168]. Releasing the vacuum allows easy removal of the device. This concept can be implemented with rigid plastics only for extremely clean and smooth surfaces, but has a much better performance with elastomeric materials. Though not a widely used method, it has been used for

performing assays over pre-cultured cells such as neural progenitor cells. The interesting aspect of this integration is that the cells were cultured in a petri dish and the microfluidic device was assembled on the petri dish later for the post culture assay [169].

Magnet assisted bonding has been pursued in different ways. Tkachenko *et al.* used magnets [170] to reinforce PDMS chips bonded to glass by self-adhesive property. Rafat *et al.* reported magnet assisted bonding via magnetic slabs attracting iron particles embedded in PDMS [171].

2.3.2.3 Reversible bonding with adhesives

Double side adhesive tapes are a good candidate for aiding the bonding process. This process does not require any external bonding equipment or any solvent or liquid adhesives. Thompson *et al.* demonstrated this reversible bonding technique with three variants of Scotch® tape [34]. This concept has been rated for non-specialized users, since the adhesive part from the tape is interacting with the liquid sample in the channel, which could lead to contamination. Considering the application, the choice of tapes is limited, with the tapes used in literature [34, 172], being in Polyester (structural) with Silicone adhesive.

2.4 World to chip interfaces

World to Chip interfaces provide for macro to micro conversion fixtures at the inlet and outlet of the microfluidic chips. These interface is probably the least reliable component of a LOC device, and is often neglected by the microfluidics community [173]. One reason for the complications in these components, especially from a commercial stand point is the lack of standardization associated with interfacing components [120]. Some of the functional characteristics desired for the world to chip interfaces are,

- Minimal dead volume
- Reuseable
- Inert material
- Easy interfacing
- Leak free

While sealing of microfluidics and providing interconnections are two independent functions, most of the sealing concepts in polymers can be extended for world to chip interfaces. Using modified syringe needles or pins (New England) or metal tubes etc. directly plugged into elastomeric materials [174] (Fig. 14 (a)), or sealed with epoxies (Fig. 14 (b)) or curing polymers has been the norm. Providing for interconnects on silicon is complicated and requires extensive fabrication. There are modern low cost innovative solutions being proposed frequently. One such method involves using a double sided adhesive tape Fig. 16 [175].

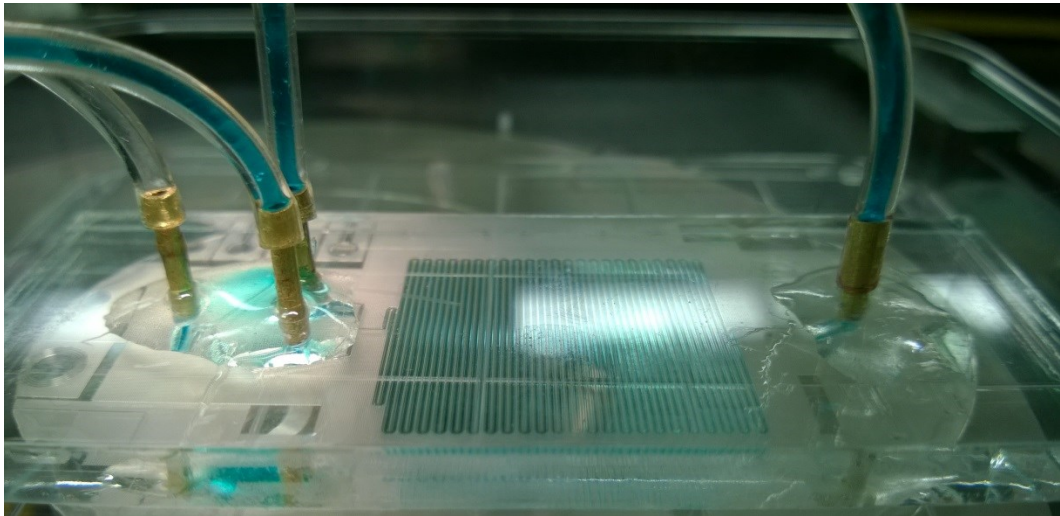
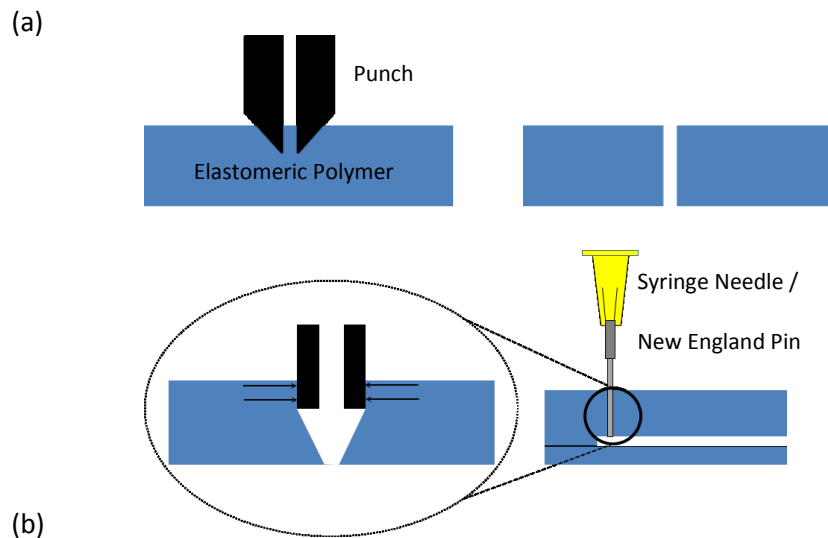
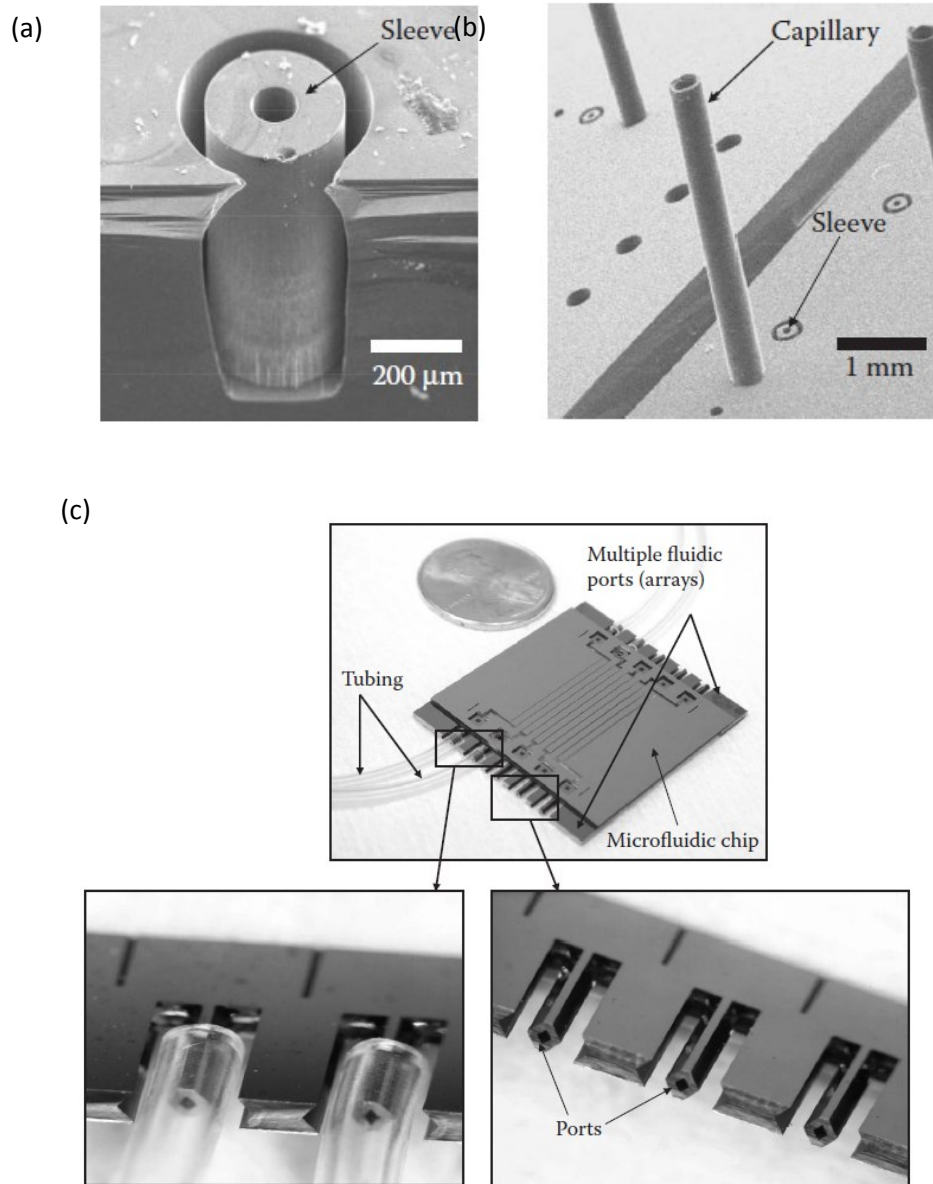


Fig. 14. (a) Schematic of the punching process and the interconnect fabrication method (Adapted from [174]) (b) Metal interconnects embedded in PMMA holder chip and sealed by a two part epoxy.



X

Fig. 15. (a,b) “sleeve”-type coupler that fits the inner and outer diameter of the capillary tubing and prevents adhesive seeping into the microchannel.[Reprinted from [176], with permission from Elsevier] (c) Interconnect modules in silicon , for interfacing on a silicon microfluidic chip [Reprinted with permission [177], Copyright © 2002, Kluwer Academic Publishers]

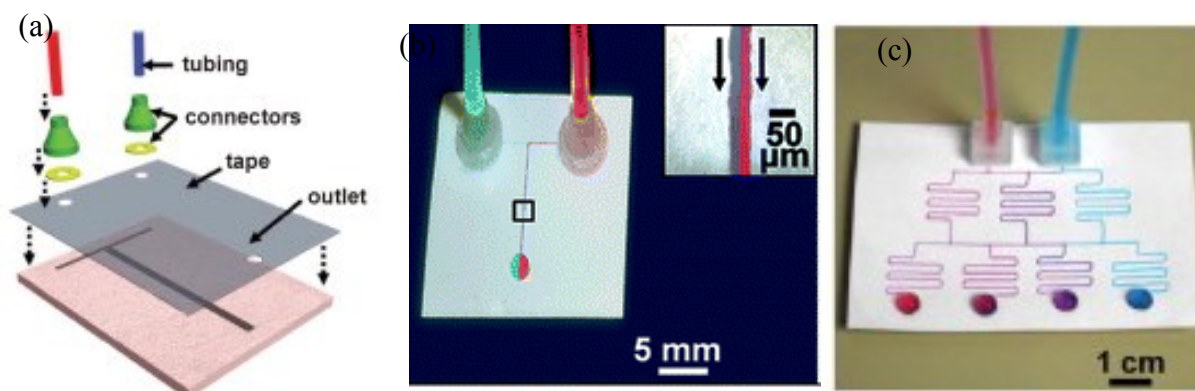


Fig. 16. Double side adhesive tape bonded world to chip inter connects for paper based microfluidics.(a) Schematic arrangement for the WTC interconnects (b) sample unit T-channel for and (c) serial dilution device. [Reproduced from [175] with permission from The Royal Society of Chemistry]

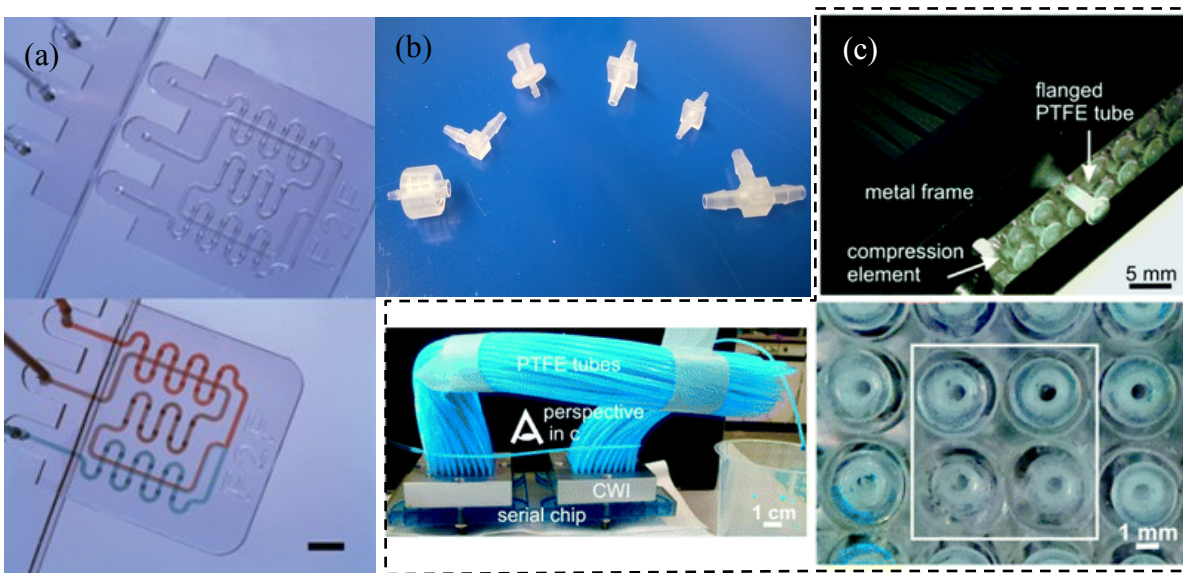


Fig. 17. (a) Microfluidic Fit to Flow adapter[Reprinted from [178] with permission from The Royal Society of Chemistry] (b)press and screw fit connectors (c) Force fit interconnects in PTFE (the force is applied with a holder by means of tightening screws) [Reprinted from [179] with permission from The Royal Society of Chemistry]

Modular interfacing units like luer locks, and adhesive, press and screw fit connectors, are available in standard sizes, which is the first of the standardization

initiatives in the field of microfluidics. Few other modular systems like fit to flow interconnect [178] and flanged multichannel world to chip interface [179] have been developed for mass integration.

Atencia *et al.* proposed magnetic connectors for world to chip interface. The concept relies on holding a magnetic needle holder against the inlet/ outlet port with a backing magnet on the back side of the chip. Different sealing interfaces have been tested and a maximum rupture pressure has been reported with polyimide tape [180].

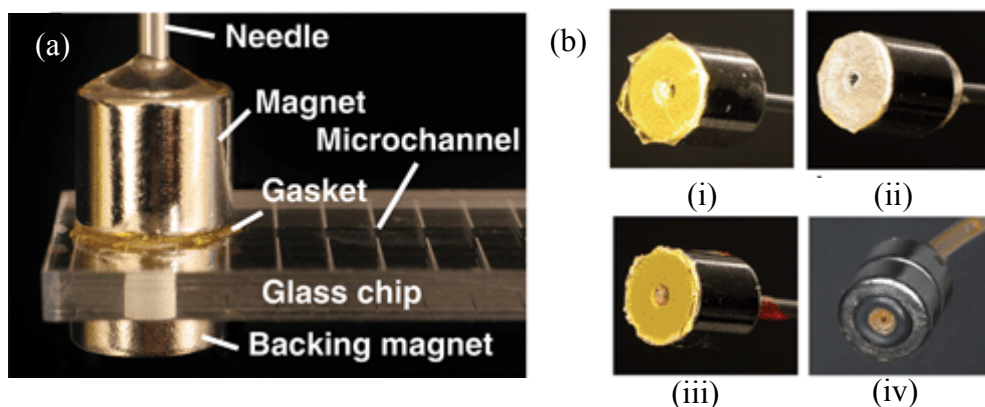


Fig. 18. (a) Magnet based world to chip interconnects (b) Interface gasketing provided by (i) Polyimide tape (ii) Polyester tape (iii) PDMS and (iv) rubber O-ring [Reprinted from [180] with permission from The Royal Society of Chemistry]

Extending an adhesive based bonding and interfacing concept but integrating it with van der Waals forces assisted bonding technique, we propose a novel bonding technique involving gecko inspired dry adhesives. This concept has never been attempted before and we are the first group to extend the application of dry adhesives to the field of microfluidics. Details of the integration will be discussed in the subsequent chapters.

Before delving into the integration aspect, it is important to understand the concept of adhesion in context to gecko inspired dry adhesives.

2.5 Gecko Inspired Adhesives

Gecko adhesion is perhaps one of the most extensively studied phenomenon in the field of biomimetics. Tockay Geckos (*Gekko gekko* body weight $\approx 43.4 \pm 1.48$ gm[181] and can support ~ 47 times their body weight (Clinging ability $\sim 20.04 \pm 1.33$ N per pad[181]) in shear loading and detach at will. This adhesion is facilitated by van der Waals intermolecular forces [37].

Van der Waals forces are weak intermolecular forces between two electrically neutral molecules and thus arise out of dipole interactions. The types of dipoles can be classified into three types, permanent dipole, instantaneous dipole and induced dipole. Permanent dipoles are evident in neutral molecules with the significant difference in the electronegativities of the constituent atoms. In molecules with atoms of similar electronegativity, instantaneous dipoles are observed. These dipoles keep oscillating the polarities on their constituent atoms. When instantaneous dipoles is in proximity to a permanent dipole, the oscillation of polarity in the instantaneous dipole is lost and gets regulated by the permanent dipole. This is called an induced dipole.

The van der Waals forces comprises are of three types of forces, London dispersion forces, the Debye forces and Keesom forces[182]. The forces between an instantaneous dipole and an induced dipole are called the London dispersion forces, between two permanent dipoles are the Keesom Forces, and between a permanent and induced dipole are the Debye forces. They have a long range electromagnetic character which is proportional to r^{-6} , where r is the distance between the molecules; $r \geq$ molecular diameter.

Between two parallel surfaces the van der Waals force is given by

$$f_{vdW} = \frac{A}{6\pi D^3} \quad \dots\dots \text{Eq. 7}$$

where A is the Hamaker constant and is intrinsic to the material (in dry air $\sim 10^{-19}$ J[183]), whereas D is the distance between the surfaces (~ 0.2 nm for solids in contact[183]).

Several attempts have been made to replicate gecko adhesion, mostly in soft elastomeric materials. Hence an insight into the physics of soft material adhesion is necessary.

While van der Waals forces still remain relevant for synthetic gecko inspired adhesives, other adhesion mechanisms observed in polymers are based on diffusion, mechanical, molecular, chemical and thermodynamic interaction phenomenon. These mechanisms have been reviewed comprehensively by Awaja *et al* in bulk polymers[184].

The energy required to overcome the adhesive forces between two bodies in contact is called the free surface energy. Liquids in contact with another liquid or solid achieve equilibrium at the lowest surface energy state, as in the case of rain drops, whereas for solids in contact, the equilibrium is attained by the distribution of elastic forces in the contacting bodies. However in case of light loading in elastic solid bodies, surface forces can be significant. This correlation was both theoretically and experimentally proved by Johnson *et al*, [185] also famously referred to as the JKR theory (Johnson, Kendall and Roberts). According to JKR Theory, the pull off force between two elastic spheres of radii, R_1 and R_2 is given by,

$$P = \frac{3}{2}\pi\gamma R \quad \dots\dots\text{Eq. 8}$$

Where, γ is the work of adhesion,

$$\gamma = \gamma_1 + \gamma_2 - \gamma_{12} \quad \dots\dots\text{Eq. 9}$$

$\gamma_1, \gamma_2 =$ surface energies of the materials in air/vaccum

$\gamma_{12} =$ interface energy when the two surfaces are in contact

and R is the effective radius, given by

$$R = R_1 R_2 / (R_1 + R_2) \quad \dots\dots \text{Eq. 10}$$

This equation can be adjusted for one flat surface by equating its radius to be infinitely large.

This equation concludes that the pull off force is not related to the effective contact area, but to the contact perimeter. Hence, a splitting of the contact surface can effectively increase the net pull off force. This was experimentally demonstrated by flat punch contacts by Varenberg *et al.* [186]. It should also be understood that the work against adhesion energy is not available to drive the next detachment, thereby requiring more net pull off force than a monolith surface [187]. Other advantages include rough surface adaptability and defect tolerance.

When the contact is split into N fibers of radius, $R_n = R/\sqrt{N}$, considering self similar scaling, then

$$P_T = \frac{3}{2} \gamma \pi R \sqrt{N} \quad \dots\dots \text{Eq. 11}$$

While in case of radius invariance scaling model,

$$P_T = \frac{3}{2} \gamma \pi R N \quad \dots\dots \text{Eq. 12}$$

Kendall [188] calculated the pull off force between a rigid disc, of radius a , and an semi-infinite half space of elastic material of modulus E to be,

$$P = \sqrt{8\pi E^* a^3 \gamma} \quad \dots\dots \text{Eq. 13}$$

Where,

$$E^* = \frac{E}{(1-\nu^2)} \quad \dots\dots \text{Eq. 14}$$

ν being the poissons ratio , E being the Young's modulus of the elastic half space.

Spolenak *et al.* [189] calculated the pull of force for fibers of different contact shape elements in various animals. This work considered a vertical cylinder of radius a and

modulus E_1 , and a semi infinite half space of modulus E_2 and reworked the effective modulus to be,

$$\frac{1}{E^*} = \frac{1-\nu_1^2}{E_1} + \frac{1-\nu_2^2}{E_2} \quad \dots\dots\text{Eq. 15}$$

Incase of contact splitting for this flat punch vertical fiber, $N = (a/r)^2$. Applying scaling laws, the force would scale proportional to $N^{0.25}$. Hence the effective pull off force, P_T is given by

$$P_T = PN^{0.25} \quad \dots\dots\text{Eq. 16}$$

This increase has also been validated by the work of Greiner *et al.*[190]. This work also experimentally studies in detail the effect of aspect ratios of the pillars (λ) and the radii (r). The pull off force was demonstrated to scale as a function of $r^{-0.4}$, is scaled as $\lambda^{0.3}$. In order to accommodate the separation of each feature for practical purposes, an areal density ' ρ ' may also be included, which is always directly proportional, and $N = \rho(R/R_n)^2 = \rho(a/r)^2$.

Varenberg *et al.*[191] revisited the hypothesis of area-independent/perimeter dependent model and concluded that the area does have an effect and the adhesion would be equal between a two structured and non-structured surfaces as long as the contact area is same, but added that the presence of thin film based terminal elements are critical in the development of a successful adhesive. Griener *et al.*'s [190] work also proposes accounting for the apparent area of contact in order to have a better comparison. Also recently, the contact splitting theory has been reported to be a non-accurate model [192], though the experimental studies support the claim of increase in pull of force with increasing splitting. While theoretically increasing the aspect ratio and decreasing the radius may be advantageous, there are physical limitations from a manufacturing perspective. Also, based on some experimental work carried out in our research group [193], for a similar effective contact area (~50% fill factor) the variation in peak adhesion strengths of Sub-100 μm

mushroom shaped fibers was very small. Although attempts have been made to fabricate nanostructured [194] surfaces for adhesion, but condensation effects caused by clustering of the fibers have been observed, which led to reduced adhesion [190]. This has also been referred to as the matting condition or lateral collapse.

Also most of the theories studying adhesion consider the material as a linear elastic material, while most of the polymer samples often demonstrate hyperelastic behavior.

In the process of studying the adhesion in some of the beetle species, Carbonne *et al.*'s work also lends credence to the observation that thin film contact elements would improve the adhesion. This study compares the different failure modes between a flat punch and a mushroom shaped contact element. Comparing the pull of strengths, the peak strength required for a mushroom shaped contact element under a central debonding mechanism, which is the typical mode of failure, was identified to be [192],

$$\sigma = \left[\frac{\pi^3 \Delta\gamma^3 E^{*2}}{12 \Delta U_B} \right]^{1/4} \dots\dots \text{Eq. 17}$$

Where, ΔU_B is the stress dependent energy barrier $\sim 1\text{eV}$, at room temperature ($T=300\text{ K}$).

The effect of surface roughness is critical for adhesion in Geckos. While the contact forces typically decrease with sliding between two rigid bodies, Geckos rely on shear displacements to initiate adhesion. A small vertical preload combined with a short drag against the contact surface engages the Gecko spatulae [195]. Considering this mechanism, Gecko adhesion also includes a component of 'frictional adhesion' via microscopic interference, cold welding or other bonding mechanisms. This adhesion is proportional to the shear force [196]. Peng *et al.* also identified that the adhesion of a thin nanofilm over a sinusoidal roughness varies with the amplitude and wavelength of the roughness. The normal adhesion decreases with increasing surface roughness for film lengths larger than

the wavelength, while it decreases initially and then increases for the shorter films [197]. This work also identifies that Geckos have optimized their spatula thickness in a way so as to maximize the adhesion force. In case of mushroom shaped contact geometries, the adhesion strength has also been found to increase with decreasing roughness. At the same time, depending on the size of the adhesive fibers, the adhesion was observed to be very low with surface asperities that very fine and very large compared to the adhesive fibers [198]. Hence, microstructured surfaces provide flaw insensitivity as an added benefit apart from improved adhesion compared to plane unstructured surfaces.

Synthetic versions of gecko inspired adhesives have been manufactured in a wide variety of polymers with variable results depending on the presence of any thin film element or without. Thermoset elastomers like PDMS [199], Polyurethane (PU), Polyurethane acrylate (PUA) and Polyvinylsiloxane have been the most preferred choice of materials. Of late thermoplastic elastomers have also been used for the same [200]. Various geometries of microscopic/nanoscale microfibrils, fabricated by different methods at different orientations have been studied. Since there is no standard measurement technique, the results that have been reported cannot be directly compared against each other. Few versions have also demonstrated under water adhesion [201] and adhesion in vacuum [199]. Sameoto *et al.* have reviewed many of these synthetic dry adhesives [202]. Most of the synthetic adhesives have been fabricated to perform under shearing forces, which also tends to provide the anisotropic adhesion due to orientation of the fibres. Some of the fibre geometries are shown as in Fig. 19. Del Campo *et al.* conducted a study of effect of length scale and tip geometry on adhesion performance and concluded that the tip geometry plays the most significant role. Pillars with mushroom shaped tips had the greatest pull off force compared to other geometries like flat tipped, round tipped and spatula tipped fibers [203].

These synthetic adhesives have been used as the locomotion mechanism for vertical climbing robots and for space applications [204]. Our group has extended this research for MEMS pick and place [193]. The anisotropic adhesion helps in reliable picking and easy release [205]. Gecko adhesives used in tandem with mussel adhesive protein have been demonstrated to improve performance, especially under water [206]. M.K Kwah *et al.* [207] and Mahdavi [208] have reported the development of gecko inspired tissue adhesives.

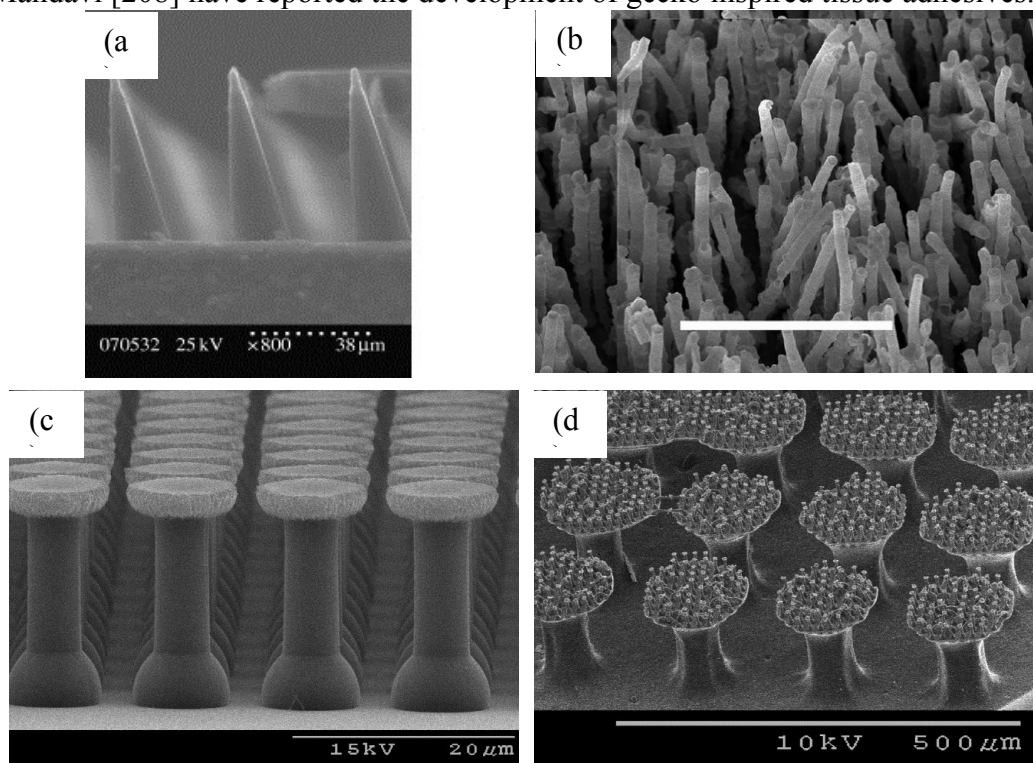
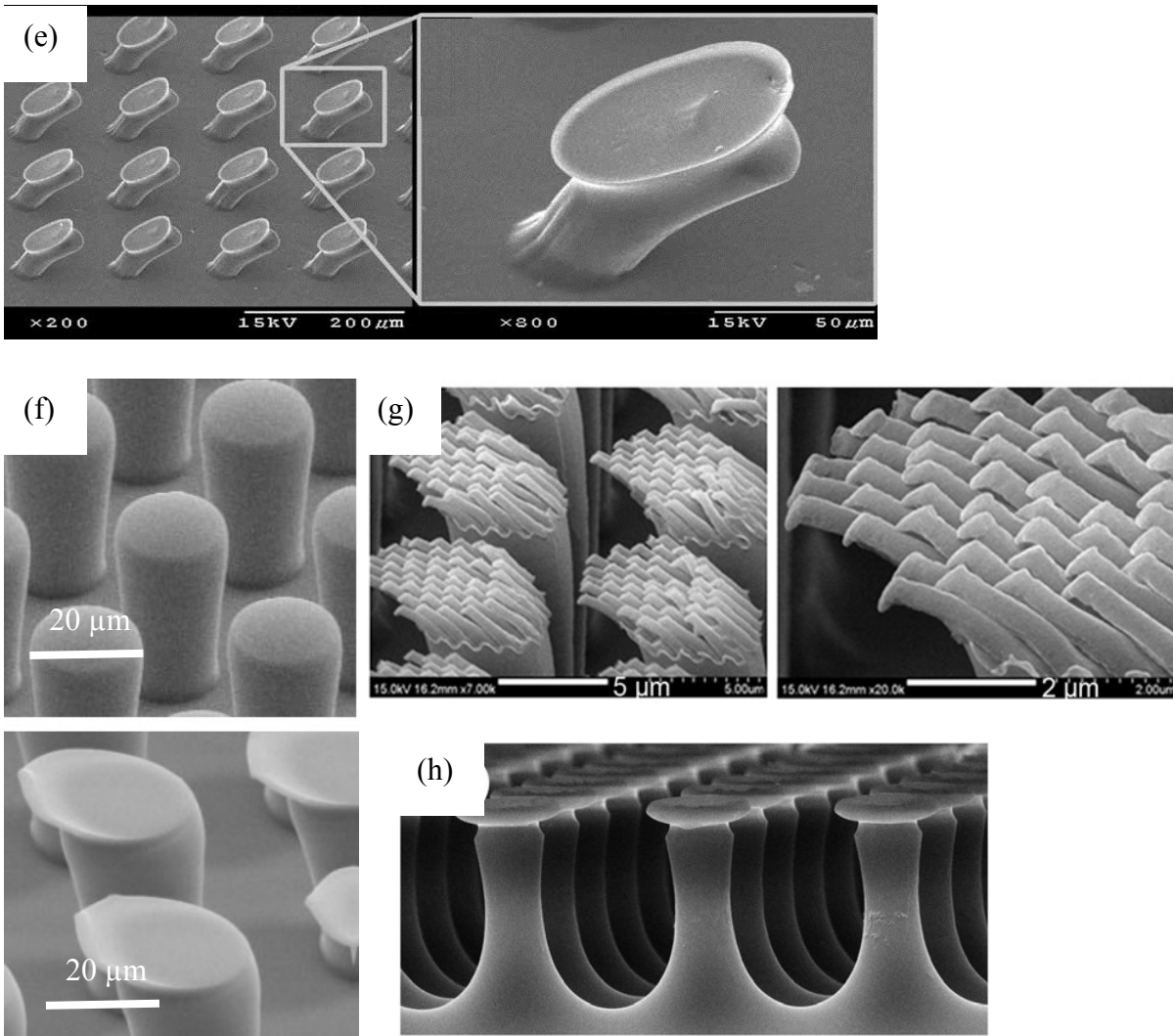


Fig. 19. Synthetic gecko inspired adhesives: (a) Wedge shaped adhesive fibers in PDMS manufactured by dual layer SU-8 lithography in on quartz wafer [209] (b) vertical fibres in polypropylene manufactured over polycarbonate filter by pressure filling in vacuum at 200 °C, scale bar equals 10 microns [Reprinted with permission from [210], Copyright 2006 by the American Physical Society] (c) polyurethane mushroom shaped fibers [Reprinted with permission from [211] Copyright 2009 American Chemical Society] (d) hierarchical mushroom shaped adhesives in polyurethane with each layer hierarchical layer formed in separate steps and assembling by joining interfaces with liquid polyurethane and curing. [Reprinted with permission from [212] Copyright 2009 American Chemical Society].



(e) Angled mushroom shaped polyurethane fibers fabricated by dipping angled fibers in liquid polyurethane and curing against a flat surface under an applied pressure [[213], [Reprinted by permission of John Wiley & Sons, Inc.]] f) Sylgard-184 fibers, fabricated by thin film inking of Sylgard 184 followed by downward curing and tilted printing and curing respectively and [214] [Reprinted by permission of John Wiley & Sons, Inc.] g) angled high aspect ratio nanofibers fabricated in polyurethane acrylate by replica molding from a directional etched polysilicon substrate [215]. h) Polyurethane fibers fabricated from commercial PMMA master molds in a single molding process Reproduced with permission [202], © IOP Publishing].

CHAPTER 3: STUDY OF MANUFACTURING FEASIBILITY WITH SEBS

3.1 Introduction

In order to make synthetic gecko inspired adhesive integrated microfluidic devices, this chapter studies a novel low cost material, which has been demonstrated to be acceptable for microfluidics, from a manufacturing perspective. The gecko inspired adhesives present an aggressive geometry that is challenging compared to a conventional microfluidic fabrication technique. Hence a replication fidelity study involving Scanning Electron microscopy and Optical profilometer based deductions is presented here.

Thermoplastic elastomers provide an alternative to both elastomers and thermoplastics in a way that assimilates the best of both the materials, The material of choice from the TPE family that has been studied extensively is styrene-ethylene-butylene-styrene.

Styrenic block copolymers have a typical structure of Styrene-other polymer-Styrene complex. In the case of SEBS, the intermediate polymer is polybutadiene, polyisoprene, making a SEBS a linear triblock copolymer. It may be manufactured by the hydrogenation of Styrene-butadiene-styrene [216]. The glassy styrene is distributed in a continuous elastomeric matrix of Ethylene-Butylene. These organized sections of styrene act as physical, rather than chemical crosslinks, and are free to move, break and re-organise at elevated temperatures which provides the elastomer its thermoplastic properties. SEBS has two glass transition temperatures associated with the ethylene-butylene and polystyrene domains at $\sim -55^{\circ}\text{C}$ and $\sim 95^{\circ}\text{C}$ respectively.

Sections of this chapter have been published in: [217] and are reproduced with permission

Between these glass transition temperatures, the styrenic domains remain glassy and provide for the physical crosslinks, thereby preventing the flow of the rubbery domains. The melting temperature of polystyrene is ~ 165 °C. The physical morphology of the SEBS is spherical, for the solid phase ratios < 0.20 [216].

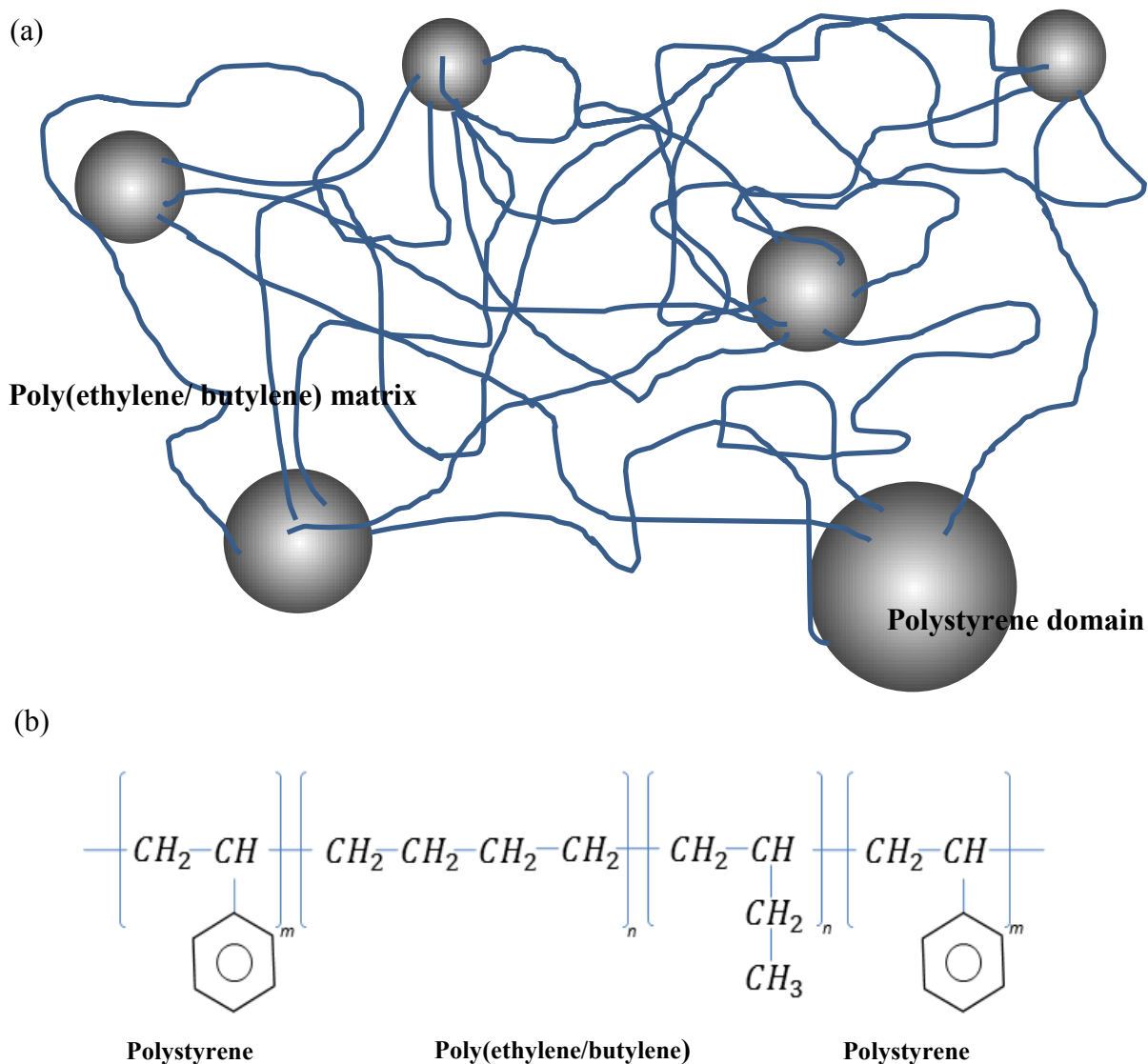


Fig. 20. (a) Physical structure of SEBS (adapted from [218]) (b) Chemical formula of SEBS

SEBS is commercially available in different proportions of polystyrene, and poly(ethylene/butylene). There also are variants with polypropylene, sometimes classified under a special category, SEPS (styrene-ethylene-propylene-styrene)[219, 220]. Apart from the basic variations, these polymers may also contain various plasticisers, solvents and oils. Hence not all commercially available SEBS variants could be of use for microfluidics. Also different companies brand it under different names making it difficult to identify except via material data sheets. Kraton Performance Polymers has a G series lineup mostly of SEBS and have been graded for medical application. GLS has a small line of clear/transparent SEBS in the Versaflex CL series. Polimeri Europa has a SOL TH series of modifier free SEBS. Dynasol's CH series and AlphaGary's Evoprene G series polymers are UV and Ozone resistant and FDA approved for food storage. Hexpol TPE has different TPEs including SEBS (Dryflex T series) with customizable TPEs available for specific uses including medical device grade and chemical resistant formulations.

A few studies have been performed to test the viability of SEBS for microfluidics. Borysiak *et al.*, [86] studied two different grades of SEBS, SEBS 42(42 wt % PS) and SEBS 12(12 wt % PS), and compared it with PDMS and Polystyrene. SEBS 42 devices demonstrated wettability, stable surfaces (for both contact angle and electro-osmotic charge) thermal stability, low autofluorescence and high transmissivity. The material was also tested for cell attachment and proliferation. It was also concluded to be superior to PDMS in terms of molecular adsorption (Fig. 22). Features as small as 2 μ m (dia) and aspect ratios as high as 4:1, were demonstrated to be feasible. The polymer was dissolved in toluene and fabricated via soft lithography techniques. The silicon surfaces needed to be silane treated for efficient and reliable demolding. The authors also tested reversible, plasma treated and thermal bonding, and found the maximum pressure to be 20-30psi, 30-35psi

and 60psi respectively. Cell culture studies found SEBS (SEBS42 and SEBS12) to promote cell adhesion and proliferation, which was comparable or slightly exceeded the growth on PDMS (adsorbed with Fibronectin). Sudarsan *et al.* performed EcoRI restriction enzyme digestion to prove biocompatibility with SEBS CP-9000 in molecular biology grade mineral oil. A solvent compatibility study has also been performed and concluded to be compatible with most solvents, and with minimal swelling, except for toluene and chloroform [84]. Geissler demonstrated localized DNA array formations on Versaflex CL30 [87]. These studies can be interpreted to imply that SEBS should be appropriate for many basic microfluidic applications. Borysiak *et al.* confirmed the feasibility of performing advanced microfluidic analysis using dielectrophoresis and isotachopheresis, which involved studying the polymers electric and surface charge properties, which were concluded to be highly stable and conducive. Since there are different types of assays and cell cultures [221] a universal acceptance of SEBS for microfluidics can only be made after further studies.

Melt processing has been the preferred choice of processing thermoplastics and thermoplastic elastomers. While the high dimension control , short cycle time and high productivity make it more lucrative , the capital cost involved in fabrication via injection molding is exorbitantly high The typical cost of injection molding machines ranges around 50,000USD, for low end versions while the high end variants could cost upwards of 100,000 USD . Based on economy of scale function defined as[222],

$$C_{dev}(n) = C_{mat} + \frac{C_{NRE}}{n} + C_o e^{-\left(\frac{\log n}{N}\right)} \quad \dots\dots Eq. 18$$

C_{dev} : Cost per device for a volume production of n parts; C_{mat} : Cost of raw materials;
 C_{NRE} : Non recurring cost (Capital cost, production automation etc); C_o :Initial process cost for the first device (towards process optimisation)

the cost per chip scales as a function of number of parts being manufactured, which will further scale down depending on the number of components and the processing steps. This high initial capital investment could be justified only after an initial success of the product.

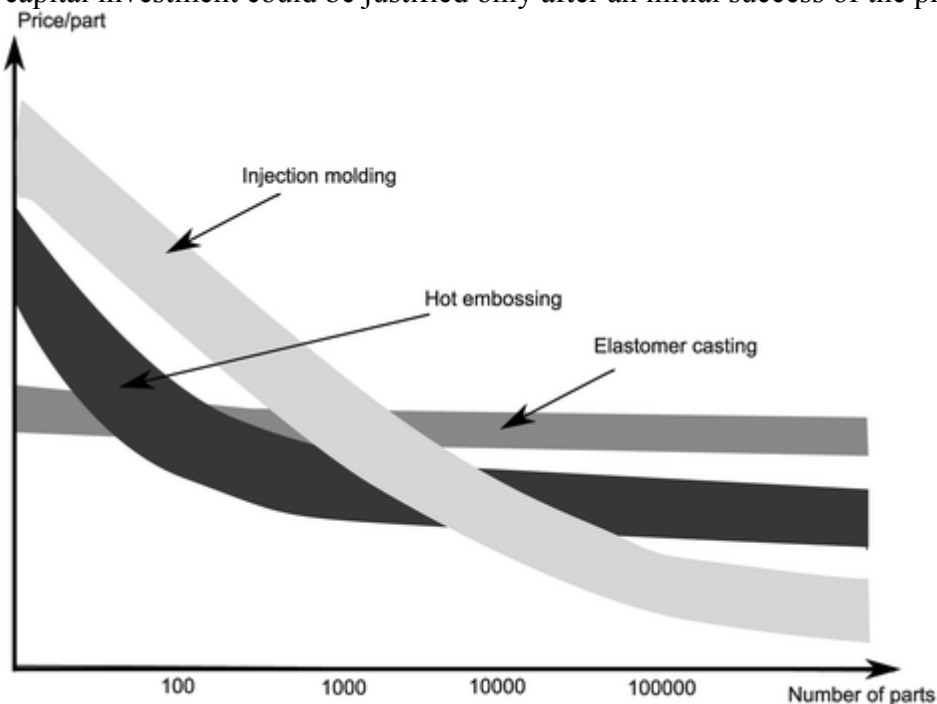


Fig. 21. Economics of scale based on manufacturing process. [Reprinted from [222] with permission from The Royal Society of Chemistry]

As evident from, Fig. 21, melt fabrication, via injection molding is the better choice of fabrication in a large scale compatible process for thermoplastics, but as the modulus of the thermoplastics scales down with thermoplastic elastomers, the initial capital investment can be minimised by using low cost molds and other modified molding machines and the break even volume much shortened possibly by a serial continuous process, as discussed in Chapter 5. Solvent processing of thermoplastics has shown to yield differences in the structural morphology of the polymers due to factors like rate of solvent evaporation and the

choice of solvents.[223]. Hence a melt processing approach may be better for large scale manufacturing to ensure uniform quality.

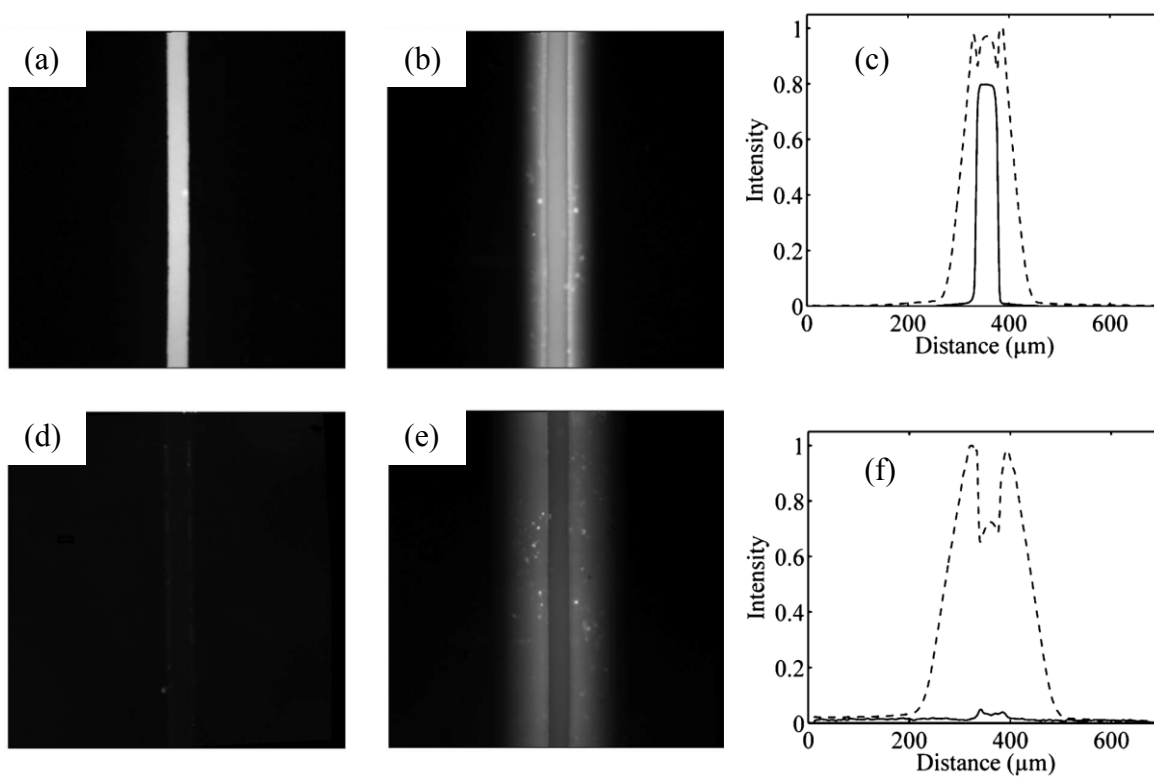


Fig. 22. The Rhodamine dye test analysis performed by Borysiak *et al.* With Rhodamine B dye filled channel: (a), SEBS (b), PDMS and (c); the intensity variation along the width of the channel . after flushing the dye, (d), SEBS (e) PDMS and (f) intensity variation. [Reprinted with permission from The Royal Society of Chemistry].

Table 3: Comparison of SEBS to PDMS and PS (partially adapted from [86])

Property	PDMS (10:1 mix)	PS	SEBS
Elastic modulus	1–3 MPa (Flexible)	3 GPa (Rigid)	<10MPa (Flexible)
Advancing contact angle	108°	~94°	borderline hydrophobic (93-104°)
Surface stability	–	++	++
Cell culture	++	+++	++
Zeta potential (pH 7)	–25–32 mV	–20–30 mV	–39 mV (for SEBS 42) and stable
Thermal stability (DSC)	+	–	+
Molecule sorption	–	++	++
Optical transparency	++	+	+
Autofluorescence	+	+	+
Gas permeability	+++	+	++
Cost of material	high	low	low
Resolution	50nm	10nm	10nm
Ease of demolding	easy	Moderate-difficult (Mold dependent)	easy
Bonding	via extensive processes (reversible-easy)	thermal bonding (reversible not possible)	Thermal bonding (reversible-easy)
Ease of fabrication: Rapid prototyping	easy	melt processing (expensive) *solvent processing (easy)	melt processing (moderate-expensive) *solvent processing (easy)
Large scale manufacturing	expensive	low to moderate	low to moderate

3.2 Replication studies

Since SEBS is available in different compositions, a preliminary guideline was set to have the ease and simplicity for manufacturing and check for possible use of valves, which required the use of low moduli SEBS variants, which are generally available as pellets. As the polystyrene content increases, the crystallinity increases and hence these materials are available in amorphous/ fluffy crumb state. While the Geckofluidics concept discussed later in detail, in this thesis is compatible with other elastomeric polymers, a few polymers were studied for the manufacturing feasibility. Five variants of SEBS, two versions of a thermoplastic polyurethane and one formulation of Ethylene Vinyl Acetate (EVA) were studied. The study was important, because demolding interlocked features after manufacturing could possibly damage the features. Some torn and/or fractured features embedded inside the molds may render the mold damaged for any subsequent processing, while some polymers may undergo plastic deformation either perpetrated by adhesion or mechanical interlocking.

The most well characterized SEBS polymers in academia have been sourced from Kraton polymers. The low polystyrene content variations used in this thesis are G1657 and G1645, with 12.3-14.3% PS and 11.5-13.5% PS content respectively. The detailed composition of the Dryflex SEBS polymers was not available. The thermoplastic polyurethanes are shape memory polymers. The fluffy crumb variants of SEBS are the high polystyrene content samples (Fig. 23(b)), though certainly compatibly with processes like injection molding, were excluded from testing due to incompatibility with the scale and mode of the manufacturing process being explored. The manufacturing process is via thermo-compressive molding with a silicone master which is discussed later in this thesis. Polymers like EVA had to be manufactured at lower temperatures, because the degradation

temperature is ~200 °C, while MM4520 required a temperature of 215 °C and dual pressure cycling. G1645 has a lower melt flow index, meaning that it is much slower to flow under a given load and temperature, which may also require a dual compression molding cycle to adequately fill in the smallest features. A brief overview is as in Table 4.

Table 4: Overview of the thermoplastic elastomers

Polymer	Type	Shore Hardness	Tg	Raw form
Kraton G1657 ¹²	SEBS	~ 47 A	-42C and 95 C	Clear dusted pellets
Kraton G1645 ¹³	SEBS (With Enhanced Rubber Segment)	~35 A	-35 C and 95 C	Clear dusted pellets
SMP MM4520 ¹⁴	Thermoplastic polyurethane	Temperature dependent 30 D for rubbery zone	25 C	Clear cylindrical pellets
SMP MM2520 ¹⁴	Thermoplastic polyurethane	Temperature dependent 26 D for rubbery zone	45 C	Clear cylindrical pellets
Proform ^{TM15}	Ethylene-Vinyl-Acetate (EVA)	~85 A	-10 C and 31-40 C	Translucent sheet
Dryflex C3 6068 ¹⁶	SEBS/carbon composite	~ 70 A	N/A	Black pellets
Dryflex T509 ¹⁷	SEBS	~ 50 A	-50C and 100C	Translucent pellets
Dryflex T909 ¹⁷	SEBS	~ 90 A	-50C and 100C	Translucent pellets

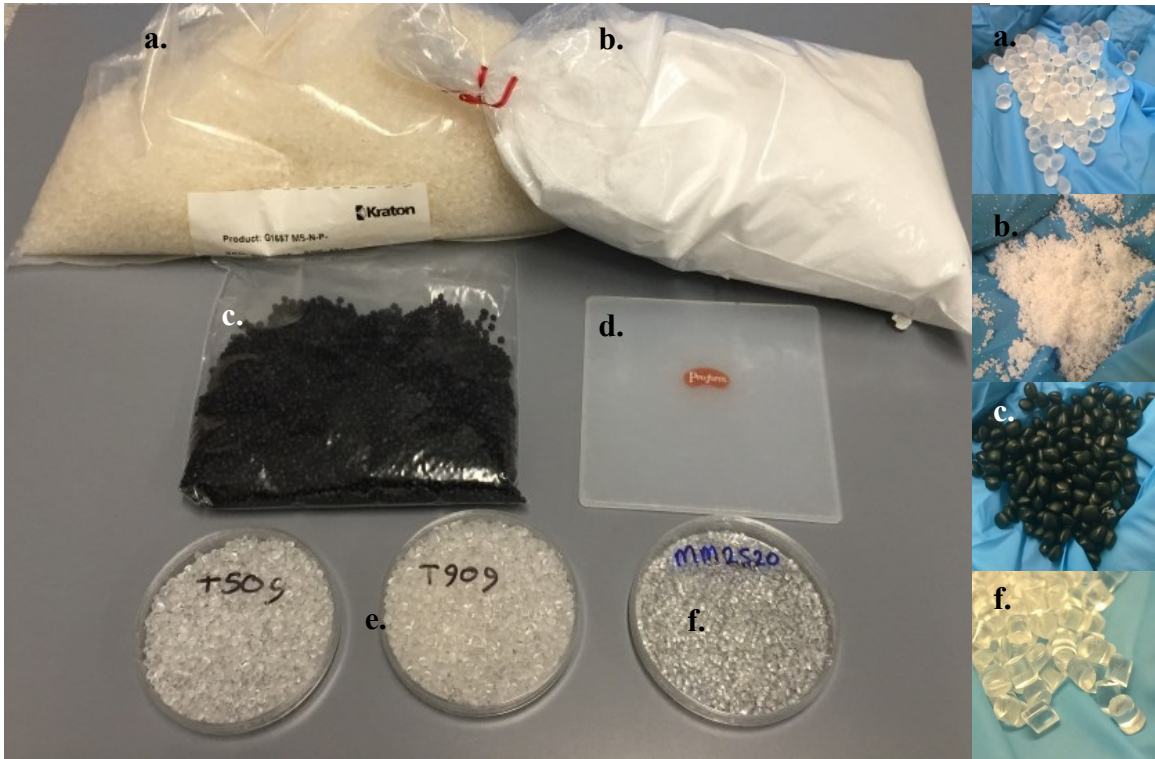
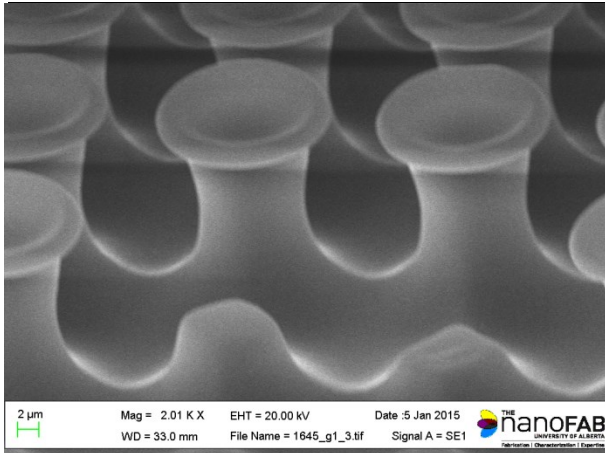
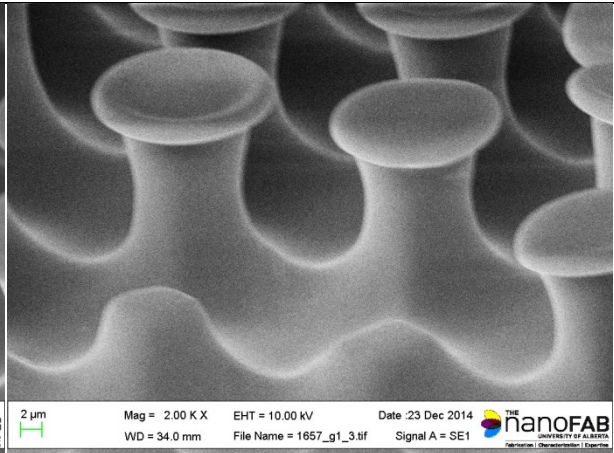


Fig. 23. a. Kraton G 1657 (pellet form) b. Kraton G1651 (Fluffy crumbs) c. Dryflex C series (SEBS-carbon black composite pellets) d. Proform EVA (Sheet) e. Dryflex SEBS T series f. thermoplastic polyurethane (cylindrical pellets)

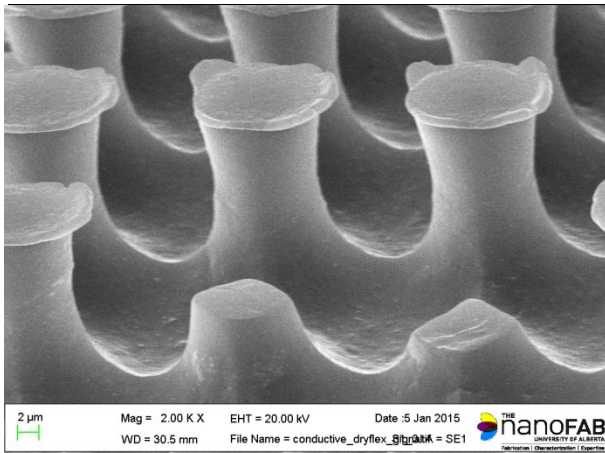
Qualitative inferences were drawn based on scanning electron microscopy and quantitative measurements from optical profilometer scans along with rating for the manufacturing feasibility. The SEM imaging data for 16 μ m diameter (cap) mushroom shaped features is shown in Fig. 24.



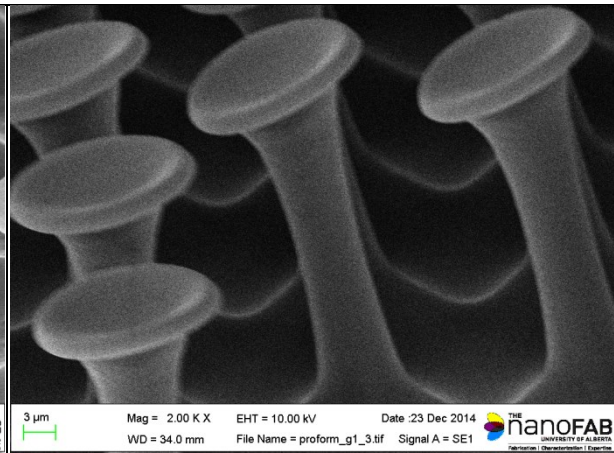
G1645



G1657



C3 6068



Proform EVA

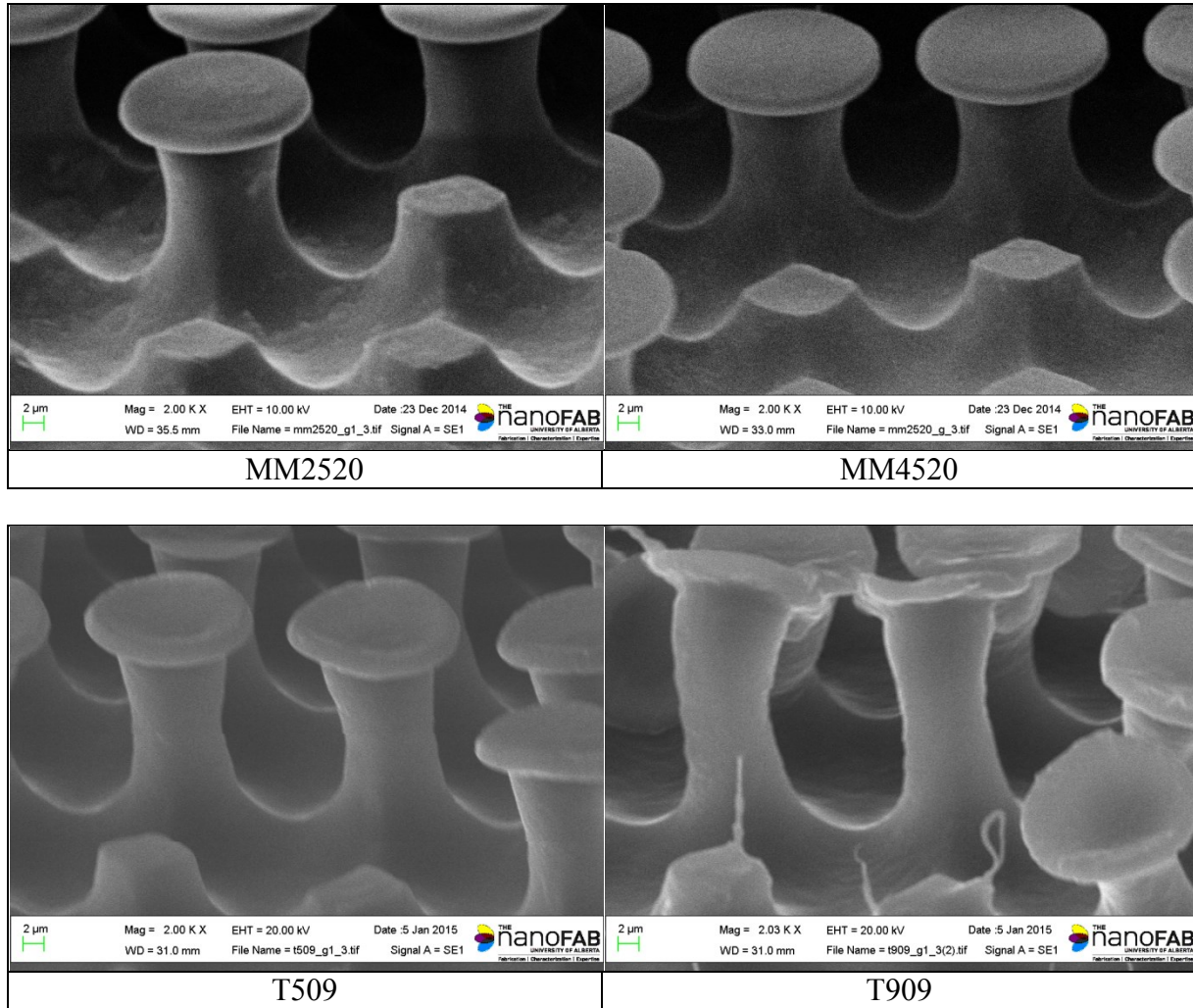


Fig. 24: Replication study results for various polymers*

*The fractured fibres in the SEMs are faithful replicas of induced damage in the master molds.

Polymers imaged under low gun voltages (2kV) had poor resolution (Fig. 25(b)), while higher voltages cause surface charging Fig. 25(a)). Hence a thin gold layer was deposited using Denton sputter. The warping of the mushroom heads (referred as caps in the due course of this thesis) is due to the stresses induced by the deposition of gold (~10nm) for SEM imaging purposes.

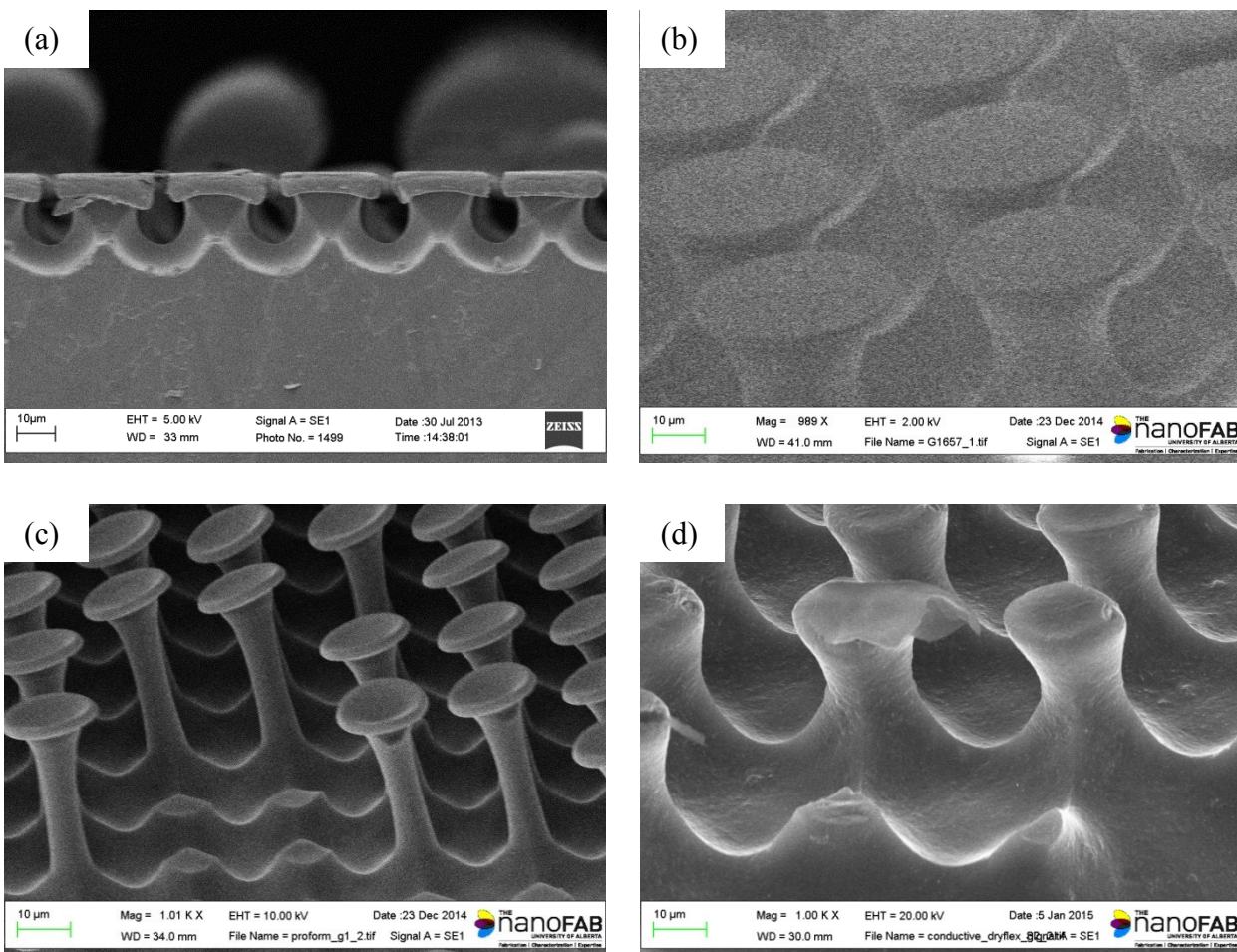


Fig. 25.(a) Charging plumes (in the background) at gun voltages of ~5kV in a PS sample without gold coating (b) Low resolution images with low gun voltages (G1657) Extent of poor replication with (c) Proform EVA and (d) C3 6068

3.3 Results and discussion

The ease of fabrication and the replication quality could be factorized based on the manufacturing of the samples and SEM imaging. From an ease of manufacturing perspective, Proform EVA was the easiest polymer to work with. It has a higher melt index and hence showed good filling properties. Dryflex C3 6068 was the most difficult to replicate. From the SEM images, it could be concluded that Kraton G 1657, 1645 and SMP MM4520 had the most complete and perfect filling. Proform EVA showed plastic deformation of almost 100 % during the demolding process(Fig. 25(c))which was also partially evident with Dryflex T509 and T909.

Speckles were observed with the Thermoplastic Polyurethanes. This could be because of the inherent phases in the polymer, or the phase separation occurring during the molding process. Dryflex C3 6068 appeared to have poor filling (Fig. 25(d)) in certain areas accompanied by significant roughness. The smaller cap features appeared to be brittle, which could be induced by the presence of carbon black. The evident roughness was clearly due to the presence of carbon black. Some outgassing of volatiles could be predicted due to the clouding of the Silicone mold. Dryflex TPEs (T509 and T909) were expected to have a good potential to be used for microfluidics, but the significantly high surface roughness (Table 5), outgassing of volatiles and lower than expected optical properties were observed. Based on ease of manufacturability and replication fidelity, Kraton G1657 would be the material of choice followed by Kraton G1645. SMPs can be an interesting choice which allows for materials to be bonded when soft at elevated temperatures, and then turn rigid when cooled.

A detailed roughness measurement analysis was also attempted. Zygo Optical Profilometer was used for this analysis. Some curvature was observed on some of the polymers, which

would eventually disappear when in contact with another surface, but was an issue for the roughness measurements. The roughness values were heavily amplified depending on the curvature as the measurements would be absolute values without accounting for the curvature (Fig.26). To account for the curvature, a surface profile fit of 4th order was used. While other profiles exist, the curvature was inconsistent with varying materials and samples, hence a safer option was used. All the profiles confirmed to a flat horizontal surface, after the profile removal (Fig.27).

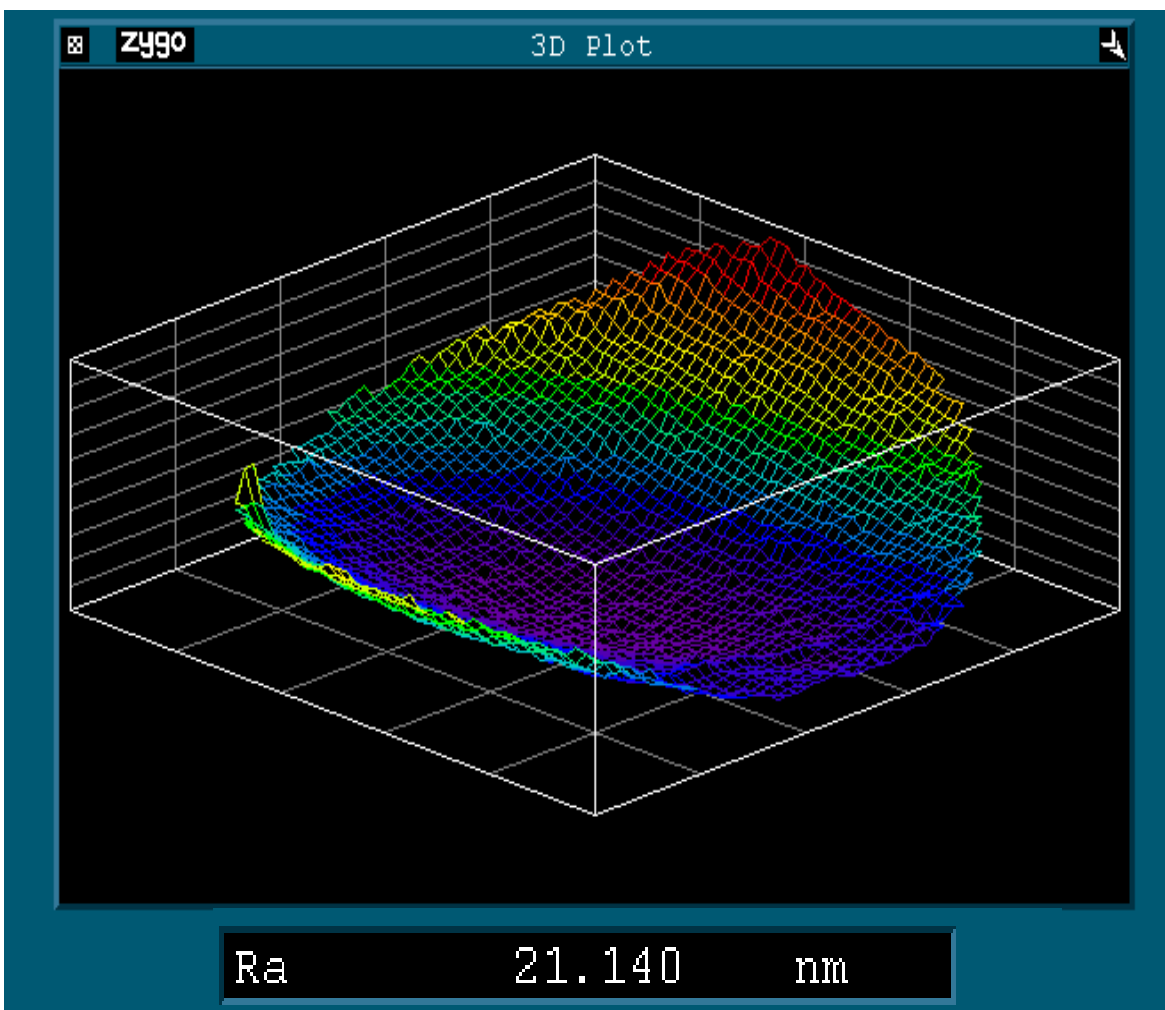


Fig. 26. Surface profile for Kraton G1657, without curve fitting

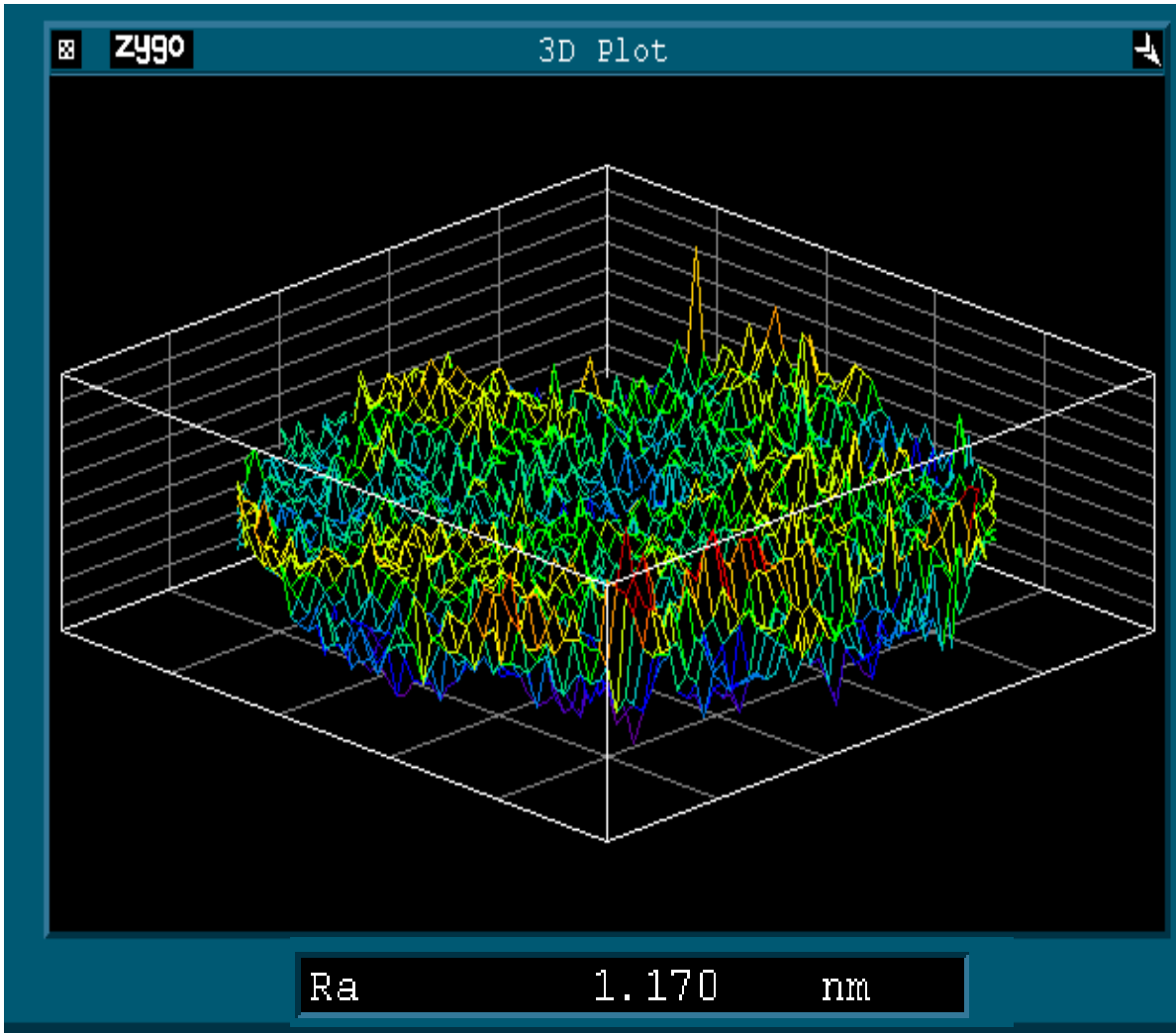


Fig. 27. Surface profile for Kraton G1657,after curve fitting,

An average value of the average roughness was calculated across three different sites. Since the kraton pellets are dusted pellets, aggregation of the dust could be observed on samples with improper mixing. The silica dust approximately contributed to a 3 fold increase in the roughness for G1645. The average roughness (R_a) values are tabulated as in Table 5.

Table 5 :Average roughness values for different replicated polymers (The details of the scans are as in Appendix A)

Material	Average Rougness (Ra) nm
T509	15.86933
T909	127.4463
G1645M	4.064
G1657M	1.108667
MM 2520	5.949667
MM 4520	1.217667
C3 6068	64.2205
EVA Proform	2.505333
SiliconeMold	1.157667

The typical roughness was fairly minimal for Kraton SEBS, shape memory polymers and EVA, while they are extremely high was Dryflex T909 and Carbon black filled Dryflex C3 6068. The extreme variations have been illustrated as in Fig. 28

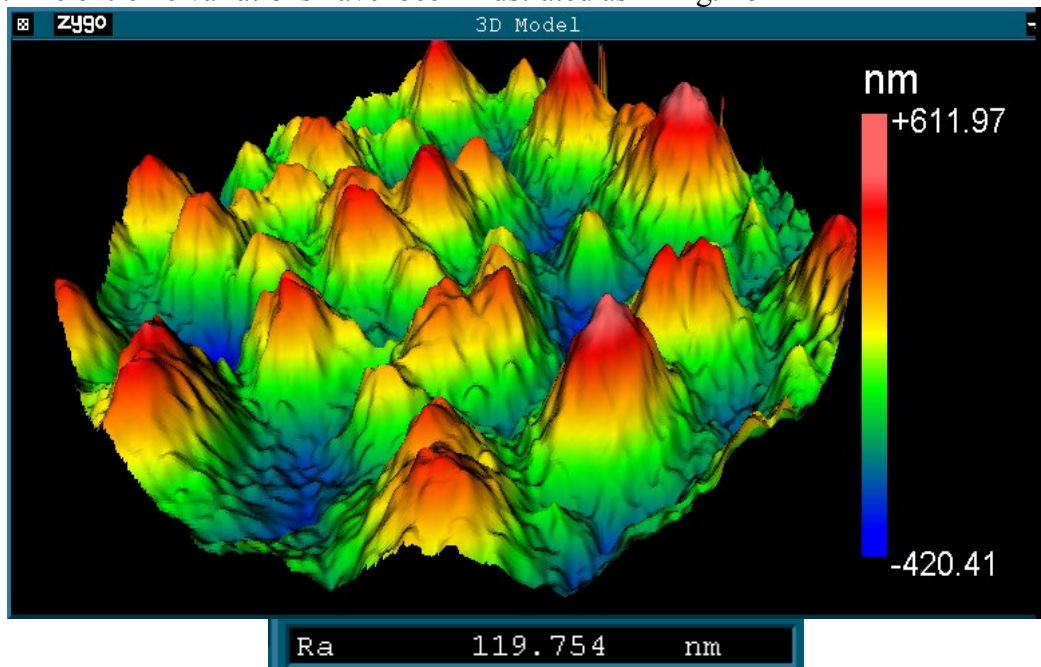


Fig. 28. T909 (Maximum Roughness)

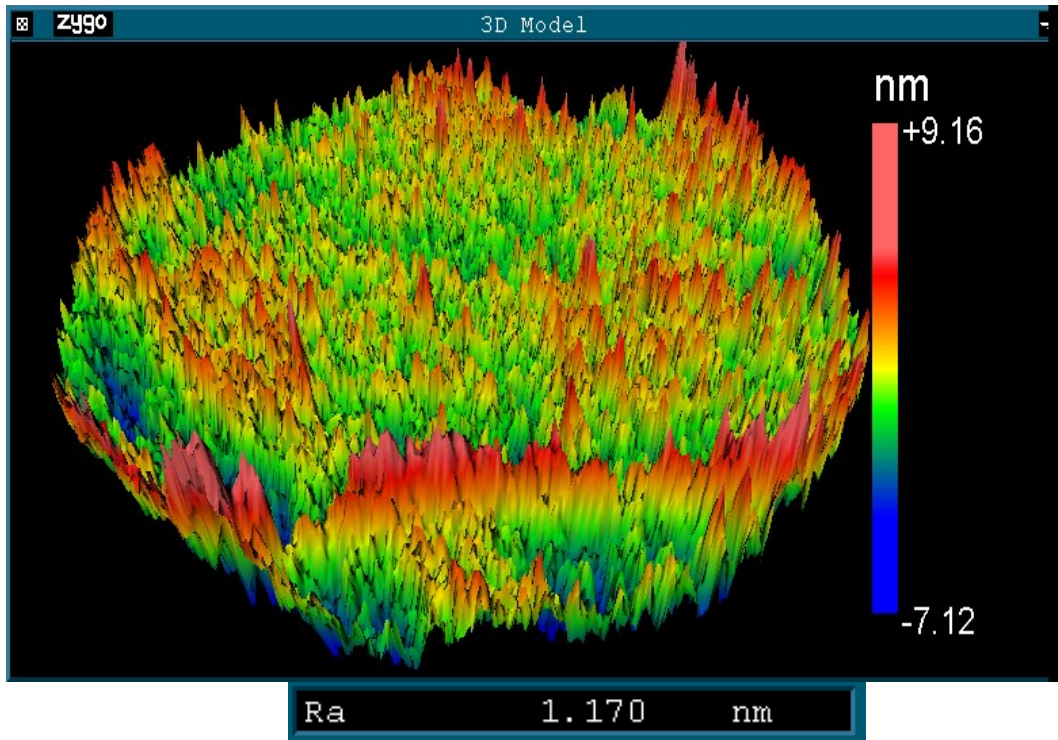


Fig. 29. Kraton G1657M (Minimum Roughness)

The optical profilometer scans doesn't require deposition of gold and hence the measured values are true representative of the absolute surface roughness. Also certain caps were ripped or did not fill during the molding process, but no absolute judgement could be made about the incomplete caps. The measurements were limited to the center of the clean fibers. Kraton G165M demonstrates close to a perfect replication and hence would be the most ideal choice purely on the basis of surface quality. Followed by G1657 was MM4520. The surface looked glassy, but the manufacturing process often leads to significant trapped gasses.

Table 6: Summary of results

Polymer	Molding Parameters	Ease of Fabrication	Replication Quality	Notes
Kraton G1657	200°C/30 seconds	++	+++	Best combination of flow and visual appearance. High fidelity and ~100% roughness replication.
Kraton G1645	200°C/30 seconds	+	++	Harder to flow than G1657, more variation in surface quality. Polymer pull back was observed during the unloaded cooling process. The quality of replication was close to G1657 from SEM but very fine speckles were observed under optical profilometer. May be used in applications with thermal assisted bonding (details in chap 6)
SMP MM4520	215°C/60 seconds	-	+++	Very slow to flow and required higher temperatures than all other varieties tested. Some freckles were observed underside of the caps. Very low surface roughness and a glassy appearance. Some air pockets were observed, but are due to the manufacturing process, and may be eliminated under high pressure molding methods.
SMP MM2520	200°C/30 seconds	+	++	Similar flow to G1645. Heavy speckles were observed. The surface roughness was moderately high, quite evidently from the phase separation, which is also the reason for the speckles.
EVA Proform™	160°C/30 seconds	+++	++	Extremely easy to flow and lower temperatures can be used. Matte texture appearance, but may be visual scattering from the semi-crystalline polymer which makes the

				material translucent. Though the replication quality looked smooth, the fibers were plastically deformed more than 100% and bent in the direction of peeling (from the mold)
Dryflex C3 6068	200 °C/30 seconds	--	--	Significant polymer pull back during cooling was observed- elastic behavior. The fibers that remain filled look good when imaged through silicone but once demolded show extreme damage and surface roughness. Poor filling was also observed in certain areas. A cloudy appearance of the silicone mold occurs within a few minutes of demolding implying some release of volatiles.
Dryflex T509	200 °C/30 seconds	+	-	Similar flow to G1657, and appears to fill well when imaged through the mold, but has more adhesion to silicone and surface roughness is greater. The caps appeared very wavy and the overhangs tend to tear in a few locations.
Dryflex T909	200 °C/30 seconds	+	---	Similar flow to G1657, and appears to fill well when imaged through the mold, but after demolding the fibers look more damaged and rough. This is a much stiffer elastomer than the others tested and can be plastically deformed during demolding. The degree of light scattering in this polymer is very temperature sensitive (nearly opaque at high T).Moderate pitting was also observed. The surface roughness was the highest amongst the polymers tested.

3.4 Conclusion

Though SEBS has been demonstrated as a favorable material for microfluidics, this study reports the manufacturing feasibility of commercially available variants of SEBS and a few other thermoplastic elastomers by manufacturing aggressive adhesive geometries of the geckofluidic devices. While a few of the tested materials gave promising results, others had challenges which couldn't be predicted from analysing the datasheets of the individual polymers. Many of the data sheets do not explicitly state the additives added to the polymers, which present challenges during the fabrication process. Release of volatiles and oily residues were observed with a few materials, while phase separation was observed from the SEM images.

From an cumulative analysis and the ease of fabrication, G1657 was the most preferred choice and G1645, with a slight manufacturing difficulty and relatively higher roughness, would be a close second choice.

CHAPTER 4: FIBER DESIGN GUIDELINES

4.1 Introduction

While the synthetic Gecko adhesives has been accepted to be function of van der Waals forces, the discussion that ensues is how to emulate this adhesion. A significant number of solutions have been proposed and different contact geometries have been experimented with, a few of which were illustrated in (Fig. 19). Many plants and animals also exhibit adhesion via microstructuring of their contact surface, but Gecko adhesion has become the generic term to reference to all microstructuring based adhesion systems. While a few of the insects with flat mushroom contact achieve adhesion by the mix of van der Waals and capillary forces[224], most synthetic versions have achieved it by pure van der Waals forces.

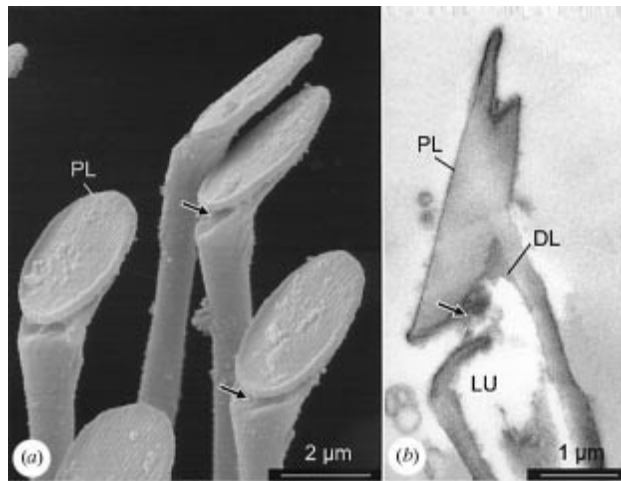


Fig. 30: Setae geometry on feet of *Episyrrhus balteatus*, a fly. PL- End Plate; Lu- Lumen and DL- electron dense layer [Reproduced from [225], The Royal Society]

Synthetic adhesives can demonstrate as high as a 1MPa of shear adhesion. Most of them have been designed to demonstrate anisotropic adhesion, and rely on shear force loading of

the fibres. Non-angled fibres, depending on the tip geometry can exhibit normal , shear and/or mixed adhesion. Considering the application to microfluidics, a non directional adhesive is desired.

Experimental studies were performed by del Campo *et al.* [226] towards identifying the optimum tip shape for maximum adhesion. The study was performed on fiber radii varying between 2.5 and 25 μm . The aspect ratio of the fibers was fixed at 1. A flat punch geometry was set as the base for reference to compare the effect of the tip geometries. A spherical end contact, a flat contact with filleted edges, a spatula overhang tip, a flat mushroom overhanged tip and a concave tip were tested (Fig. 31). All geometries were fabricated via photolithography in SU-8 and then replicated in PDMS via an intermediate.

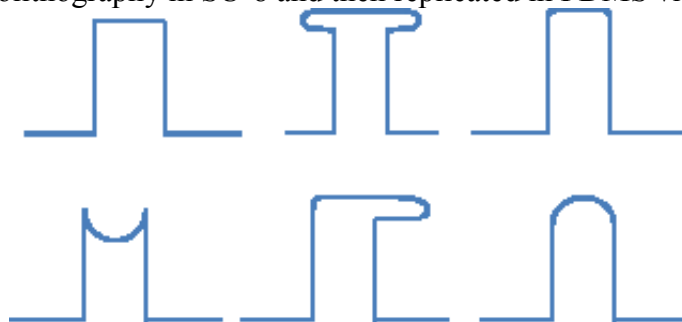


Fig. 31. Fiber geometries tested for maximum adhesion strength.

The tests were performed using a sapphire sphere with a diameter of 5mm, with a constant retraction rate of $1\mu\text{m s}^{-1}$. The flat punch reference geometry (10 μm) had a pull off force of $\sim 0.7\text{mN}$ for a preload of $\sim 2.5\text{mN}$. The round tip yielded at $\sim 0.35\text{mN}$ for a preload of $\sim 2.25\text{mN}$, while the spatula tip had a pull off force of $\sim 6\text{mN}$ for preload of $\sim 2\text{mN}$. The maximum pull off force however, was demonstrated by the mushroom shaped geometry at $\sim 13.5\text{mN}$ for a preload of $\sim 2.25\text{mN}$. The adhesions strengths were proportionally lower for larger diameter tips. The flat tip with fillet edges performed slightly poorer than flat punch

geometry. After accounting for the effective contact area, the maximum adhesion strengths reported for flat mushroom overhang structures were ~ 30 times of the flat punch geometry. The authors suggested further studies to explain the better performance of the mushroom shaped adhesives, which were performed by Carbone *et al.*[227]. The contact geometry has also been correlated to the type of adhesion in biological systems by Gorb *et al.*[224] a reports that a spatula shaped contact is preferred in case of an active quick release adhesion , and a mushroom shaped contact is the preferential termination element for long term passive adhesion.

The theoretical explanation into debonding mechanism shows that a flat punch geometry and the mushroom shaped geometry have completely different debonding mechanisms. The detachment mechanism for a flat punch geometry initiates at the outer edge and propagates inwards, while for a mushroom shaped geometry, is vice versa (Fig. 32. Idealized failure modes). It also concludes that this detachment is independent of the pillar dimensions and that the overhang doesn't support any additional load but eliminates the stress singularity (Fig. 33(a),(c)) . The stress singularity is mitigated by an optimum design of the cap thickness, if not, the singularity again appears at the outer edge of the fiber (Fig. 33(d)). This work also proves that, the mushroom shaped fibers are also tolerant to defects almost as large as 25% of the fiber diameter. In continuation with the efforts to determine the perfect geometry, Carbone *et al.* [228] identified that the cap aspect ratio and the cap to neck ratio are the critical design aspects for achieving the best adhesion possible. They also identified the optimum ratios to be, 0.2-0.3 for cap thickness to neck diameter ratio, and cap diameter to neck diameter ratio be pegged at greater than 2. The fiber aspect ratio was shown to have some effect for cylindrical fibres by Greiner *et al.*[190]. The pull off strength increases linearly with the pillar aspect ratio until after which they could buckle

under self weight. While as per St.Venant's principle, different loads of similar intensity have similar effect at a sufficiently larger distance, a very low aspect ratio fiber would be lesser than that optimal distance, and may fail due to improper load redistribution.

Based on these optimized set of conditions, if we set the cap diameter to 100 μm , the neck diameter should be less than 50 μm and the cap thickness should be $\sim 10\text{-}15\mu\text{m}$.

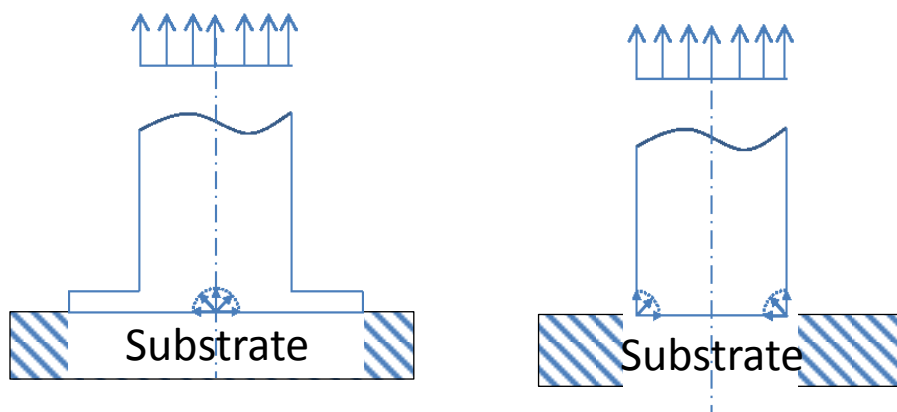


Fig. 32. Idealized failure modes [Adapted from [227], with permission from The Royal Society of Chemistry]

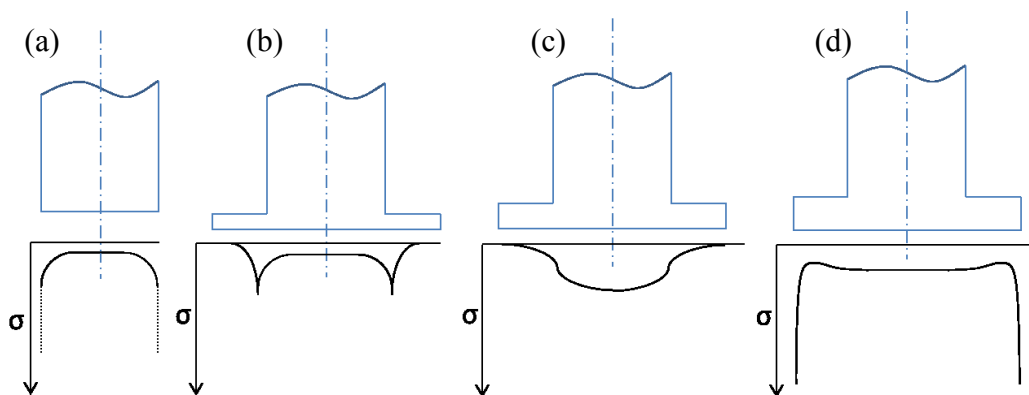
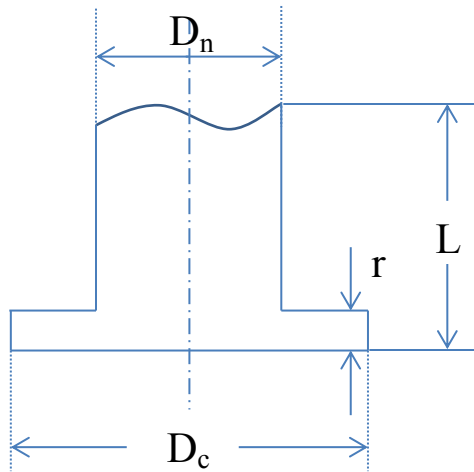


Fig. 33. Stress distribution for (a) flat punch and Mushroom Caps : (b) thin, (c) optimum and (d) thick [Adapted from [227], with permission from The Royal Society of Chemistry]



$$\text{Cap Aspect Ratio} = \frac{r}{D_c}$$

$$\text{Fiber Aspect Ratio} = \frac{r}{D_c}$$

Fig. 34: Geometry and geometric definitions for mushroom shaped micro fibers

4.1 Integration with microfluidics.

Extending the concept of dry adhesives to microfluidics can provide for a bonding solution devoid of any surface treatments, clamps (incl. magnets), thermo-compression bonding and liquid adhesives. This can be worked out by creating a sweep of the basic design geometry to create a microfluidic channel wall. This gasket, will serve to hold the fluid in the desired path at the same time provide a good adhesion to the contact substrate. The surroundings of this gasket are populated with other primary adhesive structures which in tandem with the gasket increase the reliability and adhesion strength (as in Fig. 35). The work of these supporting adhesive can be maximized when the adhesive is integrated with a rigid backing layer. The rigid backing layer helps to re-distribute the point force / localized pressure over the surrounding fibres, thereby providing for a higher pull off force.

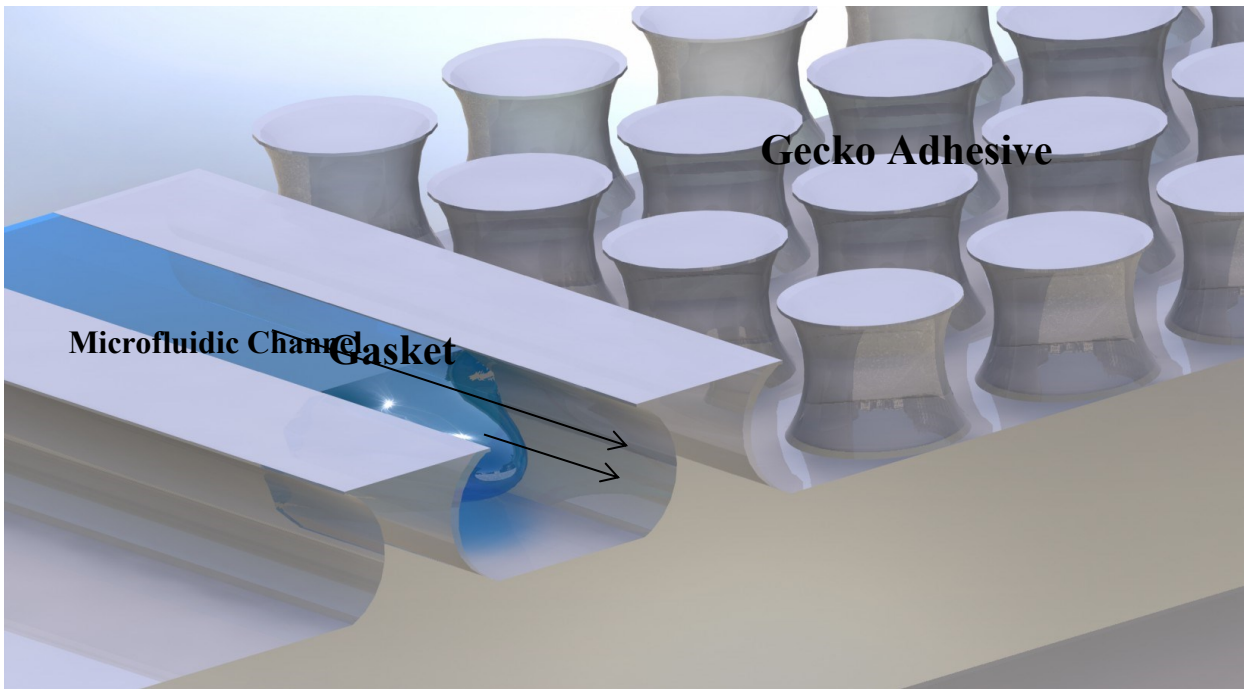


Fig. 35. A schematic layout of a geckofluidics device

The prime reason for failure of conventional microfluidic channels under pressure driven flows is because of the stress singularity arising at the edge of the interfacing geometry inside the channel, similar to the flat punch geometries. A simulation study was performed in COMSOL, to study this stress distribution in the gasket, and also to show the effect of a rigid backing. This study builds up on a similar study undertaken on gecko inspired adhesives [229] but extends it to the concept of Geckofluidics.

A 3mm blister was modelled with 100 μm gasket cap width and 100 μm adhesive fibre cap diameter. The neck diameter at the lowest was 55micron at $\sim 40\%$ height. While these values are close to the idealized models, the geometry of the fibers is slightly different from the proposed models, owing to the fabrication feasibility, which is discussed in the manufacturing part of this thesis. Elastomeric materials like PDMS or SEBS demonstrate viscoelastic behavior and thus need to be modelled using hyperplastic models in COMSOL.

A detailed experimental and FEA study has been performed by Ben Bscheiden [229], in order to develop numerical models for accurate material behavior. Mooney- Rivlin, 2nd order, 3rd order and 5th order models were tried, and the 5th order model provided the best fit for the values read from uniaxial elongation tests on Instron (300% displacement and more). The values of Mooney Rivlin parameters determined for Kraton G1657 are

C1 (kPa)	C2 (kPa)	C3 (kPa)	C4(kPa)	C5 (kPa)
-69.5	532	3.49	58.8	-17.5

While further studies pertaining to cyclic testing were performed, they were beyond the scope of the requirements for Geckofluidics, as the devices should ideally be for single use or at best a few (<10 cycles), under which there is no degradation or significant variation of the material properties.

The FEA study was performed with triangular elements and an axis symmetric boundary condition. Since the major focus was to show the stress distribution in the gasket, a 2D geometry was used and the simulation was performed on a revolved extension of this 2D model. The cap of the fibres are the most stressed parts of the fibre, and are very small, hence a ‘extra fine’ physics controlled mesh size was used . A mesh convergence study based on earlier waork [229] was performed (See Appendix E). The maximum pressure used in this study is 200kPa (~29psi) in order to compare all the models with a similar basis. All the fibre boundaries ideally in continuum are bounded with a roller boundary condition and the top surface of the cap was fixed. The stress values in the adhesives gaskets were compared with rounded edge flat punch geometry gasket, under a case of 5 additional fibers supporting the gasket.

4.3 Results

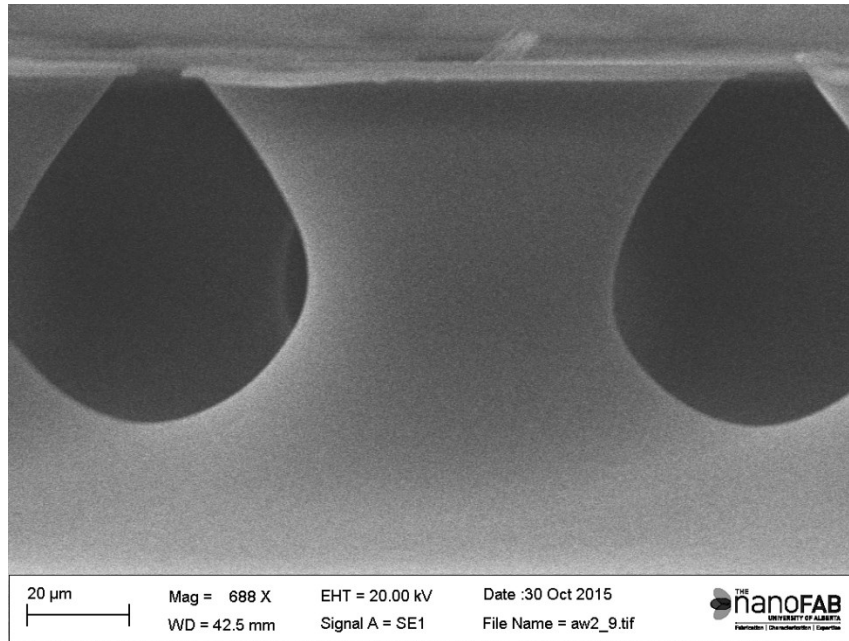


Fig. 36: SEM of the modelled adhesive fiber

4.3.1 MESH:

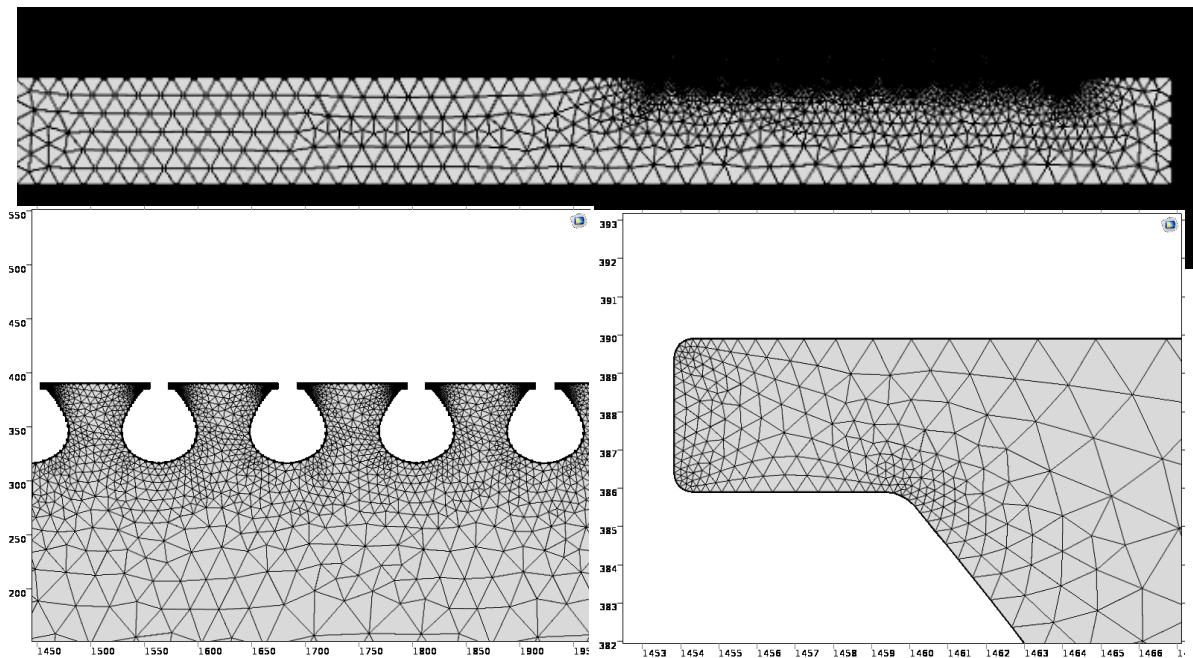


Fig. 37. Illustration of modelled geometry and meshing scheme

4.3.2 BOUNDARY CONDITIONS

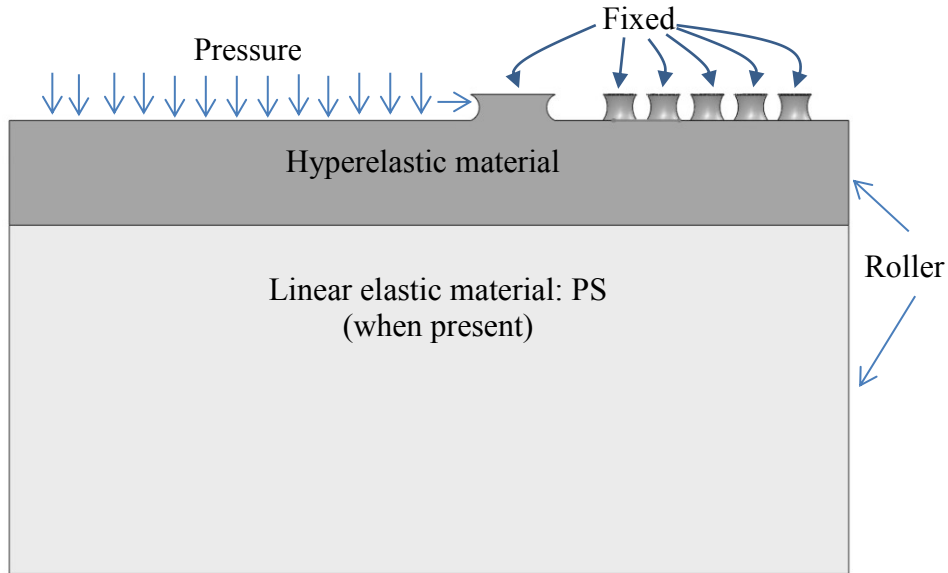


Fig. 38. Description of boundary conditions used for simulation

4.3.3 GOVERNING EQUATIONS

From [230] and [231],

Based on Newton's second law,

$$\nabla \cdot \sigma + F_v = \rho \ddot{u} \quad \dots \text{Eq. 19}$$

Where,

σ is the Cauchy's stress,

F_v is the body force per unit volume,

ρ is the mass density and

u is the displacement vector.

But since a stationary analysis is carried out, $\ddot{u}=0$, Hence,

$$\nabla \cdot \sigma + F_v = 0 \quad \dots \text{Eq. 20}$$

For modelling the linear elastic material:

Towards identifying the stresses in the deformed geometry, the cauchy's stress (σ) is replaced with First Piola- Kirchoff stress tensor (P), which is obtained as a product of deformation gradient tensor (F) and Second Piola- Kirchoff(S) stress

$$\begin{aligned} \nabla \cdot P + F_v &= 0 \\ \Rightarrow \nabla \cdot (FS) + F_v &= 0 \end{aligned} \quad \dots\dots\text{Eq. 21}$$

Where,

$$F = I + \nabla u$$

I is the initial deformation gradient tensor

Based on Hookes law,

$$S = S_0 + C : (\epsilon - \epsilon_0 - \epsilon_{inel}) \quad \dots\dots\text{Eq. 22}$$

C is the 4th order elasticity tensor , ‘:’ implies double dot tensor product; S_0 is the intitial stress and ϵ_0 denotes initial strain. ϵ_{inel} represents the inelastic strain

Since the measurements are with respect to a deformed body, the strain measurements corresponding to Piola-Kirchoff stress is the Green-Lagrange strain, given by

$$\epsilon = \frac{1}{2} (\nabla u + (\nabla u)^T + (\nabla u)^T \nabla u) \quad \dots\dots\text{Eq. 23}$$

For modelling hyperelastic material

Continuing from the stationary analysis,

$$\nabla \cdot \sigma + F_v = 0$$

and

$$\sigma = \int F S F^T \quad \dots\dots\text{Eq. 24}$$

Where,

$$\begin{aligned} F &= \nabla u + I \\ S &= \frac{\partial W_s}{\partial \epsilon} \end{aligned} \quad \dots\dots\text{Eq. 25}$$

Where, W_s is Strain energy density.

The corresponding Green-Lagrange strain tensor , ϵ is given by

$$\epsilon = \frac{1}{2} (F^T F - 1) \quad \dots\dots\text{Eq. 26}$$

To accommodate for the hyperelastic properties of the polymer, a numerical model was developed in an earlier study [229] to fit the material behavior from the Instron tests. The polymer was assumed to be incompressible, isotropic and non-linearly elastic. While there are various models that are prescribed for hyperelastic materials, the simplest model with the lowest order was identified to minimize the numerical instabilities. Two models, Ogden and Mooney Rivlin 5 parameter models gave a good fit, but The Mooney Rivlin model produced a numerically stable solution. The equation used is

$$W_s = C_{10}(\bar{I}_1 - 3) + C_{01}(\bar{I}_2 - 3) + C_{20}(\bar{I}_1 - 3)^2 + C_{02}(\bar{I}_2 - 3)^2 + C_{11}(\bar{I}_1 - 3)(\bar{I}_2 - 3) + \frac{1}{2}(K(J_{el} - 1))^2 \dots \dots \text{Eq. 27}$$

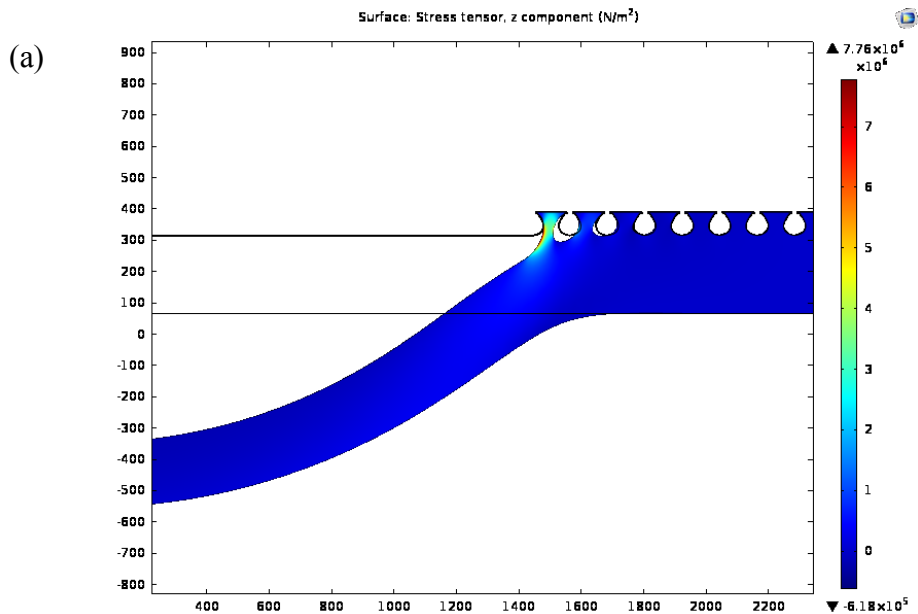
Where, J_{el} = elastic volume ratio = $\det(F_{el})$,

K = Bulk modulus,

$C_{10}, C_{01}, C_{20}, C_{02}, C_{11}$ are the mooney-rivlin model parameters derived from experimental analysis,

I_1, I_2 two invariants of the elastic right Cauchy-Green deformation tensors

4.3.4: STRESS DISTRIBUTION WITHOUT BACKING LAYER



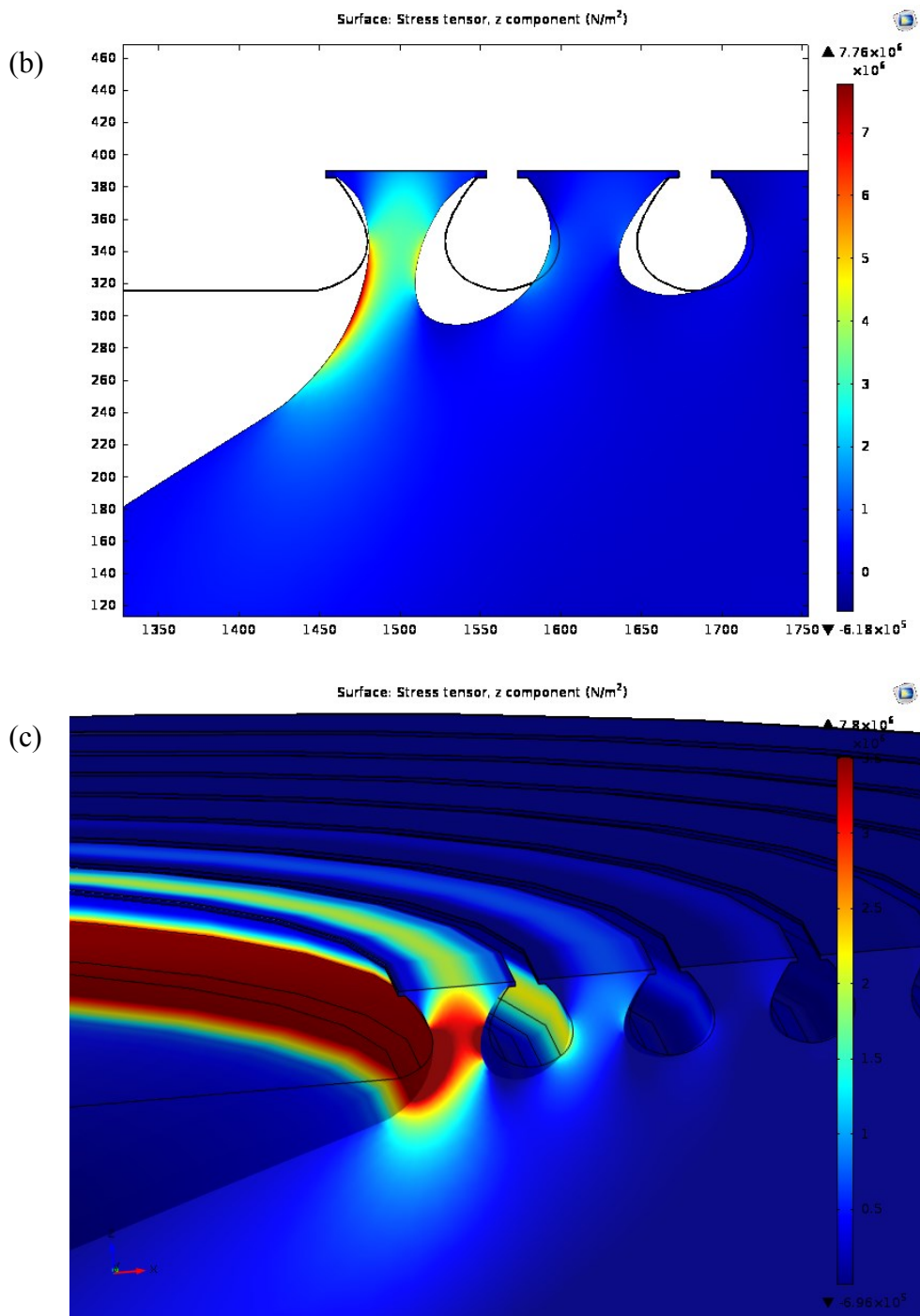
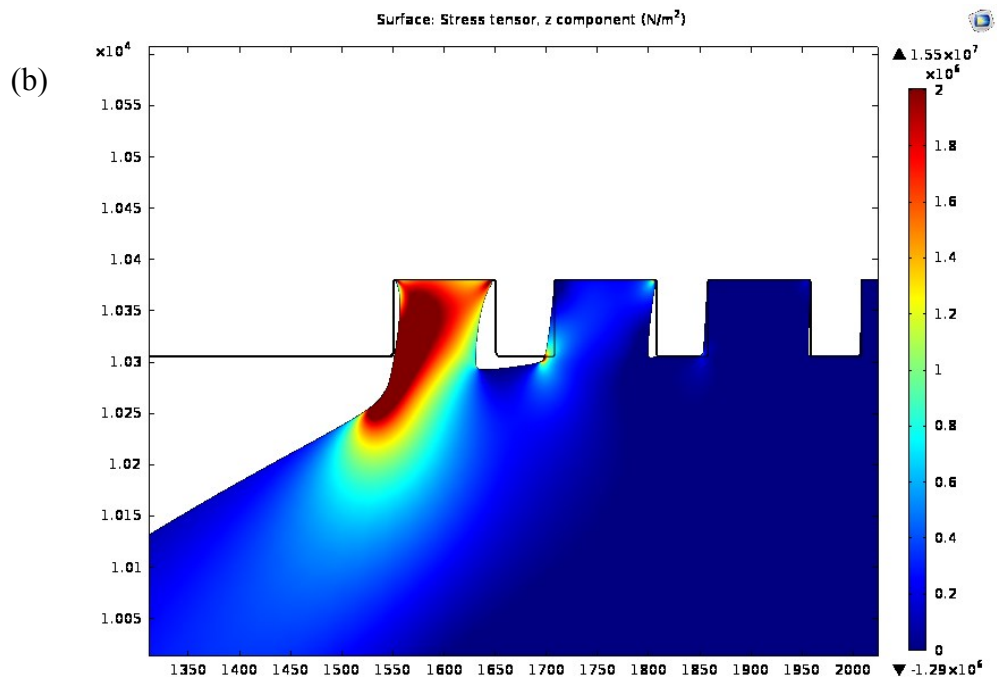
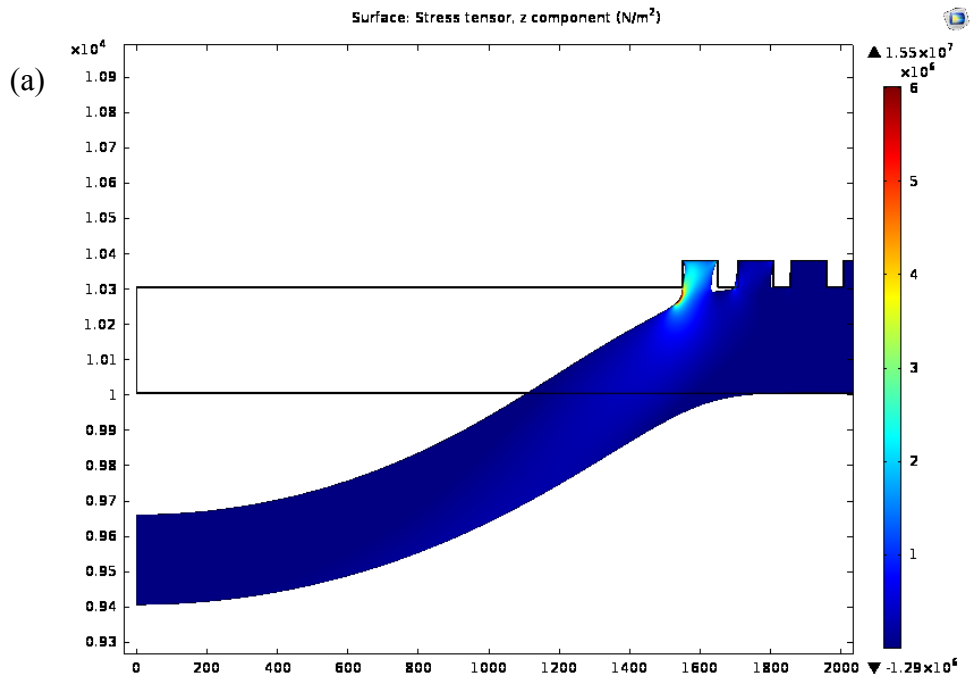


Fig. 39. Geckofluidics: (a) Normal stress distribution (deflected). (b) Normal stress distribution in Gasket (c) 3D stress distribution in the gasket.



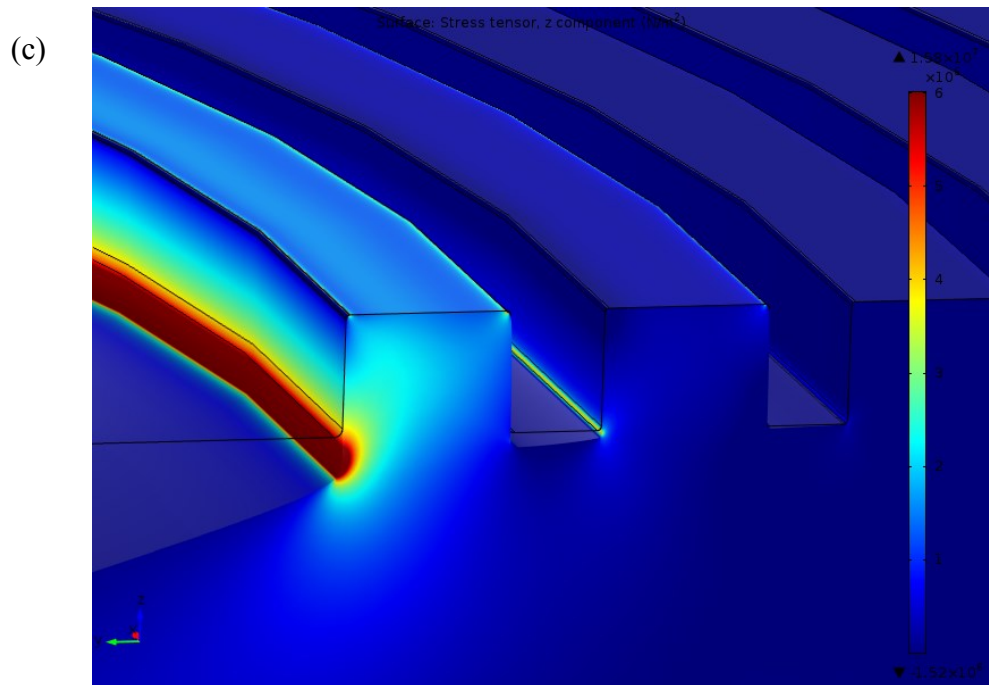


Fig. 40. Vertical punch geometry: (a) Normal stress distribution (deflected). (b) Normal stress distribution in Gasket (c) 3D stress distribution in the gasket.



Fig. 41. The inflation of the blisters as observed in practical application

The inflation of the blisters, as observed by simulation and in practicality, is significant for very thin devices. This inflation creates a peel angle which leads to detachment at lower pressures. The variation of pull of force with respect to the peel angle is given by the

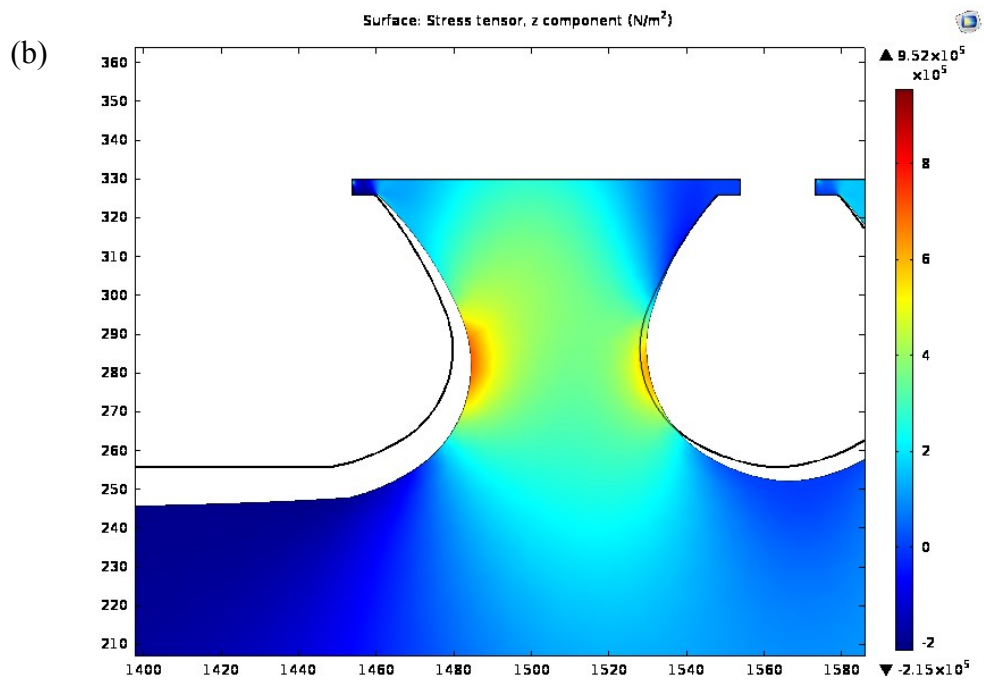
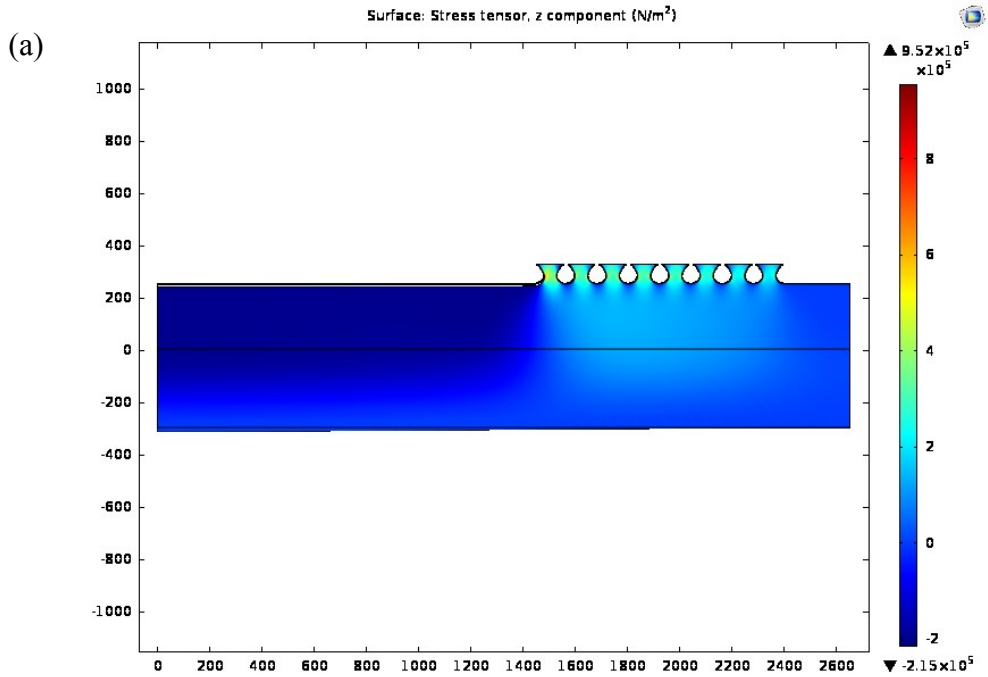
Kendall theory as [232, 233],

$$\frac{F}{b} = \frac{\gamma}{1-\cos \theta} + \textit{Elastic energy term} \quad \dots\dots\dots \text{Eq. 28}$$

Where, F = peeling force in the peeling direction, b is the tape width, γ is the adhesion energy, and θ is the peeling angle (with the horizontal).

While the geometry of the fibers or the frictional interface is unaccounted for in this study, it is clear that for lower peeling angles the adhesion energy is higher. When the applied pressure, inside the blister increases, the peel angle increases, and the blister thereby fails at lower pressures. Also, the stress distribution of the Geckofluidics sample (Fig 39 (a)), shows that the supporting fibers have a minimal contribution and are not engaged. In order to keep this induced peel angle as small as possible and to engage the supporting fibers for stress redistribution, a rigid backing was added to the blisters. The simulations and results ahead demonstrate the effect of backing layer for both the geckofluidics and verticle geometry contact blisters.

4.3.5 : STRESS DISTRIBUTION WITH RIGID BACKING



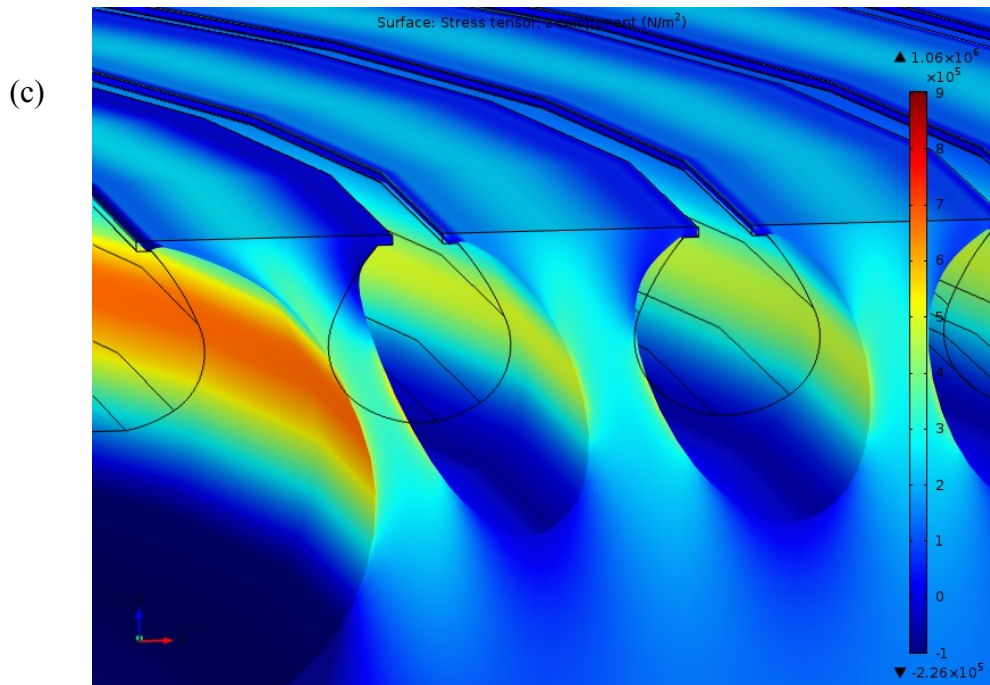


Fig. 42. Geckofluidics with rigid backing: (a) Normal stress distribution (deflected). (b) Normal stress distribution in Gasket (c) 3D stress distribution in the gasket.

4.4 RESULTS AND DISCUSSION

Fig. 39, 40 and 42 help visualize the stress distribution in a Geckofluidic device, in cases with and without the rigid backing layer. Under the Geckofluidic geometry, the peak stress was observed at the neck of the fibers, while a very high stress concentration as observed at the step for the vertical punch geometry. As reasoned, the introduction of the rigid backing evidently decreases the bulging effect of the blister, at the same time helps to engage the supporting adhesive fibers. While the stress distribution throughout the device is certainly important, the stresses distribution responsible for indicating the performance of the adhesive, is the stress distribution in the gasket at the contact interface. The stress distributions in the gaskets are as in Fig 43-46.

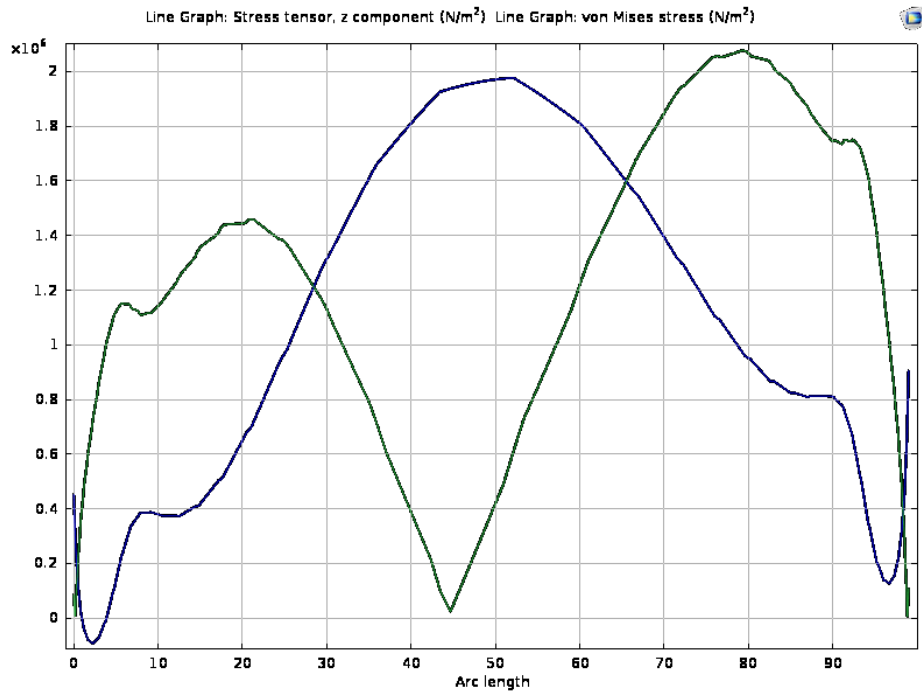


Fig. 43. Geckofluidics without Rigid Backing: (Green: von mises; Blue: Normal Stress)

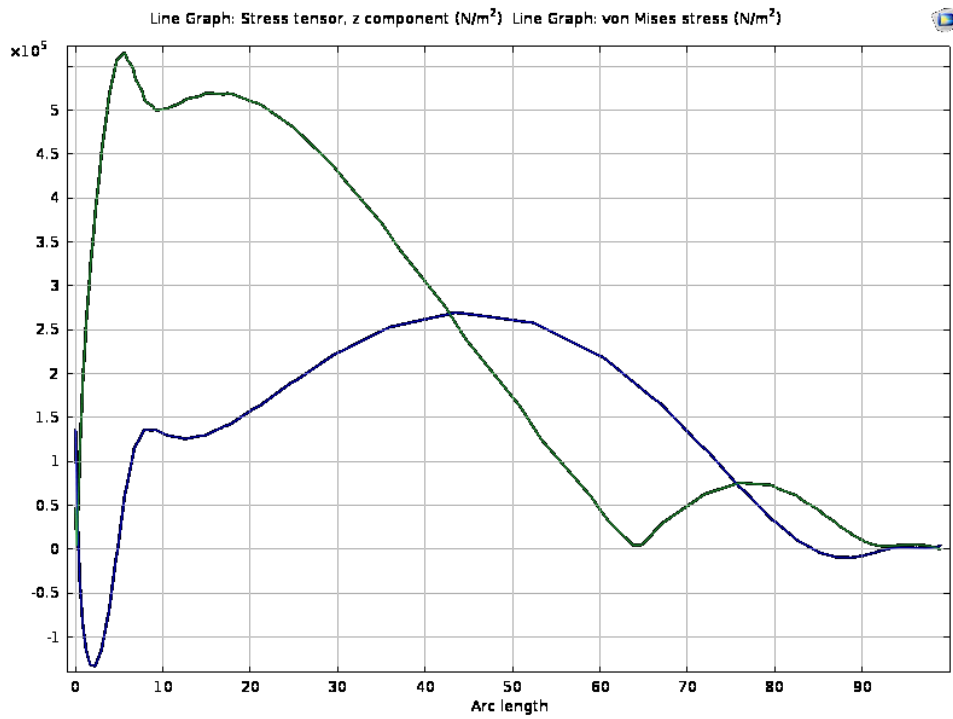


Fig. 44. Geckofluidics with Rigid Backing:

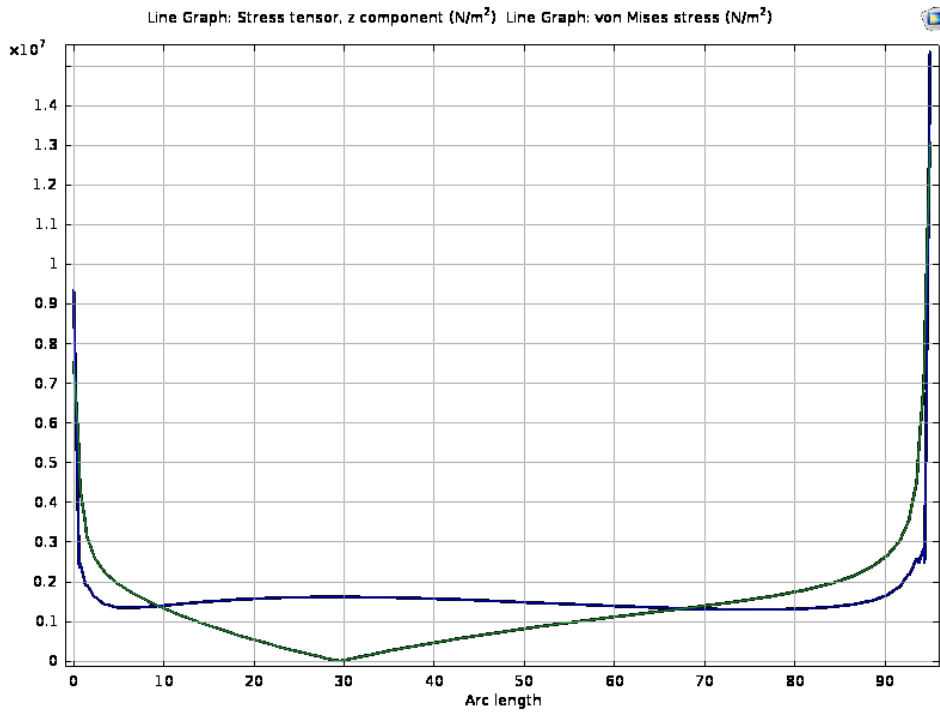


Fig. 45. Vertical Punch geometry: without Rigid backing

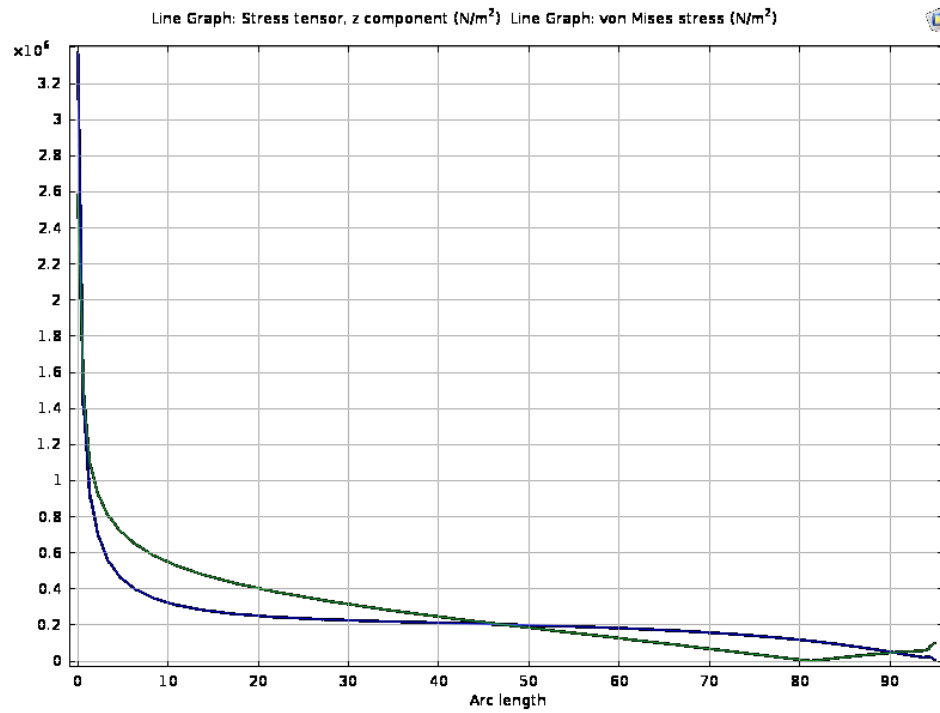


Fig. 46. Vertical Punch geometry: With Rigid backing

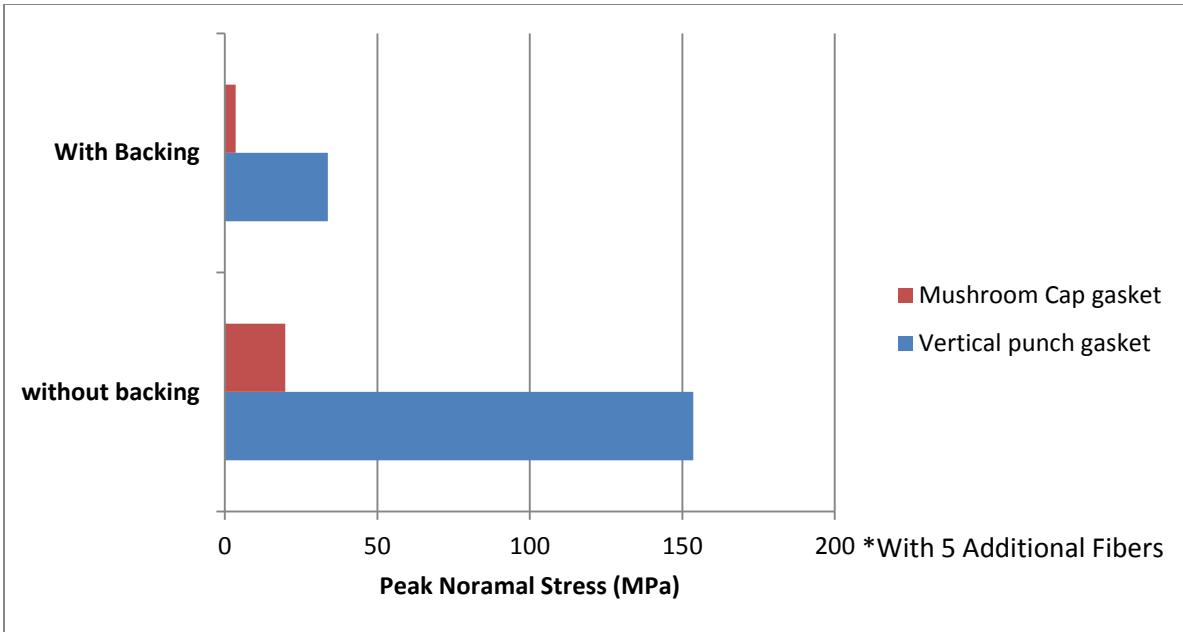


Fig. 47.A relative comparison of the peak Normal Stresses

As observed for these simulations, the effect of the fiber geometry is quite apparent with a decrease of more than an order of magnitude of peak stress and the mitigation of this peak stress from the periphery to the center. The distribution is also similar to the ideal stress distribution as illustrated earlier in Fig. 33(c). The small peaks observed at the periphery, in the graphs for gecko-fluidics blisters were due to small stress concentration arising at the interface of the fillet and the flat contact. Also the peak stress for vertical punch filleted geometries is reduced by the presence of the fillet, which otherwise would reach singularity, and thereby not resolve.

Effect of number of supporting fibers and backing layer thickness

Apart from the design of the fibres, it is also important to understand how other design factors like the thickness of the backing layer, the modulus of the material and also the number of load bearing fibres, help make a robust integration of dry adhesives with microfluidics. While the variation of adhesion strength with the reduced Young’s modulus

(E^*) is important, the choice of material is dictated by the application and may thereby not be a design variable.

A simulation study was performed to identify the variation of peak normal stress in the gasket in correlation with the variation in backing layer thickness and the number of fibers. In regard to the boundary conditions used for the study of number of load bearing fibers, it is to be noted that, the effect of the applied pressure in the blister induces different responses in unconstrained fibres, depending on the presence or absence of the backing layer. In case of absence of the backing layer, the unconstrained fibres will experience a net upward moment (

Fig. 48), which is ideally curtailed by the presence of the bonding interface,. A roller boundary condition may be used to avoid this, but since the number of fibers required to have stable distribution is the subject of focus, the upward moment has been neglected. On the other hand, the presence of a rigid backing layer causes the fibers to be pushed down almost an equivalent displacement as the elongation of the blister itself (Fig. 49).

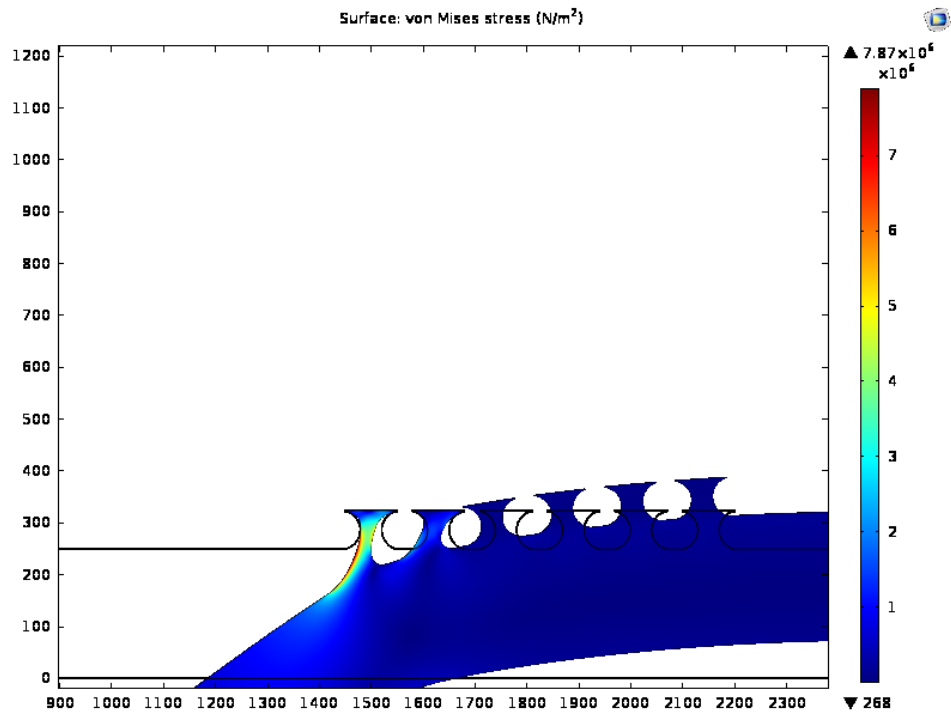


Fig. 48. Geckofluidics: Without backing: one fixed fiber beyond the gasket

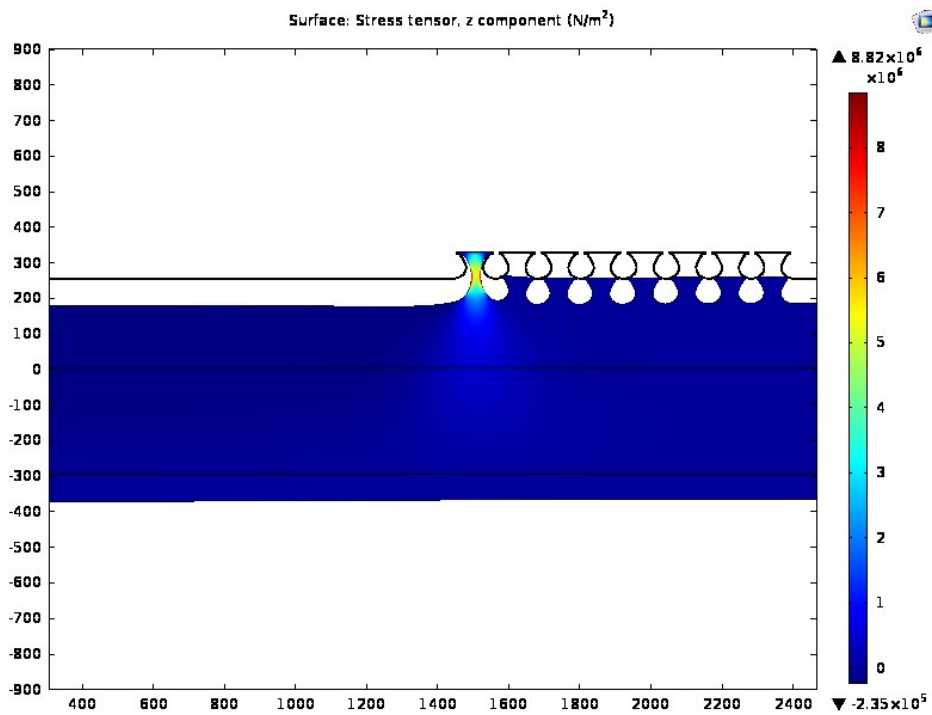


Fig. 49. Geckofluidics with rigid backing

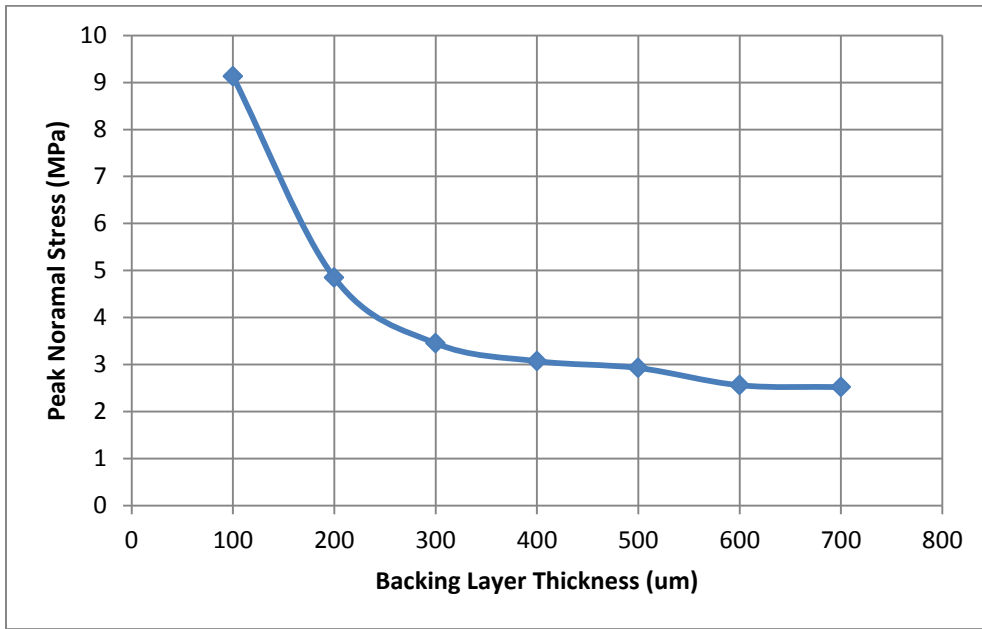


Fig. 50. The variation of peak stress in the geckofluidic gasket with respect to variation in backing layer thickness

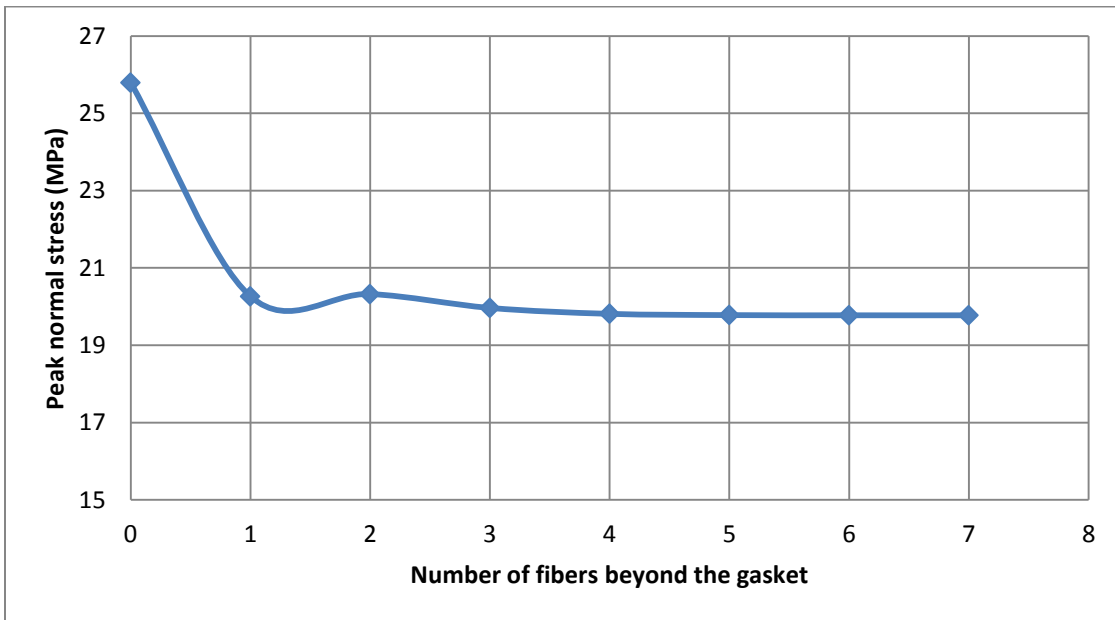


Fig. 51: The variation of peak stress in the geckofluidic gasket with respect to number of fibers in loading beyond the gasket, without backing layer

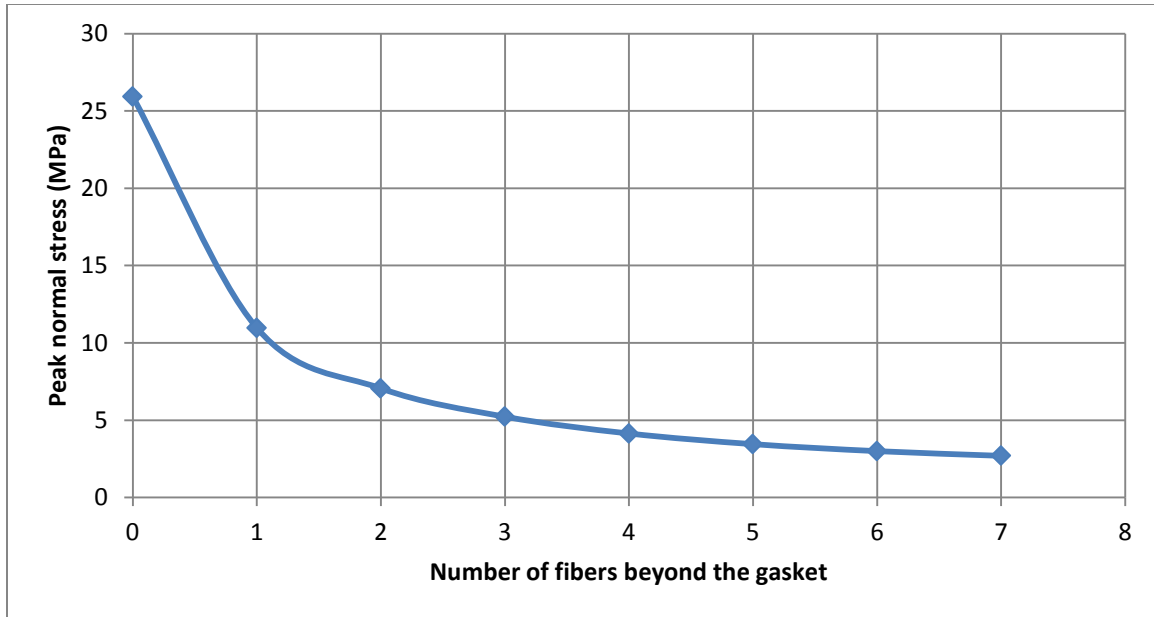


Fig. 52. The variation of peak stress in the geckofluidic gasket with respect to number of fibers in loading beyond the gasket, with backing layer

The effect of thickness of the backing layer (Fig. 50) is significant until 300-400 μm in case of polystyrene, beyond which the effect is small. Hence in order to eliminate/minimize the variations likely to be induced by the manufacturing strategy, a minimum thickness value of around $\sim 500 \mu\text{m}$ can be set. From a practical perspective, this thickness can also effectively minimize any pressure induced cracking, which is evident with very thin backing layers.

The number of fibers beyond the gasket does play a significant effect in supporting the net pressure in the blister (Fig. 51, Fig. 52). This effect is significantly higher in case of the geckofluidics blister supported by a rigid backing. While the trends are similar, the variation between 0 and 2 fibers supporting the gaskets is small but significant, while the variation between 2 and 6 is minimal. Hence in a typical application of geckofluidics about 3 rows of additional fibers can help have a better net adhesion. This number can vary with

the material of the sample device. In case of high pressure applications, devices supported by a rigid backing, demonstrated significant reduction in the stress with the presence of even a single fibre, compared to no fibers, and this stress keeps decreasing with the addition of every additional fibers. The stress in the single gasket is significantly higher compared to a non rigid backing case, as the rigid backing constraints the deflection of the blister, unlike in the case without a rigid backing, resulting in a stress concentration.

4.5 Conclusion

An FEA study was performed to study the design deviations away from the idealised geometry, which were included for the manufacturing feasibility. The study takes into account the hyperelastic properties of SEBS, modeled by a 5th order Mooney Rivlin equation. In order to study the adhesion centric design improvement of the geckofluidic sample over a vertical punch geometry, the stress distribution profile in the interfacing gasket demonstrated both the migration and mitigation of peak stress for the Geckofluidic design. The rigid backing improved the net adhesion performance and under a thickness of at least 500 μm was demonstrated to have an optimal performance. With the backing layer engaging the supporting fiber, the stress sharing effects are significant until 3 rows of adhesive fibers.

Hence, appropriate design measures may be taken depending on the type and aggressiveness of the application.

CHAPTER 5: FABRICATION

5.1 Introduction

With the choice of material set, and the design guidelines in place, the Geckofluidic devices could then be manufactured. The underlying theme for fabrication is to provide a fabrication alternative, which would be cost effective and have the adhesive infrastructure grafted in it, with minimal extra processing steps, and thereby be simple enough to be adopted in MEMS integration. Many different microfluidic chip designs, including a few designs for Dr. Stephan Warnat (Dr. Ted Hubard Group) at Dalhousie University, who had collaborated with us on the integration of MEMS with Geckofluidics, were included on the mask. The entire design and fabrication was carried out at University of Alberta Nanofab facility and the equipment at the research group's lab.

Gasket sizes of 50 μm , 100 μm and 250 μm were designed to be tested across various microfluidic devices and blisters. All the adhesive fibers were fixed at 100 μm based on previous work at the group as they yield the best adhesion performance and are very mechanically robust, and were arranged in a square array with a gap of 20 μm . A cap aspect ratio of 1:1 was targeted. Different heights of the channels and the blisters were fabricated. A proof of concept mask with 25 μm square shaped fibers caps, with 5 μm gaps and ~20 μm height fibers was also used in this study.

While a wide variety of designs were fabricated, a few could be tested for their intended use, while others were adapted for reuse in a other projects. A few designs were tested, but required optimization for better and characterizable performance.

(See Appendix B for mask designs)

While some of the most common manufacturing methods for large scale manufacturing of microfluidics are hot embossing and injection molding, the cost of tooling is a significant deterrent. Silicon based mold inserts could be significantly cheaper compared to the ones fabricated by the LIGA method, but the brittle nature of silicon makes it a very risky proposition [235]. The interlocking of very small features or thermal fatigue can lead to the fracture of the insert, apart from the constant risk of oxidizing the substrate over time, and thereby the resulting geometric variations.

Replica molding is a fairly standard practice of replicating silicon or photoresist on silicon based microstructures in thermosetting elastomers. The generated replica is an inverse of the original master, and in order to generate a polymeric replica of the positive master, the elastomeric daughter mold used for another replica molding step which results in a positive replica. This could be a simple direct replica molding with a dissimilar polymer, or may require some surface treatments in order to prevent bonding of the two polymers. While this is simple with elastomers, a successful replication in thermoplastics ideally requires that the polymers be in liquid state, which is possible by dissolving the polymers in solvents. The general approach to casting liquid thermoplastics like PMMA is via spin coating. This approach can be used when solidification of the polymer requires the evaporation of the solvent which is complete and uniform in thin film. In case of thick films, directional solidification takes place from outer to inner surface, which could in some cases lead to incomplete evaporation at the interior thereby leading to an incomplete replication and compromised density [236]. Hence thick devices are often made out of multiple thin films [237], which could be a laborious and time consuming process. Wrinkles may also appear on the outer surfaces depending on the thickness and the shrinkage coefficient of the polymer. For these reasons, if a thick replica is desired, solvent

casting is usually avoided. Imprinting thermoplastics with soft masters has been demonstrated by a very small number of groups. Carlvaho *et al.*, demonstrated a dual silicone master embossing of PMMA [238], Benner *et al.* demonstrated a replication of PMMA master in COC [239] and Goral *et al.* demonstrated it with similar PDMS molds in polystyrene [240]. The hesitation in wide adoption of this technology pertains to the durability of the master mold and the minimum feature size. While these fears are justified, the use of thermoplastic elastomers should be without many of these concerns. The fabrication process layout is shown in Fig. 53.

5.2. Mask Designs

The masks were designed in a mask designing software, called Tanner L-Edit. Other softwares like AutoCAD may also be used for the same, but depending on the type of mask writer, a GDSII (Gerber Data Stream Information Interchange) format may be required. The photomask is generated in a 5" x 5" Chrome coated sodalime glass (0.09" Thick)

As stated earlier, the geometry of the microfluidic channel was defined by sweeping the basic geometry of the adhesive fiber. The mask contains parallel lines of the gasket thickness defining the geometries, terminating into ports for inlets and outlets. The blisters and a few other geometries have single independent gaskets. The surroundings of these channels were populated with 100 μ m dots. In the case of 3D microfluidics, localized alignment marks can be used with the other layers on the same or a different mask. Microfluidic mixers, droplet generator, capillary electrophoresis and valve designs, simple straight channels, and gaskets for world to chip interface were some of the designs implemented on the mask. (See Appendix B)

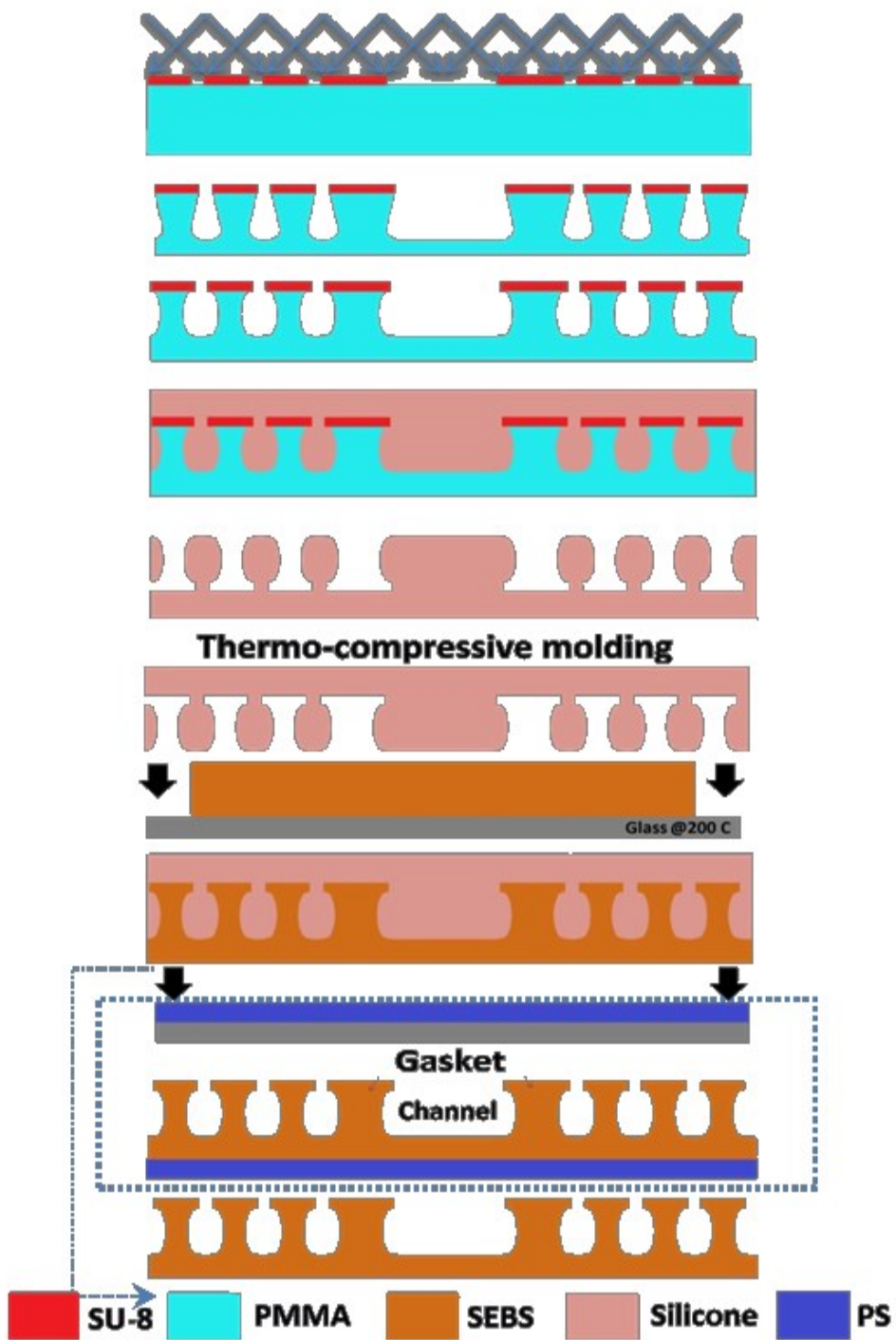


Fig. 53. Process layout for fabrication of Geckofluidic devices

5.3 Master mold fabrication

The mold fabrication process is a two part process involving creating a master mold and a replica daughter mold. The daughter mold is the one used for creating the final device. A typical approach to fabricating fibers with an integrated overhang would be via the use of two photoresists, each for the stub and the cap, on a silicon wafer [241]. Alternatively, to decrease the cost and integrate the adhesive in a single mold, we exploit the poor selectivity of PMMA for deep UV lithography. A prepatterned SU-8 layer acts as the master for the UV exposure, while it itself serves as the cap. Similar process has been described in other works by our group [200, 229, 242] in regard to fabrication of dry adhesives, while this work expands it in the context of fabrication of microfluidics.

PMMA is often referred to as acrylic, and is sold under different brand names like, Plexiglas®, Perspex®, Lucite, Optix® etc. Most commercial grades have significant additives, for suitable commercial uses. A brief study of commercial versions of PMMA was performed by M.Rahbar [243] and Optix and UVT were found to be good options for microfluidics. Though, PMMA is not used directly for microfluidics in this work, the low cost and ease of availability make OPTIX®, by Plaskolite a preferred choice. Large sheets of PMMA were purchased from Home Depot or McMaster Carr and cut into 5” x 5” substrates, to match the typical chrome mask, with Laser engraver (VLS 3.5, Universal Laser systems®). Warping of PMMA has been reported in some of the previous trials at our group, but decreasing the intensity of the laser source, and cutting the substrates in multiple passes has shown to minimize the warping. The PMMA sheets are covered with a sheet of polyethylene, which is removed only after taking the substrates to the clean room. This ensures minimal contamination by debris after laser cutting and simplifies the future cleaning process. The substrates were washed with DI water and dried in nitrogen. Cleaning

with or rubbing the PMMA substrate against kimwipes etc was avoided to prevent any scratches on the surface. The 5"x5" substrates were mounted on the vacuum chuck on the Head-Way resist spinner. SU-8 2002 was spin coated at 500rpm for 5 sec., followed by 1000rpm for 40 sec. to achieve a thickness of $\sim 3.4\mu\text{m}$. The substrates were then soft baked at 90 °C for 3 minutes. The ideal prebake temperature is 95 °C, but taking into account that the substrates tend to warp around this temperature, a slightly lower temperature was adopted, which was compensated by an increase in the prebake time duration, which would ideally be 1-2 minutes.

The SU-8 is mounted along with the chrome mask on a customized jig [193], and is held in place using bulldog clips. This is carried out to ensure a maximum contact is made between the mask and the SU-8 coated PMMA substrate. The quality of the caps is primarily dependent on the quality of contact, and the normal warping of the PMMA cannot be compensated for by the typical aligner equipment in the nanofab. The jig has nylon bolts which are threaded into the jig plate. An appropriate tightening of the bolts will show newton's rings that indicate the quality of contact with the mask. A exposure dose of 450mJ cm^{-2} was incident using a 365nm UV light source, which is far beyond the recommended dosage on other selected substrates as per datasheets (SU-8 2000.5-2015)[244]. This value has been optimized in previous works at the research group. Though the exposure could account for an over exposure, the intimate contact of the mask will ensure a minimal bloating of features. The unpolymerised SU-8 can be developed via a spin rinse on the head-way spinner, by jetting with SU-8 developer and IPA in alternate cycles. While a dip rinse could be used, a spin rinse ensures no residue, which could be trapped in a high density structured surface. This process ultimately produced the caps of the required gaskets and fibers from SU-8 on acrylic.

In order to generate the supporting pillars for overhanging caps, the region surrounding the caps needs to be removed, which includes an undercut. This is achieved by exposing the PMMA to deep UV (254 nm). PMMA is known to be a good positive photoresist for deep UV, and x-ray exposures breaking down the larger molecular weight PMMA molecules into smaller molecules, referred to as main chain scission. UV light is incident in region between the caps, and depending on the type of light, collimated or uncollimated, it will undergo a variable extent of diffraction. SU-8, despite its transparency in optical and near UV ranges is nearly opaque at the DUV wavelengths used, and serves as an effective mask even for these small cap thicknesses. For smaller undercuts and high aspect ratio fibers, a collimated source may be used, while for relatively larger undercuts, semi-collimation arrangements or uncollimated source may be used. The development rate of the exposed PMMA is determined by the energy intensity and the time of exposure, and thereby defines the height of the channels and fibers. The source used is a 254nm Deep UV (DUV) oven (Stratalinker™ 2400) with a nominal intensity of $4.4 \pm 0.2 \text{ mW cm}^{-2}$. [193]

While not a regular problem, some substrates may develop significant crazing (micro-stress cracks) [245], during the subsequent processing of the substrates, This could be because of the significant stresses induced during the exposure process. This is also quite evident from the fact that all wafers warp by the end of the DUV step. This crazing effects can be minimized by annealing the wafer at 85 °C for a few hours, preferably over night. after the exposure dose.

After exposure, it is necessary to develop the exposed PMMA. This is done by removing the lower molecular weight PMMA in a developer solution. The substrates were moved back to nanofab to continue this process. Some of the standard developers for PMMA are methyl isobutyl ketone (MIBK): Isopropanol (IPA), IPA:water [246] and G-G

developer[247]. IPA generally tends to be absorbed by PMMA and results in swelling of PMMA, and the G-G developer is highly toxic. The IPA based developers are also temperature sensitive, and have better development rates at $\sim 28^\circ\text{C}$ [243]. Propylene glycol monomethyl ether acetate (PGMEA), primarily used in nanofab as SU-8 developer has also been shown to demonstrate good development rates of exposed PMMA, but the selectivity is poor. The development rate of PMMA (Optix®) (unexposed) with SU-8 developer was observed to be $\sim 300\text{-}330\text{ nm min}^{-1}$. (Temperature: $18.5\pm 0.2^\circ\text{C}$; Relative Humidity: $42\pm 2\%$) The wafers are developed in SU-8 Developer for ~ 1 hr, inspecting in between to observe the undercut. If a satisfactory feature is observed, the etch may be stopped. (This is likely for fibers nearing 1:1 aspect ratio for the cap and is about $\sim 5\text{-}10$ min before the actual stop). A common problem that has been reported with the development of PMMA is the re-deposition of PMMA as scum on the substrate, which is aggravated in our case due to high density features. One approach generally followed is to spin develop the patterned substrate. SU-8 developer is sprayed on the spinning wafer, similar to the SU-8 development process. But since the substrates tend to be warped, using spin development requires the wafer to be held on the chuck by a double sided tape. Despite use a good quality scotch tape, the wafers tend to occasionally fly off the chuck and crash, thereby damaging the mold. Hence a new post-development process was investigated.

5.3.1 THE DEVELOPMENT PROCESS

The study involved using different compositions of the developers for the post-development process. SU-8 developer and IPA (with DI water) have been used independently for the development process in some of the previous works [193, 229, 243]. The new post-development method, aimed at trying to rinse the substrates in a mix of both the solvents in different proportions. The proportion of the mix tested were,

- 75%SU-8 Developer -25%IPA
- 50%SU-8 Developer- -50% IPA
- 25%SU-8 Developer -75%IPA
- 100% IPA

The patterned PMMA substrates are immersed in the solutions for ~1 min and stirred gently after which they can be dried with nitrogen.

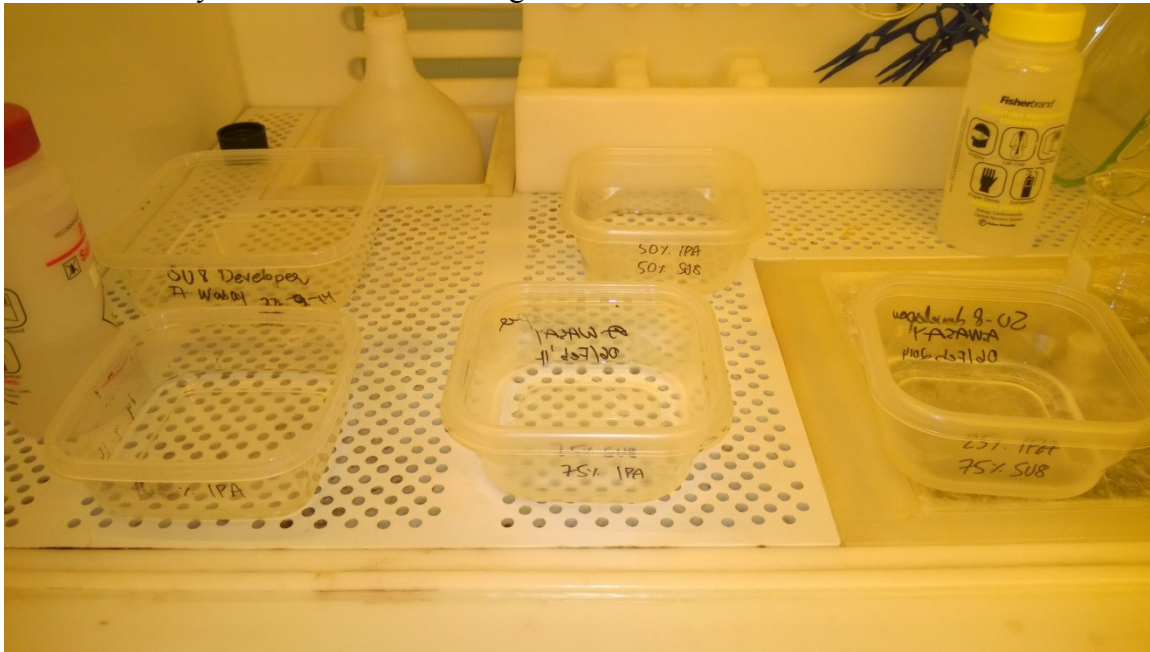


Fig. 54. Prepared post development solvent compositions

If the substrates are dried directly off the SU-8 developer bath, the continued etching of PMMA even during the drying process and the aggregation of the PMMA as a precipitate from the evaporated developer (in which the PMMA had dissolved) would create variable heights depending on the variability and direction of the drying process and the size of the substrate. Hence a 100% SU-8 developer based post development process is fallible. The results of the other compositions are as illustrated as in Fig. 55, Fig. 56, Fig. 57 and Fig. 58,

5.3.1.1 75% SU-8 Developer-25% IPA

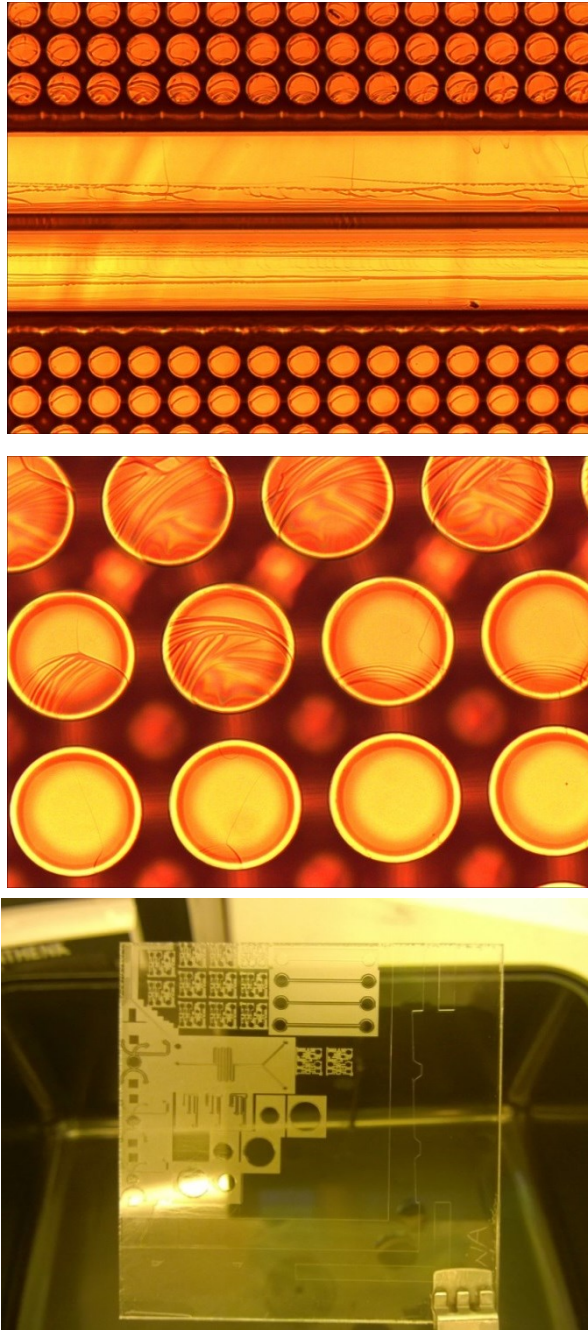


Fig. 55. Post development in 75% SU-8 Developer-25% IPA, (a) 5X (b) 20X
(c) Naked eye view

5.3.1.2 50%SU-8 Developer-50% IPA

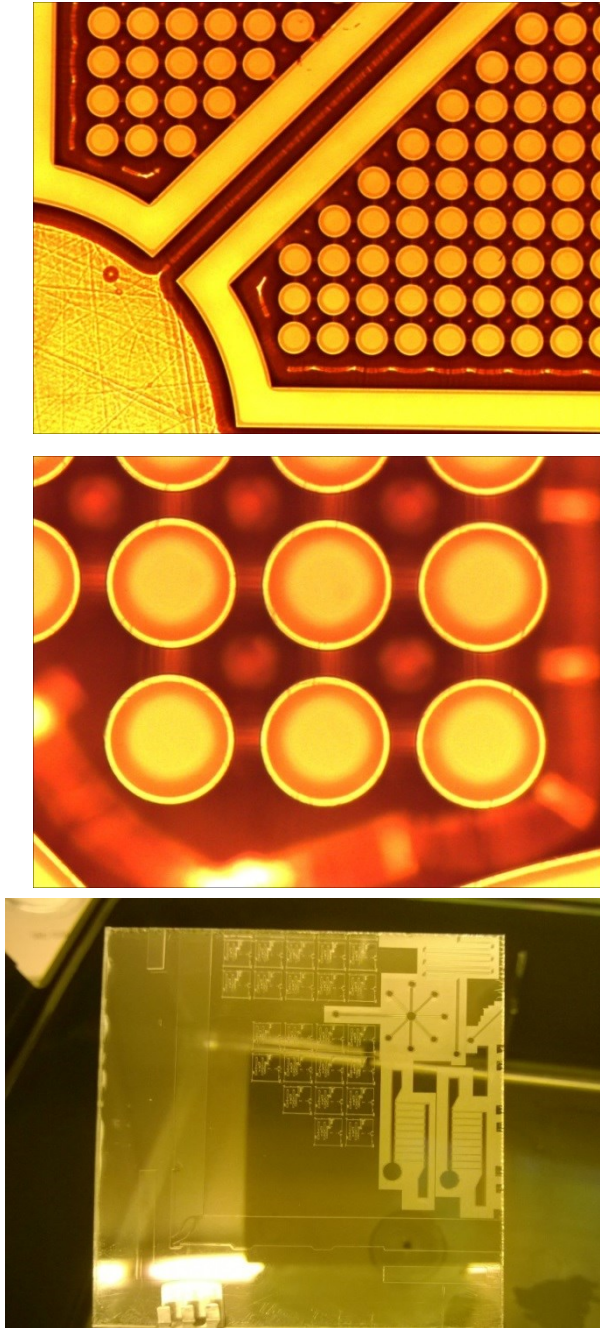


Fig. 56. Post development in 50% SU-8 Developer-50% IPA, (a) 5X (b) 20X
(c) Naked eye view

5.3.1.3 25%SU-8 Developer-75%IPA

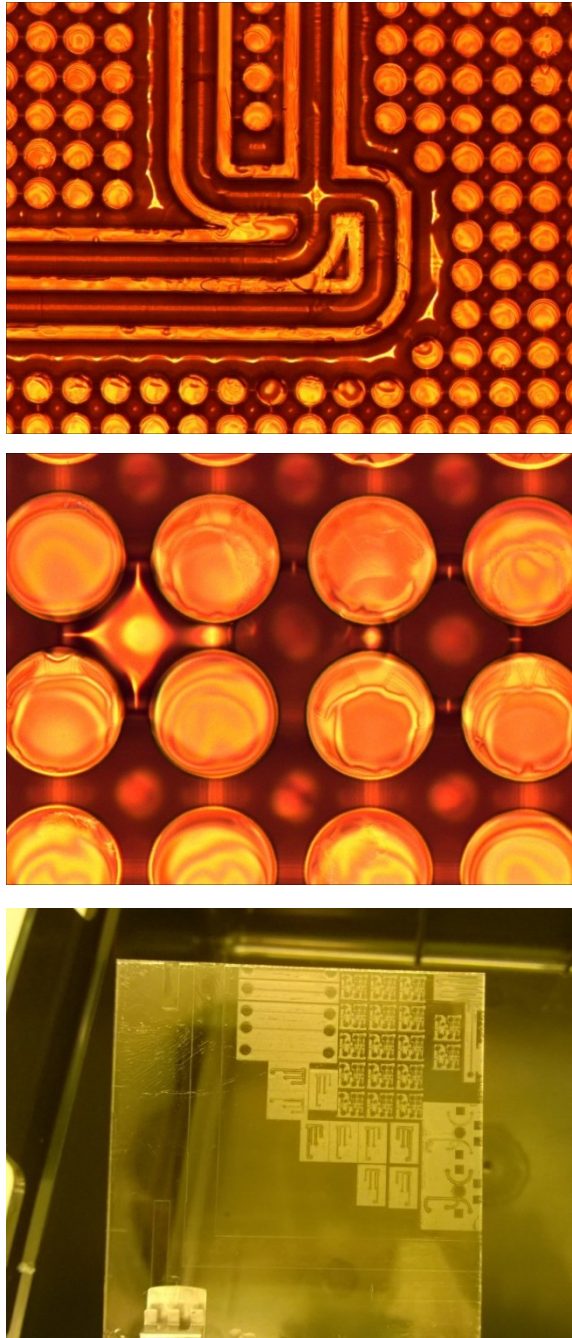


Fig. 57. Post development in 25% SU-8 Developer-75% IPA, (a) 5X (b) 20X
(c) Naked eye view

5.3.1.4 100% IPA

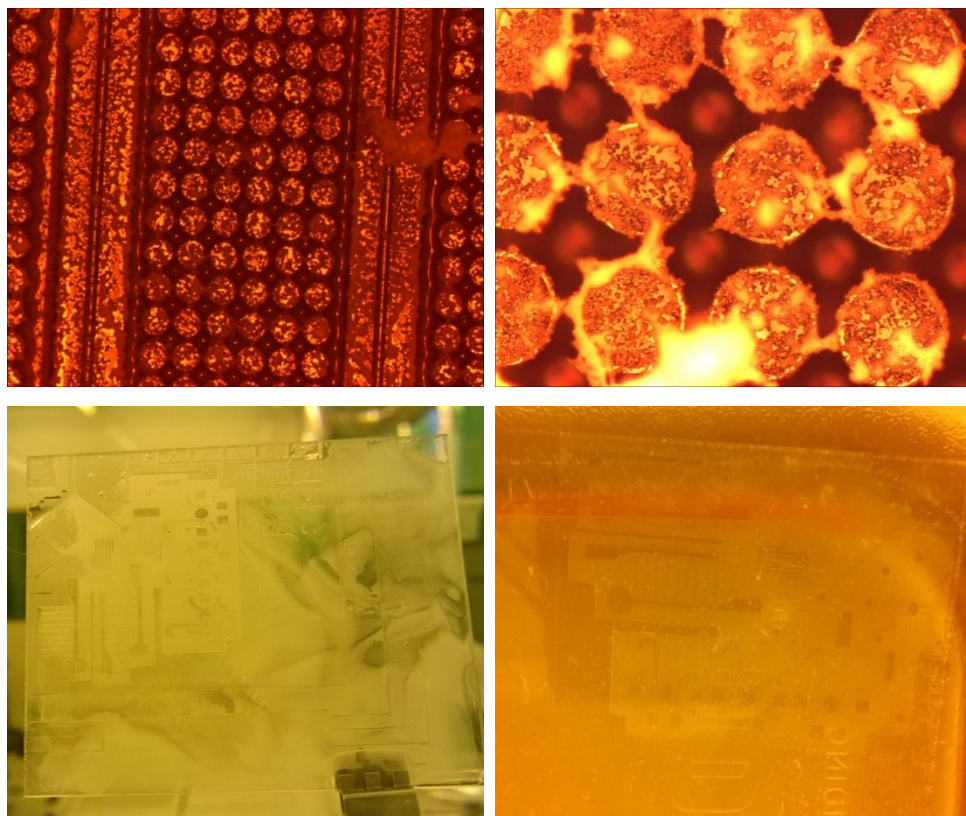


Fig. 58. Post development in 100% IPA: (a) 5X (b) 20X (c) Naked eye view (d) Inside the developer bath

As observed from the images above, 25% SU-8 developer -75 %IPA and 75% SU-8 developer -25 %IPA mix compositions produced some re-deposition as evident on the caps in the images, while the residue produced in 25% SU-8 developer -75 %IPA mix along with some redeposition was evident even to the naked eye. The visual appearance of the 75% SU-8 developer -25 %IPA was mostly clear, except for some aggregation near the gaskets. The 50% each composition of SU-8 Developer and IPA, produced the best results, no evident scum or redeposition was observed. The undercuts of the fibers were clear of the uncrosslinked PMMA. The over hang on the fibers was pronounced.

Severe re-deposition and scum was observed for a 100% IPA mix. The entire surface turned milky, with the redeposition, which was evident even when the substrates were under the solution. The dissolved PMMA would precipitate out immediately during an IPA dip and produced the worst results by far of all the final rinse steps. Severe crazing has also been observed in a few cases, when post developed in wafers which were not annealed after UV exposure.

Hence a 50%SU-8 Developer-50% IPA mix is the ideal post development rinse solvent in instances where spin rinsing is not feasible. A 75% SU-8 developer -25 %IPA mix may also be used for longer times to generate similar results as 50% SU-8 developer-50% IPA mix. Occasionally some specks of residue may remain on the wafer, which can be removed by a quick rinse with water. In the process of developing about 15 wafers in the due process of this thesis, a few tips could be suggested for a good development process. The designs on the mask could be organized with the larger structures in the centre of the wafer, while the smaller ones can be towards the periphery. The structures may be ideally oriented radially (or at least close) to aid in spin-rinsing of that process is used to clear off solvents. The nitrogen drying process can start from the centre of the wafer and progress spirally outwards to ensure that remaining solvent with dissolved PMMA is dried near the least critical features.

The height of the channels is expected to vary with respect to the exposure dose, the gap between features, development time, and the development conditions like humidity and temperature. Most of these wafers were developed in clean room conditions as follows; temperature = $18.5 \pm 0.5^{\circ}\text{C}$, RH= 41 ± 2 %. The variation in channel heights after development with respect to the exposure dose (in hrs) is shown in Fig. 59.

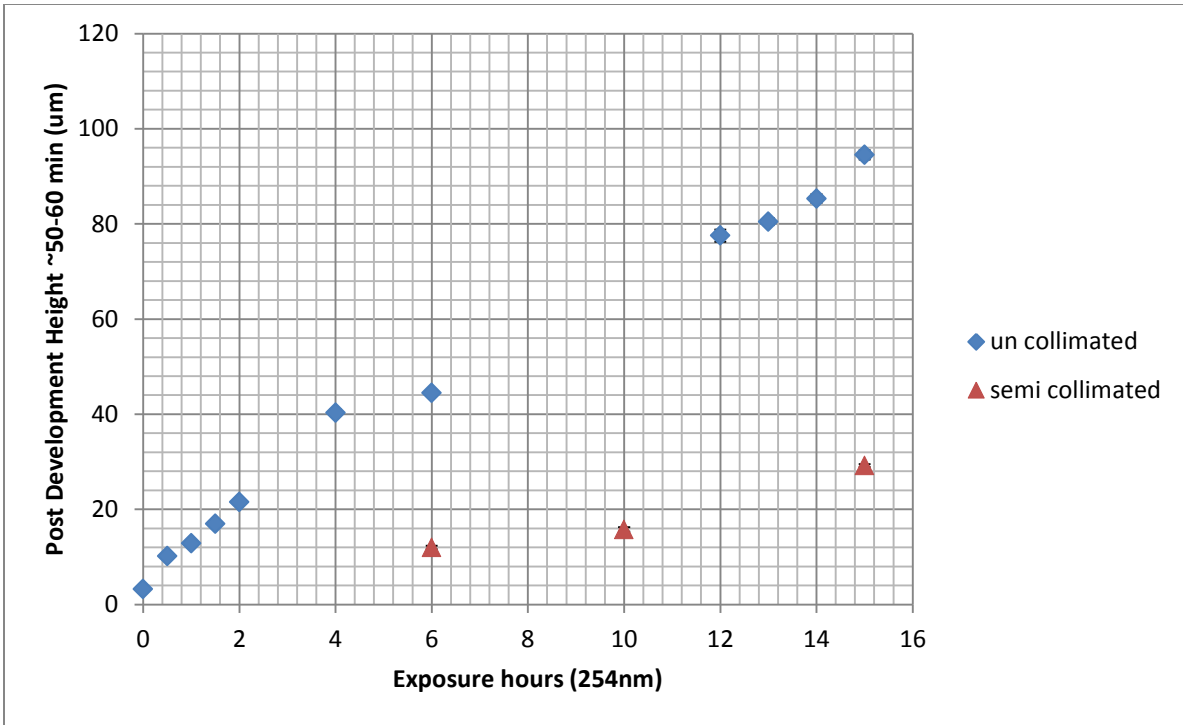


Fig. 59. Variation of channel height with respect to exposure dose (in hrs) [See Appendix C for height details]

5.4 Daughter Mold Fabrication

Once the post development process is completed, The wafers were moved back into the lab. Since the resultant features in the PMMA master mold are positive, a negative daughter mold has to be cast in a thermoset polymer using the PMMA master mold. When narrowing down to the choice of polymers to be used, it is important to consider the high density of structures in the substrate and also that all the structures will be interlocked after curing of the polymer. The overhang cap features are also sub 5 μm , and can easily tear during demolding, if a high modulus polymer or low tear strength polymer is used for the negative mold. Based on all these requirements, a low Shore A hardness addition/ platinum curing silicone rubber, TC-5030 (BJB Enterprises®) was used. It also has a higher tear

strength and durability than Sylgard 184 (11.4kN/m for TC-5030 vs. 2.6kN/m for Sylgard 184), which will ensure an intact one-piece mold.

TC-5030 has a shorter working time (~25 minutes) and a higher viscosity (45,000cps) compared to Sylgard 184, and with the high density structures on the master molds, it requires that the degassing be performed after pouring the pre-polymer mix (Part A+Part B ; ratio: Part A:Part B= 10:1) on the master mold. During the degassing process, the polymer doesn't foam as much compared to polymers like Sylgard 184, which in combination with the high viscosity, can ensure that the polymer doesn't overflow over the master mold for a stock of 20-22gm TC-5030 resulting in a 1.5-1.7mm thick molds. The regular curing process can be completed at room temperature but requires close to 24hrs, which can be catalyzed by baking at ~80 °C , under which case it can be demolded in less than 2 hours. The low shore hardness of the Silicone (~30A) ensures an easy demolding. Other polymers can be cast against the silicone mold to attain a positive replica of the PMMA master mold. Silicones can be cast after performing a silane treatment on the silicone mold [201]. Thermoplastics may be used either in in a solvent casting process or via an injection molding or hot embossing process. But the scope for Geckofluidics is more promising with thermoplastic elastomers.

5.5 Device preparation

5.5.1 THERMOCOMPRESSIVE MOLDING

The prime candidates for thermoplastic elastomers were SEBS Kraton® G1657M and G1645M. Other polymers like shape memory polymers were also tested towards extending the geckofluidics concept with rigid polymers. A typical compression molding process (also referred to as thermo-compressive molding) employs a thermosetting polymer.

It involves placing the uncured thermoset resin in an open heated mold, followed by closing the mold under a high pressure. We employ the compression molding mechanism with SEBS Kraton polymers, with a small modification of using a removeable soft mold.

Pucks were fabricated by melting a few pellets of SEBS on a hot plate at 200 °C on a glass slide. The pellets are dusted pellets, and hence have a small silica content. The puck fabrication process also helps to intermix the silica dust, and thereby reduces the silica dust concentration at the interfacial surface. These pucks may be pre-fabricated and stored at room temperature, or may be prepared and used immediately. The silicone mold is kept in contact with the heated puck upon which a glass slide is placed to ensure a uniform distribution of the applied load. The hot plate setup is under a Branson ultrasonic welder (2000X f/aef), which can regulate the applied load under the ‘hold force’ load setting. The ultrasonics cannot be turned off completely, but the lowest weld time setting of 0.01 sec is small enough to render the applied ultrasonic weld power insignificant. A controlled load can be applied depending on the required thickness of the backing layer and the height of the fibers. Loads as low as 20 lb have also been able to fill the molds, while higher loads will yield thinner devices. Thinner devices of SEBS are preferred as the backing layer thickness inversely affects the adhesion strength [248], and more area of devices can be produced with the same volume of material. The silicone molds can deform under very high applied loads, hence moderating the applied load to ~100lbs should be reasonable enough to minimize the deformations. After the load is removed, the glass-mold-polymer-glass assembly is moved to a cooler surface. After attaining a room temperature, the polymer samples can be peeled off from the silicone mold, and can be bonded to the desired substrate immediately (after punching holes for ports, if required)

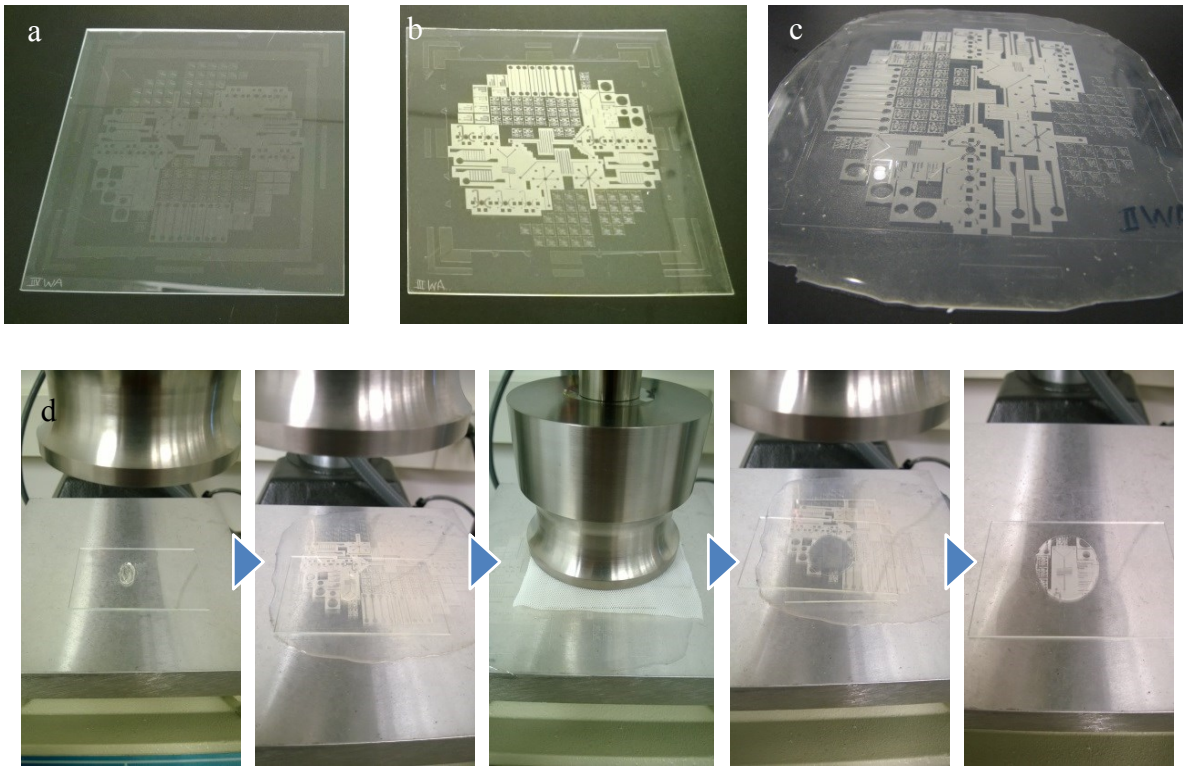
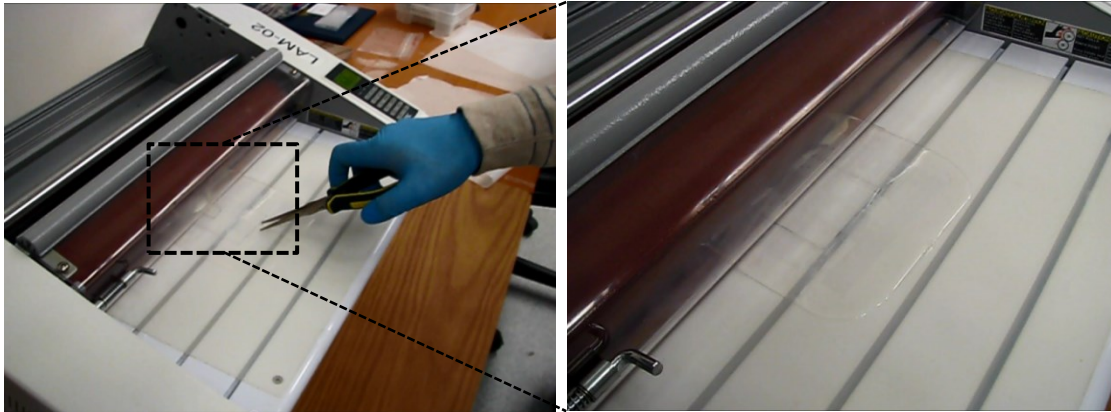


Fig. 60. Visual depiction of the fabrication process. a) SU-8 patterned PMMA Wafer. b) UV exposed, post etched PMMA wafer, c) silicone daughter mold d) thermo-compressive molding process

In order to create a rigid backing for the geckofluidics devices, thick pucks of polystyrene, ~2mm thick were fabricated by melting polystyrene petri dishes. Post cooling of the thermo-compressive molded SEBS devices, the silicone mold- SEBS composite is brought in contact with the PS puck on the SEBS side on a hot plate at 200 °C. A load of ~100lbs was applied via the ultrasonic welder for ~20 sec. The composite structure is then cooled, after which the devices can be peeled from the silicone mold for subsequent use. The device geometry and cross section is as observed under an SEM in Fig. 62(a,b).

5.5.2 ROLLER THERMOCOMPRESSIVE MOLDING

The molding process has also been tested with a roller based thermo-compressive molding technique in EVA. Proform EVA has a melt flow temperature $<100\text{ }^{\circ}\text{C}$, while the melt flow temperature for SEBS would be $\sim 220\text{ }^{\circ}\text{C}$. The laminator had a maximum temperature setting at $160\text{ }^{\circ}\text{C}$ which made it difficult to test SEBS so the EVA is used as proof of concept for the technique. The polymer was preheated at $160\text{ }^{\circ}\text{C}$ on a hot plate and then put through the laminator at $160\text{ }^{\circ}\text{C}$. The laminator had two sets of rollers. After the glass-EVA-Silicone mold-glass composite emerges at the second roller, it is moved to a cooler surface, where after attaining the room temperature; it could be demolded, and bonded. The typical roller embossing speeds are under 2mm s^{-1} , as stated earlier, while the lowest speeds operated under for this roller compressive molding were $\sim 3.5\text{mm s}^{-1}$. The higher operating speeds yielded almost similar type of filling. This demonstration sets a tone for the possible use of this process for large scale serial manufacturing, compared to the batch processing as earlier, and at a faster processing speed.

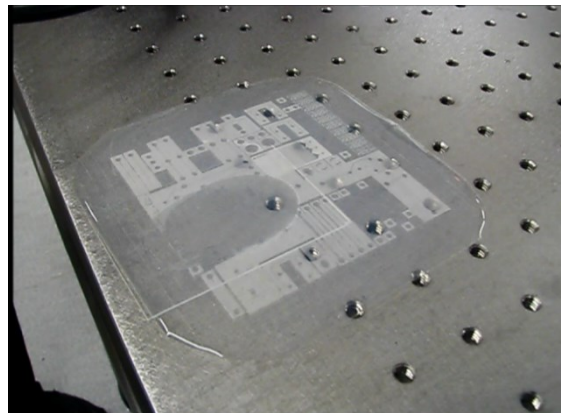


(a) Loading to the roller



(b) Exit from Roller 1

(c) Exit from Roller 2



(d) Cooling to room temperature before demolding

Fig. 61. Roller- Thermo compressive molding

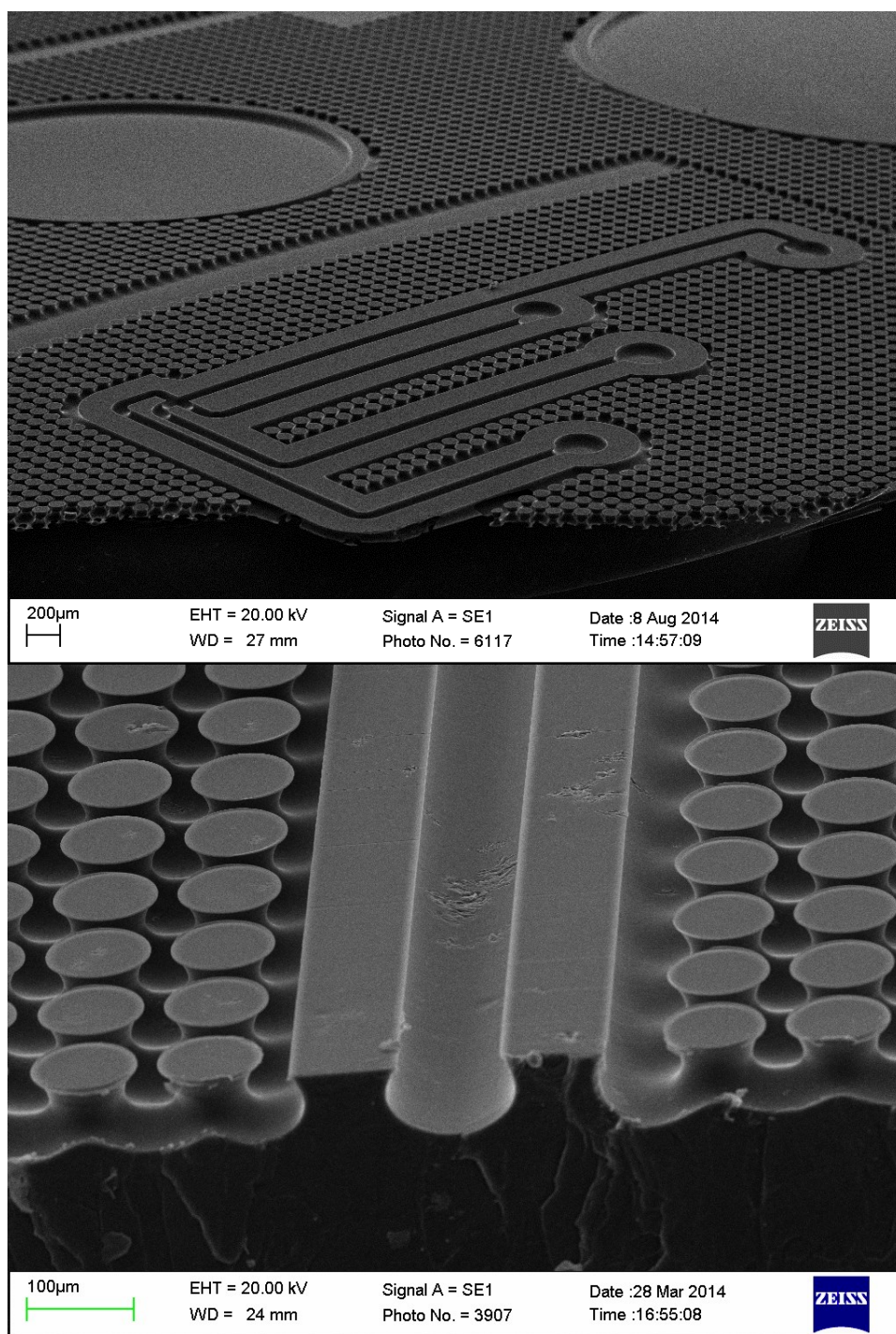


Fig. 62 (a) SEM Image of a Geckofluidic device replica in PS (b) cross section of a geckofluidics channel

5.6 World to chip interface manufacturing

The world to chip interfaces consists of a wide variety of options, of which only a few have been standardized. Most of the simpler options provide interconnect which are either press fit, screw fit or adhesively bonded and integrated manufactured ports, apart from the advanced options which involve magnetic and screw holders and silicon micromachined interconnection modules. This thermocompressive molding technique may also be attractive for manufacturing double sided adhesive integrated microfluidic channels. The press and the screw fit connectors require machining into the backing of the wafer, while the adhesively bonded and some press fits interconnects, still require some thickness on the backing to incorporate the metal pins. Considering the typical thickness of the Geckofluidic devices, it is necessary to develop a world to chip interface for these devices. The manufacturing of these devices involves using Geckofluidic blisters either patterned directly on the backing layer or bonding a geckofluidics blister onto a rigid material, with holes drilled through the material into the blister. Patterning a geckofluidics blister on the other side of the device involves fabricating the device and the gaskets in a single thermocompressive molding step. The SEBS puck is sandwiched between two layers of silicon master mold, one having the design negative, while the other with the gasket negative. The traditional methods of press fitting metal pins can be used for applications involving low pressures since, the adhesion strength varies inversely with the thickness of the backing layer [248]. These interconnects could be interesting for application involving sequential operation, wherein interconnects could be reversible interface with the chip, and then can be transferred to another chip. Since SEBS is hydrophobic, and has been demonstrated for applications under water[201], any reagent contact with the interconnects should not affect performance, unless with reagents that have a significantly lower contact angle.

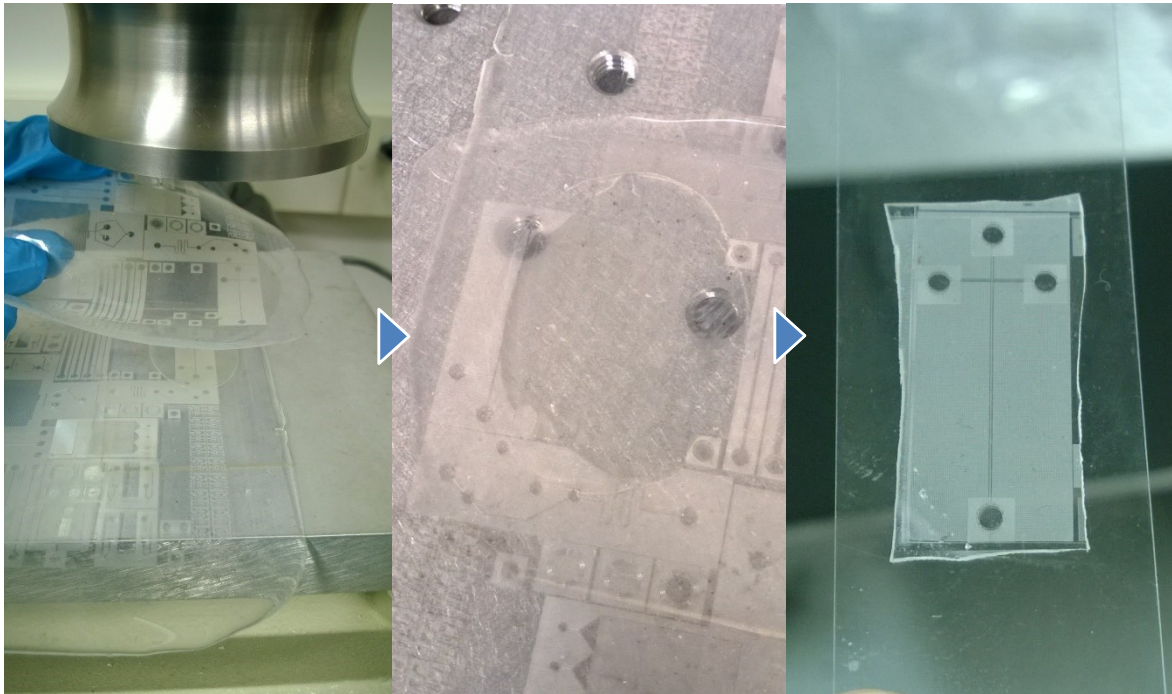


Fig. 63. Dual master thermocompressive molding.

A few types of interconnect were also fabricated by thermocompressive molding of replica molding of desired dimensioned features and also a few standard size connectors. Blisters may also be patterned on them, in a similar dual master thermo-compressive molding process. Holes are punched into the interconnects using a biopsy punch, which are available in various dimensions and may be selected based on the subsequent interconnection feature, a metal pin or polymer tube.

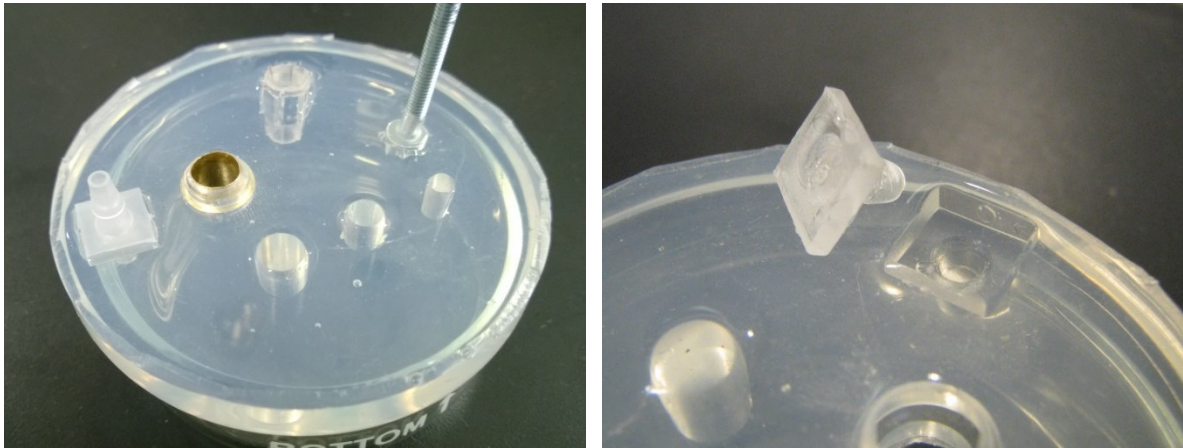


Fig. 64. (a) A casting with some of the molded features (b) Dual master thermocompression molded interconnect with a patterned gasket

5.7 Conclusion

A detailed manufacturing process has been demonstrated in this chapter via the three main fabrication steps, the fabrication of the PMMA mastermold, the replica molding in Silicone and the thermocompressive molding. The challenges associated with spin development have been addressed via the use of a mixture of SU-8 developer and IPA solutions. An mix of 1:1 ratio was identified to be an appropriate recipe for a clear development.

The thermo compressive molding process has been demonstrated with the flexibility of including the PS stiff backing layer. The roller thermo-compressive molding process has also been demonstrated via a proof of concept demonstrated in EVA polymer. This method has ample scope to be developed into a serial mass manufacturing process. The extension of the thermocompressive moldingwith dual molds, can also help pattern channels and world to chip interfacing features in a simultaneous operation. The demolded samples have been demonstrated for mainstream microfluidic applications in the following chapter.

CHAPTER 6: TESTS AND APPLICATIONS

6.1 Introduction

While adhesive tape based microfluidic systems were deemed appropriate for non-specialized users[34], Gecko inspired dry adhesives provides tools for specialized microfluidics users. Occasional references in the previous chapters provide a insight into the typical scope and application of microfluidics, this chapters illustrates the adaptation of geckofluidic devices to replicate the functionality of those typical microfluidic applications. All these applications are independently or integratively well characterised , but the attempts in this chapter only seek to demonstrate a proof of concept scale of the underlying principles on the geckofluidic platform. Flow driving modes like electroosmotic flow are governed by material properties and the geckofluidics concept doesn't interfere with it, but the flexibilitiy of integration and reusability, the geckofluidics concept provides is noteworthy and hence demonstrated.

A high level classification of results was to demonstrate the use of Geckofluidic devices for both pressure driven microfluidics and non pressure driven microfluidics..

6.2 Non pressure driven systems:

6.2.1 PINCH INJECTION IN A CAPILLARY ELECTROPHORESIS DEVICE:

Capillary Electrophoresis has been one of the most efficient and simple separation technique to separate diverse analytes, like small molecules to proteins , DNA and viruses in presence of a high electric field. [249, 250] The separation occurs dues to differences in

charge to mass ratio, allowing particles of higher ratio to separate ahead of the low ratio species. The use of fused silica capillaries or microfluidic channels helps in the dissipation of the heat generated due to high electric fields and also utilizes very small sample volumes, thereby facilitating handling of biological samples.

Precise short plugs of the sample solution are separated out for detailed analysis of the sample in a capillary electrophoresis device. This is achieved in a process called pinch injection, which involves generating creating a voltage bias in order to pinch a fraction of the sample driven by electro osmosis. The electroosmotic flow drives streams of sample (S) and buffer (B) from two independent inputs and is driven to sample waste (SW) and buffer waste (BW) ports respectively. The plugs of the sample input are pinched towards the buffer waste by the creation of a high magnitude voltage bias across the buffer and buffer waste. In specialized tests, fluorescent dyes and voltages as high as 2kV would be used.

The fluidics were manufactured in SEBS Kraton G1657, via thermo-compression molding. The adhesive infrastructure utilising Gecko inspired adhesives were 20 μ m square micropillars as in Fig. 65 . These geckofluidics devices were bonded on to a polystyrene petri dish with gold electrodes patterned on it. The electrodes were patterned on a denton gold sputter unit via a laser cut mask which had openings for the electrode. A 240 sec deposition would yield approximately ~15-16 nm thick electrodes. Since regular metal solders have a melting point higher than that of polystyrene, it is highly likely for the polystyrene at the gold and polystyrene interface to melt and thereby crack the gold film. In order to avoid this, Fields metal, a low temperature melting metal, was used with a low temperature setting on a hot glue gun to solder the electrodes to copper wires[251]. [See Appendix D for details] The device set up, is as in Fig. 67 (a).

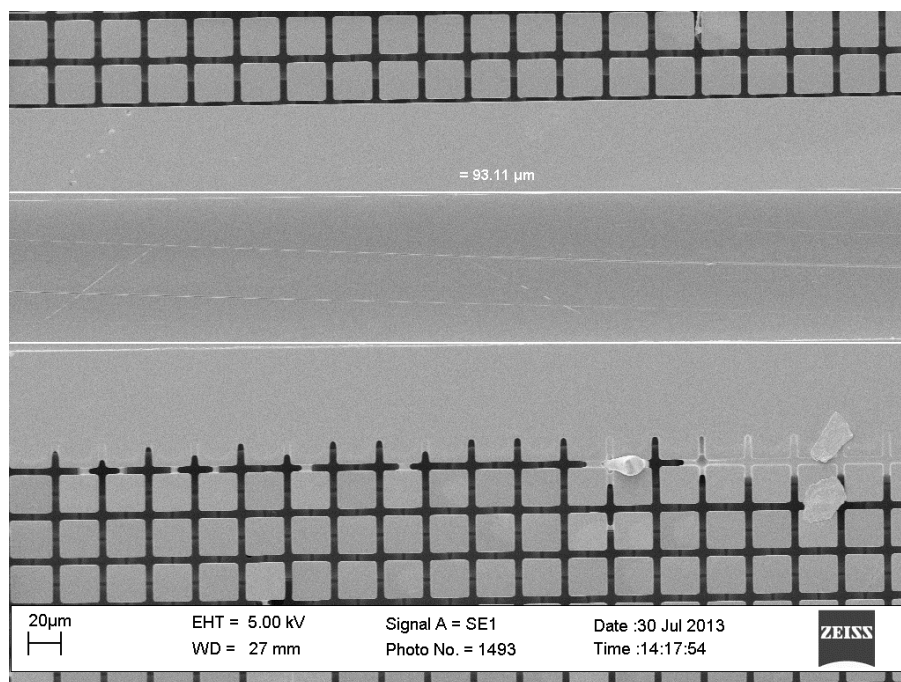


Fig. 65. A Geckofluidic channel with square tipped fibers

The pinch injection process demonstrated here is similar to the technique demonstrated by Chinna *et al.* [252] with a few modifications. Since characterizing the process or material was not the prime motive, a proof of concept demonstration was appropriate and attempted with minimal instrumentation. Food coloring dyes with Sodium borate was used as a sample and Sodium borate (pH: 9.5) was used as a buffer. A manual switching of voltages required larger times for the voltages at each well to be changed, which prevented creation of small plugs, hence a high magnitude negative voltage was applied across the buffer and buffer waste. The magnitudes of voltages used by Chinna *et al.*, were beyond 400V, which was the limitation of the voltage source being used. This required using a small negative pressure to aide the pinching for sample injection, similar to a process demonstrated by Zhang *et al.* [253]. The equilibrium potential can be achieved in symmetric geometries, but, in the current context of the design, which is a part of a larger

design, the ports had to be re organized to achieve an equilibrium potential at the intersection. The modified conceptual design is as illustrated in Fig. 66.

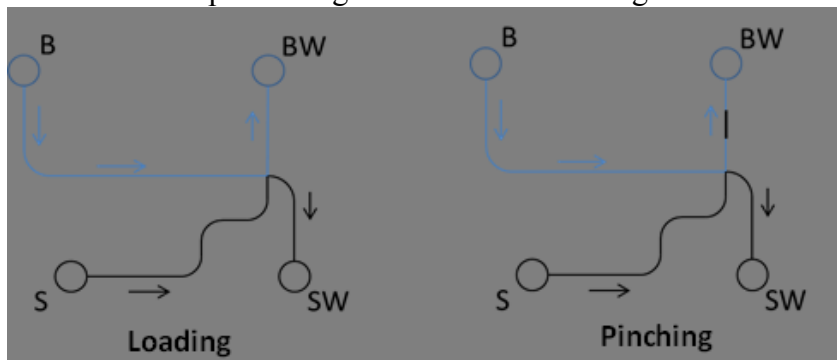


Fig. 66. Conceptual illustration of pinch injection

During the sample loading phase, a voltage of 200V was applied across the sample and the buffer input, while the sample waste and buffer waste were kept at zero. Once a steady state was achieved, a negative voltage of -400V was applied on the buffer waste terminal to pinch the sample into the buffer waste channel. The pinch injection process is as illustrated in Fig. 67(b).

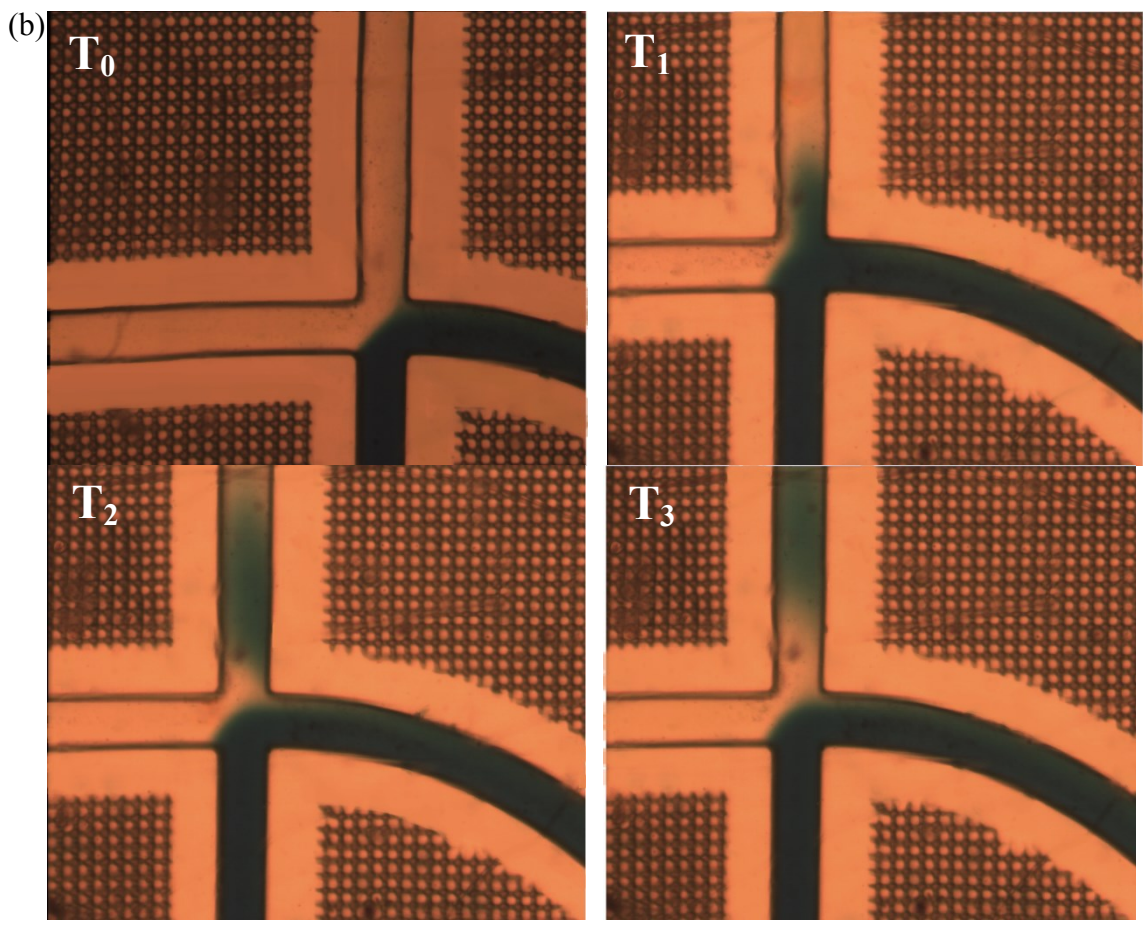
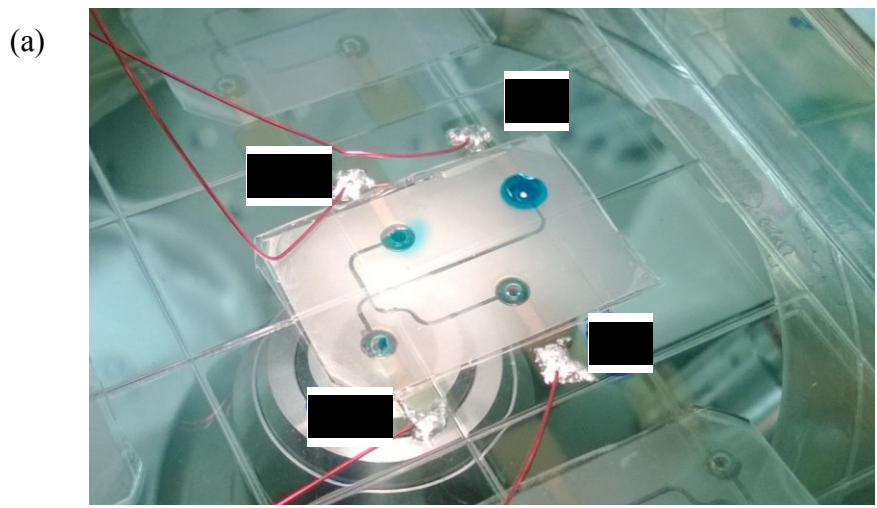


Fig. 67. (a) An assembled Capillary Electrophoresis Chip (b) Demonstration of pinch injection

6.2.3 FLEXILE MICROFLUIDICS

Most geckofluidic devices can conform to irregular yet smooth surfaces, and can be adapted for integration with flexible electronics and any other surface conformal microfluidic applications. They may also be used for stretchable electronics.

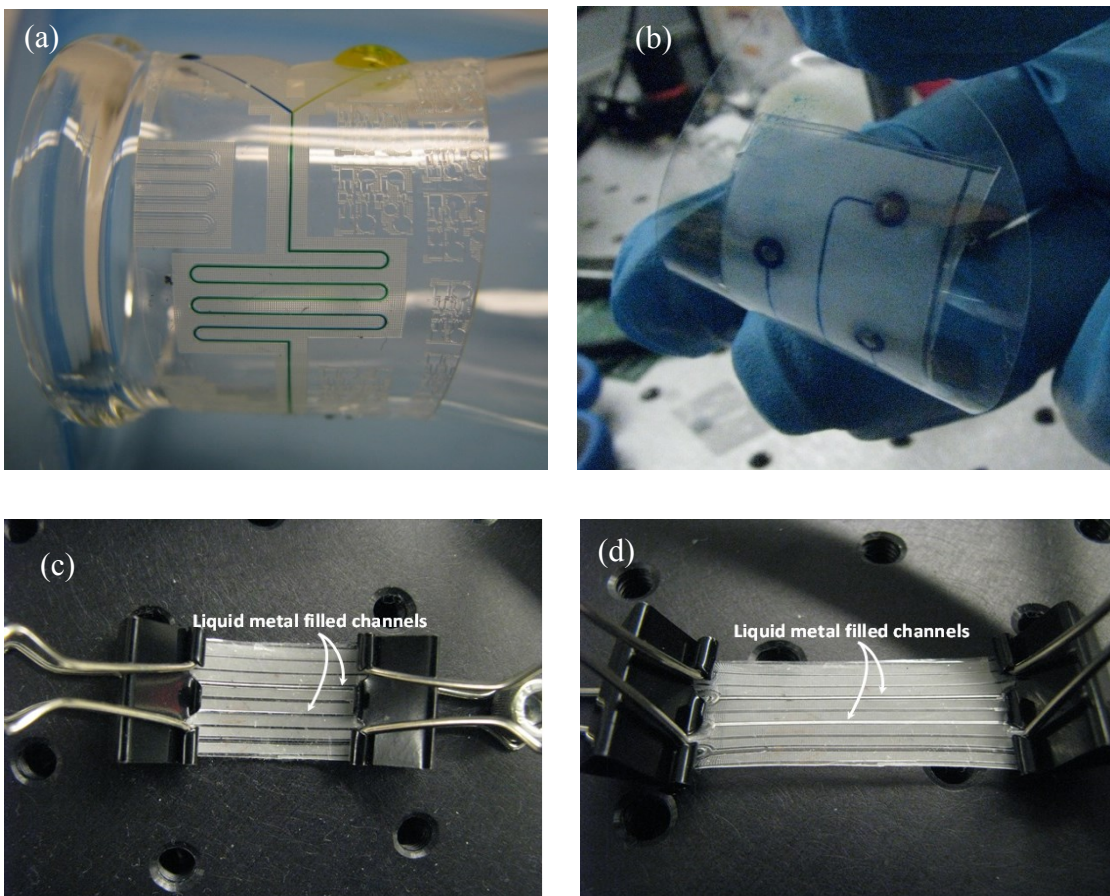


Fig. 68. (a) A micromixer on the neck of an erlenmeyer flask (b) Flexible electrodes patterned on thin PS, integrated with a CE device (c) Ga-In (liquid metal) filled channels for stretchable antennas.

6.2.4 INTEGRATION WITH MEMS

In this work, geckofluidic devices were developed for a MEMS based cell gripper. The study involves studying properties of various cells on a polyMUMPs chip, on which cells were pumped using dielectrophoresis. Since the pressures in the chip are minimal, the supporting adhesive fibers were kept to a minimum, and were avoided at places with thick wires. The bonding support and the channels are defined by the gasket, which helps prove the robustness of the concept.

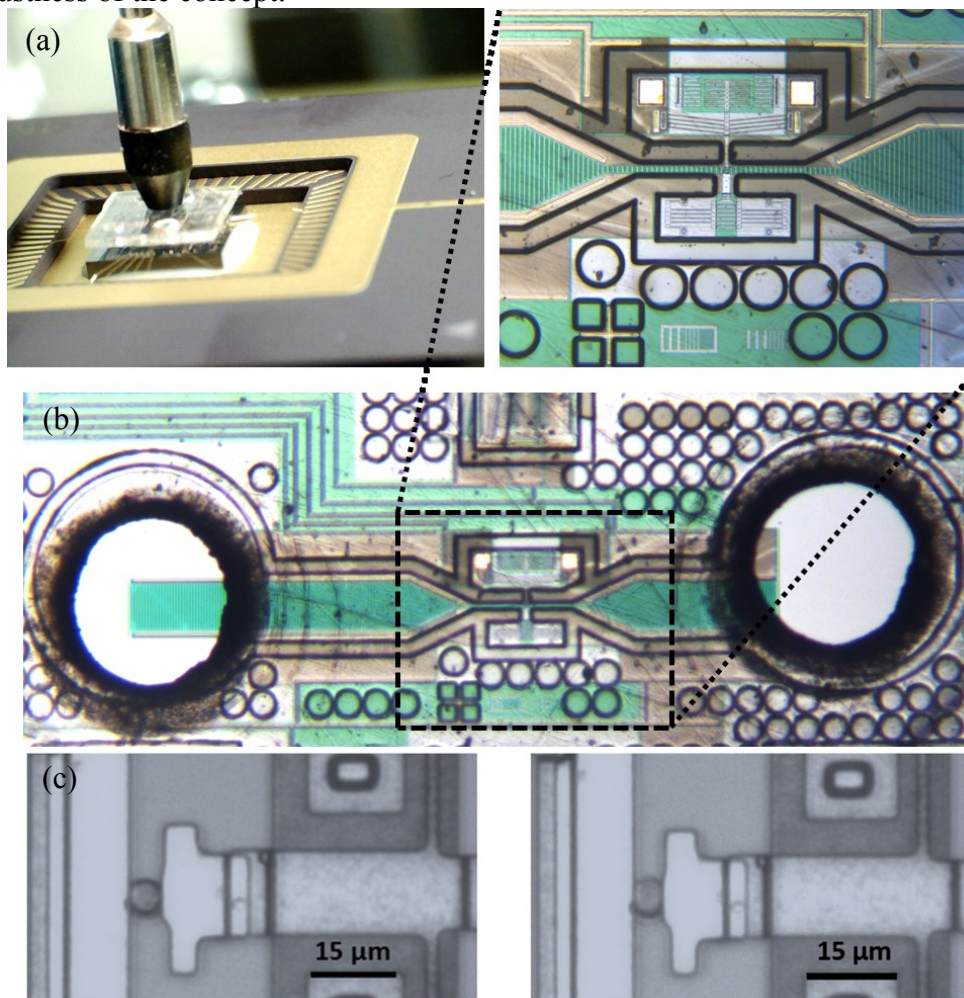


Fig. 69. (a) Assembly of the MEMS chip with the geckofluidic channel. (b) The assembled device an enlarged view of the MEMS gripper section [Partially adapted from [234]](c) the gripper in action (image courtesy: Dr.Stephan Warnat, Dalhousie University)

6.3 Pressure driven microfluidics:

6.3.1 BLISTER BURST TEST

Considering the typical adhesion strengths of Gecko inspired adhesives, it was most logical to extend the scope of geckofluidics to pressure driven microfluidics. Towards studying the feasibility for pressure driven microfluidics, a study was conducted to identify the maximum pressure sustenance of a geckofluidic blister. The blister was a simple o-ring formed of the continuous gasket and is fabricated in Kraton G1657, G1645 and shape memory polymers. Also considering the presumption of having the flexibility to use with different contact elements potentially of different materials on a Lab on a chip device, it was important to test this adhesion with different interfacing materials. A normal pull off adhesion strength for different interfacing materials like glass, gold and polystyrene has been conducted in an earlier work with G1657 and was measured to be 1 MPa, 1.25 Mpa and 1.4 MPa [229]. The dimensions of the blister were, blister diameter: 3mm; fiber cap thickness: 3.2 μm , fiber cap diameter: 100 μm , height of the fibers: 72 μm .

The blisters were mounted on the suitable substrates. The holes were drilled in the polymer substrates, while for silicon and glass, the holes were made through the blister. The pressure supply was routed through the blister via a pressure sensor (Measurement specialities™-M5100). The pressure sensor has an input from a LabView controlled power supply (National instruments™ PXI 4110), and the output connected to a Digital Multimeter, (National instruments™ PXI 4070), interpreted by LabView(Fig (55(b))). Before starting the test, a calibration curve was established to correlate the input pressure with the read voltage, using known regulated pressures, interpreted by a mechanical guage device installed on the air supply supply line. The input to the blister were manually held, to prevent any detachments from the interconnections. All the blisters tested had a rigid backing, as it was established that the blisters would begin to inflate(Fig. 55(a)) at pressures as low as 10 psi and eventually fail at ~20psi against PMMA and ~40psi against G1657. During the process of the test, a secondary confirmation test was employed by means of surrounding the gasket with water, to include a visual confirmation of leak.

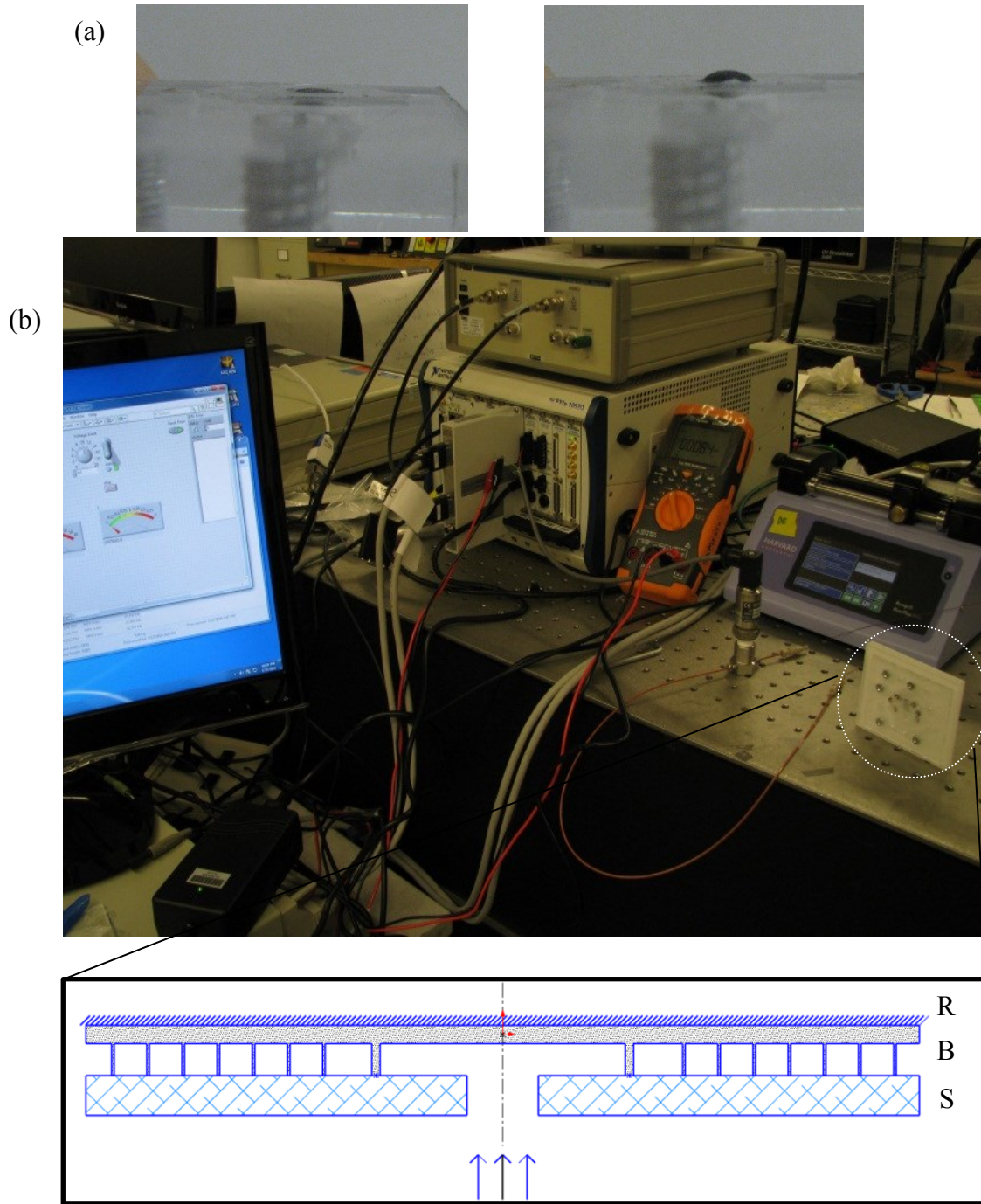
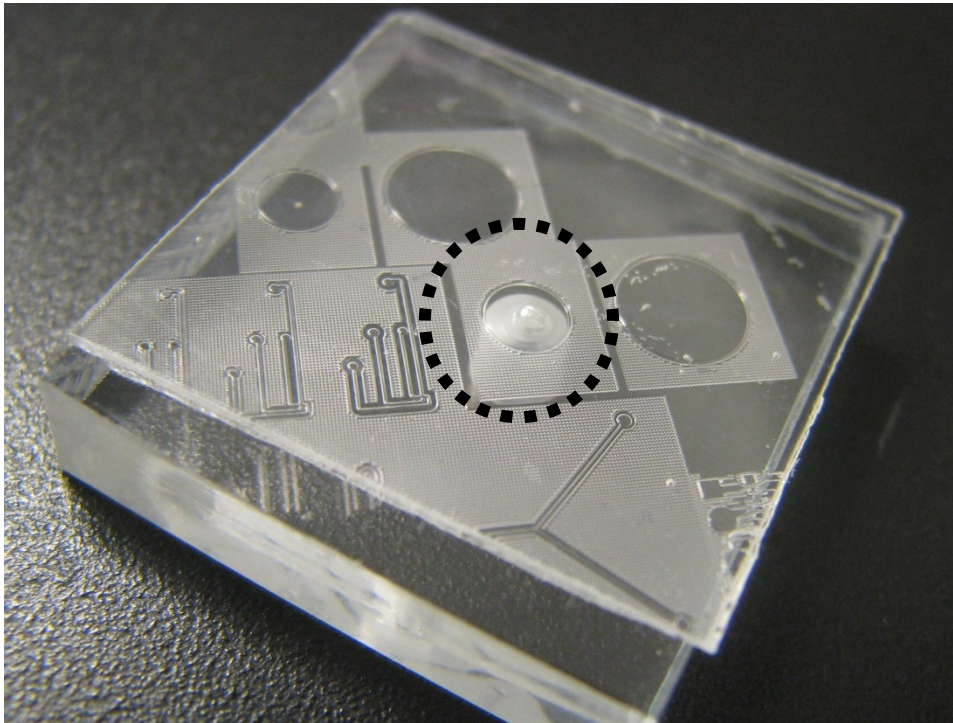


Fig. 70. (a) Inflation in Geckofluidic blisters (b) Set up of the burst pressure test (inset: Schematic of the blister arrangement (R)igid backing- (B)lister- (S)ubstrate) [Partially adapted from [234]]

(a)



(b)

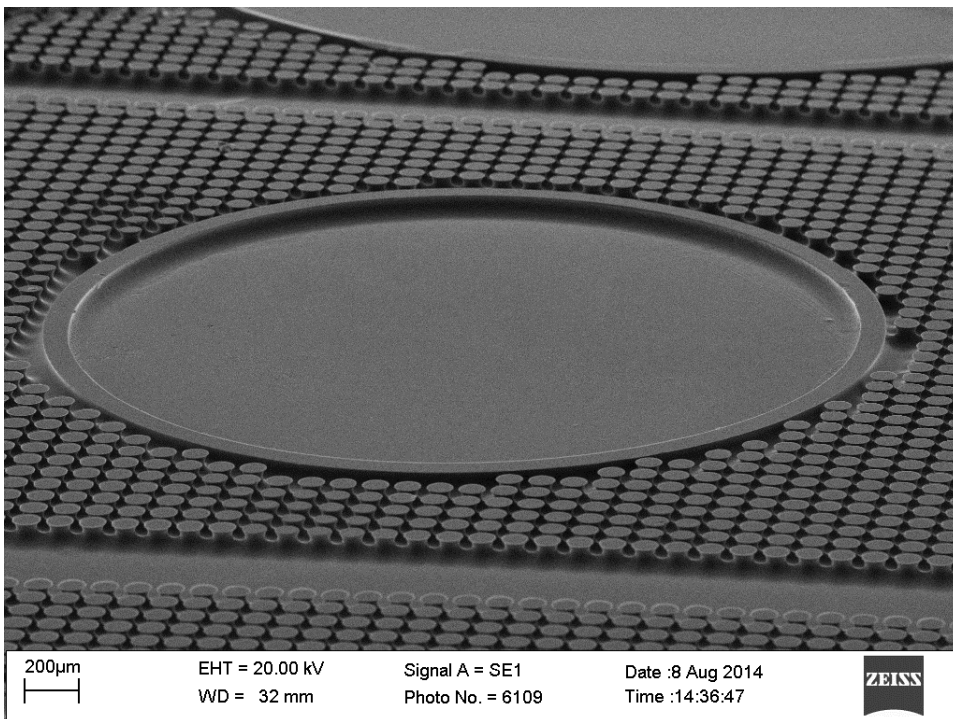


Fig. 71. (a) The blister arrangement on the substrate (b) SEM of the Blister
128

The geckofluidic blisters demonstrate a wide range of adhesion strength depending on the interfacing material. Pressures as high as 95psi were observed for G1657 interfacing with G1657, while the maximum reported strength under reversible SEBS bonding was 20-30psi [86]. While this high a pressure endurance may appear as an irreversible bond, the devices can be demolded under a mixed application of normal and shear force (The PS backing would crack in the process of demolding). Also the observed maximum pressures are limited by the pressure source availability and may be slightly higher than the observed values of 95 psi. It was also observed that, a short annealing step, at 85 C for 5min, helped to improve the adhesion by 40-75%, in different interfacing materials. Irreversible bonding may also be achieved at similar temperatures but under longer time durations[86]. The maximum reported bonding pressures under reversible bonding for PDMS is ~5psi and the irreversible bond strength of 74 ± 2 psi [130].

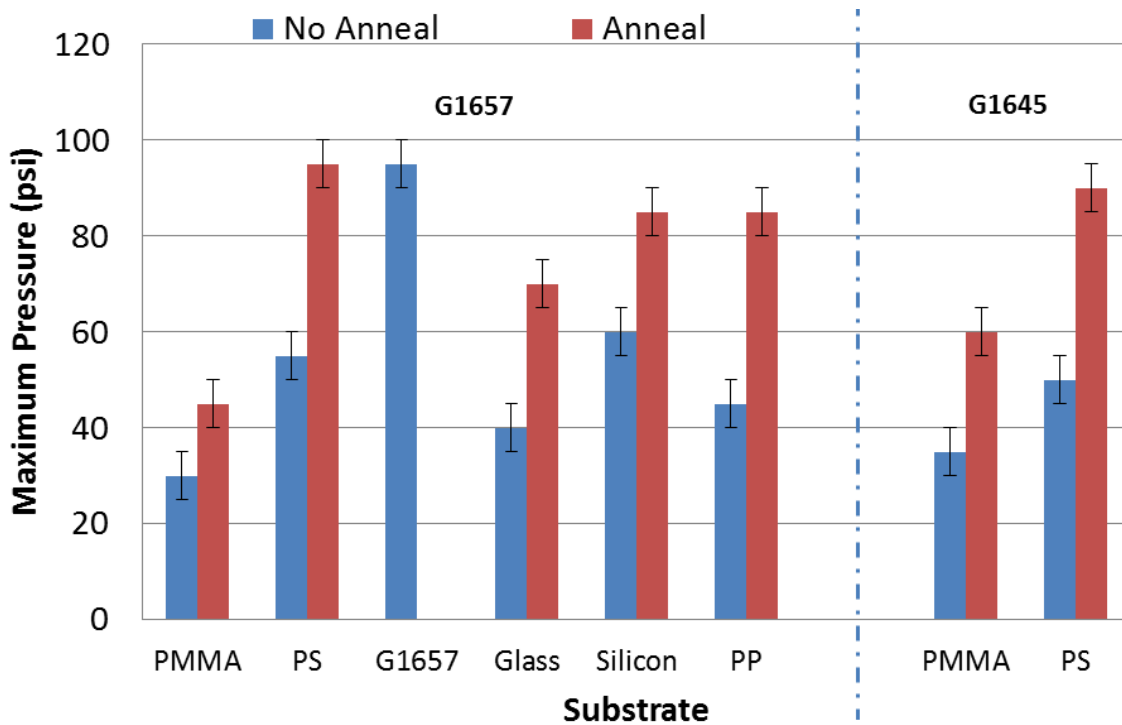


Fig. 72.: Burst pressure test results against different substrates.[Partially adapted from [234]]

The burst pressure tests were also performed with shape memory polymers, MM2520 and MM4520 [254]. These polymers have been shown to demonstrate adhesion at temperatures higher than T_g of the polymers.(Babak Soltannia and Dan Sameoto, *Adhesion Society Meeting 2015*). These polymers appear to have some adhesion after being bonded at temperatures of T_g+20 °C, but tend to instantaneously debond under the application of pressures as low as 10psi at room temperature.. Hence these polymers may be attractive for non pressure driven systems, but are not ideal for pressure driven microfluidics.

While the adhesion strength is variable depending on the structural material and the interfacing material, the effect of gecko adhesives is quite evident, with at least a 200% increase over a nonstructured surface. The maximum reversible adhesion with glass (~70psi) is almost on par with the reported irreversible adhesion of PDMS on glass, under which the failure is either by tearing or the failure of interconnect. Based on this observed data, Geckofluidics presents a strong case for use with pressure driven microfluidics.

6.3.2 MICROMIXING:

Mixing in macro environment is achieved by turbulent flow. But, as stated earlier, in microfluidics, the fluid flow regime is laminar, which creates challenges for mixing. Mixing in this case is achieved purely by diffusion. Various methods have been proposed for micromixing, using both active and passive methods [255-257]. Apart from the properties of the liquids, the geometry of the channels also governs the rate of mixing. Many complex geometries have been tested and have established that introducing irregularities in the channel surface and / or the geometry improves mixing via passive methods. A simple such irregularity is a serpentine channel, which has been demonstrated in Fig. 74. The channel height is $\sim 73\mu\text{m}$, and the channel width is $\sim 100\mu\text{m}$. The net length of the micromixer is $\sim 100\text{mm}$ with the serpentine section being $\sim 65\text{ mm}$ long. The maximum pressures haven't been qualified, but a difference in mixing can help identify the scale of pressure variation.

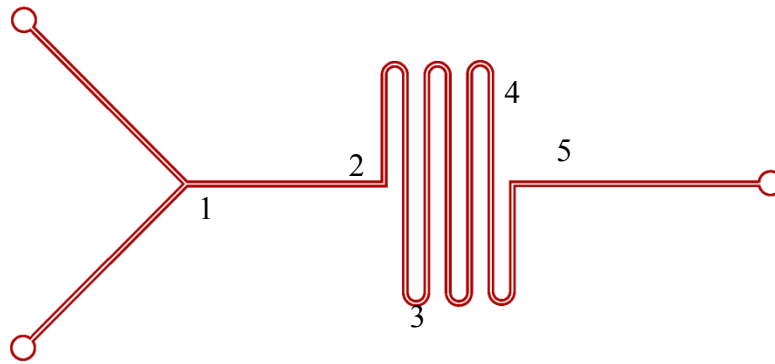


Fig. 73. Micromixer with focus regions

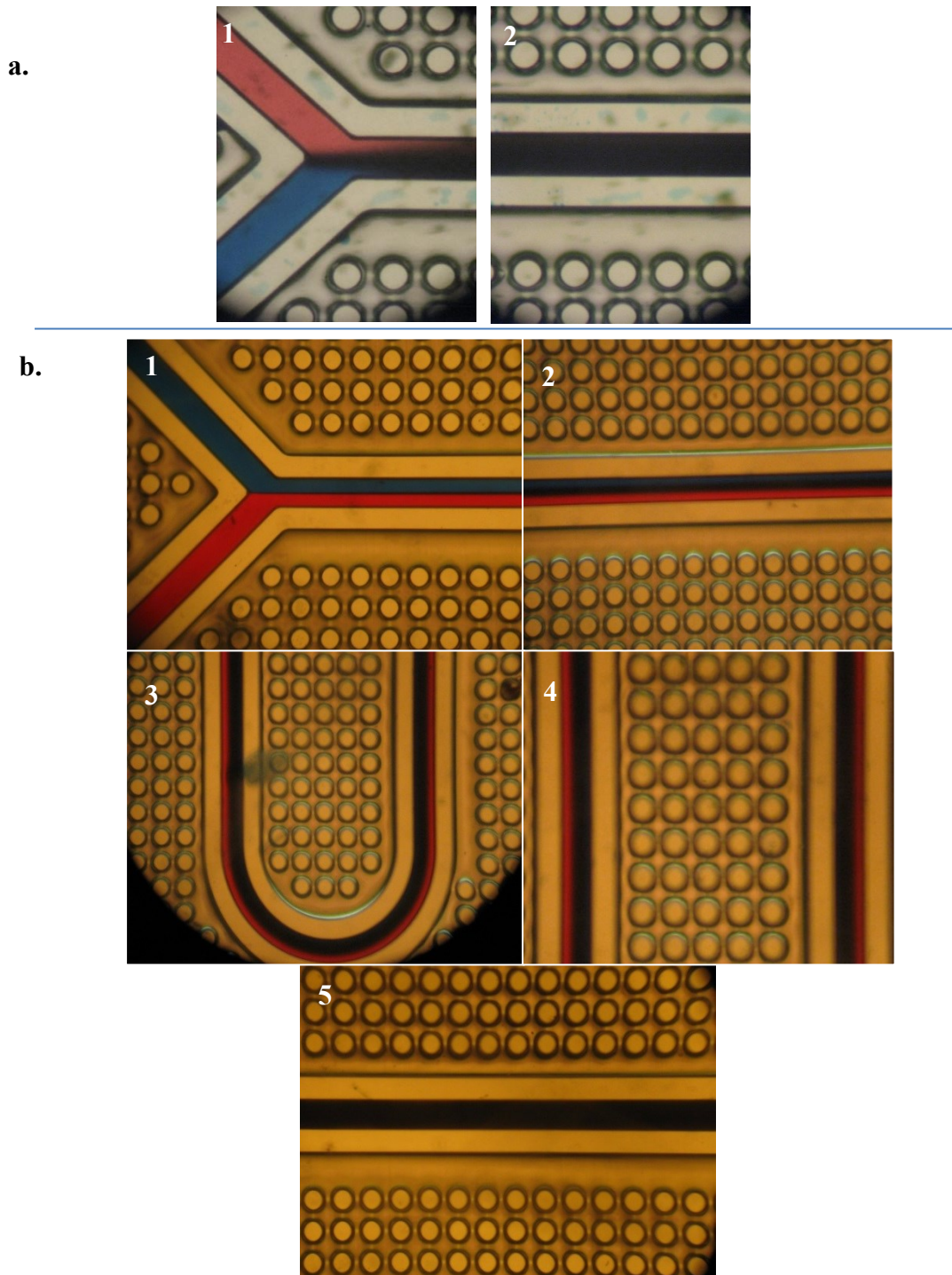


Fig. 74. Mixing in a Y-channel with a serpentine section – (a) High flow rates, (b) Low flow rate (at specified focus regions)

6.3.3 DROPLET GENERATOR

Droplet microfluidics is one of the more promising modes of engineering reagent interactions in microfluidics. Both samples and reagents are introduced into microfluidics devices as droplets in a driving inert medium like oil. Small amounts of reagents of the order of picoliters to femto liters, can be introduced as droplets and mechanisms like mixing and chemical reactions can be precisely achieved. They are lucrative for single cell studies as single cells can be introduced into droplets with precise amount of reagent[258]. Air droplets have also been introduced into liquid driving medium to study the gas dissolution rates [259]. Bubble logic was conceived by Manu Prakash *et al* which looked into performing boolean computations with droplets [260]. Creations of droplets requires a moderately high flow rate which requires reasonably high pressures to drive the fluids due to the channel resistances.

A very long serpentine channel with small intermediate constrictions of ~10 microns created the resistance and 3 channels converging into 15 micron channels formed the '+' bubble generator. Of the three channels, one was formed by two pre-intersecting channels, while the other 2 were formed from one diverging channel. The three channels were connected to three inputs on two syringe pumps, as in Fig. 75(a).

Flow rates as high as 250 μ l/min were tested but the bubbles generated were too fast to be captured by the available camera. The results in Fig. 76. are from experiments carried out at 2.5 μ l/min (Q_{water}), and flow rate ratios($Q_{\text{oil}}: Q_{\text{water}}$) of, 2:1 and 1:1 and 4:1 for $Q_{\text{water}}=5\mu$ l/min. The coalescence also varies with the sizes and flow rates of the droplets. The generated droplets are also evident at the exit tube, as in Fig. 75.(b), and may be stored for any subsequent use.

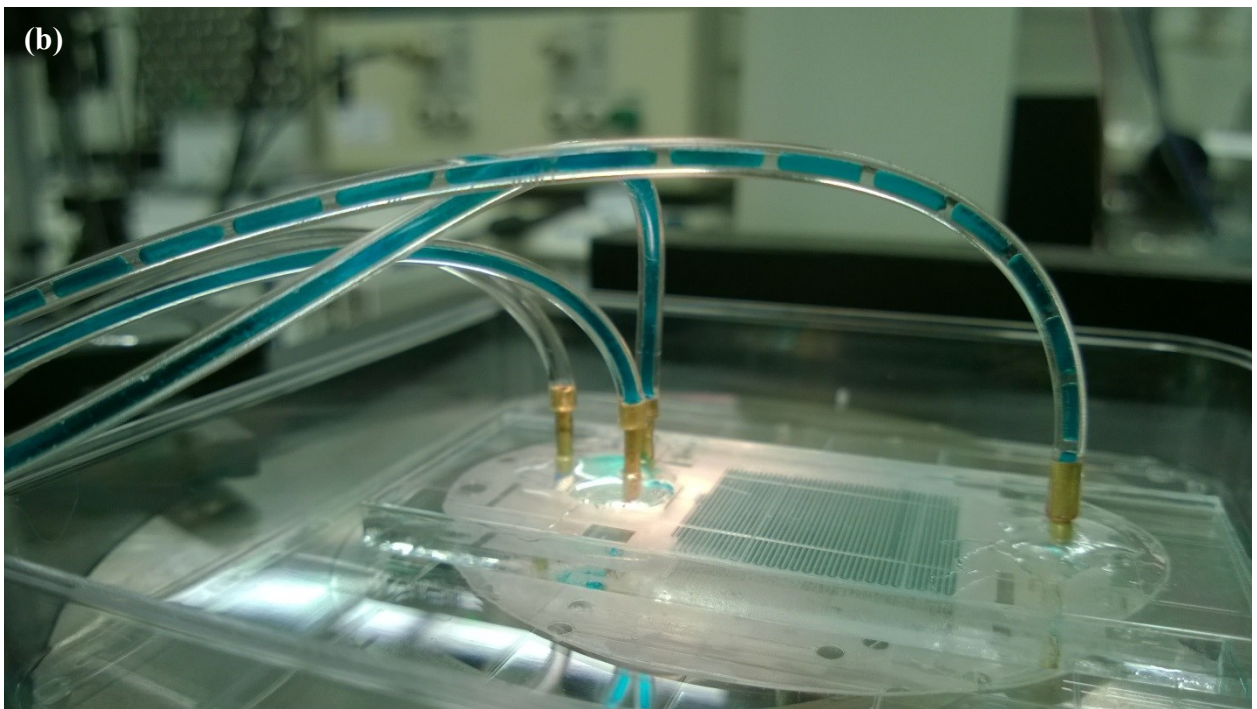
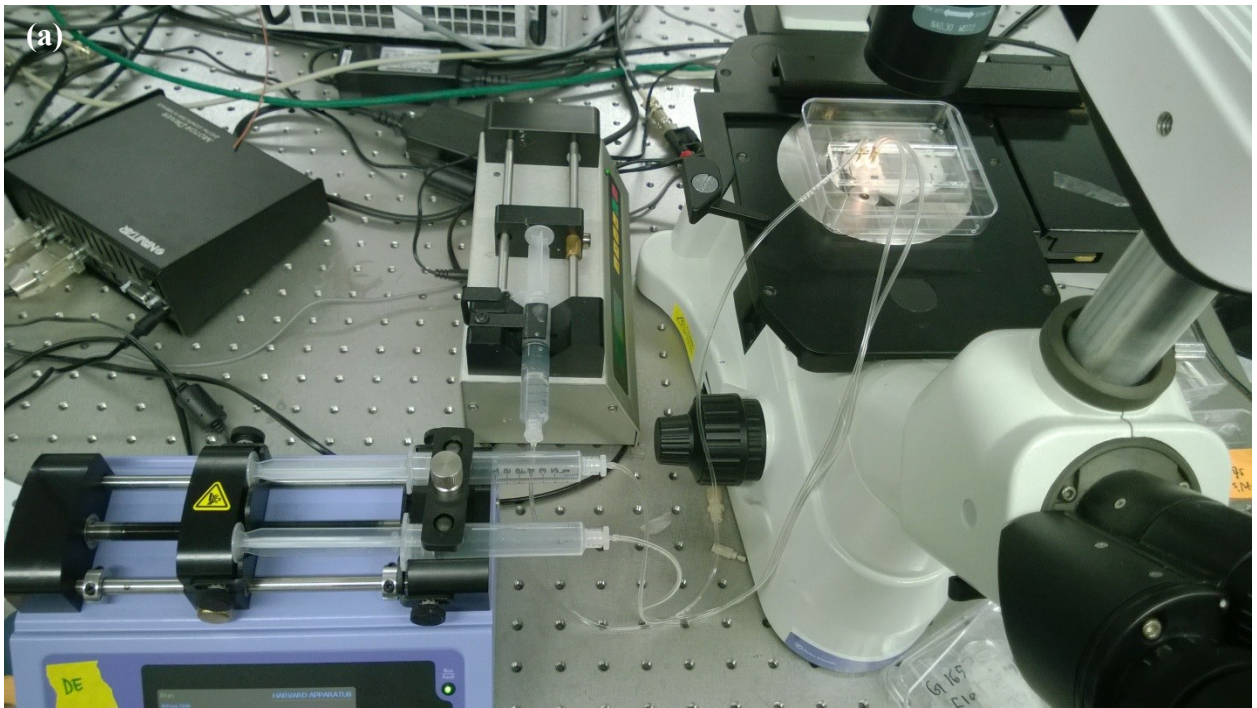


Fig. 75.(a) The droplet generation equipment set-up (b) the droplet generator chip[Partially adapted from [234]]

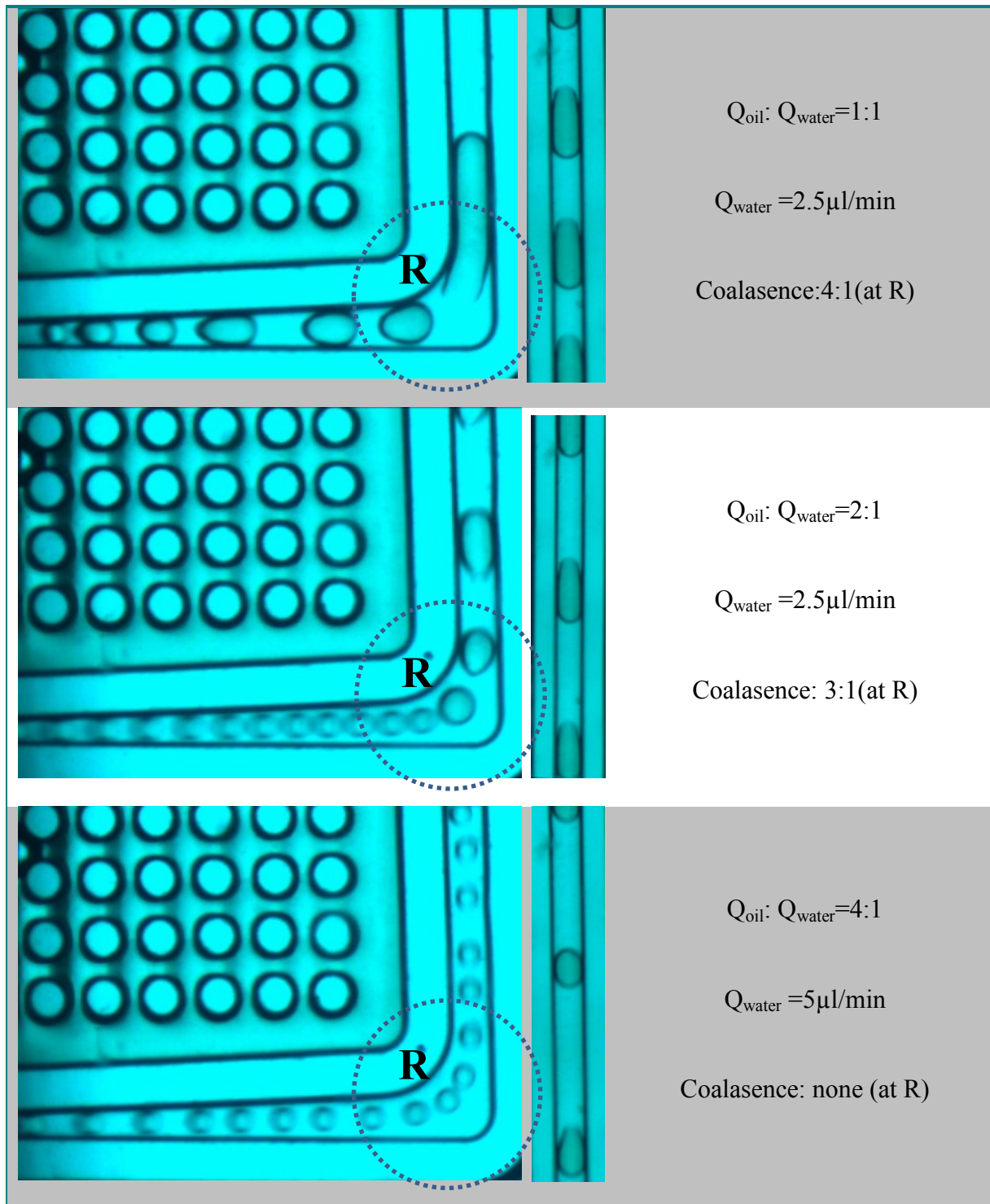


Fig. 76. Droplet Generation and coalescence results[Partially adapted from [234]]

6.3.4 VALVES

One of the underlying criterion for using thermoplastic elastomers was to allow for maximum mechanical functionality to the microfluidic devices via the provision for valves. The valves proposed by Groover *et al.*[30] and Unger *et al.* [29] have a wall with deflectable membrane below which needs to be deflected to overcome or generate the valve resistance respectively and are often challenging to integrate with microfluidic systems. While most of the valves can be actuated with smaller pressures, actuating doormat/diode style valves requires higher pressures.. Diode valves similar to Groover *et al.*, integrated with gecko adhesive infrastructure were fabricated using the method, described earlier in this thesis..The thin intermediate membrane was fabricated by spin coating SEBS (Kraton G1657) dissolved in hexane on a glass slide.The membrane can be easily transferred because of the surface energy variations between glass and SEBS. The assembly of the main channel and the underlying cavity was carried out under a microscope after appropriate alignment. The valves were actuated manually using a syringe (~30psi at maximum compression). The results are as illustrated in Fig. 77. The actuation of the valve is only at a small section of central wall. The air trapped during the fluid introduction, across the incomplete breach, pushes back the liquid after resealing. This may not be evident in an optimised device.The current design in the thesis requires further optimisation and requires adequate characterisation but the current experiments, as shown in Fig. 77, may be considered a proof of concept of Geckofluidics for valves

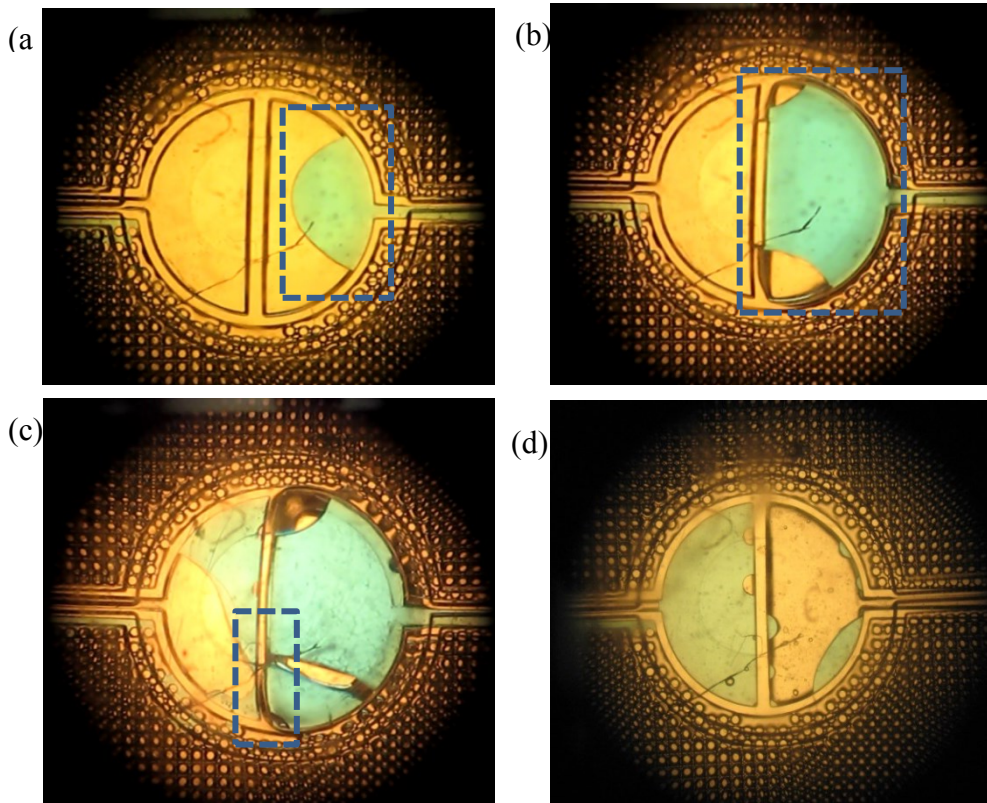


Fig. 77. (a) Fluid introduction (b) fluid deflecting the memberane (c) the breach (d) reseal

6.3.5 ELECTROMAGNETIC FIELD BASED MICROBEAD CAPTURE

Simple Geckofluidic straight channels were used to study the trapping efficiency of supermagnetic beads (MyOne™ Dyna beads Carboxylic acid) on a PCB trace. The study involved identifying the maximum flow rates that can be used to trap the maximum amount of magnetic beads under a fixed electromagnetic field generated due to 1 Amp of current in the underlying PCB trace. A very thin flat surface was created over the PCB traces using a UV curing adhesive (Loctite 3525). The adhesive was sandwiched between the PCB trace and a freezer bag (flattened by a glass slide) and exposed to UV (365nm) (Stratlinker 2400). A ~75 μm tall, simple geckofluidic straight channel was reversibly bonded to a flat UV cured adhesive surface of a PCB while holes were drilled into the PCB and brass tubing

were connected with an epoxy on the back side of the PCB. The bead solution was injected via a syringe pump (Pico pump plus Elite 11) for a precise regulation of flow rates. One PCB trace meandered to form 3 active electromagnetic sources for the fluidic channel. Maximum flow rates for efficient capture were measured, which will be discussed in a future work. Flow rates as high as $3\mu\text{l min}^{-1}$ were tested on this unit. Some of the observations are as in Fig. 79, which the concept is elucidated in Fig. 78.

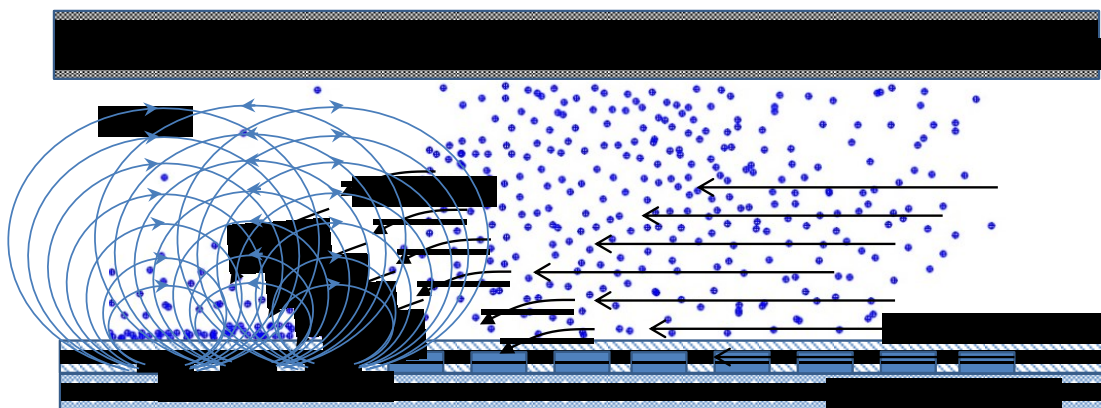


Fig. 78. Conceptual illustration of the electromagnetic field based bead capture.

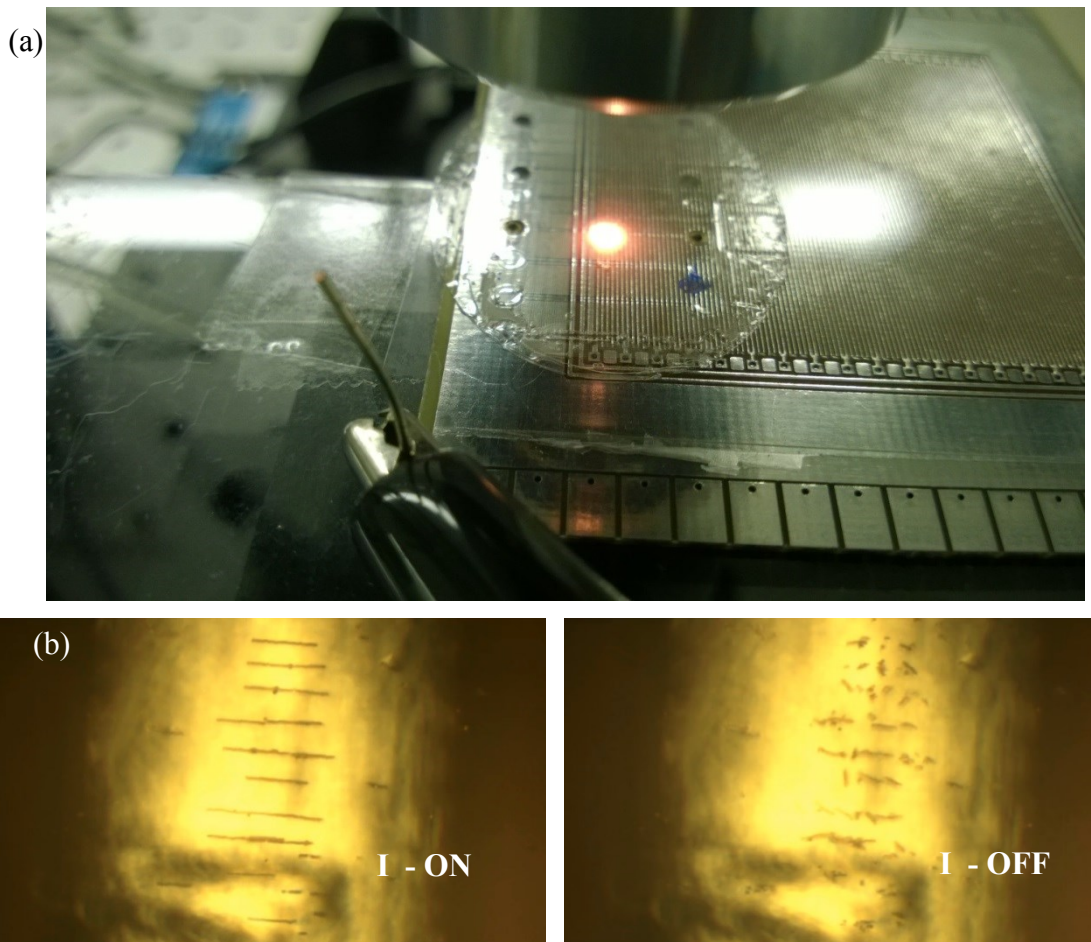


Fig. 79 (a) A Geckofluidic channel on a PCB (b) Aggregation of magnetic beads in the magnetic field lines with an input current of 1 A and immediately after turning off the field .

6.4 World to chip interface

While the brief configurations and manufacturing were explained in the previous chapter, the conceptual and fabricated devices are illustrated here. Depending on the choice of flow driving mechanisms, ports or connectors may be used. The ports can hold reagent or sample volumes for non-pressurized driving modes while connectors can be used for direct

interfacing with the injection source. In Fig 62 (b) the PMMA port block was fabricated by countersinking a laser punched hole. The port block can be aligned easily against the patterned interconnection adhesive. Using a bigger port block may cause interfacing challenges if the device thickness is not uniform in which case smaller port blocks may be used. Fig. 63(a) demonstrates the stick and play interfaces fabricated via an adhesive bonding of a multi gasketed geckofluidic blister and a centrally laser punched PMMA block. These composite adapters can be attached or detached at will. Fig. 63 (b,c) demonstrate typical interfacing modules for microfluidics.

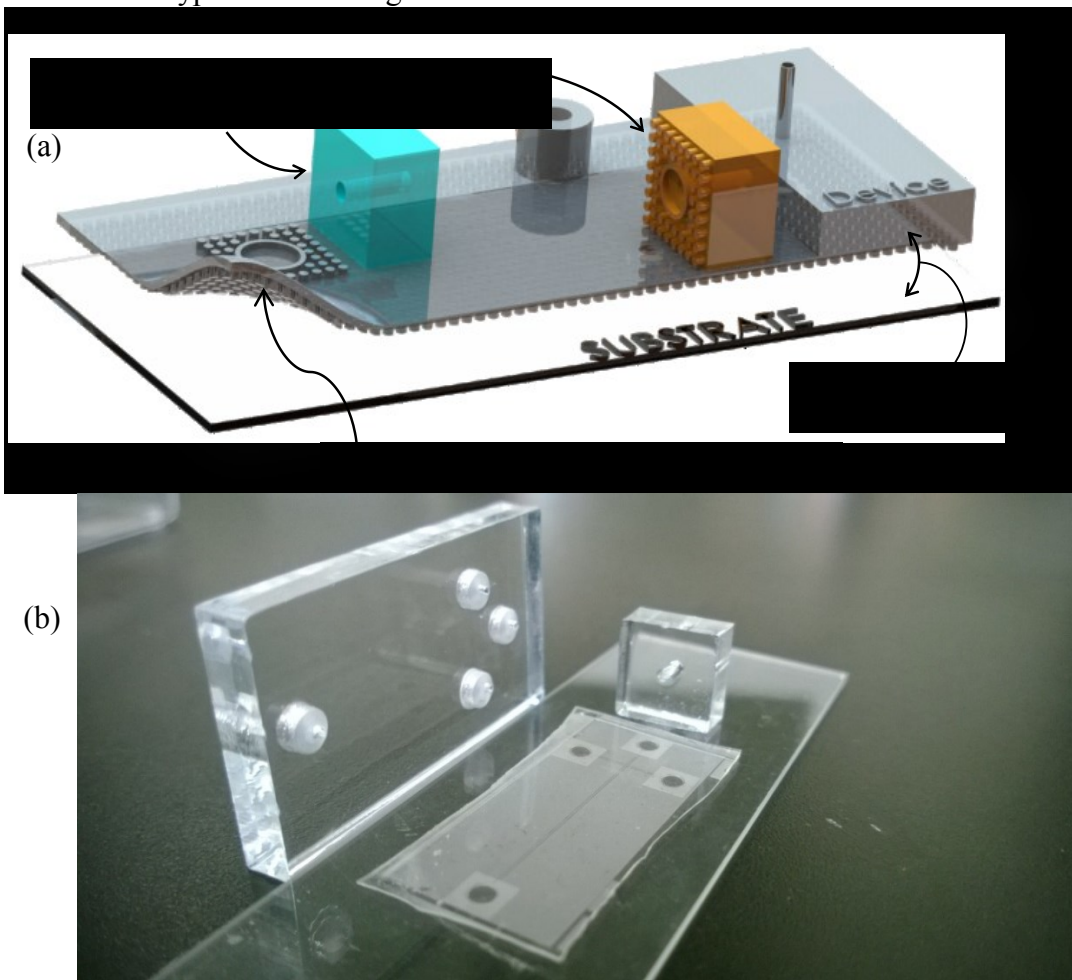
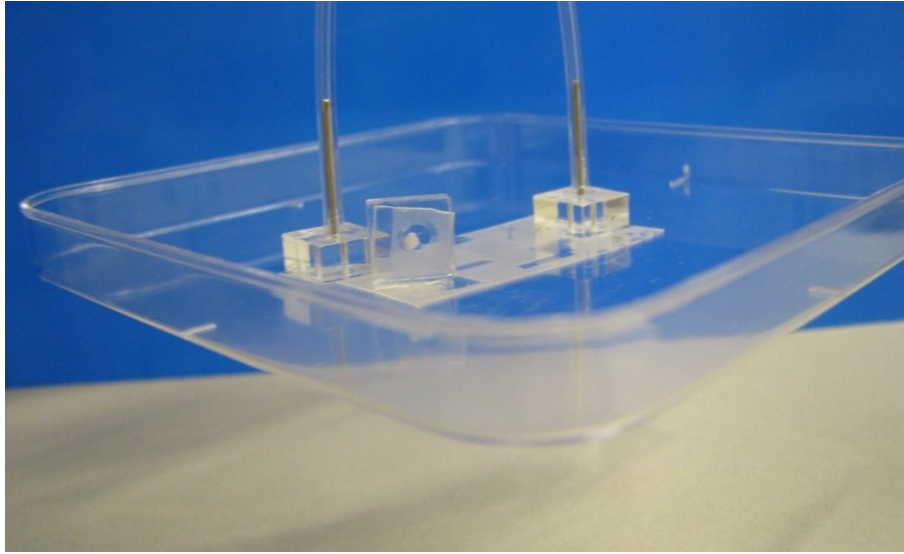
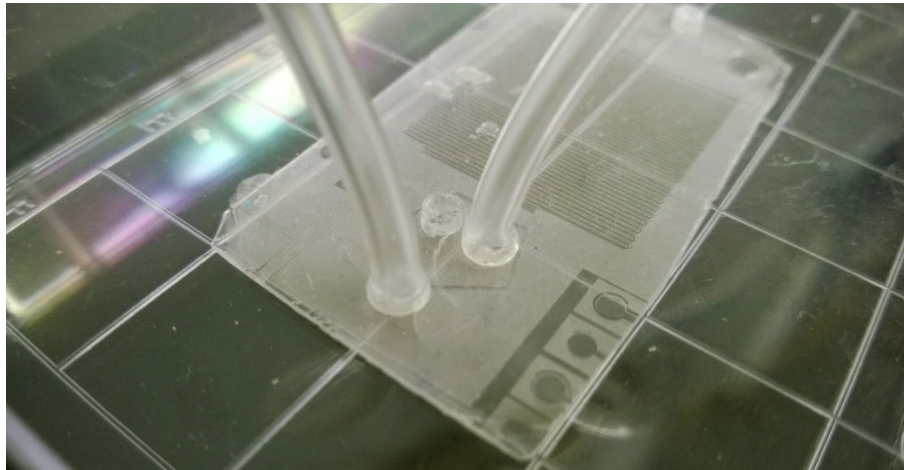


Fig.62 (a) Schematic of the possible configurations (b) port and/or connect configuration

(a)



(b)



(c)

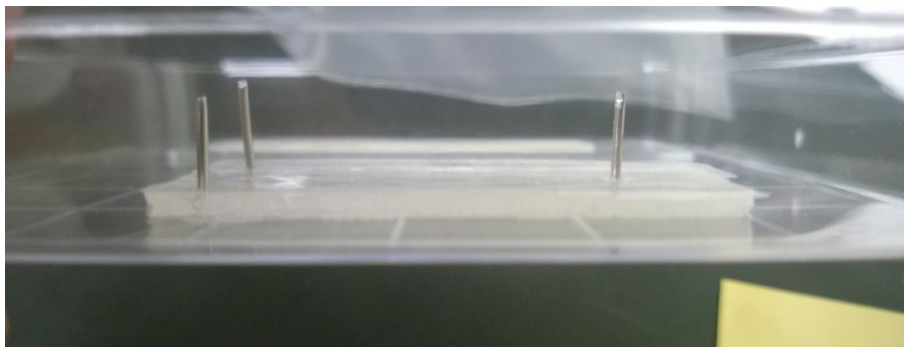


Fig.63 (a) A micromixer channel on PS petri dish suspended by stick and play interconnects (b) A droplet generator device with a modified rigid backing (c) Press fit pins for interconnection

Chapter 7: Conclusion

7.1. Summary

The goal of the project was to extend the application of Gecko inspired adhesives to the field of microfluidics to provide for an instant bonding technique. The work in this thesis builds up on the extensive work done at the group towards manufacturing and characterizing synthetic gecko inspired adhesives. Studies were performed to identify and characterize the manufacturing feasibility of various thermoplastics. Design guidelines were developed to define ideal characteristics of the adhesive integrated microfluidic systems. With the design and manufacturing guidelines in place, the ‘Geckofluidic’ chips were designed and manufactured to demonstrate a wide range of typical microfluidic application. Apart from providing a an instant bonding solution, the integration of gecko adhesives helps to provide a robust solution for the world to chip interfaces.

The manufacturing feasibility study involves studying approximately 10 commercially available bio compatible thermoplastic elastomers. The guidelines for suitability involved perfect feature replication without adhesive fiber collapse or plastic deformation. This was based on optical microscopy and SEM imaging. Beyond the superficial visualisation, optical profilometer based study helps details the extent of replication fidelity. While SEBS has been demonstrated as a good choice of material for microfluidics, the conclusion to this chapter identifies SEBS Kraton G1657 to have the best replication fidelity and thereby the best potential to integrate the Gecko inspired Adhesives.

Chapter 4 builds up extensively on the simulation parameters laid out by the previous study [229] to generate parameters in context with geckofluidics. Since the acceptability of a bonding mechanism has to inherently do with its performance under a wide range of operating condition, the simulation identifies the limitations of the standalone concept, and

then highlights the effect of the measures taken to increase the functionality of the concept over a wider range. While the standalone concept is significantly well apt at withstanding upto 40psi of pressure (SEBS to SEBS bonding), the significant deformations at this limit effect the performance of the microfluidic system, and hence need reinforcements to negate that effect. This is provided as a rigid backing layer. The polymer used for the backing layer was PS, which increased the adhesion strength by 50% to more than 100% compared to the samples without the rigid backing. The SEBS to SEBS bonding can withstand more than 95psi with a rigid backing, while annealing the samples helped increase the adhesion strength by atleast 40%. The effect of the backing layer thickness has also been studied , which found a plateauing effect for thickness beyond 500-600 micron thick PS layers. Also the number of fibers beyond the gasket required to effectively mitigate the effect of pressure in the channel was ~3-4 rows, which is specific to the current design of 100 micron pillars. The manufacturing process deployed was thermocompressive molding, which can help fabricate the adhesive integrated microfluidic chip in less than a minute, providing a complete assembled chip, from start to finish, in under 2 minutes. This method also does away with expensive tooling like injection molders or mold inserts. While a controlled hold force was applied via an ultrasonic welder (without the ultrasonics), the process has been effectively demonstrated with handheld weights in some of the previous works in the lab [200]. The mold manufacturing process required a few modifications for the PMMA development process which was troubleshooted by the use of 50-50% mixture of SU-8 developer and IPA for a prefinal rinse.

A variety of proof of concept microfluidic applications with geckofluidic devices were demonstrated in chapter 6 of this thesis. The applications broadly are classified as pressure driven and non pressure driven . Applications such as microfluidic valves

demonstrate the proof for 3d microfluidics , while at the same time demonstrate the flexibility of bonding by being forgiving to any misalignments. Any misalignments can be dealt with by simple delaminating of the misaligned layer and reattempting the bonding process, which is not flexible for conventional bonding techniques. The applications with MEMS systems and simple microelectronics can be extrapolated to include the flexibility of integration with complex microelectronics and MEMS. The extension of the geckofluidics concept to world to chip interconnects greatly simplifies the interfacing challenge.

This work brings to fore an unconventional yet simplistic approach to microfluidic chip bonding, which is robust and reliable and is achievable in a process which is fairly cost effective. The manufacturing process doesn't require any new tools or does it add to the fabrication complexity or time and can be adopted as easily by research labs and industries alike.

7.2. Future Work

The applications demonstrated in the thesis are only a subset of the possible applications. There could be applications within the domain of microfluidics which haven't been explored in this thesis or may not be compatible for integration. Being first of its kind, the integration of dry adhesives with microfluidics, there is ample scope to extend the work in the similar direction. Some of the possible studies could include,

- During the thermo-compressive molding process, the use of silicone mold under higher loads tends to create dimensional variations compared to the target dimensions (observed as high as 10%). The thickness of the sample also varies with

the applied load. Hence either fixed tolerance may be set in place depending on the preset values for the loads and temperature. The study therein, could include identifying a different silicone or loads under which the variations are minimal.

- Fabrication of larger samples via roller thermo-compressive molding process can be pursued, as it could help regulate the variations in thickness of the samples, at the same time be more attractive for large scale manufacturing.
- While the adhesion is primarily a function of the aspect ratio of the cap, the range of pillar aspect ratios under which this assumption holds true can be studied.
- Adhesion pressure against bare silicon has been characterised in this work, but integration with MEMS and microelectronics may require characterisation with a range of polymers like polyimides, parylene etc., and other metal and materials.
- Characterisation of interface roughness and its influence on adhesion may also need to be pursued to increase the range of application.

LIST OF PUBLICATIONS

Journal:

- Wasay, A; Sameoto, D. Gecko Gaskets For Self-Sealing And High-Strength Reversible Bonding Of Microfluidics. Lab On A Chip. 15, 13, 2749-2753, 2015. Issn: 14730197.

Conferences:

- A.Wasay And D. Sameoto ,“Geckofluidics”: A New Concept In Reversible Bonding Of Microfluidic Channels, Solid-State Sensors, Actuators And Microsystems Workshop, Hilton Head 2014, Hilton Head, Sc, USA
- D. Sameoto ; A. Wasay; Materials Selection And Manufacturing Of Thermoplastic Elastomer Microfluidics, Proc. Spie 9320, Microfluidics, Biomems, And Medical Microsystems Xiii, 932001 (March 5, 2015); Doi:10.1117/12.2081291
- A.Wasay And D. Sameoto, Geckoadhesives For Microfluidics: A Strong And Reversible Bonding Technique, Proc. Int. Conf. Miniaturized Syst. Chem. Life Sci., 18th, 2014, 2530–2531.
- Abdul Wasay, Dan Sameoto; Geckofluidics: Gecko Inspired Adhesives For Reversible Bonding Of Microfluidics, , Canadian Microsystems Corporation-Texpo 2014, Ottawa , CA
- D. Sameoto And A. Wasay; Multi-Layer Strong Reversible Bonding Via Gecko-Inspired Gasket Architecture , Napa Institute 2015, Enabling Future Health Care-The Role Of Micro And Nano Technologies, Napa, CA, USA

Presentation:

- “Geckofluidics” : Dry Adhesives For Reversible Bonding Of Microfluidic Devices, Abdul Wasay, Faculty Of Engineering Graduate Research Symposium 2014, University Of Alberta.

REFERENCES

References

- [1] L. Gervais, N. de Rooij and E. Delamarche. Microfluidic chips for point-of-care immunodiagnosics. *Adv Mater* 23(24), pp. H151-H176. 2011. . DOI: 10.1002/adma.201100464.
- [2] N. Nguyen and S. T. Wereley. *Fundamentals and Applications of Microfluidics. [Electronic Resource]* 2006.
- [3] Jean-Baptiste Salmon, "Lecture notes: Microfluidics for lab-on-chips:2010 http://www.lof.cnrs.fr/IMG/pdf/Microfluidic_Lectures_2010.pdf," 2010.
- [4] G. M. Whitesides. The origins and the future of microfluidics. *Nature* 442(7101), pp. 368-373. 2006. . DOI: 10.1038/nature05058.
- [5] S. Prakash and J. Yeom. "Chapter 2 - fundamentals for microscale and nanoscale flows," in *Nanofluidics and Microfluidics*, S. Prakash and J. Yeom, Eds. 2014, . DOI: <http://dx.doi.org/10.1016/B978-1-4377-4469-9.00002-0>.
- [6] M. T. Guo, A. Rotem, J. A. Heyman and D. A. Weitz. Droplet microfluidics for high-throughput biological assays. *Lab Chip* 12(12), pp. 2146-2155. 2012. . DOI: 10.1039/c2lc21147e.
- [7] J. Liu, C. Hansen and S. R. Quake. Solving the 'world-to-chip' interface problem with a microfluidic matrix. *Anal. Chem.* (18), pp. 4718. 2003.
- [8] M. Ghodbane, E. C. Stucky, T. J. Maguire, R. S. Schloss, D. I. Shreiber, J. D. Zahn and M. L. Yarmush. Development and validation of a microfluidic immunoassay capable of multiplexing parallel samples in microliter volumes. *LAB ON A CHIP* 15(15), pp. 3211-3221. 2015.
- [9] M. K. Araz, A. M. Tentori and A. E. Herr. Microfluidic multiplexing in bioanalyses. *J LAB AUTOMATION* 18(5), pp. 350-366 17p. 2013. . DOI: 10.1177/2211068213491408.
- [10] J. Wu and M. Gu. Microfluidic sensing: State of the art fabrication and detection techniques. *J. Biomed. Opt.* 16(8), 2011.
- [11] C. A. Baker, C. T. Duong, A. Grimley and M. G. Roper. Recent advances in microfluidic detection systems. *BIOANALYSIS* 1(5), pp. 967-975. 2009.

- [12] X. Li, D. R. Ballerini and W. Shen. A perspective on paper-based microfluidics: Current status and future trends. *Biomicrofluidics* 6(1), pp. 011301. 2012. . DOI: 10.1063/1.3687398.
- [13] O. Mudanyali, S. Dimitrov, U. Sikora, S. Padmanabhan, I. Navruz and A. Ozcan. Integrated rapid-diagnostic-test reader platform on a cellphone. *Lab Chip* 12(15), pp. 2678-2686. 2012. . DOI: 10.1039/c2lc40235a.
- [14] C. D. Chin, V. Linder and S. K. Sia. Commercialization of microfluidic point-of-care diagnostic devices. *Lab Chip* 12(12), pp. 2118-2134. 2012. . DOI: 10.1039/c2lc21204h.
- [15] Available: <http://www.barchart.com/headlines/story/1785750/microfluidic-device-system-market-2013-2019>.
- [16] Y. Zhu and Q. Fang. Analytical detection techniques for droplet microfluidics-A review. *Anal. Chim. Acta* 787pp. 24-35. 2013.
- [17] H. Zhu, S. O. Isikman, O. Mudanyali, A. Greenbaum and A. Ozcan. Optical imaging techniques for point-of-care diagnostics. *Lab Chip* 13(1), pp. 51-67. 2013. . DOI: 10.1039/c2lc40864c.
- [18] S. Spindel and K. E. Sapsford. Evaluation of optical detection platforms for multiplexed detection of proteins and the need for point-of-care biosensors for clinical use. *Sensors (14248220)* 14(12), pp. 22313-22341. 2014. . DOI: 10.3390/s141222313.
- [19] M. Hitzbleck and E. Delamarche. Reagents in microfluidics: An 'in' and 'out' challenge. *Chem. Soc. Rev.* 42(21), pp. 8494-8516. 2013.
- [20] R. Gorkin, J. Park, J. Siegrist, M. Amasia, B. S. Lee, J. Park, J. Kim, H. Kim, M. Madou and Yoon-Kyoung Cho. Centrifugal microfluidics for biomedical applications. *Lab on a Chip - Miniaturisation for Chemistry & Biology* (14), pp. 1758-1773. 2010. . DOI: 10.1039/b924109d.
- [21] Z. Yu, K. Yong and J. P. Fu. Microfluidic blood cell sorting: Now and beyond. *SMALL* 10(9), pp. 1687-1703. 2014.
- [22] A. G. Crevillén, M. Hervás, M. A. López, M. C. González and A. Escarpa. Review: Real sample analysis on microfluidic devices. *Talanta* 74(-), pp. 342-357. 2007. . DOI: 10.1016/j.talanta.2007.10.019.
- [23] J. Kim, M. Johnson, P. Hill and B. K. Gale. Microfluidic sample preparation: Cell lysis and nucleic acid purification. *INTEGRATIVE BIOLOGY* 1(10), pp. 574-586. 2009.

- [24] S. Wyatt IV, C. D. Reyes and G. P. López. Microfluidic cell sorting: A review of the advances in the separation of cells from debulking to rare cell isolation. *Lab on a Chip - Miniaturisation for Chemistry & Biology* 15(5), pp. 1230-1249. 2015. . DOI: 10.1039/c4lc01246a.
- [25] F. Abhari, H. Jaafar and N. Yunus. A comprehensive study of micropumps technologies. *INTERNATIONAL JOURNAL OF ELECTROCHEMICAL SCIENCE* 7(10), pp. 9765-9780. 2012.
- [26] R. Mukhopadhyay. When PDMS isn't the best. what are its weaknesses, and which other polymers can researchers add to their toolboxes? *Anal. Chem.* 79(9), pp. 3248-3253. 2007.
- [27] Holger Becker. Mind the gap! *Lab Chip* 10(3), pp. 271-273. 2010.
- [28] E. Berthier, E. Young and D. Beebe. Engineers are from PDMS-land, biologists are from polystyrenia. *Lab Chip* 12(7), pp. 1224-1237. 2012.
- [29] M. A. Unger, H. Chou, T. Thorsen, A. Scherer and S. R. Quake. Monolithic microfabricated valves and pumps by multilayer soft lithography. *Science* 288(5463), pp. 113-116. 2000.
- [30] W. H. Grover, A. M. Skelley, C. N. Liu, E. T. Lagally and R. A. Mathies. Monolithic membrane valves and diaphragm pumps for practical large-scale integration into glass microfluidic devices. *Sensors and Actuators, B: Chemical* 89pp. 315-323. 2003. . DOI: 10.1016/S0925-4005(02)00468-9.
- [31] L. Gervais, M. Hitzbleck and E. Delamarche. Capillary-driven multiparametric microfluidic chips for one-step immunoassays. *Biosens. Bioelectron.* 27(1), pp. 64-70. 2011.
- [32] Natalya V. Zaytseva, Vasiliy N. Goral, Richard A. Montagna and Antje J. Baeumner. Development of a microfluidic biosensor module for pathogen detection. *Lab Chip* 5(8), pp. 805. 2005.
- [33] K. Anwar, T. Han and S. M. Kim. Review: Reversible sealing techniques for microdevice applications. *Sensors & Actuators: B. Chemical* 153pp. 301-311. 2011. . DOI: 10.1016/j.snb.2010.11.002.
- [34] C. S. Thompson and A. R. Abate. Adhesive-based bonding technique for PDMS microfluidic devices. *Lab Chip* 13(4), pp. 632-635. 2013.

- [35] X. L. Luo, A. T. Lewandowski, H. M. Yi, G. F. Payne, R. Ghodssi, W. E. Bentley and G. W. Rubloff. Programmable assembly of a metabolic pathway enzyme in a pre-packaged reusable bioMEMS device. *Lab Chip* 8(3), pp. 420-430. 2008.
- [36] S. Choi and J. Chae. Reusable biosensors via in situ electrochemical surface regeneration in microfluidic applications. *Biosens. Bioelectron.* 25(2), pp. 527. 2009. . DOI: 10.1016/j.bios.2009.08.003.
- [37] K. Autumn, M. Sitti, Y. A. Liang, A. M. Peattie, W. R. Hansen, S. Sponberg, T. W. Kenny, R. Fearing, J. N. Israelachvili and R. J. Full. Evidence for van der waals adhesion in gecko setae. *Proc. Natl. Acad. Sci. U. S. A.* (19), pp. 12252. 2002.
- [38] K. Autumn, Y. A. Liang, S. T. Hsieh, W. Zesch, W. P. Chan, T. W. Kenny, R. Fearing and R. J. Full. Adhesive force of a single gecko foot-hair. *Nature* 405(6787), pp. 681. 2000.
- [39] K. Autumn and W. Hansen. Ultrahydrophobicity indicates a non-adhesive default state in gecko setae. *Journal of Comparative Physiology. A, Sensory, Neural, and Behavioral Physiology* 2006.
- [40] N. W. Rizzo, K. H. Gardner, D. J. Walls, N. Keiper-Hrynko, T. S. Ganzke and D. L. Hallahan. Characterization of the structure and composition of gecko adhesive setae. *JOURNAL OF THE ROYAL SOCIETY INTERFACE* 3(8), pp. 441-451. 2006.
- [41] A. MANZ, N. GRABER and H. M. WIDMER. Miniaturized total chemical-analysis systems - a novel concept for chemical sensing. *SENSORS AND ACTUATORS B-CHEMICAL* 1(1-6), pp. 244-248. 1990.
- [42] K. N. Ren, J. H. Zhou and H. K. Wu. Materials for microfluidic chip fabrication. *Acc. Chem. Res.* 46(11), pp. 2396-2406. 2013.
- [43] D. R. Reyes, D. Iossifidis, P. A. Auroux and A. Manz. Micro total analysis systems. 1. introduction, theory, and technology. *Anal. Chem.* 74(12), pp. 2623-2636. 2002.
- [44] H. Becker and U. Heim. Silicon as tool material for polymer hot embossing. *Technical Digest IEEE International MEMS 99 Conference Twelfth IEEE International Conference on Micro Electro Mechanical Systems (Cat No99CH36291)* pp. 228. 1999.
- [45] J. Elders, H. V. Jansen, M. Elwenspoek and W. Ehrfeld. DEEMO: A new technology for the fabrication of microstructures. *Proceedings IEEE Micro Electro Mechanical Systems 1995* pp. 238. 1995.

- [46] S. Tanzi, P. F. Ostergaard, M. Matteucci, T. L. Christiansen, J. Cech, R. Marie and R. Taboryski. Fabrication of combined-scale nano- and microfluidic polymer systems using a multilevel dry etching, electroplating and molding process. *J Micromech Microengineering* 22(11), 2012.
- [47] C. H. Lin, G. B. Lee, Y. H. Lin and G. L. Chang. A fast prototyping process for fabrication of microfluidic systems on soda-lime glass. *J Micromech Microengineering* 11(6), pp. 726-732. 2001.
- [48] K. Sugioka and Y. Cheng. Fabrication of 3D microfluidic structures inside glass by femtosecond laser micromachining. *Appl. Phys. A* 114(1), pp. 215-221. 2014. . DOI: 10.1007/s00339-013-8107-3.
- [49] A. T. Woolley and R. A. Mathies. Ultra-high-speed DNA fragment separations using microfabricated capillary array electrophoresis chips. *Proc. Natl. Acad. Sci. U. S. A.* (24), pp. 11348. 1994.
- [50] C. Iliescu, H. Taylor, M. Avram, J. Miao and S. Franssila. A practical guide for the fabrication of microfluidic devices using glass and silicon. *Biomicrofluidics* 6(1), pp. 016505. 2012. . DOI: 10.1063/1.3689939.
- [51] S. Y. Chou, P. R. Krauss and P. J. Renstrom. Imprint lithography with 25-nanometer resolution. *Science* (5258), pp. 85. 1996.
- [52] J. W. Stansbury and M. J. Idacavage. 3D printing with polymers: Challenges among expanding options and opportunities. *Dental Materials* . DOI: <http://dx.doi.org/10.1016/j.dental.2015.09.018>.
- [53] H. Becker and L. E. Locascio. REVIEW: Polymer microfluidic devices. *Talanta* 56pp. 267-287. 2002. . DOI: 10.1016/S0039-9140(01)00594-X.
- [54] M. P. Groover. *Fundamentals of Modern Manufacturing: Materials, Processes, and Systems* 2002.
- [55] H. Becker and C. Gärtner. Polymer microfabrication technologies for microfluidic systems. *Analytical and Bioanalytical Chemistry* 2008.
- [56] M. Rabe, D. Verdes and S. Seeger. Understanding protein adsorption phenomena at solid surfaces. *Adv. Colloid Interface Sci.* 162pp. 87-106. 2011. . DOI: 10.1016/j.cis.2010.12.007.

- [57] P. C. Thomas, S. R. Raghavan and S. P. Forry. Regulating oxygen levels in a microfluidic device. *Anal. Chem.* (22), pp. 8821. 2011.
- [58] C. J. Ochs, J. Kasuya, A. Pavesi and R. D. Kamm. Oxygen levels in thermoplastic microfluidic devices during cell culture. *LAB ON A CHIP* 14(3), pp. 459-462. 2014.
- [59] M. P. Groover. *Fundamentals of Modern Manufacturing: Materials, Processes, and Systems* 2002.
- [60] P. G. Debenedetti and F. H. Stillinger. Supercooled liquids and the glass transition. *Nature* (6825), pp. 259. 2001.
- [61] T. Whelan. *Polymer Technology Dictionary* 1994.
- [62] K. E. Kear and T. L. Rapra. *Developments in Thermoplastic Elastomers* 2003.
- [63] F. C. Cabrera, de Souza, João C. P., A. E. Job and F. N. Crespilho. Natural-rubber-based flexible microfluidic device. *RSC Advances* 4(67), pp. 35467. 2014.
- [64] K. Domansky, D. C. Leslie, J. McKinney, J. P. Fraser, J. D. Sliz, T. Hamkins-Indik, G. A. Hamilton, A. Bahinski and D. E. Ingber. Clear castable polyurethane elastomer for fabrication of microfluidic devices. *Lab Chip* 13(19), pp. 3956-3964. 2013. . DOI: 10.1039/c3lc50558h.
- [65] K. W. Bong, J. Lee and P. S. Doyle. Stop flow lithography in perfluoropolyether (PFPE) microfluidic channels. *Lab Chip* 14(24), pp. 4680-4687. 2014. . DOI: 10.1039/c4lc00877d.
- [66] R. M. van Dam. Solvent-resistant elastomeric microfluidic devices and applications. 2006.
- [67] J. P. Rolland, R. M. Van Dam, D. A. Schorzman, S. R. Quake and J. M. DeSimone. Solvent-resistant photocurable liquid fluoropolymers for microfluidic device fabrication [corrected]. *J. Am. Chem. Soc.* 126(8), pp. 2322-2323. 2004.
- [68] T. Renckens, D. Janeliunas, H. van Vliet, J. van Esch, G. Mul and M. T. Kreutzer. Micromolding of solvent resistant microfluidic devices. *LAB ON A CHIP* 11(12), pp. 2035-2038. 2011.
- [69] G. Maltezos, E. Garcia, G. Hanrahan, F. A. Gomez, S. Vyawahare, R. M. van Dam, Y. Chen and A. Scherer. Design and fabrication of chemically robust three-dimensional microfluidic valves. *Lab Chip* 7(9), pp. 1209-1211. 2007.

- [70] G. Sharma Author, L. Klintberg Author, K. Hjort Author and Uppsala universitet, Teknisk-naturvetenskapliga vetenskapsområdet, Tekniska sektionen, Institutionen för teknikvetenskaper, Mikrosystemteknik, Originator. Viton-based fluoroelastomer microfluidics. *J Micromech Microengineering* pp. 25016. 2011.
- [71] J. C. McDonald and G. M. Whitesides. Poly(dimethylsiloxane) as a material for fabricating microfluidic devices. *Acc. Chem. Res.* (7), pp. 491. 2002.
- [72] D. C. Duffy, J. C. McDonald, O. J. Schueller and G. M. Whitesides. Rapid prototyping of microfluidic systems in poly(dimethylsiloxane). *Anal. Chem.* 70(23), pp. 4974-4984. 1998. . DOI: 10.1021/ac980656z.
- [73] X. Z. Niu, S. L. Peng, L. Y. Liu, W. J. Wen and P. Sheng. Characterizing and patterning of PDMS-based conducting composites. *Adv Mater* 19(18), pp. 2682-+. 2007.
- [74] J. Li, M. Zhang, L. Wang, W. Li, P. Sheng and W. Wen. Design and fabrication of microfluidic mixer from carbonyl iron--PDMS composite membrane. *Microfluidics and Nanofluidics* (4), pp. 919. 2011.
- [75] J. W. Zhou, D. A. Khodakov, A. V. Ellis and N. H. Voelcker. Surface modification for PDMS-based microfluidic devices. *Electrophoresis* 33(1), pp. 89-104. 2012.
- [76] J. Zhou, A. V. Ellis and N. H. Voelcker. Recent developments in PDMS surface modification for microfluidic devices. *Electrophoresis* 2010.
- [77] Z. Almutairi, C. L. Ren and L. Simon. Evaluation of polydimethylsiloxane (PDMS) surface modification approaches for microfluidic applications. *Colloids Surf. Physicochem. Eng. Aspects* 415pp. 406-412. 2012. . DOI: 10.1016/j.colsurfa.2012.10.008.
- [78] H. Schmid and B. Michel. Siloxane polymers for high-resolution, high-accuracy soft lithography. *Macromolecules* 33(8), pp. 3042-3049. 2000.
- [79] D. W. Inglis. A method for reducing pressure-induced deformation in silicone microfluidics. *Biomicrofluidics* 4(2), pp. 026504. 2010. . DOI: 10.1063/1.3431715.
- [80] K. Hosokawa and R. Maeda. A pneumatically-actuated three-way microvalve fabricated with polydimethylsiloxane using the membrane transfer technique. *J. Micromech. Microeng.* 10(3), pp. 415-420. 2000.
- [81] P. M. Pilarski, S. Adamia and C. J. Backhouse. Research paper: An adaptable microvalving system for on-chip polymerase chain reactions. *J. Immunol. Methods* 305pp. 48-58. 2005. . DOI: 10.1016/j.jim.2005.07.009.

- [82] A. K. Au, H. Y. Lai, B. R. Utela and A. Folch. Microvalves and micropumps for BioMEMS. *Micromachines* 2(2), pp. 179-220. 2011.
- [83] E. Roy, J. C. Galas and T. Veres. Thermoplastic elastomers for microfluidics: Towards a high-throughput fabrication method of multilayered microfluidic devices. *LAB ON A CHIP* 11(18), pp. 3193-3196. 2011.
- [84] A. P. Sudarsan, J. Wang and V. M. Ugaz. Thermoplastic elastomer gels: An advanced substrate for microfluidic chemical analysis systems. *Anal. Chem.* (16), pp. 5167. 2005.
- [85] D. Trimbach, K. Feldman, N. D. Spencer, D. J. Broer and C. Bastiaansen. Block copolymer thermoplastic elastomers for microcontact printing. *Langmuir* 19(26), pp. 10957-10961. 2003.
- [86] M. D. Borysiak, K. S. Bielawski, N. J. Sniadecki, C. F. Jenkel, B. D. Yogt and J. D. Posner. Simple replica micromolding of biocompatible styrenic elastomers. *Lab Chip* 13pp. 2773-2784. 2013.
- [87] M. Geissler, E. Roy, G. Diaz-Quijada, J. C. Galas and T. Veres. Microfluidic patterning of miniaturized DNA arrays on plastic substrates. *ACS APPLIED MATERIALS & INTERFACES* 1(7), pp. 1387-1395. 2009.
- [88] A. P. Sudarsan and V. M. Ugaz. Fluid mixing in planar spiral microchannels. *LAB ON A CHIP* 6(1), pp. 74-82. 2006.
- [89] M. D. Borysiak, E. Yuferova and J. D. Posner. Simple, low-cost styrene-ethylene/butylene-styrene microdevices for electrokinetic applications. *Anal. Chem.* (24), pp. 11700. 2013.
- [90] M. D. Borysiak, K. W. Kimura and J. D. Posner. NAIL: Nucleic acid detection using isotachopheresis and loop-mediated isothermal amplification. *Lab on a Chip - Miniaturisation for Chemistry & Biology* 15(7), pp. 1697-1707. 2015. . DOI: 10.1039/c4lc01479k.
- [91] V. Z. Peter. The ten-step patterning Process—Surface preparation to exposure. *Microchip Fabrication: A Practical Guide to Semiconductor Processing, Fifth Edition* 2004.
- [92] Y. N. Xia, J. J. McClelland, R. Gupta, D. Qin, X. M. Zhao, L. L. Sohn, R. J. Celotta and G. M. Whitesides. Replica molding using polymeric materials: A practical step toward nanomanufacturing. *Adv Mater* 9(2), pp. 147-149. 1997.

- [93] A. KUMAR and G. M. WHITESIDES. Features of gold having micrometer to centimeter dimensions can be formed through a combination of stamping with an elastomeric stamp and an alkanethiol ink followed by chemical etching. *Appl. Phys. Lett.* 63(14), pp. 2002-2004. 1993.
- [94] X. M. Zhao, Y. N. Xia and G. M. Whitesides. Fabrication of three-dimensional microstructures: Microtransfer molding. *Adv Mater* 8(10), pp. 837-&. 1996.
- [95] E. Kim, Y. Xia and G. M. Whitesides. Polymer microstructures formed by moulding in capillaries. *Nature* (6541), pp. 581. 1995.
- [96] E. Kim, Y. N. Xia, X. M. Zhao and G. M. Whitesides. Solvent-assisted microcontact molding: A convenient method for fabricating three-dimensional structures on surfaces of polymers. *Adv Mater* 9(8), pp. 651-654. 1997.
- [97] J. A. Rogers and K. E. Paul. Using an elastomeric phase mask for sub-100 nm photolithography in the optical near field. *Appl. Phys. Lett.* 70(20), pp. 2658. 1997.
- [98] S. Jeon, E. Menard, J. U. Park, J. Maria, M. Meitl, J. Zaumseil and J. A. Rogers. Three-dimensional nanofabrication with rubber stamps and conformable photomasks. *Adv Mater* 16(15), pp. 1369-1373. 2004.
- [99] Q. B. Xu, R. M. Rioux, M. D. Dickey and G. M. Whitesides. Nanoskiving: A new method to produce arrays of nanostructures. *Acc. Chem. Res.* 41(12), pp. 1566-1577. 2008.
- [100] D. Qin, Y. Xi and G. M. Whitesides. Soft lithography for micro- and nanoscale patterning. *Nature Protocols* (3), pp. 491. 2010.
- [101] D. J. Guckenberger, T. E. de Groot, A. M. D. Wan, D. J. Beebe and E. W. K. Young. Micromilling: A method for ultra-rapid prototyping of plastic microfluidic devices. *Lab Chip* 2015. . DOI: 10.1039/C5LC00234F.
- [102] C. G. Khan Malek. Laser processing for bio-microfluidics applications (part II). *Analytical and Bioanalytical Chemistry* (8), 2006.
- [103] C. Malek. Laser processing for bio-microfluidics applications (part I). *ANALYTICAL AND BIOANALYTICAL CHEMISTRY* 385(8), pp. 1351-1361. 2006.
- [104] H. W. Li, Y. Q. Fan, R. Kodzius and I. G. Foulds. Fabrication of polystyrene microfluidic devices using a pulsed CO2 laser system. *MICROSYSTEM TECHNOLOGIES-MICRO-AND NANOSYSTEMS-INFORMATION STORAGE AND PROCESSING SYSTEMS* 18(3), pp. 373-379. 2012.

- [105] T. F. Hong, W. J. Ju, M. C. Wu, C. H. Tai, C. H. Tsai and L. M. Fu. Rapid prototyping of PMMA microfluidic chips utilizing a CO₂ laser. *MICROFLUIDICS AND NANOFUIDICS* 9(6), pp. 1125-1133. 2010.
- [106] H. Klank, J. P. Kutter and O. Geschke. CO₂-laser micromachining and back-end processing for rapid production of PMMA-based microfluidic systems. *LAB ON A CHIP* 2(4), pp. 242-246. 2002.
- [107] M. Li, S. Li, J. Wu, W. Wen, W. Li and G. Alici. A simple and cost-effective method for fabrication of integrated electronic-microfluidic devices using a laser-patterned PDMS layer. *Microfluidics and Nanofluidics* (5), pp. 751. 2012.
- [108] A. Toossi, M. Daneshmand and D. Sameoto. A low-cost rapid prototyping method for metal electrode fabrication using a CO₂ laser cutter. *J Micromech Microengineering* 23(4), 2013.
- [109] C. K. Chung and K. Z. Tu. Application of metal film protection to microfluidic chip fabrication using CO₂ laser ablation. *MICROSYSTEM TECHNOLOGIES* 20(10-11), pp. 1987-1992. 2014.
- [110] S. Nikumb, Q. Chen, C. Li, H. Reshef, H. Y. Zheng, H. Qiu and D. Low. Precision glass machining, drilling and profile cutting by short pulse lasers. *Thin Solid Films* 477pp. 216-221. 2005. . DOI: 10.1016/j.tsf.2004.08.136.
- [111] M. Masuda, K. Sugioka, Y. Cheng, N. Aoki, M. Kawachi, K. Shihoyama, K. Toyoda, H. Helvajian and K. Midorikawa. 3-D microstructuring inside photosensitive glass by femtosecond laser excitation. *Appl. Phys. A* 76(5), pp. 857. 2003.
- [112] P. J. Heaney, A. V. Sumant, C. D. Torres, R. W. Carpick and F. E. Pfefferkorn. Diamond coatings for micro end mills: Enabling the dry machining of aluminum at the micro-scale. *Diamond & Related Materials* 17pp. 223-233. 2008. . DOI: 10.1016/j.diamond.2007.12.009.
- [113] A. Bertsch, P. Renaud, C. Vogt and P. Bernhard. Rapid prototyping of small size objects. *RAPID PROTOTYPING JOURNAL* 6(4), pp. 259-266. 2000.
- [114] A. K. Au, N. Bhattacharjee, L. F. Horowitz, T. C. Chang and A. Folch. 3D-printed microfluidic automation. *Lab on a Chip - Miniaturisation for Chemistry & Biology* 15(8), pp. 1934-1941. 2015. . DOI: 10.1039/c5lc00126a.
- [115] P. F. O'Neill, A. Ben Azouz, M. Vázquez, J. Liu, S. Marczak, Z. Slouka, H. C. Chang, D. Diamond and D. Brabazon. Advances in three-dimensional rapid prototyping of

microfluidic devices for biological applications. *Biomicrofluidics* 8(5), pp. 1-11. 2014. . DOI: 10.1063/1.4898632.

[116] B. C. Gross, J. L. Erkal, S. Y. Lockwood, C. P. Chen and D. M. Spence. Evaluation of 3D printing and its potential impact on biotechnology and the chemical sciences. *Anal. Chem.* 86(7), pp. 3240-3253. 2014.

[117] T. Hanemann, M. Hecke and V. Piottter. Current status of micromolding technology. *POLYMER NEWS* 25pp. 224-228. 2000.

[118] J. Zhao, R. H. Mayes, G. Chen, H. Xie and S. C. Poh. Effects of process parameters on the micro molding process. *Polymer Engineering & Science* 43(9), pp. 1542. 2003.

[119] J. Giboz, T. Copponnex and P. Mele. Microinjection molding of thermoplastic polymers: A review. *J Micromech Microengineering* 17(6), pp. R96-R109. 2007.

[120] C. M. Klapperich. Microfluidic diagnostics: Time for industry standards. *Expert Review of Medical Devices* (3), pp. 211. 2009.

[121] Chin-Chi Cheng, Sen-Yeu Yang and D. Lee. Novel real-time temperature diagnosis of conventional hot-embossing process using an ultrasonic transducer. *Sensors* (14248220) 14(10), pp. 19493-19506. 2014. . DOI: 10.3390/s141019493.

[122] L. F. Peng, Y. J. Deng, P. Y. Yi and X. M. Lai. Micro hot embossing of thermoplastic polymers: A review. *J Micromech Microengineering* 24(1), 2014.

[123] M. Sahli, C. Millot, C. Roques-Carmes, C. Khan Malek, T. Barriere and J. C. Gelin. Quality assessment of polymer replication by hot embossing and micro-injection moulding processes using scanning mechanical microscopy. *Journal of Materials Processing Tech.* 209pp. 5851-5861. 2009. . DOI: 10.1016/j.jmatprotec.2009.06.011.

[124] E. W. Becker, W. Ehrfeld, P. Hagmann, A. Maner and D. Münchmeyer. Fabrication of microstructures with high aspect ratios and great structural heights by synchrotron radiation lithography, galvanofforming, and plastic moulding (LIGA process). *Microelectronic Engineering* 4pp. 35-56. 1986. . DOI: 10.1016/0167-9317(86)90004-3.

[125] M. Hecke and W. K. Schomburg. Review on micro molding of thermoplastic polymers. *J Micromech Microengineering* 14(3), pp. R1-R14. 2004.

[126] E. Wilhelm, C. Neumann, Sachsenheimer, K., Länge, K. and B. E. Rapp, "Uv-light structured silanization for selective bonding and fabrication of paper-based microfluidic

channels," in *18th International Conference on Miniaturized Systems for Chemistry and Life Sciences*, San Antonio, Texas, USA, 2014, pp. 1784-1786.

[127] C. Tsao and D. L. DeVoe. Bonding of thermoplastic polymer microfluidics. *Microfluidics and Nanofluidics (1)*, pp. 1. 2009.

[128] X. Li, N. Wu, Y. Rojanasakul and Y. Liu. Selective stamp bonding of PDMS microfluidic devices to polymer substrates for biological applications. *Sensors & Actuators: A. Physical* 193pp. 186-192. 2013. . DOI: 10.1016/j.sna.2012.12.037.

[129] L. E. Locascio, A. C. Henry, T. J. Johnson and D. Ross. "Surface chemistry in polymer microfluidic systems," in *Lab-on-a-Chip*, R. E. Oosterbroek and A. v. d. Berg, Eds. 2003, . DOI: <http://dx.doi.org/10.1016/B978-044451100-3/50004-8>.

[130] S. Bhattacharya, A. Datta, J. M. Berg and S. Gangopadhyay. Studies on surface wettability of poly(dimethyl) siloxane (PDMS) and glass under oxygen-plasma treatment and correlation with bond strength. *J Microelectromech Syst* 14(3), pp. 590-597. 2005.

[131] Y. Xu, C. X. Wang, L. X. Li, N. Matsumoto, K. Jang, Y. Y. Dong, K. Mawatari, T. Suga and T. Kitamori. Bonding of glass nanofluidic chips at room temperature by a one-step surface activation using an O₂/CF₄ plasma treatment. *LAB ON A CHIP* 13(6), pp. 1048-1052. 2013.

[132] B. Xu, X. Yan, J. Xu and H. Chen. One step high quality poly(dimethylsiloxane)-hydrocarbon plastics bonding. *Biomicrofluidics* 6(1), pp. 016507. 2012. . DOI: 10.1063/1.3694251.

[133] P. Rezai, P. R. Selvaganapathy and G. Rwohl. Plasma enhanced bonding of polydimethylsiloxane with parylene and its optimization. *J Micromech Microengineering* 21(6), 2011.

[134] Y. Kusano. Atmospheric pressure plasma processing for polymer adhesion: A review. *J. Adhesion* 90(9), pp. 755-777. 2014.

[135] M. J. Shenton, M. Lovell-Hoare and G. C. Stevens. Adhesion enhancement of polymer surfaces by atmospheric plasma treatment. *JOURNAL OF PHYSICS D-APPLIED PHYSICS* 34(18), pp. 2754-2760. 2001.

[136] A. Kruse, G. Kruger, A. Baalman and O. D. Hennemann. Surface pretreatment of plastics for adhesive bonding. *J. Adhes. Sci. Technol.* 9(12), pp. 1611-1621. 1995.

- [137] C. W. Tsao, L. Hromada, J. Liu, P. Kumar and D. L. DeVoe. Low temperature bonding of PMMA and COC microfluidic substrates using UV/ozone surface treatment. *LAB ON A CHIP* 7(4), pp. 499-505. 2007.
- [138] A. Bhattacharyya and C. M. Klapperich. Mechanical and chemical analysis of plasma and ultraviolet-ozone surface treatments for thermal bonding of polymeric microfluidic devices. *LAB ON A CHIP* 7(7), pp. 876-882. 2007.
- [139] S. Roy, C. Y. Yue, S. S. Venkatraman and L. L. Ma. Low-temperature (below T-g) thermal bonding of COC microfluidic devices using UV photografted HEMA-modified substrates: High strength, stable hydrophilic, biocompatible surfaces. *JOURNAL OF MATERIALS CHEMISTRY* 21(38), pp. 15031-15040. 2011.
- [140] C. W. Beh, W. Zhou and T. H. Wang, "Oxygen plasma-free microfluidic device sealing," in *14th International Conference on Miniaturized Systems for Chemistry and Life Sciences*, Groningen, The Netherlands, 2010, pp. 1217-1219.
- [141] W. Wu, J. - Wu, J. - Kim and N. Y. - Lee. Instantaneous room temperature bonding of a wide range of non-silicon substrates with poly(dimethylsiloxane) (PDMS) elastomer mediated by a mercaptosilane. *Lab Chip* (13), pp. 2819. 2015. . DOI: 10.1039/C5LC00285K.
- [142] S. H. Ng, Y. X. Wu, Z. F. Wang and Z. P. Wang. Rapid thermal bonding of polymer microfluidic devices assisted by corona discharge. *2009 Symposium on Design, Test, Integration & Packaging of MEMS/MOEMS* pp. 343. 2009.
- [143] D. Olivero and Z. H. Fan, "Chips & tips: lamination of plastic microfluidic devices," *Lab Chip*, 2008.
- [144] K. Kistrup, C. E. Poulsen, M. F. Hansen and A. Wolff. Ultrasonic welding for fast bonding of self-aligned structures in lab-on-a-chip systems. *Lab Chip* 15(9), pp. 1998-2001. 2015. . DOI: 10.1039/c5lc00174a.
- [145] R. Truckenmuller, Y. Cheng, R. Ahrens, H. Bahrs, G. Fischer and J. Lehmann. Micro ultrasonic welding: Joining of chemically inert polymer microparts for single material fluidic components and systems. *MICROSYSTEM TECHNOLOGIES-MICRO-AND NANOSYSTEMS-INFORMATION STORAGE AND PROCESSING SYSTEMS* 12(10-11), pp. 1027-1029. 2006.
- [146] Z. Zhang, X. Wang, Y. Luo, S. He and L. Wang. Thermal assisted ultrasonic bonding method for poly(methyl methacrylate) (PMMA) microfluidic devices. *Talanta* 81pp. 1331-1338. 2010. . DOI: 10.1016/j.talanta.2010.02.031.

- [147] R. Truckenmuller, Y. Cheng, R. Ahrens, H. Bahrs, G. Fischer and J. Lehmann. Micro ultrasonic welding: Joining of chemically inert polymer microparts for single material fluidic components and systems. *MICROSYSTEM TECHNOLOGIES-MICRO-AND NANOSYSTEMS-INFORMATION STORAGE AND PROCESSING SYSTEMS 12(10-11)*, pp. 1027-1029. 2006.
- [148] Y. Luo, Z. Zhang, X. Wang and Y. Zheng. Ultrasonic bonding for thermoplastic microfluidic devices without energy director. *Microelectronic Engineering* 87pp. 2429-2436. 2010. . DOI: 10.1016/j.mee.2010.04.020.
- [149] Z. Zhang, Y. Luo, X. Wang, Y. Zheng, Y. Zhang and L. Wang. A low temperature ultrasonic bonding method for PMMA microfluidic chips. *Microsystem Technologies (4)*, pp. 533. 2010.
- [150] K. F. Lei, S. Ahsan, N. Budraa, W. J. Li and J. D. Mai. Microwave bonding of polymer-based substrates for potential encapsulated micro/nanofluidic device fabrication. *Sensors and Actuators A: Physical* 114(2-3), pp. 340-346. 2004. . DOI: <http://dx.doi.org/10.1016/j.sna.2003.12.018>.
- [151] A. Toossi, H. Moghadas, M. Daneshmand and D. Sameoto. Bonding PMMA microfluidics using commercial microwave ovens. *Journal of Micromechanics & Microengineering* 25(8), pp. 1-1. 2015. . DOI: 10.1088/0960-1317/25/8/085008.
- [152] J. H. Hildebrand. *Solubility of Non-Electrolytes* 1936.
- [153] C. M. Hansen. The universality of the solubility parameter. *Product R&D* 8(1), pp. 2-11. 1969. . DOI: 10.1021/i360029a002.
- [154] N. E. Jackson, L. X. Chen and M. A. Ratner. Solubility of nonelectrolytes: A first-principles computational approach. *J Phys Chem B* 118(19), pp. 5194-5202. 2014.
- [155] F. Umbrecht, D. Müller, F. Gattiker, C. M. Boutry, J. Neuenschwander, U. Sennhauser and C. Hierold. Solvent assisted bonding of polymethylmethacrylate: Characterization using the response surface methodology. *Sensors and Actuators A: Physical* 156(1), pp. 121-128. 2009. . DOI: <http://dx.doi.org/10.1016/j.sna.2009.03.028>.
- [156] R. T. Kelly, T. Pan and A. T. Woolley. Phase-changing sacrificial materials for solvent bonding of high-performance polymeric capillary electrophoresis microchips. *Anal. Chem.* (11), pp. 3536. 2005.
- [157] I. R. G. (. Ogilvie, C. F. A. (. Floquet, H. Morgan, V. J. (. Sieben and M. C. (. Mowlem. Solvent vapor bonding and surface treatment methods. 2012.

- [158] (). *Norland Optical Adhesives*. Available: <https://www.norlandprod.com/adhesiveindex2.html>.
- [159] H. K. Wu, B. Huang and R. N. Zare. Construction of microfluidic chips using polydimethylsiloxane for adhesive bonding. *LAB ON A CHIP* 5(12), pp. 1393-1398. 2005.
- [160] R. Arayanarakool, S. Le Gac and d. B. van. Low-temperature, simple and fast integration technique of microfluidic chips by using a UV-curable adhesive. *LAB ON A CHIP* 10(16), pp. 2115-2121. 2010.
- [161] S. Tuomikoski and S. Franssila. Free-standing SU-8 microfluidic chips by adhesive bonding and release etching. *Sensors & Actuators: A. Physical* 120pp. 408-415. 2005. . DOI: 10.1016/j.sna.2005.01.012.
- [162] M. A. Eddings and B. K. Gale. A PDMS-based gas permeation pump for on-chip fluid handling in microfluidic devices. *J Micromech Microengineering* 16(11), pp. 2396-2402. 2006.
- [163] J. S. Go and S. Shoji. A disposable, dead volume-free and leak-free in-plane PDMS microvalve. *Sensors & Actuators: A. Physical* 114pp. 438-444. 2004. . DOI: 10.1016/j.sna.2003.12.028.
- [164] E. Sollier, C. Murray, P. Maoddi and D. Di Carlo. Rapid prototyping polymers for microfluidic devices and high pressure injections. *Lab Chip* 11(22), pp. 3752-3765. 2011. . DOI: 10.1039/c1lc20514e.
- [165] H. Chen, A. A. McClelland, Z. Chen and J. Lahann. Solventless adhesive bonding using reactive polymer coatings. *Anal. Chem.* (11), pp. 4119. 2008.
- [166] P. Kim and K. Y. Suh. Rigiflex, spontaneously wettable polymeric mold for forming reversibly bonded nanocapillaries. *Langmuir* 23(8), pp. 4549-4553. 2007.
- [167] A. Khademhosseini, J. Yeh, G. Eng, J. Karp, H. Kaji, J. Borenstein, O. C. Farokhzad and R. Langer. Cell docking inside microwells within reversibly sealed microfluidic channels for fabricating multiphenotype cell arrays. *LAB ON A CHIP* 5(12), pp. 1380-1386. 2005.
- [168] M. Le Berre, C. Crozatier, G. Velve Casquillas and Y. Chen. Reversible assembling of microfluidic devices by aspiration. *Microelectronic Engineering* 83(-), pp. 1284-1287. 2006. . DOI: 10.1016/j.mee.2006.01.257.

- [169] G. C. Bong, W. P. Jeong, S. H. Jia, C. Huang, E. S. Monuki and N. L. Jeon. A hybrid microfluidic-vacuum device for direct interfacing with conventional cell culture methods. *BMC Biotechnology* 7pp. 60-66. 2007. . DOI: 10.1186/1472-6750-7-60.
- [170] E. Tkachenko, E. Gutierrez, M. H. Ginsberg and A. Groisman. An easy to assemble microfluidic perfusion device with a magnetic clamp. *LAB ON A CHIP* 9(8), pp. 1085-1095. 2009.
- [171] M. Rafat, D. R. Raad, A. C. Rowat and D. T. Auguste. Fabrication of reversibly adhesive fluidic devices using magnetism. *LAB ON A CHIP* 9(20), pp. 3016-3019. 2009.
- [172] G. A. Cooksey and J. Atencia. Pneumatic valves in folded 2D and 3D fluidic devices made from plastic films and tapes. *LAB ON A CHIP* 14(10), pp. 1665-1668. 2014.
- [173] Y. Temiz, R. D. Lovchik, G. V. Kaigala and E. Delamarche. Review article: Lab-on-a-chip devices: How to close and plug the lab? *Microelectronic Engineering* 132pp. 156-175. 2015. . DOI: 10.1016/j.mee.2014.10.013.
- [174] A. M. Christensen, D. Chang-Yen and B. K. Gale. Characterization of interconnects used in PDMS microfluidic systems. *J Micromech Microengineering* 15(5), pp. 928-934. 2005.
- [175] A. C. Glavan, R. V. Martinez, E. J. Maxwell, A. B. Bala Subramaniam, R. M. D. Nunes, S. Soh and G. M. Whitesides. Rapid fabrication of pressure-driven open-channel microfluidic devices in omniphobic RF paper. *Doi:10. 1039/c3lc50371b* 2013. . DOI: 10.1039/c3lc50371b.
- [176] B. L. Gray, D. Jaeggi, N. J. Mourlas, B. P. van Drieënhuizen, K. R. Williams, N. I. Maluf and G. T. A. Kovacs. Novel interconnection technologies for integrated microfluidic systems1Paper presented as part of the SSAW-98 workshop.1. *Sensors & Actuators: A. Physical* 77pp. 57-65. 1999. . DOI: 10.1016/S0924-4247(99)00185-5.
- [177] B. Gray. "Fluidic interconnects for microfluidics," in Anonymous 2011, . DOI: doi:10.1201/b11188-13.
- [178] A. Chen and T. R. Pan. Fit-to-flow (F2F) interconnects: Universal reversible adhesive-free microfluidic adaptors for lab-on-a-chip systems. *Lab Chip* 11(4), pp. 727-732. 2011.
- [179] E. Wilhelm, C. Neumann, T. Duttenhofer, L. Pires and B. E. Rapp. Connecting microfluidic chips using a chemically inert, reversible, multichannel chip-to-world-interface. *Lab Chip* 13(22), pp. 4343-4351. 2013.

- [180] J. Atencia, G. A. Cooksey, A. Jahn, J. M. Zook, W. N. Vreeland and L. E. Locascio. Magnetic connectors for microfluidic applications. *LAB ON A CHIP* 10(2), pp. 246-249. 2010.
- [181] D. J. IRSCHICK, C. C. AUSTIN, K. PETREN, R. N. FISHER, J. B. LOSOS and O. ELLERS. A comparative analysis of clinging ability among pad-bearing lizards. *Biol. J. Linn. Soc.* 59(1), pp. 21-35. 1996. . DOI: <http://dx.doi.org/10.1006/bijl.1996.0052>.
- [182] J. N. Israelachvili. "Chapter 6: Van der waals forces," in *Intermolecular and Surface Forces* (3rd ed.) Anonymous 2011, .
- [183] K. Autumn. "Properties, principles, and parameters of the gecko adhesive system," in , A. Smith and J. Callow, Eds. 2006, . DOI: 10.1007/978-3-540-31049-5_12.
- [184] F. Awaja, M. Gilbert, G. Kelly, B. Fox and P. J. Pigram. Adhesion of polymers. *Progress in Polymer Science* 34(9), pp. 948-968. 2009. . DOI: <http://dx.doi.org/10.1016/j.progpolymsci.2009.04.007>.
- [185] K. L. Johnson, K. Kendall and A. D. Roberts. Surface energy and the contact of elastic solids. *Proceedings of the Royal Society of London. Series A, Mathematical and Physical Sciences* (1558), pp. 301. 1971.
- [186] M. Varenberg, A. Peressadko, S. Gorb and E. Arzt. Effect of real contact geometry on adhesion. *Appl. Phys. Lett.* 89(12), pp. 121905. 2006. . DOI: 10.1063/1.2356099.
- [187] M. Kamperman, E. Kroner, A. del Campo, R. M. McMeeking and E. Arzt. Functional adhesive surfaces with "gecko" effect: The concept of contact splitting. *ADVANCED ENGINEERING MATERIALS* 12(5), pp. 335-348. 2010.
- [188] K. Kendall. The adhesion and surface energy of elastic solids. *Journal of Physics: D Applied Physics* 4(8), pp. 1. 1971.
- [189] R. Spolenak, S. Gorb, H. Gao and E. Arzt. Effects of contact shape on the scaling of biological attachments. *Proceedings: Mathematical, Physical and Engineering Sciences* (2054), pp. 305. 2005.
- [190] C. Greiner, A. del Campo and E. Arzt. Adhesion of bioinspired micropatterned surfaces: Effects of pillar radius, aspect ratio, and preload. *Langmuir* 23(7), pp. 3495-3502. 2007.

- [191] M. Varenberg, B. Murarash, Y. Kligerman and S. Gorb. Geometry-controlled adhesion: Revisiting the contact splitting hypothesis. *Appl. Phys. A* 103(4), pp. 933-938. 2011. . DOI: 10.1007/s00339-011-6394-0.
- [192] R. D. O'Rorke, T. W. J. Steele and H. K. Taylor. Bioinspired fibrillar adhesives: A review of analytical models and experimental evidence for adhesion enhancement by surface patterns. *Journal of Adhesion Science & Technology* 30(4), pp. 362-391. 2016. . DOI: 10.1080/01694243.2015.1101183.
- [193] B. J. Ferguson. *Improved Gecko Inspired Dry Adhesives Applied to the Packaging of MEMS* .
- [194] S. Kim, M. Sitti, Ji-Hyun Jang and E. L. Thomas. Fabrication of bio-inspired elastomer nanofiber arrays with spatulate tips using notching effect. *2008 8th IEEE Conference on Nanotechnology* pp. 780. 2008.
- [195] N. Gravish, M. Wilkinson, S. Sponberg, A. Parness, N. Esparza, D. Soto, T. Yamaguchi, M. Broide, M. Cutkosky, C. Creton and K. Autumn. Rate-dependent frictional adhesion in natural and synthetic gecko setae. *JOURNAL OF THE ROYAL SOCIETY INTERFACE* 7(43), pp. 259-269. 2010.
- [196] K. Autumn, A. Dittmore, D. Santos, M. Spenko and M. Cutkosky. Frictional adhesion: A new angle on gecko attachment. *J. Exp. Biol.* (18), pp. 3569. 2006.
- [197] Z. L. Peng and S. H. Chen. Effects of surface roughness and film thickness on the adhesion of a bioinspired nanofilm. *PHYSICAL REVIEW E* 83(5), 2011.
- [198] N. Cañas, M. Kamperman, B. Völker, E. Kroner, R. M. McMeeking and E. Arzt. Effect of nano- and micro-roughness on adhesion of bioinspired micropatterned surfaces. *Acta Biomaterialia* 8(1), pp. 282-288. 2012. . DOI: <http://dx.doi.org/10.1016/j.actbio.2011.08.028>.
- [199] M. Henrey, J. P. Díaz Téllez, K. Wormnes, L. Pambaguian and C. Menon. Towards the use of mushroom-capped dry adhesives in outer space: Effects of low pressure and temperature on adhesion strength. *Aerospace Science and Technology* 29pp. 185-190. 2013. . DOI: 10.1016/j.ast.2013.03.003.
- [200] W. Bin Khaled and D. Sameoto. Fabrication and characterization of thermoplastic elastomer dry adhesives with high strength and low contamination. *ACS APPLIED MATERIALS & INTERFACES* 6(9), pp. 6806-6815. 2014.

- [201] B. Soltannia and D. Sameoto. Strong, reversible underwater adhesion via gecko-inspired hydrophobic fibers. *ACS Appl. Mater. Interfaces* 6(24), pp. 21995-22003. 2014. . DOI: 10.1021/am5075375.
- [202] D. Sameoto and C. Menon. Recent advances in the fabrication and adhesion testing of biomimetic dry adhesives. *Smart Mater Struct* 19(10), 2010.
- [203] A. del Campo, C. Greiner and E. Arzt. Contact shape controls adhesion of bioinspired fibrillar surfaces. *Langmuir* 23(20), pp. 10235-10243. 2007.
- [204] Y. S. Li, A. Ahmed, D. Sameoto and C. Menon. Abigaille II: Toward the development of a spider-inspired climbing robot. *Robotica* 30pp. 79-89. 2012.
- [205] W. Bin Khaled and D. Sameoto. Anisotropic dry adhesive via cap defects. *BIOINSPIRATION & BIOMIMETICS* 8(4), 2013.
- [206] H. Lee, B. P. Lee and P. B. Messersmith. A reversible wet/dry adhesive inspired by mussels and geckos. *Nature* 448(7151), pp. 338-341. 2007. . DOI: 10.1038/nature05968.
- [207] M. K. Kwak, H. E. Jeong and K. Y. Suh. Rational design and enhanced biocompatibility of a dry adhesive medical skin patch. *Adv Mater* 23(34), pp. 3949-+. 2011.
- [208] A. Mahdavi, L. Ferreira, C. Sundback, J. W. Nichol, E. P. Chan, D. J. D. Carter, C. J. Bettinger, S. Patanavanich, L. Chignozha, E. Ben-Joseph, A. Galakatos, H. Pryor, I. Pomerantseva, P. T. Masiakos, W. Faquin, A. Zumbuehl, S. Hong, J. Borenstein, J. Vacanti, R. Langer and J. M. Karp. A biodegradable and biocompatible gecko-inspired tissue adhesive. *Proc. Natl. Acad. Sci. U. S. A.* (7), pp. 2307. 2008.
- [209] A. Parness, D. Soto, N. Esparza, N. Gravish, M. Wilkinson, K. Autumn and M. Cutkosky. A microfabricated wedge-shaped adhesive array displaying gecko-like dynamic adhesion, directionality and long lifetime. *JOURNAL OF THE ROYAL SOCIETY INTERFACE* 6(41), pp. 1223-1232. 2009.
- [210] C. Majidi, R. E. Groff, Y. Maeno, B. Schubert, S. Baek, B. Bush, R. Maboudian, N. Gravish, M. Wilkinson, K. Autumn and R. S. Fearing. High friction from a stiff polymer using microfiber arrays. *Phys. Rev. Lett.* 97(7), 2006.
- [211] S. Kim, E. Cheung and M. Sitti. Wet self-cleaning of biologically inspired elastomer mushroom shaped microfibrillar adhesives. *Langmuir* 25(13), pp. 7196-7199. 2009.

- [212] M. P. Murphy, S. Kim and M. Sitti. Enhanced adhesion by gecko-inspired hierarchical fibrillar adhesives. *ACS APPLIED MATERIALS & INTERFACES* 1(4), pp. 849-855. 2009.
- [213] M. P. Murphy, B. Aksak and M. Sitti. Gecko-inspired directional and controllable adhesion. *SMALL* 5(2), pp. 170-175. 2009.
- [214] A. del Campo, C. Greiner, I. Alvarez and E. Arzt. Patterned surfaces with pillars with controlled 3D tip geometry mimicking bioattachment devices. *Adv Mater* 19(15), pp. 1973-+. 2007.
- [215] H. E. Jeong, J. Lee, H. N. Kim, S. H. Moon, K. Y. Suh and R. Langer. A nontransferring dry adhesive with hierarchical polymer nanohairs. *Proc. Natl. Acad. Sci. U. S. A.* (14), pp. 5639. 2009.
- [216] N. R. Legge, G. Holden and H. E. Schroeder. *Thermoplastic Elastomers : A Comprehensive Review* 1987.
- [217] D. Sameoto and A. Wasay. Materials selection and manufacturing of thermoplastic elastomer microfluidics. 2015, .
- [218] I. K. Robert Shanks. *Thermoplastic Elastomers* 2012Chapter 8.
- [219] (). *Kraton G1701: SEP*. Available:
<http://docs.kraton.com/pdfDocuments/2009091316272757864244.PDF>.
- [220] (). *G1730 :SEP*. Available:
<http://docs.kraton.com/pdfDocuments/200909280835411564890.PDF>.
- [221] S. Halldorsson, E. Lucumi, R. Gómez-Sjöberg and R. M. T. Fleming. Advantages and challenges of microfluidic cell culture in polydimethylsiloxane devices. *Biosensors and Bioelectronics* 63pp. 218-231. 2015. . DOI: 10.1016/j.bios.2014.07.029.
- [222] Holger Becker. It's the economy.... *Lab on a Chip - Miniaturisation for Chemistry & Biology* 9(19), pp. 2759-2762. 2009.
- [223] E. Pedemonte, G. Dondero, G. C. Alfonso and F. d. Candia. Three-block copolymers: Morphologies and stress - strain properties of samples prepared under various experimental conditions. *Polymer* 16pp. 531-538. 1975. . DOI: 10.1016/0032-3861(75)90013-0.

- [224] S. N. Gorb and M. Varenberg. Mushroom-shaped geometry of contact elements in biological adhesive systems. *Journal of Adhesion Science & Technology* 21(12), pp. 1175-1183. 2007. . DOI: 10.1163/156856107782328317.
- [225] S. N. Gorb. The design of the fly adhesive pad: Distal tenent setae are adapted to the delivery of an adhesive secretion. *Proceedings: Biological Sciences (1398)*, pp. 747. 1998.
- [226] A. del Campo, C. Greiner and E. Arzt. Contact shape controls adhesion of bioinspired fibrillar surfaces. *Langmuir* 23(20), pp. 10235-10243. 2007.
- [227] G. Carbone, E. Pierro and S. N. Gorb. Origin of the superior adhesive performance of mushroom-shaped microstructured surfaces. *SOFT MATTER* 7(12), pp. 5545-5552. 2011.
- [228] G. Carbone and E. Pierro. Sticky bio-inspired micropillars: Finding the best shape. *SMALL* 8(9), pp. 1449-1454. 2012.
- [229] B. S. Bschaden. *Developing Design Guidelines for Improved Gecko Inspired Dry Adhesive Performance* 2014.
- [230] G. T. Mase and G. E. Mase. *Continuum Mechanics for Engineers* 1999.
- [231] *COMSOL Reference Manual : Structural Mechanics Module*.
- [232] K. Kendall. Thin-film peeling-the elastic term. *Journal of Physics: D Applied Physics* 8(13), pp. 1449. 1975.
- [233] N. S. Pesika, Y. Tian, B. X. Zhao, K. Rosenberg, H. B. Zeng, P. McGuiggan, K. Autumn and J. N. Israelachvili. Peel-zone model of tape peeling based on the gecko adhesive system. *J. Adhesion* 83(4), pp. 383-401. 2007.
- [234] A. Wasay and D. Sameoto. Gecko gaskets for self-sealing and high strength reversible bonding of microfluidics. *Lab Chip* 2015. . DOI: 10.1039/C5LC00342C.
- [235] D. R. Barbero, M. Saifullah, P. Hoffmann, H. J. Mathieu, D. Anderson, G. Jones, M. E. Welland and U. Steiner. High resolution nanoimprinting with a robust and reusable polymer mold. *ADVANCED FUNCTIONAL MATERIALS* 17(14), pp. 2419-2425. 2007.
- [236] E. L. Kendall, J. Y. Han, M. S. Wiederoder, A. Sposito, A. Wilson, O. D. Rahmanian and D. L. DeVoe. Soft lithography microfabrication of functionalized thermoplastics by solvent casting. *Journal of Polymer Science Part B: Polymer Physics* (18), pp. 1315. 2015. . DOI: 10.1002/polb.23766/abstract.

- [237] J. D. Williams and W. J. Wang. Study on the postbaking process and the effects on UV lithography of high aspect ratio SU-8 microstructures. *JOURNAL OF MICROLITHOGRAPHY MICROFABRICATION AND MICROSYSTEMS* 3(4), pp. 563-568. 2004.
- [238] B. L. Carvalho, E. A. Schilling, N. Schmid and G. J. Kellogg. Soft embossing of microfluidic devices. *MICRO TOTAL ANALYSIS SYSTEMS* 1pp. 959-962. 2003.
- [239] T. Brenner, C. Muller, H. Reinecke, R. Zengerle and J. Ducree. Fabrication chain for prototyping of microfluidic chips in polymers. 2005, .
- [240] V. N. Goral, Y. C. Hsieh, O. N. Petzold, R. A. Faris and P. K. Yuen. Hot embossing of plastic microfluidic devices using poly(dimethylsiloxane) molds. *J Micromech Microengineering* 21(1), 2011.
- [241] D. Sameoto and C. Menon. A low-cost, high-yield fabrication method for producing optimized biomimetic dry adhesives. *J Micromech Microengineering* 19(11), 2009.
- [242] Anonymous Improved gecko inspired dry adhesives applied to the packaging of MEMS.
- [243] M. Rahbar. PMMA microfluidics technology: Development and characterization. *ProQuest Dissertations and Theses* 2010.
- [244] <http://www.microchem.com/Prod-SU82000.htm>. Available: <http://www.microchem.com/Prod-SU82000.htm>.
- [245] E. H. Andrews and G. M. Levy. Solvent stress crazing in PMMA: 1. geometrical effects. *Polymer* 15(9), pp. 599-607. 1974. . DOI: [http://dx.doi.org/10.1016/0032-3861\(74\)90160-8](http://dx.doi.org/10.1016/0032-3861(74)90160-8).
- [246] S. Yasin, D. G. Hasko and H. Ahmed. Comparison of MIBK/IPA and water/IPA as PMMA developers for electron beam nanolithography. *Microelectronic Engineering* 61–62pp. 745-753. 2002. . DOI: [http://dx.doi.org/10.1016/S0167-9317\(02\)00468-9](http://dx.doi.org/10.1016/S0167-9317(02)00468-9).
- [247] P. Meyer, A. El-Kholi and J. Schulz. Investigations of the development rate of irradiated PMMA microstructures in deep X-ray lithography. *Microelectronic Engineering* 63pp. 319-328. 2002. . DOI: 10.1016/S0167-9317(02)00547-6.
- [248] R. Long, C. Hui, S. Kim and M. Sitti. Modeling the soft backing layer thickness effect on adhesion of elastic microfiber arrays. *J. Appl. Phys.* 104(4), pp. 044301. 2008. . DOI: 10.1063/1.2968249.

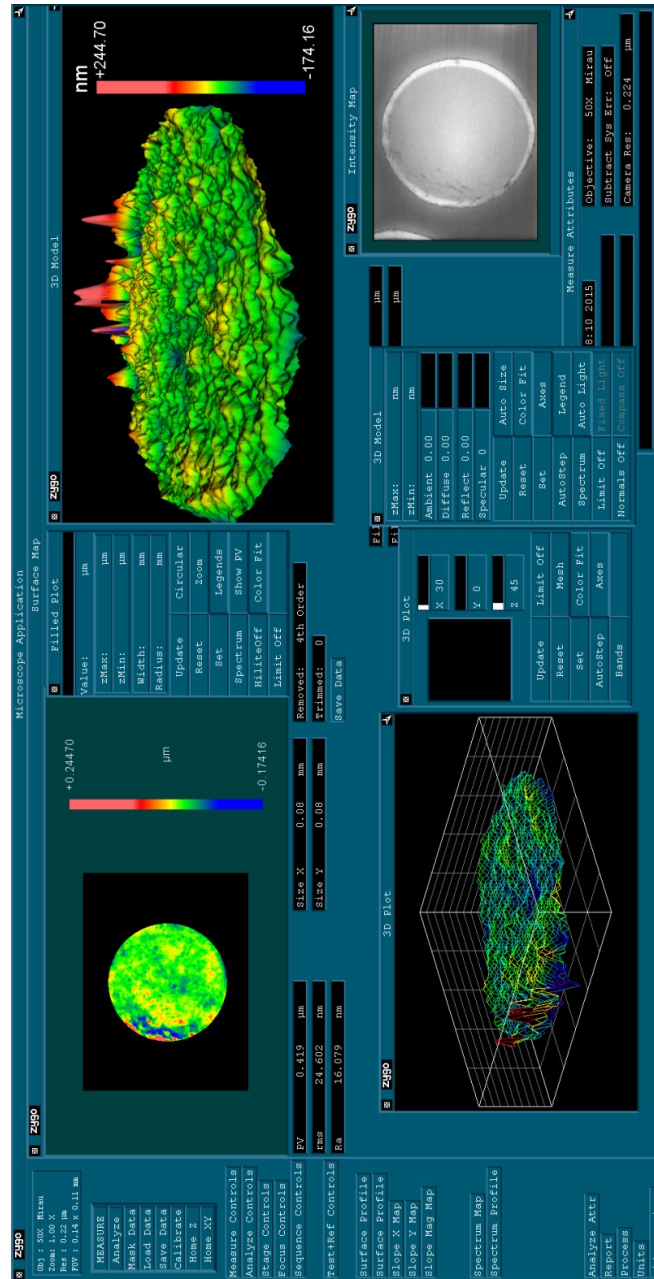
- [249] J. P. Landers. *Handbook of Capillary and Microchip Electrophoresis and Associated Microtechniques. [Electronic Resource]* 2008.
- [250] G. Binyamin, T. D. Boone, H. S. Lackritz, A. J. Ricco, A. P. Sassi and S. J. Williams. "Plastic microfluidic devices: Electrokinetic manipulations, life science applications, and production technologies," in *Lab-on-a-Chip*, R. E. Oosterbroek and A. v. d. Berg, Eds. 2003, . DOI: <http://dx.doi.org/10.1016/B978-044451100-3/50005-X>.
- [251] *Low Temperature Melting Metal Solders For Electrical Interconnects On Plastics*. Available: <http://blogs.rsc.org/chipsandtips/2015/06/25/low-temperature-melting-metal-solders-for-electrical-interconnects-on-plastics/>.
- [252] S. K. Chhina, A. Bajwa, M. Rahbar, A. K. Aminreza, H. L. Paul Chi and A. M. Parameswaran. Ultra-low-cost PMMA microfluidic device fabrication and electrophoretic pinch injection. *Journal of Medical and Biological Engineering / 中華醫學工程學刊* (2), pp. 105. 2011.
- [253] L. Zhang, X. F. Yin and Z. L. Fang. Negative pressure pinched sample injection for microchip-based electrophoresis. *LAB ON A CHIP* 6(2), pp. 258-264. 2006.
- [254] *Datasheets for MM2520 and MM4520: Shape Memory Polymers*. <http://www2.smp techno.com/en/smp/>.
- [255] Y. K. Suh and S. Kang. A review on mixing in microfluidics. *MICROMACHINES* 1(3), pp. 82-111. 2010.
- [256] N. T. Nguyen and Z. G. Wu. Micromixers - a review. *J Micromech Microengineering* 15(2), pp. R1-R16. 2005.
- [257] Chia-Yen Lee, Chin-Lung Chang, Yao-Nan Wang and Lung-Ming Fu. Microfluidic mixing: A review. *International Journal of Molecular Sciences* 12(5), pp. 3263-3287. 2011. . DOI: 10.3390/ijms12053263.
- [258] M. T. Guo, A. Rotem, J. A. Heyman and D. A. Weitz. Droplet microfluidics for high-throughput biological assays. *Lab Chip* 12(12), pp. 2146-2155. 2012. . DOI: 10.1039/c2lc21147e.
- [259] M. Abolhasani, A. Gunther and E. Kumacheva. Microfluidic studies of carbon dioxide. *Angewandte Chemie International Edition* (31), pp. 7992. 2014.
- [260] M. Prakash and N. Gershenfeld. Microfluidic bubble logic. *Science* 2007.

APPENDICES

Appendix A

Surface Profilometer Scans for different polymer samples

T509:



Microscope Application Surface Map

Z490

Obj: 50X Mirau
Mag: 0.24 mm
FW: 0.14 x 0.11 mm

MEASURE
Analyze
Mask Data
Load Data
Save Data
Calibrate
Home Z
Home XY

Measure Controls
Analyze Controls
Stage Controls
Focus Controls
Sequence Controls

Test-Ref Controls
Surface Profile
Surface Profile
Slope X Map
Slope Y Map
Slope Mag Map

Spectrum Map
Spectrum Profile

Analyze Attr
Report
Process
Units
Video Monitor

Z490 Filled Plot

Value: μm
zMax: μm
zMin: μm
Width: mm
Radius: mm

Update Circular
Reset Zoom
Set Legends
Spectrum Show EV
HiliteOff Color Fit
Limit Off

Removed: 4th Order
Trimmed: 0
Save Data

Size X: 0.08 mm
Size Y: 0.08 mm

EV: 0.808 μm
rms: 148.425 nm
Ra: 120.909 nm

Z490 3D Model

nm
+422.54
-385.22

Z490 Intensity Map

Z490 3D Plot

X: 30
Y: 0
Z: 45

Update Limit Off
Reset Mesh
Set Color Fit
AutoStep Axes
Bands

Z490 3D Model

zMax: mm
zMin: mm

Ambient 0.00
Diffuse 0.00
Reflect 0.00
Specular 0

Update Auto size
Reset Color Fit
Set Axes
AutoStep Legend
Spectrum Auto Light
Limit Off Fixed Light
Normals Off Compass Off

Z490 3D Plot

Measure Attributes

Objective: 50X Mirau
Subtract Sys Err: OFF
Camera Res: 0.224 μm

Microscope Application Surface Map

Z490

Obj : 50X Mirau
Res : 0.224 μ m
FOV : 0.14 x 0.11 mm

MEASURE
Analyze
Mask Data
Load Data
Save Data
Calibrate
Home Z
Home XY

Measure Controls
Analyze Controls
Stage Controls
Focus Controls
Sequence Controls
Test-Ref Controls

Surface Profile
Surface Profile
Slope X Map
Slope Y Map
Slope Mag Map

Spectrum Map
Spectrum Profile

Analyze Attr
Report
Process
Units
Video Monitor

Z490 Filled Plot

Value: μ m
zMax: μ m
zMin: μ m
Width: mm
Radius: mm

Update Linear
Reset Zoom
Set
Spectrum Show FV
HiliteOff Color Fit
Limit Off

Removed: 4th Order
Trimmed: 0
Save Data

Size X 0.075 μ m
Size Y 0.08 mm
Ra 4.064 nm

Size X 0.08 mm
Size Y 0.08 mm
Ra 4.064 nm

Z490 3D Model

Value: μ m
zMax: μ m
zMin: μ m
Width: mm
Radius: mm

Update Linear
Reset Zoom
Set
Spectrum Show FV
HiliteOff Color Fit
Limit Off

Removed: 4th Order
Trimmed: 0
Save Data

Size X 0.075 μ m
Size Y 0.08 mm
Ra 4.064 nm

Size X 0.08 mm
Size Y 0.08 mm
Ra 4.064 nm

Z490 3D Plot

X 30
Y 0
Z 45

Update Limit Off
Reset Mesh
Set Color Fit
AutoStep Axes
Bands

Z490 3D Model

zMax: mm
zMin: mm
Ambient 0.00
Diffuse 0.00
Reflect 0.00
Specular 0

Update Auto Size
Reset Color Fit
Set Axes
AutoStep Legend
Spectrum Auto Light
Limit Off Fixed Light
Normals Off Compass Off

Z490 Intensity Map

Measure Attributes
Objective: 50X Mirau
Subtract Sys Err: Off
Camera Res: 0.224 μ m

Microscope Application Surface Map

Z490 Obj: 50X Mirau
Zoom: A.00 X
Mag: 1.00 X
FW: 0.14 X 0.11 mm

MEASURE
Analyze
Mask Data
Load Data
Save Data
Calibrate
Home Z
Home XY

Measure Controls
Analyze Controls
Stage Controls
Focus Controls
Sequence Controls
Test+Ref Controls

PV 0.015 μ m
rms 1.527 nm
Ra 1.164 nm

Size X 0.07 mm
Size Y 0.07 mm
Removed: 4th Order
Trimmed: 0
Save Data

3D Plot
Surface Profile
Surface Profile
Slope X Map
Slope Y Map
Slope Mag Map

Spectrum Map
Spectrum Profile

Analyze Attr
Report
Process
Units
Video Monitor

Z490 Filled Plot

Value: μ m
zMax: μ m
zMin: μ m
Width: mm
Radius: mm
Update Linear
Reset Zoom
Set Legends
Spectrum Show PV
HiliteOff Color Fit
Limit Off

Size X 0.07 mm
Size Y 0.07 mm
Removed: 4th Order
Trimmed: 0
Save Data

3D Plot
X: 30
Y: 0
Z: 45
Update Limit Off
Reset Mesh
Set Color Fit
Autostep Axes
Bands

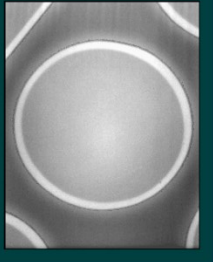
Intensity Map

Objective: 50X Mirau
Subtract Sys Err: Off
Camera Res: 0.224 μ m

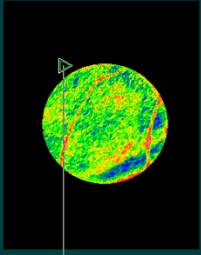
Z490 3D Model

zMax: mm
zMin: mm
Ambient 0.00
Diffuse 0.00
Reflect 0.00
Specular 0
Update Auto Size
Reset Color Fit
Set Axes
Autostep Legend
Spectrum Auto Light
Limit Off Fixed Light
Normals Off Compass Off

Z490 Intensity Map

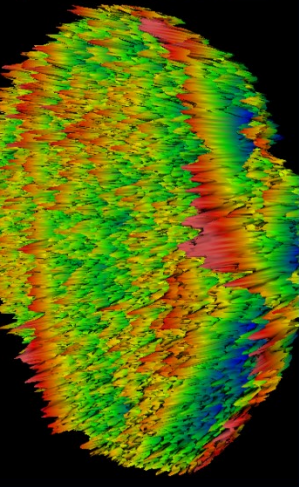


Z490 3D Plot



Value: μ m
zMax: μ m
zMin: μ m
Width: mm
Radius: mm
Update Linear
Reset Zoom
Set Legends
Spectrum Show PV
HiliteOff Color Fit
Limit Off

Z490 3D Model



Value: nm
zMax: nm
zMin: nm
Width: mm
Radius: mm
Update Linear
Reset Zoom
Set Legends
Spectrum Show PV
HiliteOff Color Fit
Limit Off

Microscope Application Surface Map

Obj : 500, Mirau
Res : 0.22 μ m
FOV : 0.14 x 0.11 mm

MEASURE
Analyze
Mask Data
Load Data
Save Data
Calibrate
Home Z
Home XY

Measure Controls
Analyze Controls
Stage Controls
Focus Controls
Sequence Controls
Rest-Ref Controls

PV 0.126 μ m
Rms 8.899 nm
Ra 5.808 nm

Size X 0.08 mm
Size Y 0.08 mm
Removed: 4th Order
Trimmed: 0
Save Data

Value: μ m
zMax: μ m
zMin: μ m
Width: mm
Radius: mm
Update Linear
Reset Zoom
set Legends
Spectrum Show PV
HiliteOff Color Fit
Limit Off

3D Model
Intensity Map

2490 2490

3D Plot
X 30
Y 0
Z 45
Limit Off
Update Reset
Mesh Color Fit
AutoStep Axes
Bands

3D Model
zMax: nm
Ambient 0.00
Diffuse 0.00
Reflect 0.00
Specular 0
Update Auto Size
Reset Color Fit
set Axes
Spectrum Auto Light
Limit Off Fixed Light
Normals Off Compass Off

Measure Attributes
Objective: 50X Mirau
Subtract Sys Err: Off
Camera Res: 0.224 μ m

3:59 2015

Video Monitor

Microscope Application Surface Map

Obj : 50X Mirau
 Beam : 0.32 nm
 FV : 0.14 x 0.11 mm

MEASURE
 Analyze
 Mask Data
 Load Data
 Save Data
 Calibrate
 Home Z
 Home XY

Measure Controls
 Analyze Controls
 Stage Controls
 Focus Controls
 Sequence Controls

FV 0.027 μm
 RMS 1.768 nm
 Ra 1.337 nm

Removed: 4th Order
 Trimmed: 0
 Save Data

Value: μm
 zMax: μm
 zMin: μm
 Width: mm
 Radius: mm
 Update Linear
 Reset Zoom
 Set Legends
 Spectrum Show FV
 Hiltetoff Color Fit
 Limit off

+0.02127 μm
 -0.00540 μm

3D Model
 zMax: μm
 zMin: μm
 Ambient 0.00
 Diffuse 0.00
 Reflect 0.00
 Specular 0
 Update Auto size
 Reset Color Fit
 Set Axes
 AutoStep Legend
 Spectrum Auto Light
 Limit Off Fixed Light
 Normals Off Compass Off

2.07 2015
 Objective: 50X Mirau
 Subtract Sys Err: Off
 Camera Res: 0.224 μm

3D Plot
 X 30
 Y 0
 Z 45
 Update Limit Off
 Reset Mesh
 Set Color Fit
 AutoStep Axes
 Bands

3D Plot
 3D Model
 Intensity Map

3D Plot
 3D Plot
 3D Plot

Analyze Attr
 Report
 Process
 Units
 Video Monitor

Microscope Application Surface Map

Obj: 50X Mirau
Zoom: 4.00 X
Mag: 0.12 µm
FOV: 0.14 X 0.11 µm

MEASURE
Analyze
Mask Data
Load Data
Save Data
Calibrate
Home Z
Home XY

Measure Controls
Analyze Controls
Stage Controls
Focus Controls
Sequence Controls
Test+Ref Controls

PV: 1.356 µm
rms: 103.885 nm
Ra: 67.422 nm

Removed: 4th Order
Frimmed: 0
Save Data

Size X: 0.08 mm
Size Y: 0.08 mm

Surface Profile
Slope X Map
Slope Y Map
Slope Map

Spectrum Map
Spectrum Profile

Analyze Attr
Report
Process
Units
Video Monitor

3D Model

nm
+880.97
-475.01

Intensity Map

µm
µm

3D Plot

X: 30
Y: 0
Z: 45

Update Limit Off
Reset MeshFill
Autostep Set
Bands

Update Color Fit
Reset Axes
Autostep Legend
Spectrum Auto Light
Limit Off Finest Light
Normals Off Compass Off

Measure Attributes
0:50 2015
Objective: 50X Mirau
Subtract Bys Err: Off
Camera Res: 0.224 µm

Microscope Application Surface Map

2490 2490

Obj : 50x Mirau
 Size : 0.32 mm
 Fov : 0.14 x 0.11 mm

MEASURE
 Analyze
 Mask Data
 Load Data
 Save Data
 Calibrate
 Home Z
 Home XY

Measure Controls
 Analyze Controls
 Stage Controls
 Focus Controls
 Sequence Controls
 Test/Ref Controls

FV 0.039 μm
 FmB 3.271 mm
 Ra 2.479 mm

Removed: 4th Order
 Trimmed: 0
 Save Data

Value: μm
 zMax: μm
 zMin: μm
 Width: mm
 Radius: mm
 Update Linear
 Reset Zoom
 set Legends
 Spectrum Show FV
 HilltsOff Color Fit
 Limit Off

+0.01295 μm
 -0.02578

3D Model
 2490 Intensity Map

3D Plot
 X 30
 Y 0
 Z 45

3D Plot
 zMax: mm
 zMin: mm
 Ambient 0.00
 Diffuse 0.00
 Reflect 0.00
 Specular 0
 Update Auto Size
 Reset Color Fit
 set Axes
 AutoStep Legend
 Spectrum Auto Light
 Limit Off Fixed Light
 Normals Off Compass Off

Measure Attributes
 Objective: 50X Mirau
 Subtract Sys Err: Off
 Camera Res: 0.224 μm

2490 2490

3D Plot
 X 30
 Y 0
 Z 45

3D Plot
 zMax: mm
 zMin: mm
 Ambient 0.00
 Diffuse 0.00
 Reflect 0.00
 Specular 0
 Update Auto Size
 Reset Color Fit
 set Axes
 AutoStep Legend
 Spectrum Auto Light
 Limit Off Fixed Light
 Normals Off Compass Off

Spectrum Map
 Spectrum Profile

Analyze Attr
 Report
 Process
 Units
 Video Monitor

Silicone: TC 5030

Microscope Application Surface Map

MEASURE

Obj: 1.00 X
Z: 1.00 X
Pos: 0.22 mm
Fov: 0.14 x 0.11 mm

Analyze
Mask Data
Load Data
Save Data
Calibrate
Home Z
Home XY

Measure Controls
Analyze Controls
Stage Controls
Focus Controls
Sequence Controls
Test/Ref Controls

Surface Profile
Surface Profile
Slope X Map
Slope Y Map
Slope Mag Map

Spectrum Map
Spectrum Profile

Analyze Attr
Report
Process
Units
Video Monitor

Value: mm
Removed: 4th Order
Trimmed: 0
Save Data

Size X: mm
Size Y: mm
Size Z: mm

Size X: mm
Size Y: mm
Size Z: mm

zMax: mm
zMin: mm

Ambient: mm
Diffuse: mm
Reflect: mm
Specular: mm

X:
Y:
Z:

Auto Size
Color Fit
Axis

AutoStep
Spectrum
Auto Light

Limit Off
Normals Off
Compass Off

Objective: 50X Mirau
Subtract Sys Err: Off
Camera Res: 0.224 μ m

Filled Plot

Value: μ m

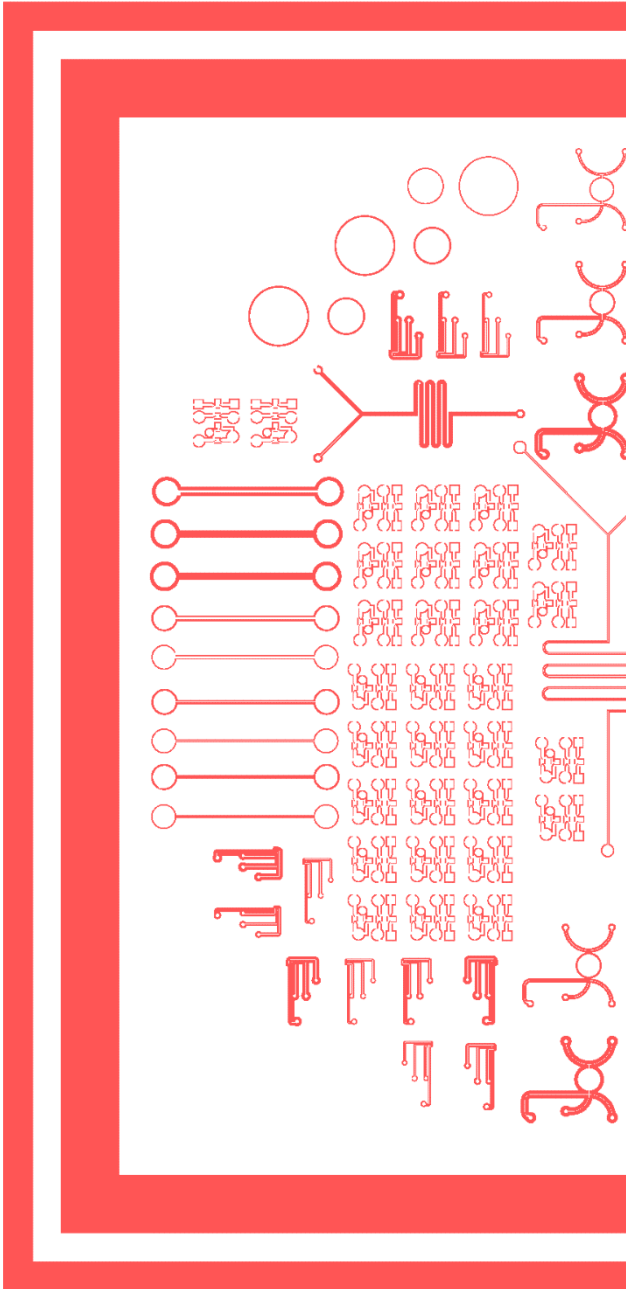
3D Model

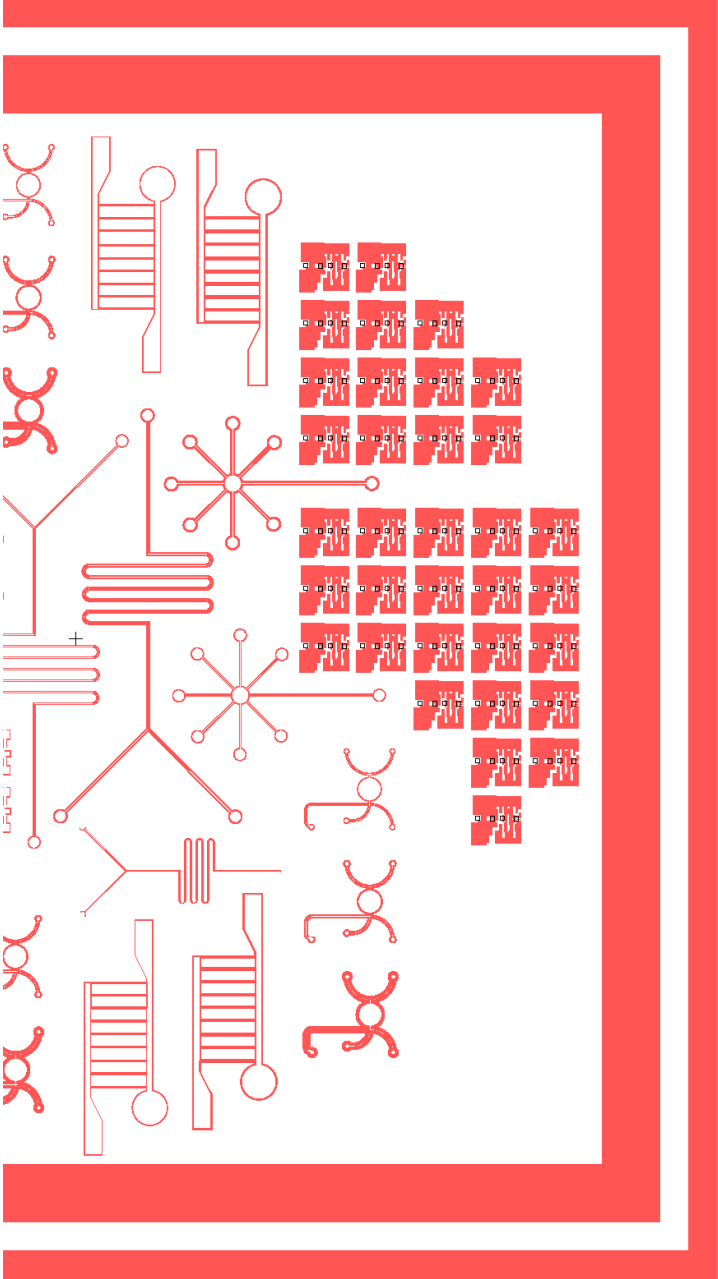
3D Plot

Intensity Map

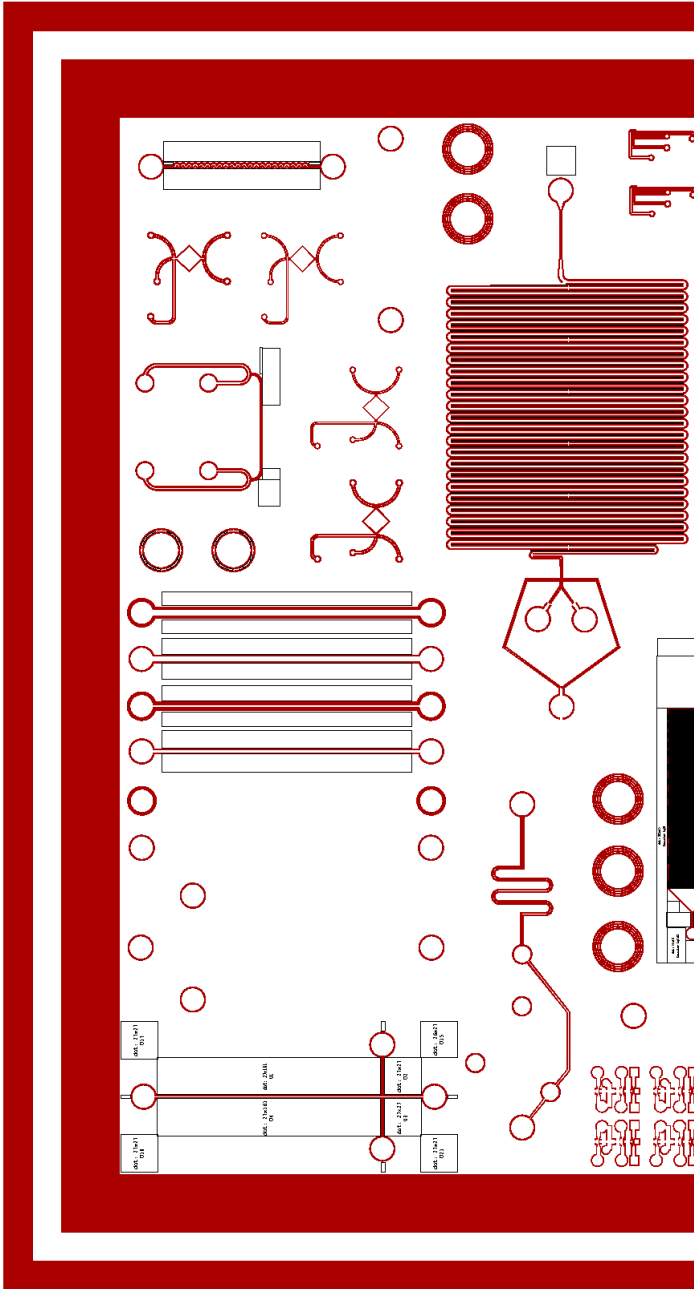
Appendix B

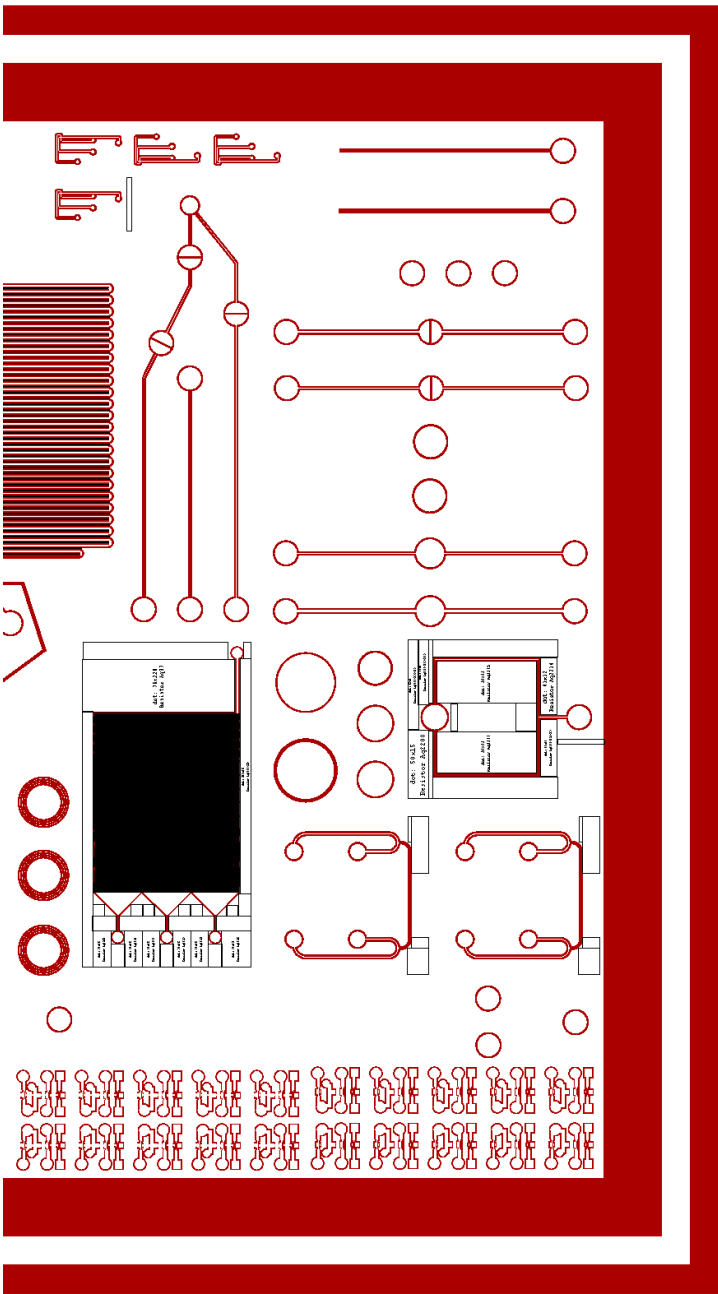
Mask 1:





Mask 2:





Appendix C

Variation of Height with respect to exposure dose

UV Exposure (Hours)	Heights (nm)					Average	SD
Uncollimated							
0	3.296	3.114	3.473	3.035	0	3.2295	0.195691
0.5	10.79	9.946	9.7	10.4	10.1	10.1872	0.483836
1	12.566	12.467	13.1	12.9	13.08	12.8226	0.29364
1.5	17.259	16.686	16.7	16.7	17.4	16.949	0.281911
2	21.626	21.502	21.5	21.3	21.6	21.5056	0.134888
4	40.816	39.83	0	0	0	40.323	0.697207
6	44.062	44.002	44.7	44.393	45.13	44.4574	0.323334
12	77.408	75.795	78.4	78.6	0	77.55075	1.2813
13	79.7	80.2	79.9	81.4	81.2	80.48	0.761577
14	86.003	84.18	85	85.9	85.5	85.3166	0.855412
15	94.469	93.1	94.6	95.5	94.8	94.4938	0.99055
Semi Collimated							
6	11.657	12	12.5	12	11.7	11.9714	0.347125
10	15.382	15.5	16.2	16.3	15.5	15.7764	0.471325
15	28.965	29.3	29.5	28.9	29.3	29.193	0.283237

Appendix D

Fields metal based solder for electrical connects on plastics

Tools and Apparatus:

- Fields Metal
- Syringe connected to tygon tube
- Copper/gold wire
- Aluminum foil dish
- Electrodes patterned on thermoplastic substrate (Here, Polystyrene)
- Hot Plate
- Shearing scissor
- Hot glue gun (Mastercraft's Dual temperature Glue gun, Operate at low temperature setting)



Fig D1: Tools and apparatus

Note: While Fields metal has been used in this demonstration, a wide variety of low temperature melting metals may be deployed for use depending on the application. The choice of metal may also warrant a need to look into the toxicity and heavy metal contents of the metal composition.

Field Metal Extrusion Process:

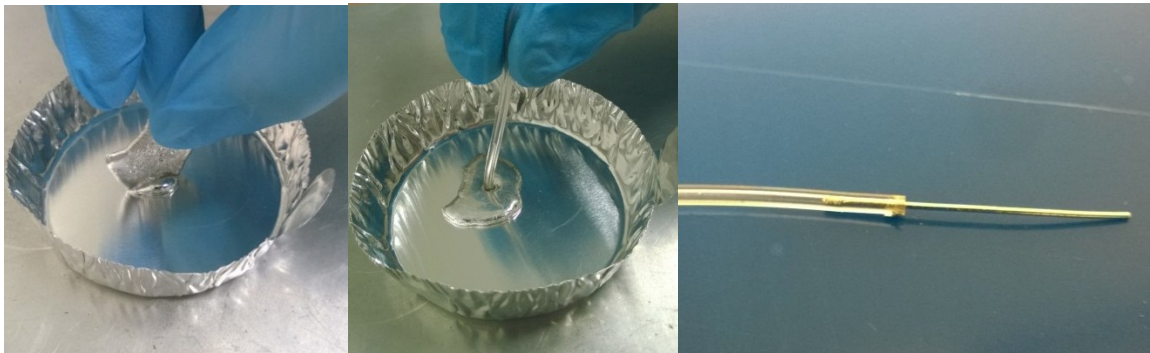


Fig. D2: metal filament forming process

- Melt the Fields metal (ROTO144) in an aluminum dish (Melting Temperature $\sim 62.2^{\circ}\text{C}$)
- Pull the liquid metal into a polymer tube of suitable diameter and length.
- Allow the metal cool to room temperature, and then pull out the metal filament using a plier.

Soldering process:

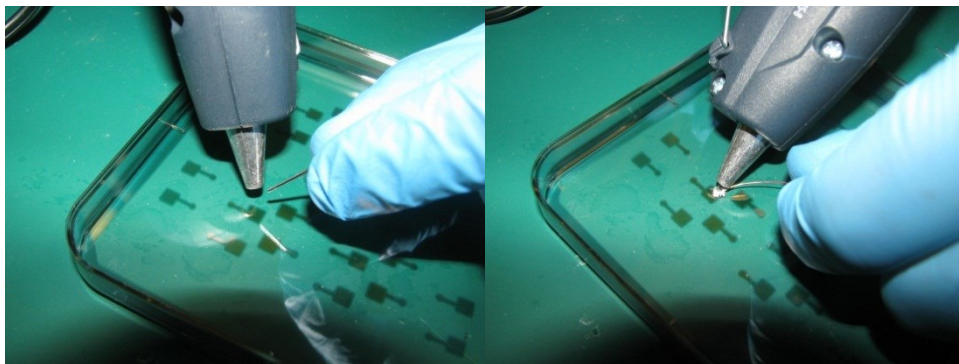


Fig D3: Soldering process

Using a low temperature gun (the hot glue gun on a lower temperature setting can heat upto $\sim 120^{\circ}\text{C}$), solder conductor wires to the gold pads with the extruded fields metal, via a process similar to a typical soldering process.

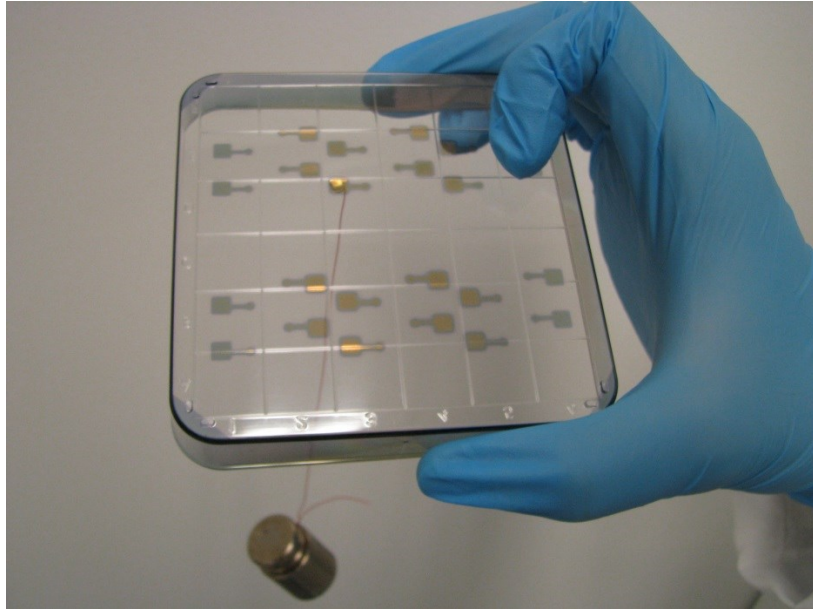


Fig D4: Proof of strength of the solder



Fig D5: Assembled Microfluidic Chip on the soldered polymer substrate.

Appendix E

